Development of Design Guidelines for Shallow Groynes

Von der

Fakultät Architektur, Bauingenieurwesen und Umweltwissenschaften

der Technischen Universität Carolo-Wilhelmina

zu Braunschweig

zur Erlangung des Grades eines

Doktor-Ingenieurs (Dr.-Ing.)

genehmigte

Dissertation

von

Bahaeldeen A. Zaid
geboren am 26. April 1978
aus Kharotum-Bahri, Sudan

Eingereicht am: 13. October 2017
Disputation am: 15. December 2017

Berichterstatter: Prof. Dr.-Ing. habil. Andreas Dittrich
Prof. Simon Tait

(2017)

Acknowledgment

I would like to thank Prof. Dr.-Ing. habil. Andreas Dittrich for the extensive support and the insightful comments which helped me completing my research and writing this thesis. I appreciate very much his time, patience and motivation.

Special thanks for Dr.-Ing. Katinka Koll for the extensive supervisions and support during HYTECH Project.

I wish to express my gratitude to all the supervisors of HYTECH EU-Project for the fruitful discussions and comments on my work during the summerschools and the meetings of the project. Special thanks to Prof. Simon Tait for his support during my secondment at the University of Sheffield and for being a second referee for my thesis.

Finally, I wish to thank my family for supporting me to accomplish this work.

This work was supported by the Research Executive Agency, through the 7th Framework Programme of the European Union, Support for Training and Career Development of Researchers (Marie Curie - FP7-PEOPLE-2012-ITN), which funded the Initial Training Network (ITN) HYTECH 'Hydrodynamic Transport in Ecologically Critical Heterogeneous Interfaces', N.316546.

Abstract

The need for river bank protection in an ecologically appropriate manner has led to the investigation of shallow groynes as a nature-oriented countermeasure against bank erosion. Shallow groynes are in-stream structures which have a horizontal crest and are submerged even during low flow conditions in order to minimize the effect on the flood level. Rather than enhancing the resisting forces like traditional bank protection measures, e.g. riprap, shallow groynes are used to redirect the attacking flow away from the river bank. In this way, the bank itself becomes available as habitat and the water-land interface is rehabilitated or preserved. Moreover, the shallow groynes increase the heterogeneity of the flow field, bed topography, and bed material, which is one of the key elements requested by the EU Water Framework Directive to improve the ecological condition of rivers. However, shallow groynes can further be used to increase attacking flow forces and thus guidelines are essential for a successful and sustainable design.

The objective of the study was to develop design guidelines for shallow groynes by investigating systematically the relevant design parameters groyne inclination, length, width, location and spacing in a river bend. The experiments were carried out in the large curved flume of the laboratory of the Leichtweiß-Institut für Wasserbau (LWI). The three-dimensional turbulent flow field was measured with an Acoustic Doppler Velocimeter (Vectrino Plus). The hydraulic boundary conditions were kept constant throughout the experiments. A reference run was carried out without a groyne providing the basis for quantification of the hydraulic effects due to the shallow groynes. The optimum groyne parameters were defined based on the highest reduction of stream-wise velocity close to the outer bank. The groyne parameters were systematically varied using a single groyne for determining the optimum angle of inclination, and investigating the effect of the width and the projected length. The manipulation of the flow field throughout the bend was investigated with a single groyne as well as with a group of groynes varying the number of groynes as well as the spacing. Further experiments were carried out with a fixed bed and a mobile outer bank.

The results of the measurements showed that the redirection of flow from the outer bank towards the inner bank due to the installation of shallow groynes was clear. The velocities close to the outer bank were decreased whereas the velocities towards the inner bank were increased. Furthermore, the installation of shallow groynes affected the secondary flow pattern, i.e. an outer bank secondary flow cell was observed.

The optimum inclination of shallow groynes was found to be 60° which showed the highest reduction on the stream-wise velocities close to the outer bank. It was also found that installing the groyne at the beginning of the curve provides the highest reduction in the velocities close to the outer bank and induces the minimum acceleration of the flow over the groyne. Regarding the groyne length, long groynes with pro-

jected length (l_p= 80cm) showed that the reduction of the velocities close to the outer bank persists throughout the curve. In the case of short groynes (l_p= 40cm) the velocities close to the outer bank recovered to those in case without groyne after the bend centre. Nevertheless, short groynes induced less acceleration of the flow compared to long ones. Different groups of groynes with different groyne lengths and spacing were tested to define the optimum groynes group setting. A geometric method to define the location of the groynes in the groynes field was developed.

The results of the mobile outer bank conditions experiments confirmed the effectiveness of shallow groynes for bank protection. The maximum scour at the outer bank in the test run without groynes was found downstream the bend exit. The installation of shallow groyne showed a significant protection to the outer bank with only minor erosion. The results of the mobile outer bank highlighted the importance of locating a groyne at the bend exit for reducing the scour downstream the bend. This is important in case the geometric method to define the location of the groyne resulted in a location for the last groyne far away from the bend exit.

Although some investigation on shallow groynes were carried out with mobile outer bank conditions, it is necessary to carry out further experiments on shallow groynes with mobile bed conditions. This allows to study the effect of shallow groynes on the river thalweg and how the groynes can relocate it away from the outer bank. The mobile bed condition tests provide information on the scour at the groyne tip which is important for the groyne stability. Furthermore, mobile bed condition tests may help to investigate in which way shallow groynes may help to diversify the bed morphology which is important for the habitat heterogeneity.

Table of Contents

List of symbols

a	[m^2]	effective area of sediment particle
A^*	[-]	drea contraction ratio
a_1... a_7	[-]	regression coefficients
A_b	[-]	relative distance (S_p/l_p)
AVR_i	[-]	average velocity ratio at the inner, centre and outer bank
C	[-]	circulation constant in the free-vortex-motion
C_D	[-]	drag coefficient
C_i	[-]	cross-section No. i
C_L	[-]	lift coefficient
c_v	[-]	relative transverse velocity
d	[mm]	grain diameter
D_B	[m]	baseline flow depth
D_e	[m]	minimum depth of penetration of vane
D_m	[m]	maximum scour depth at the bend
E		specific energy
F_D	[N]	drag force
F_G	[N]	submerged weight of sediment particle
g	[m^2/s]	acceleration of gravity
H	[m]	water depth
H_a	[m]	water depth at which mean depth and water velocity
H_v	[m]	design height of vane
h_b	[cm]	stream barb height
h_g	[m]	shallow groyne height
k_d	[m^3/N·s]	erodibility coefficient
L	[m]	length of the weir level
L_i	[-]	longitudinal profile No. i where i =1 to 7
l_p	[cm]	projected length of shallow groyne
L_v	[m]	length of vane
$L_{W\text{-}PROJ}$	[m]	projected length of weir measured from the baseline occurs perpendicular to the flow
Q	[m^3/s]	discharge
R	[m]	radius of curvature
R_a	[m]	radius at which mean depth and water velocity occurs
R_i	[m]	inner bank radius
R_o	[m]	outer bank radius
S_p	[m]	spacing between bendway weirs or vances and shallow groyne
S	[-]	channel slope
s	[m]	coordinates in s-direction

n	[m]	coordinates in s-direction
$S_{p\text{-}max}$	[m]	maximum spacing between bendway weirs
S_θ	[-]	channel slope in θ direction
t	[s]	time
T_w	[m]	channel top width
ũ	[cm/s]	depth average velocity
U	[cm/s]	mean velocity
u	[cm/s]	stream-wise velocity
U_{*a}	[m/s]	average shear velocity in the radial direction
U_a	[m/s]	average cross-sectional velocity
u_r	[m/s]	velocity in r direction
u_z	[m/s]	velocity in z direction
u_θ	[m/s]	velocity in θ direction
v	[cm/s]	transverse velocity
w	[cm/s]	vertical velocity
W	[m]	channel width
w_g	[cm]	shallow groyne width
WL	[m]	water level
W_s	[m]	submerged weight of sediment particle
$\overline{z}_b$	[m]	bed level
Δh	[m]	super-elevation
Δ_z	[m]	difference between structure crest elevation and water
ε	[m/s]	bank erosion rate
η	[-]	ratio between F_L and F_D
θ_b	[°]	bank inclination angle
θ_c	[°]	bend angle
θ_g	[°]	shallow groyne inclination angle
θ_s	[°]	planmetric angle of structure crest with bank-line tangent
θ_{sb}	[°]	stream barb inclination angle
θ_{sb}	[°]	angle between vane tip, toe and bend centre
θ_v	[°]	angle of vane with upstream tangent
κ	[-]	Kármán constant
λ_0	[-]	sheltering coefficient
μ	[-]	Coulomb static friction of sediment particles
ρ	[Kg/ m^3]	fluid density
ρ_s	[Kg/ m^3]	sediment density
	[N/m^2]	boundary shear stress applied by the flow
	[N/m^2]	critical shear stress
	[N/m^2]	critical shear stress on channel side slope
	[N/m^2]	shear stress in θ direction

List of Figures

List of Tables

List of Annexes

1 Introduction

Rivers are dynamic systems which over a long time of erosion and deposition processes develop their channel plan form. The most common characteristic regarding rivers plan form is the absence of long straight reaches; instead, the presence of frequent bends is the norm in natural rivers (Leopold & Wolman 1960). It is unusual in nature to find a river with straight reaches of more than 10 times the channel width (Leopold & Wolman 1957). Flow in river bends is complex and characterized with helical motion, super-elevation and flow separation. In association with bend flow, erosion and deposition take place at the outer bank and inner bank respectively.

Bank erosion causes loss of land and endangers stream-side infrastructures. Therefore, it has been regarded in many studies as a negative process to be halted (Piegay et al., 2005). Nevertheless, the advantages of bank erosion as a process that creates a dynamic habitat which is necessary for sustaining the ecosystem has been highlighted (Florsheim et al. 2008).

In order to protect river banks, different bank erosion counter measures are available. Bank protection methods can be divided into two categories: (i) direct methods which invest in increasing the bank resistance such as walls and gabion. (ii) Indirect methods which invest in decreasing the flow acting force on the bank such as in-stream structures. The direct methods of bank protection have some environmental drawbacks as the structures normally occupy the bank introducing discontinuity between land and water consequently, the bank area which is an important area of interfaces between water, biota and sediment is lost or extremely degraded.

In the case of the indirect bank protection methods the flow is redirected with so-called in-stream structures or nature-oriented structures away from the outer bank reducing the dynamic forces on the bank, consequently reducing the bank erosion. The redirection of the flow is done with structures projecting from the outer bank into the river at a certain angle. In addition to the bank protection, in-stream structures installation increases the hydrodynamic and morphologic heterogeneity in the river. This heterogeneity in the flow velocity, water depth and bed material creates heterogeneous habitat which intern increases biodiversity (Shields Jr. et al. 1995). Due to the environmental benefits the in-stream structures provide to the river, they are regarded as sustainable bank protection counter measure (Jamieson et al. 2013) and has become increasingly popular (Scurlock et al. 2015). Furthermore the need for ecologically-appropriate management of natural and constructed surface water bodies which has become increasingly important (Marion et al. 2014) encourage the application of nature oriented structures as bank erosion countermeasure.

Different types of in-stream structures are available e.g. bendway weirs, stream barbs and rock vane (see Chap. 2.3.2). However, the definition of some of the in-stream structure types may incorporate some inconstancy and no clear-cut distinction between the structure types is not available. Figure 1.1 shows schematically a comparison between shallow groynes and different in-stream structures. The design of in-stream structures involves different parameters, e.g. the structure parameters involve the length, projected length, width, height, inclination and spacing of the structures. Several studies were carried out to give recommendations and guidelines on some of the in-stream structures resulting from experiments (e.g. Matsuura & Townsend 2004) or physical model tests (Scurlock et al. 2015). Nevertheless, the current design guidelines of in-stream structures are based on geometric parameters whereas little is known about the hydraulic effect of the structures of different sizes and combinations on the overall flow field (Scurlock et al. 2015). Therefore a comprehensive research program is needed to elaborate on the hydraulic effect of each single parameter and to optimize the structures parameters (Matsuura & Townsend 2004).

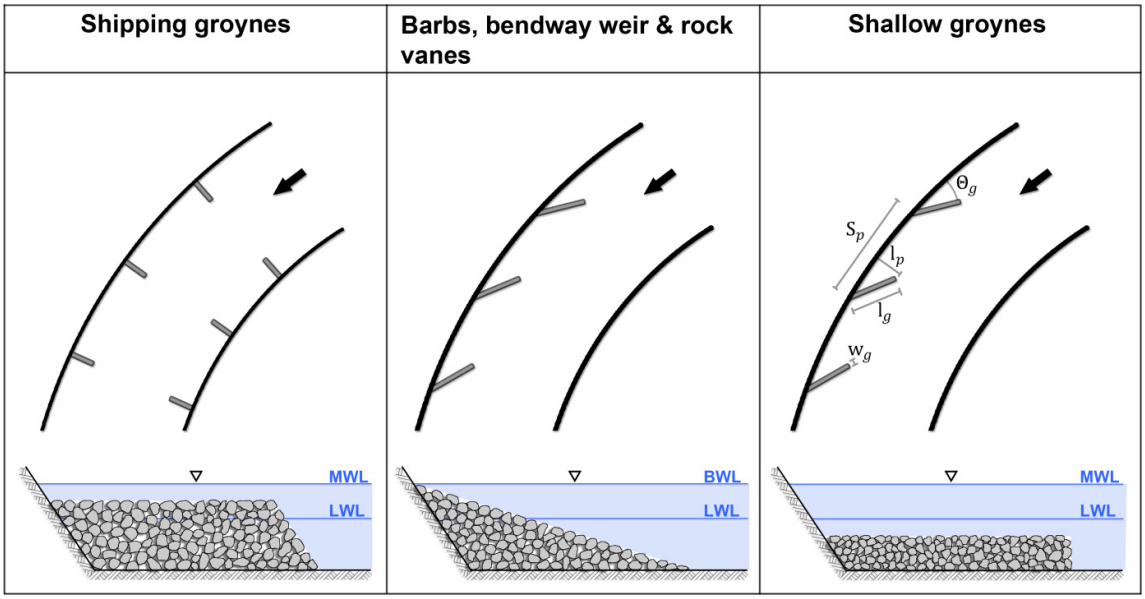

Figure 1.1 Sketch for some in-stream structures (MWL= mean water level, LWL= low water level, BWL=bank-full water level)

Definition of Shallow groynes

Shallow groynes are in-stream structures for river bank protection which are under development at the Leichtweiß-Institut (LWI). The structures are anchored to the river outer bank and protrude into the river at a certain angle. The important features of shallow groynes are: (i) the height of the structures h_g is so small that it is always submerged even during low flow conditions, (ii) the crest of the structure is horizontal (see Figure 1.1). This setup gives the shallow groynes the advantage of having the least effect on the flood level if any. In fact, this was the main reason for the devel-

opment of shallow groynes because in some areas where the flood level is highly restricted due to high land use, shallow groynes can still be applicable. In addition, the high level of submergence of the structures allows for navigation and recreation activity beside the aesthetic view of the river. The parameters of shallow groynes include length l_g, projected length l_p , width w_g , height h_g , inclination θ_g and spacing S_p and the location of the groynes in the bend (see Figure 1.1).

So far, first design guidelines for shallow groynes have been derived from experiments in a straight flume with fixed bed material by Mende (2014). Möws & Koll (2014) carried out experiments with mobile bed material in the same straight flume in order to gain information on the effect of shallow groynes on the morphology of gravel beds. However, it is not known if the data from experiments with shallow groynes in straight flumes can be applied to flumes with bends, and whether the design guidelines derived from these experiments have to be adjusted in order to obtain similar effect on the overall flow field with shallow groynes in bends.

This complex matter results in the research objectives listed below.

Research objectives

- To investigate the applicability of shallow groynes for bank protection in a curved flume.
- To systematically vary the characteristic groyne parameters such as inclination, length, width, spacing as well as position with respect to their effect on the flow field, consequently, flow force resection on the banks.
- To investigate the effect of combinations of parameters of shallow groynes in different groups of groynes in order to optimize the groynes group setup.
- Assessment of the effect of shallow groynes on local bank erosion.
- To develop design guidelines of shallow groyne taking into account the effect of the groyne parameters on the flow field.

In order to respond to these objectives a comprehensive experimental program was carried out. The experiments were done in a S-shaped flume at the laboratory of LWI. The curvature ratio (radius/width) of the curves in the flume is 1.5 which is in the range of sharp bends. The groynes were built with glued gravel to resemble as close as possible the typical groynes in the field. The groyne parameters (see Figure 1.1) were systematically varied and the 3D flow field was measured. This allows investigating the effect of each single groyne parameter on the flow field. The knowledge gained from the effect of the single groyne parameters was used in the setup and the investigations of a combination of parameters. Finally the groyne group setup was optimized based on the reduction of the stream-wise velocity close to the outer bank. The optimum setup was tested further in mobile outer bank condition experiments. The mobile outer bank experiments provided more information on the bank scour

downstream of the bend. Furthermore it helped to optimize the groynes setup to reduce the local scour around the groyne.

In Chap. 2, a literature review on bank erosion, bank erosion counter measures and in-stream structures design guidelines and studies is given. Chap. 3 describes the experimental setup including the flume setup, measurement devices, measurement grids and experimental program. In Chap. 4 the results are presented and discussed in which the investigation of the groyne inclination was addressed. Then the effect of the groyne length, width and location on the flow field is presented followed by the results of detailed measurements around a groyne located at the middle of the curve. Chap.4 addresses also the investigation of different groups of groynes and elaborates on the optimum spacing with a proposed geometric method to determine the location of the groynes in a groyne field. In addition, the results of the mobile outer bank tests are addressed and discussed. In Chap.5 conclusions and outlook are presented.

2 Literature review

A review on river bank erosion including bank erosion mechanism will be given in Chap. 2.1. Chap. 2.2 addresses the flow field and bed shear stress pattern in curved channel. Bank protection methods including classification, in-stream structure definitions and available design guidelines of in-stream structures are presented and discussed in Chap. 2.3. The introduction of shallow groynes as an alternative indirect method of bank protection is given in Chap. 2.4. Finally a synthesis of the literature review is given in Chap. 2.5

2.1 Bank erosion

Bank erosion is a key process in river morphodynamics, affecting a wide range of physical, ecological and socio-ecological issues in the fluvial environment (Papanicolaou et al. 2006). The impact of bank erosion extends to the channel morphology and flood carrying capacity by the mean of supplying sediment and large woody debris (Downs & Simon, 2001), floodplain evolution and associated habitat development (e.g. Darby and Thorne, 1996a; Rinaldi & Darby 2008). Bank erosion causes loss of land and threatens stream-site infrastructures (Figure 2.1) and flood defences. In addition, bank erosion increases fine sediment concentration which can be dangerous for the ecosystem, by decreasing the light for the aquatic plants, inhibiting the ability of fish to find food, decreasing the amount of dissolved oxygen in water and changing the water temperature (Laderoute & Bauer 2013).

Figure 2.1 *Bank erosion damages, (a) (USGS), (b) (httpswww.qld.gov.auenvironmentlands-oilerosionimpacts)*

Due to the negative impacts of bank erosion many studies exist regarding bank erosion as a process that has to be halted. Moreover, in some countries like India bank erosion causes human displacement due to the loss of agricultural land putting the displaced people in an economic insecurity (Das et al. 2014). Therefore it does not surprise that bank erosion in current river management is regarded as a natural hazard to be prevented (Piegay et al., 2005). Nevertheless it is evident, that in certain contexts bank erosion can be considered as a positive phenomenon to be preserved

(Piegay et al. 2005). Florsheim et al. (2008) explored the benefits of bank erosion to the ecosystem and regarded bank erosion as desirable attribute of rivers. Among these benefits Florsheim et al. (2008) stated the promotion of riparian vegetation and the creation of dynamic habitats which is important to sustain the ecosystem, otherwise, static banks are not norm and static rivers do not sustain the ecosystem.

Furthermore, bank erosion remains as a major contributor of sediment in some catchments. As documented in some studies bank erosion can contribute by as much as 23-54% (Palmer et al. 2014) or even up to 85% of the total sediment transported by the river in the watershed (Wallbrink et al. 1998; Trimble, 1997; Prosser et al., 2000; Simon et al., 2000). By being a source of sediment supply, bank erosion contributes to self-restoration in incised rivers where the sediment supply is limited due to anthropogenic effects (Bradvard et al. 1999). The Old Rhine is an example of the incised rivers where the concept of controlled bank erosion was introduced. The idea was to weaken the banks by removing some of the riprap and modifying of the groynes (Figure 2.2). This allows for limited bank erosion which generates alluvial dynamics, replenish sediment, and enhances sediment transport (El Kadi et al. 2014; Aelbrecht et al. 2014). The bank protection structures were modified in a pilot area. The survey of the fish before and after the modification showed that in the eroded zones the number of fish was two times higher than in the non-eroded zones (Aelbrecht et al. 2014).

Figure 2.2 Photos of the bank, (a) before the flood, (b) after the flood (Aelbrecht et al. 2014).

Considering the aforementioned impacts and benefits of bank erosion, the management of bank erosion is one of the most controversial issues in alluvial corridors (Nardi 2011). However, a reconsideration of the traditional policies for managing bank erosion is taking place, driven by the increasing awareness of (i) the unsustainable nature of some engineering bank protection measures and their associated economic cost (ii) the key role of bank erosion in channel dynamics and ecosystem services that bank erosion provides which was not considered in the previous cost-benefit analysis of bank protection works (Piegay et al. 2005).

In order to account for the ecosystem services and other benefits of bank erosion new strategies were recently followed and the river erodible corridor concept allowing the river to move within a defined corridor is increasingly adopted by the river manager. However, it is important to recognize that the erodible corridor approach is most effective where the river still has a high morphodynamic potential and sediment load (Kondolf & Piegay 2016). Further review on bank erosion can be found in Nardi (2011).

2.1.1 Main processes

River bank erosion occurs through a compilation of three mechanisms, namely sub-aerial erosion, fluvial erosion and mass failure (Lawler, 1995). The sub-aerial processes weaken the bank prior to the fluvial erosion. Fluvial erosion is linked to the mass failure through the erosion of the bank toe (Acode & Thorne 1988). The mechanisms of bank erosion are suggested to interact and operate at different special (Lawler 1995) and temporal scales (Couper & Maddock 2001).

By looking at the erosion processes throughout the river reach from the source down to the outlet, Lawler (1992) suggested a downstream change in the dominance of the bank erosion mechanisms (Figure 2.3). Lawler (1992) suggested that sub-areal processes, like preparation, freezethaw and desiccation processes may dominate the upper reaches of the river in the catchment where the stream power is low, while in the mid-basin area where the stream power is suggested to peak, the fluvial entrainments prevail. At the lower reach where the bank material is cohesive and resistant to fluid shear and bank height exceeds geotechnical instabilities mass failure is dominant (Figure 2.3).

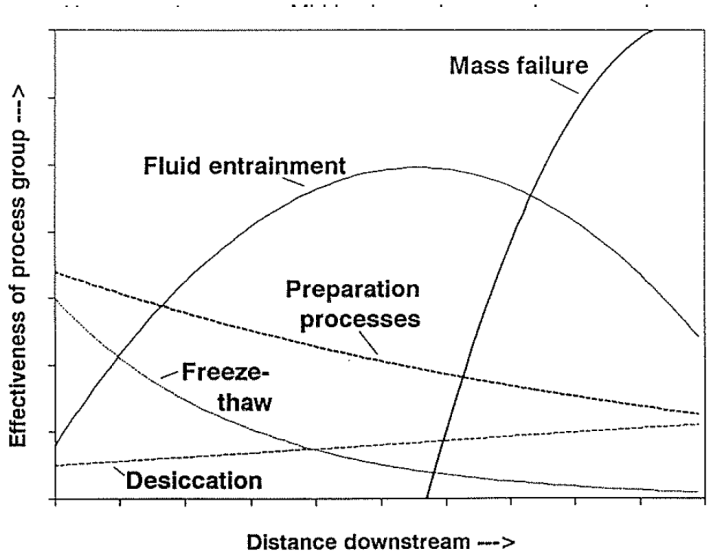

Figure 2.3 Downstream change in bank erosion process groups (after Lawler, 1995)

The three processes of bank erosion operate at different frequency and magnitude. Sub-aerial processes are the most frequent but smallest in magnitude, whereas mass failures are the rarest, highest-magnitude events, and fluvial erosion operates between the two (Couper & Maddock 2001).

2.1.1.1 Sub-aerial processes

Sub-aerial processes are a climate-related phenomenon involving number of processes known as weathering. It includes wetting and drying the bank and freeze–thaw activities which weaken the bank, and becomes as preparatory process prior to the fluvial erosion. These processes as mentioned before may dominate the upper reach where the stream power is weak. Although sub-aerial processes are often regarded as preparatory processes in the literature, Couper & Maddock (2001) found that they may be underestimated and they can be an erosive agent themselves.

According to Papanicolaou et al. (2006) the sub-aerial processes affect the temporal variation of the sediment erodibility, and partly, the shear stress property. However, no studies were carried out to quantify the effect of the sub-aerial process on the reduction of the erodibility and shear stress parameters (Papanicolaou et al. 2006).

2.1.1.2 Fluvial erosion

Fluvial erosion refers to the direct removal of the soil particle from the bank or the bed by the action of hydraulic forces. Fluvial erosion rate depends on the strength of the near-bank stream flow and the characteristics of the banks material. A widely accepted formula to quantify the fluvial erosion rate is the excess shear stress equation by (Partheniades, 1965; Arulanandan et al., 1980):

$$\varepsilon = k_d(\tau - \tau_c)^a \tag{2.1}$$

Where ε is the bank erosion rate per unit time and unit area (m/s), τ is the boundary shear stress applied by the flow (N/m^2), k_d is the erodibility coefficient $(\mathrm{m^3/N \cdot s})$, τ_c is the critical shear stress (N/m^2) and a is an empirically-derived exponent (-) typically assumed to be equal to 1.

2.1.1.3 Mass failure

Mass failure is the collapse of the river bank material under the action of gravity. Compared to fluvial erosion, mass failure is a discontinuous and large-scale detachment process (Papanicolaou et al. 2006). Bank failure takes place through several mechanisms: rotational failure, planar failure, cantilever failure and piping failure (Figure 2.4). The river bank collapses if the slope stability criterion is exceeded, i.e. when the driving force due to gravity exceeds the resisting force due to the shearing resistant of the material. A common method to evaluate the slope stability of the river

bank is the Limit Equilibrium Method (LEM) to calculate the safety factor which is the ratio between the stabilizing and destabilizing forces (Rinaldi & Darby 2008). However, the LEM method does not account for several factors which affect the bank stability, such as the changes in pore water pressure and the effect of vegetation. Studies by (Simon et al. 1991; Darby & Thorne 1996b) addressed the effect of the positive pore water pressure, whereas the effects of negative pore water pressures in the unsaturated part of the bank has been addressed e.g. by Rinaldi & Casagli (1999). Rinaldi & Darby (2008) highlighted that the effects of vegetation on the bank processes are manifold, complex and most of them are difficult to quantify. Some of the effects of vegetation on bank stability can be positive and others can be negative, therefore, the net change in the bank stability due to the vegetation is highly dependent on site specific factors (Rinaldi & Darby, 2008). However, the positive effect of the vegetation on the bank stability is usually dominant (Pollen-Bankhead & Smith 2009). The most important mechanical effect of the vegetation on the bank stability is the effect of the root system on increasing the soil strength (e.g. Pollen 2006).

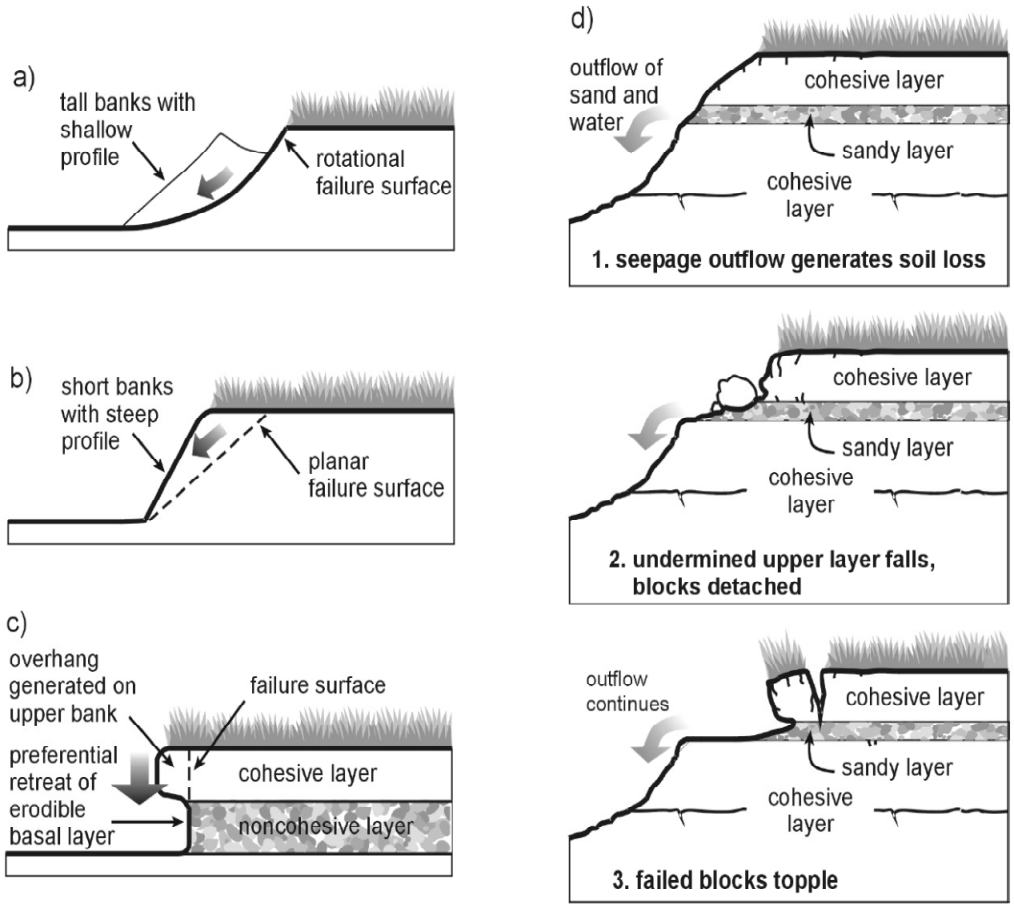

Figure 2.4 Bank failure mechanisms (modified from FISRWG 1998)

2.1.2 Stability considerations for fluvial erosion

For non-cohesive sediment the critical shear stress τ_c can be estimated using the same methods of the bed critical shear stress as given e.g. in the Shields diagram (Papanicolaou et al. 2006; Clark & Wynn 2007). Considering the high transverse slope of the bank compared to the bed longitudinal slope, a modification of the critical shear stress τ_c has to be made. To account for the channel side slope Chow 1959 presented a force balance analysis to obtain a ratio of the critical shear stress on the channel side slope to the critical shear stress on the channel bed. Figure 2.5 shows a force balance analysis on a sediment particle resting on a channel side slope ($a\tau_s$) and a particle resting on channel bed ($a\tau$).

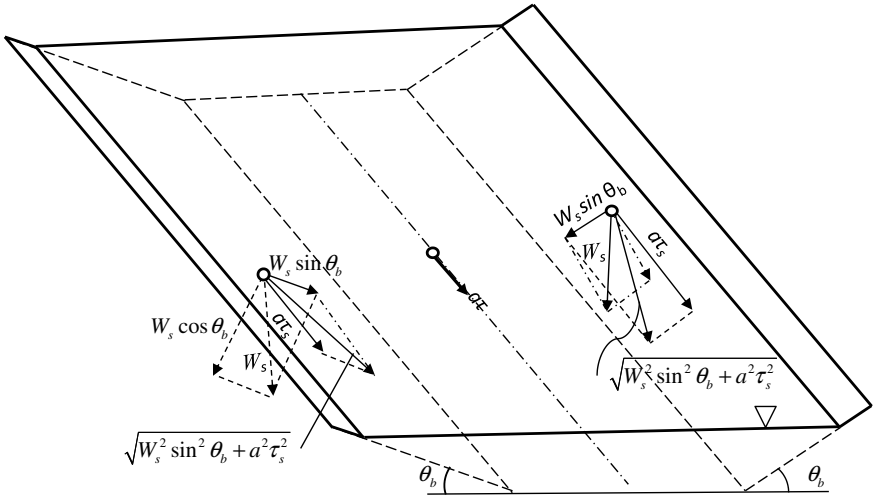

Figure 2.5 Analysis of forces on a sediment particle on side slope (modified from Chow 1959)

Considering a sediment particle resting on a side slope there are two forces causing the particle to roll. The first one is the tractive force $a\tau_s$, where a is the particle effective area and τ_s is the shear stress on the side slope. The second force is the gravity force component $W_s sin\theta_b$, where W_s is the submerged weight of the particle and θ_b is the inclination angle of the side slope. The tractive force causes the particle to roll in the downstream direction whereas the gravity component causes the particle to roll down the side slope. The resultant of these two forces is $\sqrt{W_s^2 \sin^2\theta_b + a^2\tau_s^2}$ and if it is large enough the particle will move. Thus, according to Chow (1959), the threshold condition of particle movement occurs when the driving force equals the resisting force of the particle, e.g.:

$$\sqrt{W_s^2 \sin^2\theta_b + a^2\tau_{c_s}^{\ 2}} = W_s \cos\theta_b \tan\phi \qquad 2.2$$

Where ϕ is the angle of repose and τ_{c_s} the critical shear stress on the side slope. By rearranging Eq. 2.2 τ_{c_s} can be rewritten as follows:

$$\tau_{c_s} = \frac{W_s}{a}\cos\theta_b \tan\phi\sqrt{1-\frac{\tan^2\theta_b}{\tan^2\phi}} \qquad 2.3$$

Similarly, when the motion of a particle is impending on a channel bed the force balance result in:

$$a\tau_c = W_s \tan\phi \qquad 2.4$$

or

$$\tau_c = \frac{W_s}{a}\tan\phi \qquad 2.5$$

To obtain the ratio between the critical shear stress on the side slope and the shear stress on the channel bed, the combination of Eq. 2.3 and 2.5 results in:

$$\frac{\tau_{c_s}}{\tau_c} = \cos\theta_b\sqrt{1-\frac{\tan^2\theta_b}{\tan^2\phi}} \qquad 2.6$$

Eq. 2.6 can be further simplified in:

$$\frac{\tau_{c_s}}{\tau_c} = \sqrt{1-\frac{\sin^2\theta_b}{\sin^2\phi}} \qquad 2.7$$

For example using Eq.2.7 for non-cohesive bank material with a bank angel θ_b = 31.9°, 20° and angle of repose ϕ = 34° the critical shear stress on the bank slope is $\tau_{c_s} = 0.33\tau_c$, $0.79\tau_c$ respectively. This shows that the critical shear stress on the bank is sensitive to the bank angle θ_b.

To estimate bank erosion on the basis of (e.g.) Shields diagram (see figure 2.7), the maximum shear stress along the bank has to be known. Figure 2.6 shows the boundary shear stress distribution in a trapezoidal channel for the special case of W = 4H (W = width of the channel bottom and H = water depth). The maximum boundary shear stress on the bank occurs in this case at 30% of the water depth and is estimated to $\tau_{\max} = 0.75\rho gHS$ (with: S=channle slope, ρ = the water density, g = the acceleration of gravity.).

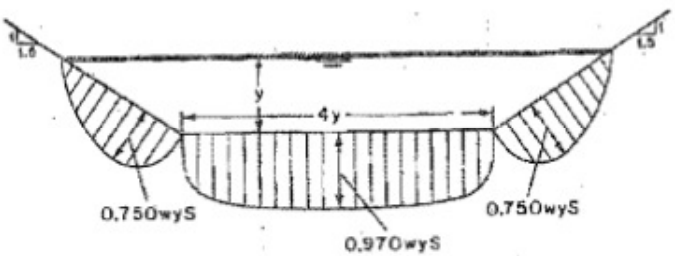

Figure 2.6 Distribution of boundary shear stresses in a trapezoidal channel section (modified from Chow 1959)

Shields (1936) investigated the initiation of motion for non-cohesive sediment particles. His approach is based, like the one of chow (1959), on balancing the driving force on a grain particle (expressed by $d^2\tau$ (with: d = characteristic grain diameter) and the stabilizing or resisting force (expressed by the weight under buoyancy). As Shields used sediment of very narrow sieve curves, the characteristic grain diameter can be replaced by the d_{50} of the sieve curves. To determine the initiation of, Shields (1936) proposed the diagram in Figure 2.7 in which the dimensionless shear stress $\tau_*(=\frac{\tau}{(\rho_s-\rho)gd})$ is plotted against the particle Reynolds number $\mathrm{Re}_*(=\frac{u_* d}{\nu}$; with: u_* = shear velocity and ν = Kinematic viscosity of water). In Figure 2.7 the experimental data of Shields (circles) and other authors are summarized. Through the data of Shields the Rouse-curve was plotted. That means, above the curve the grains are in motion and below the curve the grain rest in the river bed.

$$\tau_* = \frac{\tau}{(\rho_s - \rho) g d}$$

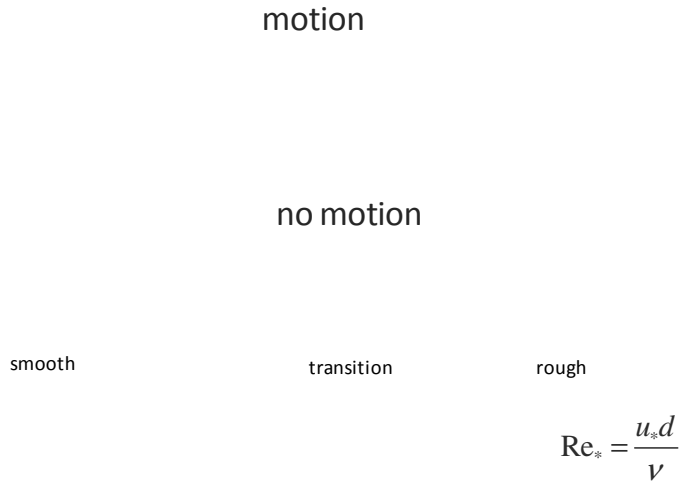

Figure 2.7 Shields diagram (modified by Dittrich, 1998)

2.2 Flow field in river bends

2.2.1 Flow pattern

Straight river channels are rare in nature and it is unusual to find straight reaches of length 10 times the channel width (Leopold & Wolman 1960). Instead, frequent bends with various sinuosities are more or less the rule in natural rivers. Flow in river bends is highly complex and three-dimensional. Yet, the applications of bend flow are important for engineers and environmentalist. Among the applications of bend flow are bank erosion, deposition, navigation and dissipation of pollutants and heat (de Vriend & Geldof 1983).

The flow in bends is characterized by secondary currents, flow separation, super-elevation due to curvature and energy losses (Han et al. 2011). The centrifugal force in the bend deflects the flow towards the outer bank in the curves. It is also responsible for creating a super-elevation of the water surface which produces a radial pressure gradient. Due to the local imbalance between the centrifugal force and the cross-stream pressure gradient, a cross-stream circulation is generated (Figure 2.8).

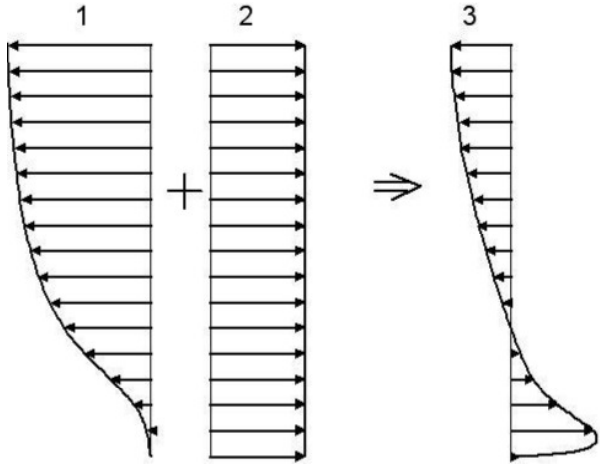

Figure 2.8 *Mechanism of a secondary current in a bend, (1) the centrifugal force, (2) the hydrostatic pressure gradient and (3) a combination of both forces (de Vriend et al. 2010)*

The combination of the secondary currents and the stream-wise velocity produces a spiral flow. If the curve is adequately long the spiral flow (helical flow) gradually reaches equilibrium state with an unchanged flow structure.

2.2.1.1 Velocity distribution

Flow in river bends has been investigated in laboratory flumes with different configurations and in the field in natural rivers. Among the laboratory studies with fixed rectangular flume walls and fixed flume bed are those of Rozovskii (1957), de Vriend (1979) and Shino & Muto (1989). Other studies employed natural bed topography in the flume such as Dietrich & Smith (1983), Odgaard & Bergs (1988), Blankaert & Graf (2001) and Blankaert et al (2013). In the studies of Dietrich et al. (1979) and de

Vriend & Geldof (1983) the flow in natural river bends was studied as well. In all of the aforementioned studies the velocity redistribution in bends has been addressed.

Investigations on the flow pattern in flumes with fixed flat bed and rectangular cross-sections and in natural developed beds with fixed walls show that the core of the higher stream-wise velocities zone moves towards the inner bank upon entering the bend followed by gradual shift of the core of the maximum velocity zone to the outer bank with a distance through the bend (Leopold & Wolman 1960; de Vreind and Geldof 1983; Chow 1959; Shukry 1950; Novak 2004; Blankaert et al 2013), see Figure 2.9.

This flow pattern can be explained by the effect of the secondary current which advects high momentum fluid toward the outer bank over the pool (see Figure 2.10) causing acceleration. Low momentum fluid close to the bottom is carried inward causing deceleration along the inside region (Dietrich et al. 1979). The velocity redistribution in sharp bends is governed by the topographic steering, curvature variation and secondary current (Ottervanger et al. 2012).

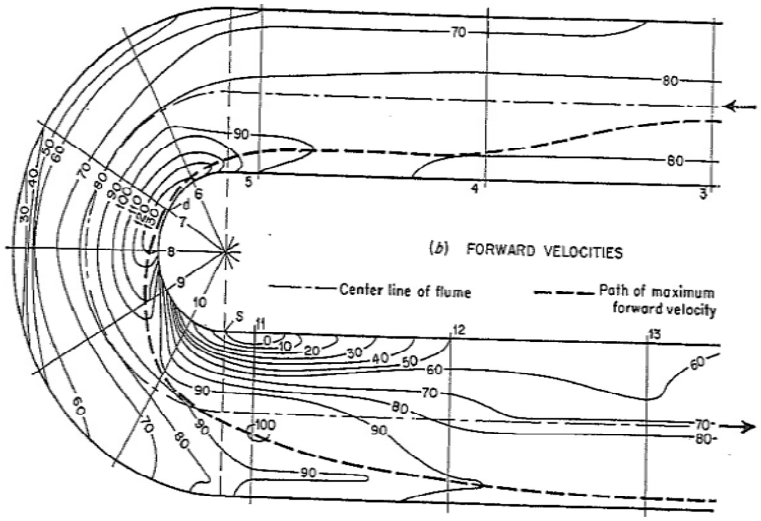

Figure 2.9 Iso-lines of the stream-wise velocities in a bend, velocities in cm/s (Shukry 1950)

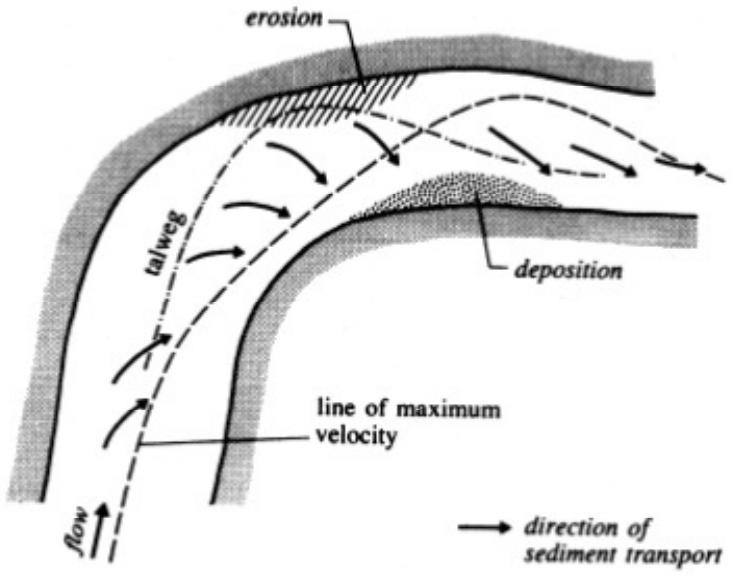

Figure 2.10 Flow in river bends (modified from Novak 2004)

In the studies of bend flow which employed natural bed topography (e.g. Dietrich et al. 1979; Blankaert et al 2013) the topographic steering effect forces the flow over the point bar toward the outer bank (Figrue 2.10). The flow pattern in studies of natural river bends confirm the laboratory investigations with fixed rectangular cross-sections and natural bed topography, in that, upon entering the bend the maximum velocity is towards the inner bank, then the maximum velocity is shifted gradually toward the outer bank as the flow goes into the bend (de Vriend & Geldof 1983).

Flume experiments conducted by Blankaert et al. (2013) on a double curved flume with mobile and immobile bed conditions showed that the flow pattern over the immobile bed show a similar pattern to the one over mobile bed and they were similar to what was found by e.g. Zeng et al. (2008) and Blanckaert (2010, 2011). This similarity indicates that the dominant hydrodynamic processes in sharp curved bends are similar in a relatively wide range of curvature ratio, bend length, roughness and Froude number conditions (Blankaert et al 2013).

A schematic picture of the 3D velocity field in a bend is shown in Figure 2.11. The cross-sectional view in Figure 2.11 shows the secondary flow cell. The flow in the upper part of the water depth is directed towards the bank increasing the attaching force of the flow. Close to the bed the flow is directed towards the inner bank which removes the sediment form the bank toe.

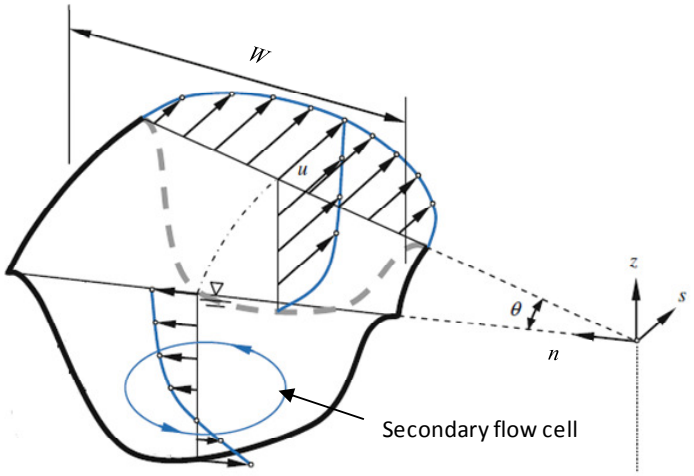

Figure 2.11 *Flow around a bend (with: θ = bend angle, s, n, z = coordinates in stream-wise, radial and vertical directions respectively, u velocity in s direction) (modified from Dey 2014)*

2.2.1.2 Secondary flow

Secondary flow (see Figure 2.11) refers to the transverse component of the flow in the cross-section plan perpendicular to the stream-wise flow (currents that occur in the plain normal to the axis of the primary flow, Bathurst et al. 1979). The combination of the secondary current and the primary flow generates the spiral flow which is the movement of the flow particles in a helical path in the general direction of the flow (Chow 1959). In curved channels the secondary flow is generated as a consequence of the local imbalance between the centrifugal force and the radial pressure gradient. The driving force in this case is the centrifugal force and the secondary flow is called 'Secondary currents of Prandtl's first kind'. Secondary currents of Prandtl's second kind are generated due to the non-homogeneity and anisotropy of turbulence in straight uniform open channel flow (Nezu & Nakagawa 1993).

The secondary current in bends determines the distribution of the velocity and shear stress by advecting the flow momentum (Blankaert & Graf 2004). The direction of the secondary flow depends on the bend geometry in plane. Looking in the flow direction, if the bend turns left the secondary flow cell is in a clock-wise direction. Counter-clock-wise secondary flow cell is encountered if the bend turns right. However, a relatively weak small outer cell close to the outer bank region that circulates in the opposite direction of the main secondary flow cell has been noted, in which turbulence was found to be important to generate it (Blankaert & de Vriend 2004), (see Figure 2.12).

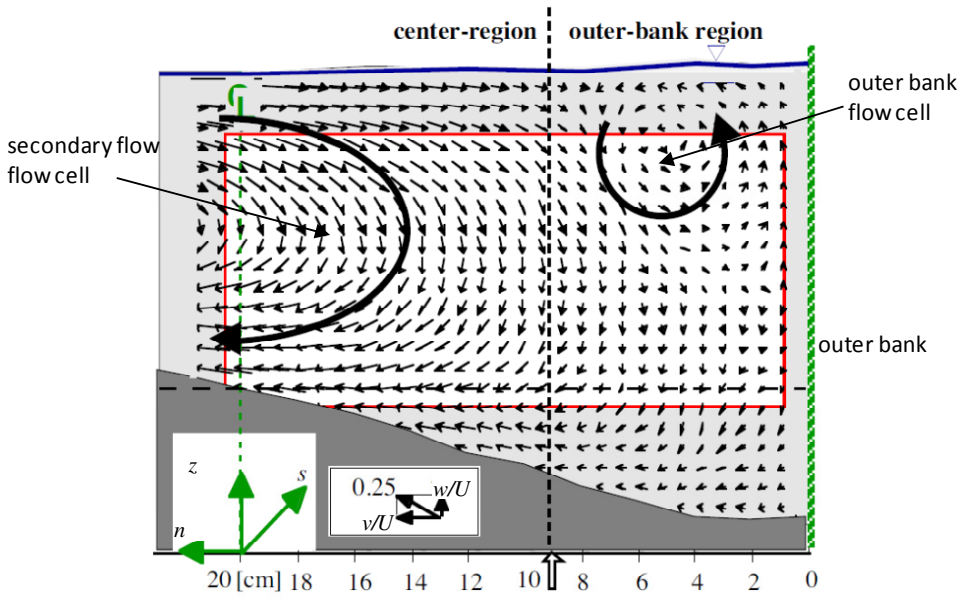

Figure 2.12 *Cross-stream motion (with u = the stream-wise velocity, v =transverse velocity, w= vertical velocity and U = average velocity (modified from Graf and Blankaert 2002)*

The outer bank flow cell was also observed in natural river bends by Bathurst et al. (1979) and their results together with Rozoviskii (1957) results suggested that the cell appears where the banks are steep. The outer bank cell was also noted in numerical studies with large eddy simulation (LES), (e.g. Kankg & Sotiropoulos 2015) who simulated rock vanes in a curve (Figure 2.13). However, the underlying mechanism of generating the outer bank cell is still poorly understood (Blankaert & de Vriend 2003).

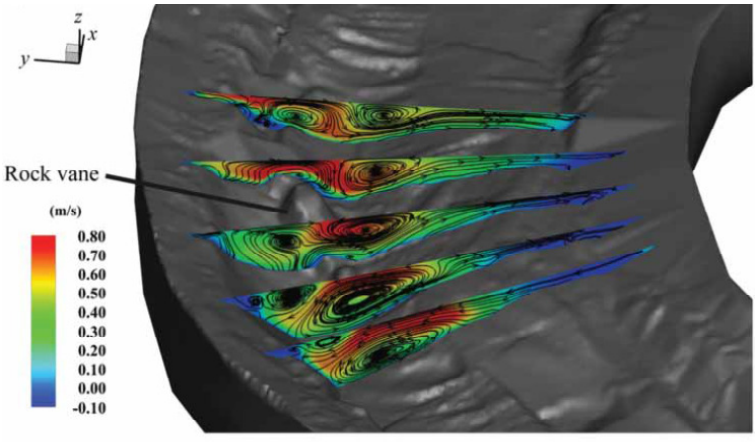

Figure 2.13 *Secondary flow cells (Kankg & Sotiropoulos 2015).*

Furthermore, in different laboratory studies on in-stream structures in bends, a large outer bank cell re-circulating in the opposite direction of the primary secondary cell was noted (Bhuiyan et al. 2010; Jamieson et al. 2013; Zaid & Koll 2016b).

2.2.1.3 Super-elevation

Flow in bends is associated with super-elevation which refers to the difference between the water level at the outer bank and the inner bank. Due to the curved path of the flow a super-elevation is generated which is correlative to the helical motion in the bend (Leopold & Wolman 1960).

The super-elevation can be calculated by balancing the centrifugal force and slope pressure force in the radial direction. Assuming that the transverse water surface slope is linear, all the filamental velocities in the bend equal to the mean velocity *U*, all the stream-lines have a radius of curvature R and neglecting the bed resistance the super-elevation $\triangle h$ can be approximated using Eq. 2.8 to Eq. 2.10 (Chow 1959).

$$\triangle h = \frac{U^2 W}{gR} \tag{2.8}$$

W and g are the channel width and the acceleration of gravity, respectively.

The accuracy of the super-elevation estimation can be improved using the free-vortex formula as:

$$\triangle h = \frac{C^2}{2gR_0^2 R_i^2}(R_0^2 - R_i^2) \tag{2.9}$$

Where C is the circulation constant in the free-vortex-motion, R_0 and R_i are outer and inner radius of the bend, respectively.

Using the following equation the constant C can be calculated iteratively if the discharge Q, R_0, R_i and the specific energy $E = H + \frac{U^2}{2g}$ are given.

$$Q = C\left(E - \frac{C^2}{2gR_0^2 R_i^2}\right)\ln\frac{R_0}{R_i} \tag{2.10}$$

2.2.2 Boundary shear stress distribution

Shear stress distribution in bends has been investigated in a laboratory curved flume by Dietrich et al. (1979) and Hooke (1975). The distribution of the maximum zone of the boundary shear stress in bends shows a comparable pattern to the maximum velocity zone. The maximum boundary shear stress zone is near the inner bank in the upstream part of the bend and crosses towards the outer bank as it reaches the central segment of the bend (see cross-section 14,18 in Figure 2.14).

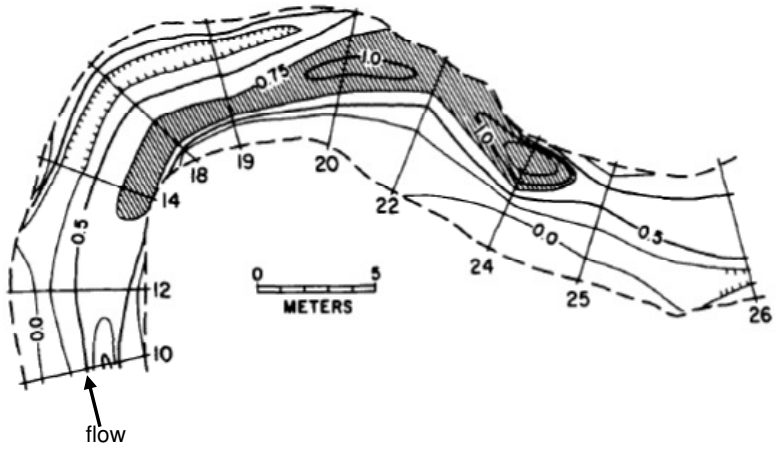

Figure 2.14 Iso-lines of boundary shear stresses (Dietrich et al. 1979)

The helical flow motion in bends transports the sediment from the outer bank towards the inner bank generating a transverse bed slope. Kikkawa et al. (1976) proposed a model to calculate the bed profile (Eqs. 2.11 to Eq. 2.13) and the maximum scour depth at river bends (Figure 2.15). According to Eqs. 2.11 to Eq. 2.13 the bed profile can be expressed by the relative water depth H/H_a:

$$\frac{H}{H_a} = \exp\left[\frac{1}{2}A\left(\frac{R^2}{R_a^2}-1\right)\right], \tag{2.11}$$

With: $$A = -\left(\frac{\frac{3}{4}\frac{\mu C_D}{1+\frac{C_L}{C_D}}}{}\right)^{1/2} \frac{U_{*_a}}{\left[\left(\frac{\rho_s}{\rho}-1\right)gd\right]^{1/2}} \frac{\lambda_0}{\kappa}\frac{U_a}{U_{*_a}} F(0) \text{ and} \tag{2.12}$$

$$F(0) = -4.167 + 2.64\frac{1}{\kappa}\frac{U_{*_a}}{U_a}. \tag{2.13}$$

Where H is the depth of the flow at a point, H_a, R_a, are the depth and the radius at which the mean depth and flow velocity occurs, R is the radius, U_a is the average cross-sectional velocity, U_{*a} is the average shear velocity in the radial direction, κ is the von Kármán constant, C_D and C_L are the drag and lift coefficients, μ is the friction coefficient and λ_0 is a sheltering coefficient. Furthermore Kikkawa et al. (1979) developed a diagram (Figure 2.15) for the relative maximum scour depth H_{max}/H_a as a function of the relative channel width W/R and the flow parameter A.

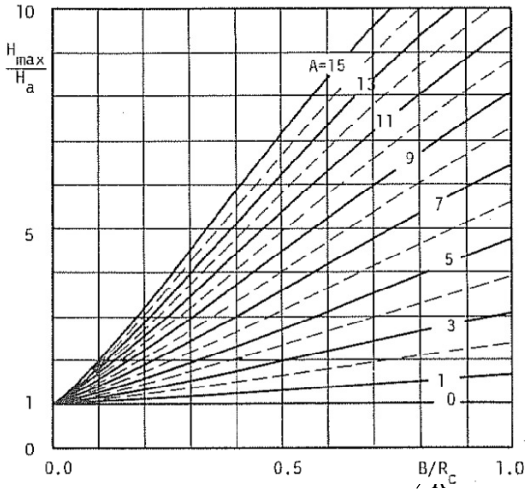

Figure 2.15 *Relative maximum scour depth H_{max}/H_a as a function of relative channel width to radius ratio W/R and the flow parameter A (modified from Kikkawa et al. 1976)*

2.2.3 Sediment sorting in river bends

Grain sizes in river bend tends to be finer in the point bar at the inner bank and courser in the pool at the outer bank due to the sorting process taking place in the bend. In addition, along the point bar at the upstream end courser grains occur whereas the downstream end is finer (Parker & Andrews 1985) see Figure 2.16. Flow in river bends is associated with erosion at the outer bank and deposition at the inner bank which over time develops a stable transverse slope. When a course sediment grain is put on the centreline it will move down the slope as it progresses through the curve, since the pull-down force due to gravity is larger than the pull-up force of the secondary flow. In contrast fine particles will move up towards the inner bank, since the pull-up force of the transverse flow is larger than the gravity force. The pull-down force due to the grain weight depends on the cube of the grain diameter whereas the inward drag force depends on the square of the grain diameter. Consequently the transverse flow in the slope of the bar provides a favourable situation for sediment sorting.

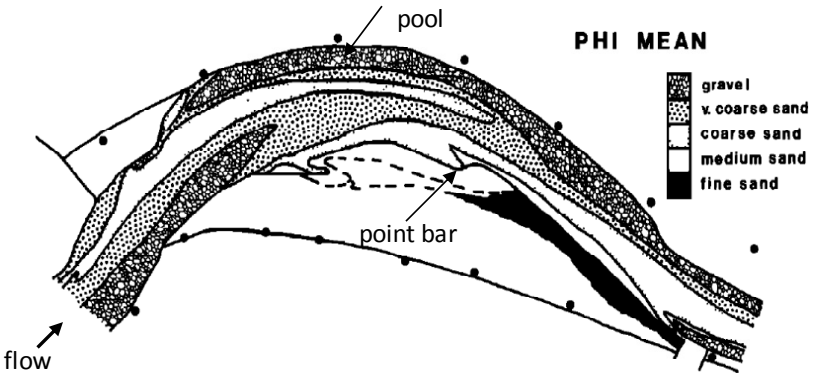

Figure 2.16 *Pattern of sediment sorting from gravel to fine sand in Esk River, flow from left to right (after Parker & Andrews 1985)*

2.3 Bank protection methods

2.3.1 Direct methods to increase bank resisting forces

There are a number of methods to protect the river bank against erosion. Yet, the environmental effectiveness and sustainability of each method can be different, depending on the degree to which it affects the river geomorphic process and, the amount of disturbance it may introduce to the riparian habitat and natural habitat (Bank Stabilization Design Guidelines, 2015). The river bank can be protected against erosion in two ways: increasing the resistance of the bank or decreasing the acting force of the flow. Accordingly, the river bank protection methods can be classified into two categories: methods that increase the resistance of the bank, referred to as direct methods, and methods which decrease the acting forces of the flow referred to as indirect methods. The direct methods address the erosion problem directly on the river bank itself. The bank resistance can be enhanced with fixed revetment methods such as riprap or walls (Table 2.1), or with flexible methods using natural material like vegetation or woods (Table 2. 2).

Table 2.1 Direct bank protection methods (after King 2015)

Protection Method	Photo	Comments
Flexible armor (concrete blocks)		• This is a quick way to stabilize a channel, providing that the capacity of the structure is not exceeded. • It is similar to full concrete lining but can be more ecologically acceptable due to the growth of vegetation between the blocks. • The ability to withstand high flow velocities is less than that of reinforced concrete. • This is an extremely expensive option.
Flexible armor (gabion mattress)		• This is similar to riprap but because smaller stones can be used, there is a greater potential for covering it with vegetation, making it ecologically more acceptable. • It is relatively easy to install. • The wire baskets can be subject to degradation by abrasion and are best protected with vegetation planted in the mattress. • Although the wire baskets are expensive, the stone can be significantly cheaper than stone required for rip-rap.
Riprap		• Properly designed riprap provides a durable protection to erosion. • Riprap can be ecologically acceptable when below the waterline where it is not visible. It can be improved by the planting of vegetation but this is not common. • Rip-rap is expensive and transport and handling costs are high. • Underwater, rip-rap construction can be easier than placing gabion mattresses.

Retaining wall (dry stacked block)		• Many systems are available and each has its own advantages and disadvantages. • Dry stacked block retaining walls can be constructed relatively quickly. • These walls can be vegetated, but the size of soil pockets within the wall often limits the types of vegetation that can be established there. • They are generally expensive, especially when transported over long distances. • The biological connectivity between the river and the bank via these structures is limited. • Users are cautioned to make sure that a progressive collapse due to local foundation failure or failure of the ends of the structure is guarded against.
etaining wall (rock filled gabion)		• Gabion walls are quick and easy to construct by semi-skilled labor providing that some basic rules are followed. • They can have the advantage of using locally available stone and in that way reduce costs. • The wire baskets can be subject to degradation by abrasion and are best protected with vegetation planted in the foundation mattress. • The biological connectivity between the river and the bank via these structures is limited.
Retaining wall (reinforced concrete)	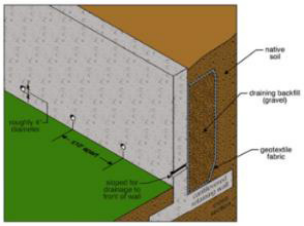	• Properly designed concrete retaining walls provide a durable protection to erosion. • They are particularly useful when a bank must be stabilized in a very confined area (such as an urban setting). • They are very expensive. • The biological connectivity between the river and the bank via these structures is extremely limited and apart from full canalization, they are the least desirable option from an ecological point of view.
Channelization		• From an ecological and cost point of view this is the last option solution for conveying water through an area within the least possible space.

Considering the ecological limitations of the traditional aforementioned bank protection methods, flexible direct bank protection techniques were proposed. In which wood or vegetation are used to increase the banks resistance to the flow. These alternative flexible techniques for bank protection provide more environmentally desirable solutions for bank protection. However, there are concerns about the ability of some of those measures to protect the bank during high floods (King 2015). Scottish Environment Protection Agency (2008) refers to these flexible techniques as green bank protection methods; because the environmental impacts are minimized by using a natural material for the protection works (WAT-SG-23 2008). These green bank protection methods are also known as bio-engineering methods (Hacker and Johannsen 2012). There are a wide range of green bank protection methods, and new

methods are being developed. For example, in the case of willow cutting the roots of the trees in the mature stage increase the stability of the bank in addition to an improvement in the habitat in the area of the bank toe. Therefore, these methods can represent a sinful complement to the indirect methods which will come later in this chapter. Detailed descriptions of some of these techniques are found in the book of Hacker and Johnassen 2012 as well as the Soil Bioengineering Construction Type Manual by Zeh (2007). Table 2.2 shows examples of green protection techniques. In practise, the bank can be protected with one or a combination of these techniques.

Table 2.2 Examples for green direct bank protection techniques

Brushwood bundles	 http://greenfix.co.uk/product/brushwood-faggots/
Woven stems	 Soil Bioengineering Construction Type Manual (Zeh 2007)
Brushwood mattresses	 Soil Bioengineering Construction Type Manual (Zeh 2007)
Willow cutting	 Soil Bioengineering Construction Type Manual (Zeh 2007)

2.3.2 Indirect methods to decrease flow acting forces

Bank erosion methods which work on reducing the acting flow forces on the bank address the bank erosion problem indirectly. The aim of these methods is to reduce the flow velocity along the outer bank by redirecting the flow away from the bank. They are therefore referred to as redirection methods. Beside the bank protection, the flow redirection methods increase the hydraulic and morphologic heterogeneity of the river and consequently increase the biodiversity (e.g. Shields et al. 1995). Unlike the direct methods where the structures are built along the banks, the structures of the indirect methods are built inside the stream close to or attached to the outer bank.

In-stream structures increase flow heterogeneity by introducing high and low velocity zones which results in heterogynous bed topography and bed material; accordingly increase habitat heterogeneity. Different studies found out that the installation of in-stream structures helped to increase biodiversity, e.g. Shields et al. (1995) found that in a restoration project with groynes the number of fish increased three times with increase of the median fish size of 50% and the number of species was increased by 25%. Due to the habitat improvement of the redirection in-stream structures, they have become increasingly popular (Scurlock et al. 2015; Shields et al. 2000).

Various types of in-stream structures like stream barbs, bendway weirs, vanes and groynes are available. However, the definition of some of these types, in different reports and publications, might incorporate confusion or inconsistency. Some structures may be referred to as one type in different publications whereas the available design guidelines of each one are different. Some relatively close types of the in-stream structures to the shallow groynes are discussed hereafter, and main characteristics are presented in definition sketches.

2.3.2.1 Stream barbs

Stream barbs are a relatively new form of stream protection structures (Matsuura & Townsend 2004). The stream barb concept was first introduced in the Soil Conservation Service, now called the Natural Resource Conservation Service, NRCS, by Donald Reichmuth (1993) who has applied these rock structures in many streams in the western United States (HEC-23). Barbs are low profile rock structures typically anchored in series, on the outside bank and extend in the upstream direction of the flow out from the bank into the stream (see Figure 2.17). Barbs should always be submerged under the bank full discharge condition (USDA 2013). The structures are used to redirect the flow from the outer bank to the centre of the stream providing bank protection and moving the stream thalweg towards the centre of the channel. In addition, they are used to improve fisheries habitat. Barbs also promote bank vegetation (Piper et al. 2001). Compared to riprap, concrete paving and gabion walls, barbs are more environmentally sustainable measures for stream stability (Jamieson et al.

2013). Considering the layout, barbs are similar in appearance to bendway weirs (Matsuura & Townsend 2004; Derrick et al. 1994).

According to Jamieson et al. (2013) barbs can be considered as a submerged variant of groyne and they are similar to spur dikes and bend way weirs. In the Integrated Stream Bank Protection Guidelines (2003), barbs, vanes or bendway weirs, referred to as one type of the in-stream structures. In fact, this highlights the confusion and the inconsistency associated with the definition of each type of in-stream structures.

The main difference between the stream barbs and shallow groynes is that, the barbs have a sloped crest and are submerged only during the bank-full discharge condition, whereas the shallow groynes have flat crest and are always submerged even during low flow conditions.

Stream barbs have a trapezoidal section, and projected from the outer bank in the upstream direction into the stream with an angle of 20-45° (Matsuura & Townsend 2004) or 20-30° according to USDA (2013). The length of the barbs is up to 1/4 of the channel width (Matsuura & Townsend 2004) or 1/3 of the channel width (USDA 2013).

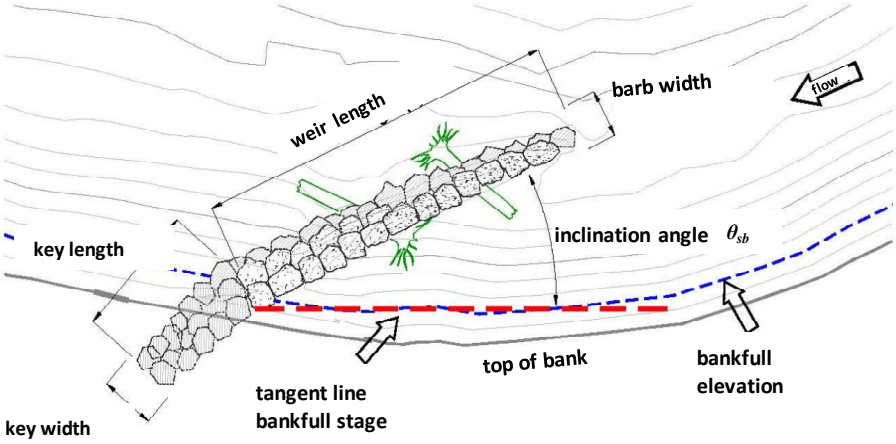

Figure 2.17 Stream barb (modified from USDA 2005)

2.3.2.2 Bendway weirs

Bendway weirs are submerged linear rock structures (see Figure 2.18), projecting at an angle from the outside bank of the river bend into the stream against the flow direction (Derrick 1999). The concept of the bendway weirs was developed by the US Army Corps of Engineer to improve the navigation in the Mississippi River (Derrick et al. 1994). Compared to other types of in-stream structures, Julian and Duncan (2003) considered bend way weirs as different from spur dikes, jetties or groynes. However, bendway weirs were considered as spur dikes, groynes or jetties by other authors (eg. Kinzli & Thornton 2009; Thornton et al. 2005). Furthermore, bend way weirs were referred to as stream barbs, bank barbs and reversed sills in HEC-23. Bend

way weirs are similar in appearance to spur dikes but have significant functional difference from spur dikes as they are always submerged unlike spur dikes which are visible above the flow (HEC-23). Referring to the aforementioned definitions, the confusion between bendway weirs and stream barbs and other in-stream structures is obvious. It can nevertheless be noted that in addition to bank stabilization, bendway weirs have been extensively used for improving navigation, whereas stream barbs were often used for bank protection and fisheries habitat improvement.

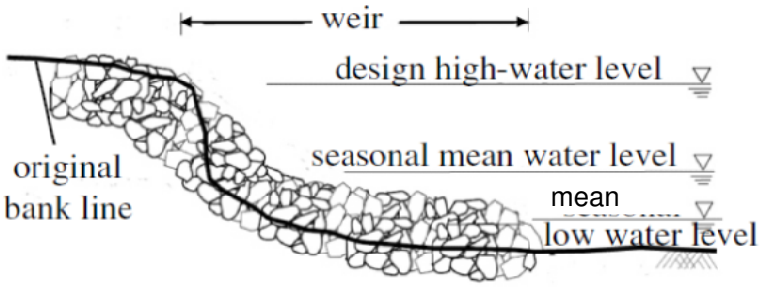

Figure 2.18 Bendway weir (Lagasse et al. 2009)

2.3.2.3 Rock vanes

Rock vanes are a single arm structure extending from the bank with an angle into the stream (see Figure 2.19) with a gradual slope from the bank to the river bed so that the tip of the vanes is submerged during low flow conditions (Johnson et al. 2001).

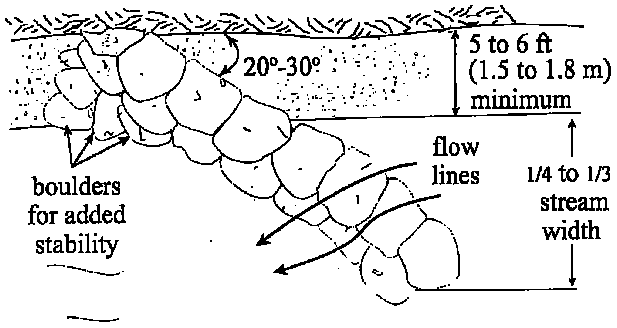

Figure 2.19 Rock vane (Johnon et al. 2001)

2.3.2.4 Bank-attached vanes

Bank-attached vanes are used for habitat improvements as well as erosion control. The structures have upstream oriented inclination angle of 25°-30° and inclined crest from the bank-full level down to the river bed (see Figure 2.20). The projected length of bank-attached vanes is typically one third of the channel width (Rosgen 1996).

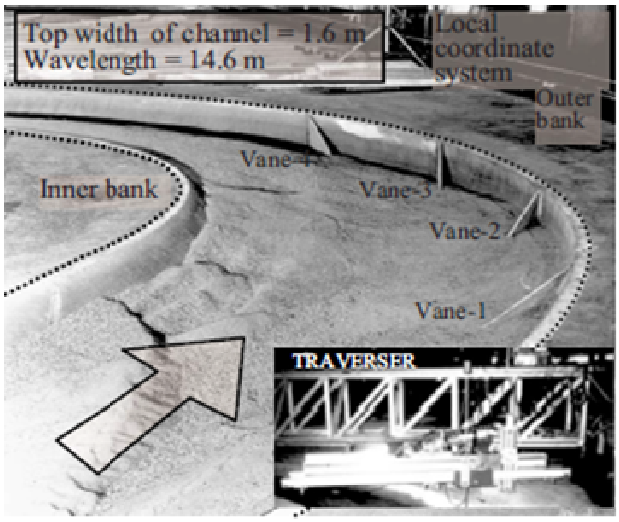

Figure 2.20 Bank-attached vanes

2.3.2.5 Submerged vanes

Submerged vanes are small flow training structures (foils) installed at an angle of attack of 15°-25° with the flow. Their initial height is 0.2 - 0.4 of the flow depth. The structures generate secondary flow circulation and modify the near bed flow pattern (Odgaard & Wang 1991a) (see Figure 2.21). Due to their size and layout, the submerged vanes are an unobtrusive and cost-effective bank erosion counter measure which can be used in a wide range of water management problems (Odgaard 2009). However, the variation of the angle of attack associated with the variation of the stage level is one of the limitations of the submerged vanes, because the vanes are constructed at a fixed angle.

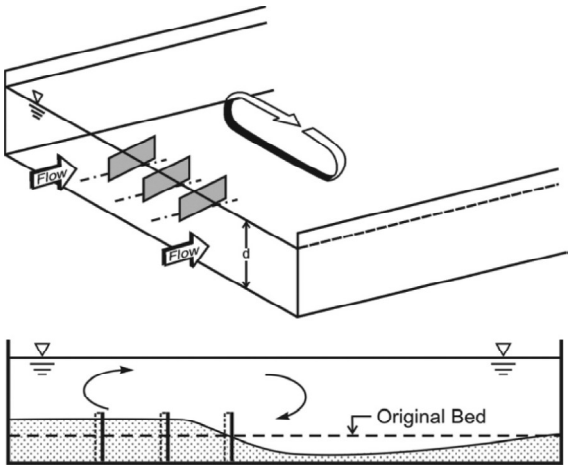

Figure 2.21 Submerged vanes (Odgaard 2009)

2.3.2.6 Groynes

Groynes, also called spur dikes, are large roughness elements that project into the channel from the bank and extend above the high-flow, water-surface elevation.

Groynes and stream barbs are often mixed. The primary difference between groynes and barbs is that groynes are higher-profile structures that tend to deepen the thalweg and narrow the stream, while barbs have less effect on the cross-sectional shape of the stream (Integrated Streambank Protection Guidelines, 2003).

According to Przedwojski et al. (1995) groynes can be classified as follow:

1- To the method and material of construction:
   - Permeable fabricated from piles, bamboo and timber.
   - Impermeable (solid) constructed from rock, gravel, gabion …etc.

2- To submergence state:
   - Submerged
   - Non-submerged

3- To the action to the stream flow:
   - Attracting, attract the flow to them and do not repel the flow to the opposite bank.
   - Deflecting, direct the flow without repelling it.
   - Repelling, pointing upstream. They serve to change the flow away from them.

4- To the layout:
   They can be straight, T-head, L-head, hockey stick, invert hockey stick, straight groynes with pier head, wings or tail groynes.

Groynes are used also in coastal engineering to protect shores and enhance sedimentation.

Figure 2.22 Groynes on River Elbe (Dittrich et al. 2010)

2.3.3 Summary on the studies of In-stream structures

2.3.3.1 Experiments and results

Associated with in-stream structures several experimental studies on the effect of in-stream structures on the bed topography have been carried out. Considered straight channels, Johnson et al. (2001) investigated the effect of a rock vane on protecting bridge abutment and found that the best setting of the rock vane includes: (i) inclination angles of 25-30° against the flow direction, (ii) distance from the abutment to the tip of the vane should be two times the channel width (ii) a number of two vanes is adequate to protect the abutment. In the same context, e.g. Fox et al. (2005), Fang et al. (2006) and Möws & Koll (2014) considered bed topographical changes associated with in-stream structures considering the scour around the head of the structure which was found to be attached to the structures head (e.g. Fang et al. 2006; Kuhnle et al. 2002).

In fact, the scour depth at the structure head endangers the stability of the structure and increases the construction costs by increasing the foundation depth. Thus, the shape of groyne head plays an important role in reducing the scour around the head. E.g. Fang et al. (2006) found that using sloped head face significantly reduces the scour around the head. Furthermore, Kadota et al. (2008) found that the permeability of the groyne significantly reduces the head scour depth.

Recently, more studies on in-stream structures addressed the application of the structures in river bends with the focus on the effect on the river morphology (e.g., Matsuura & Townsend 2004; Bejestan et al. 2010; Hemmati et al. 2012). In the aforementioned studies, no velocity measurements were done; instead, the bed topography was measured only. The topographic measurements allow to compare the initial bed topography and the resulting topography after installing the structures. Therefore the effectiveness of the structures configuration was evaluated based on the reduction on the maximum scour at the outer bank and how far it can be relocated away from the bank towards the centre of the channel. Matsuura & Townsend (2004) investigated stream barbs in a curved flume with bend angles of 90° and 135° and with mobile bed and fixed walls. They investigated groups of barbs with varying barb angles and locations to obtain recommendations on the optimum setup of the stream barb which will follow in Chap. 2.3.3.2. Bejestan et al. (2010) investigated the bendway weirs in a curved flume with a bend angle of 90°, and they found that the bend way weirs shifted the thalweg to the nose of the weirs. They found also that a spacing of three times the weir length result in the least scour at the weirs. Moreover, Hemmati et al. (2012) addressed the effect of bendway weirs angle and length on the scour at the weirs and the deposition at the point bar around the inner bank by detailed bed topographic measurement with laser distance meter.

Despite the fact that the studies mentioned above address the effect of the structures on the morphology, it is nevertheless important to combine these morphological effects with the effect on the flow field. Therefore, recent studies on in-stream structures in river bends investigated both, the channel morphology as well as the flow field (e.g. Bhuiyan et al. 2010; Jamieson et al. 2013a,b; Cunningham & Lyn 2016). 3D flow field measurements and bed topography measurements in a meander laboratory flume were carried out by Bhuiyan et al. (2010) to investigate the bank attached vanes. They found that the bank-attached vanes which have sloping crest from the bank-full level to the bed generate stronger counter-rotating secondary currents which oppose the main spiral flow responsible for bank erosion in bend compared to the low-level vanes. Moreover, they suggested some formula for the design of bank attached vanes (Chap. 2.3.3.2). Jamieson et al. (2013a,b) investigated the stream barbs in a laboratory flume with erodible bed and banks. To the knowledge of the author, it were only Jamieson et al. (2013a,b) and Cunningham & Lyn (2016) who carried out the measurements with erodible bed and bank conditions and in this respect, the two studies were comparable although different structures were investigated; bendway weirs in the case of Cunningham & Lyn (2016). Jamieson et al. (2013a,b) studied the effect of stream barbs on the flow and sediment dynamics in a curved flume with bend angle of 135° and with erodible bed and banks, varying the number of barbs (1, 2 and 4), barbs' angle (30°,35°), height, length and locations of the barbs. Extensive 3D velocity and bed topography measurements were carried out and the turbulence characteristics were addressed, however, a number of six test runs only were performed. Jamieson et al. (2013a,b) found that the setup with two barbs provides better protection for the outer bank than the setup with four barbs, and it was found that even with the barbs the outer bank can be susceptible to more erosion, particularly between the barbs, than without barbs depending on the barbs' configuration (the reason is if the barbs generate excessive secondary velocities that opposes the primary secondary flow). Similar excessive erosion of the outer bank between the structures was reported recently by Cunningham & Lyn (2016), who investigated the effectiveness of bendway weirs designed according to the guidelines of US Federal Highway Administration (HEC-23) in a curved flume with a bend angle of 90° and with erodible bed and bank. Although the bendway weirs showed an obvious deflective effect of the flow, the bendway weirs which were designed according to HEC-23 where not effective as the outer bank was still susceptible to substantial erosion for the range of studied conditions.

To the author, the setups with erodible bed and banks in the studies of Jamieson et al. (2013a,b) and Cunningham & Lyn (2016) are unique. However, in both studies a trapezoidal section with narrow bottom width and gently sloped banks was used (Figure 2.23a,b). This setup led to the implication that the structures were installed completely on the bank and no part was installed on the bed which is not a similar setup to the installation of the structures in the field in natural rivers (see e.g. Figure

2.23c). The plunging flow behind the structure goes directly onto the bank causing excessive erosion. This might be one of the reasons for the excessive outer bank scour with the presence of the structures reported in Jamieson et al. (2013a,b) and Cunningham & Lyn (2016). As the lengths of the in-stream structures in many guidelines are proportional to the channel width, the use of a wide flume would allow having longer barbs or bendway weirs which can extend into the river bed replicating more realistic configurations of the structures as they will be built in the field (see Figure 2.23c).

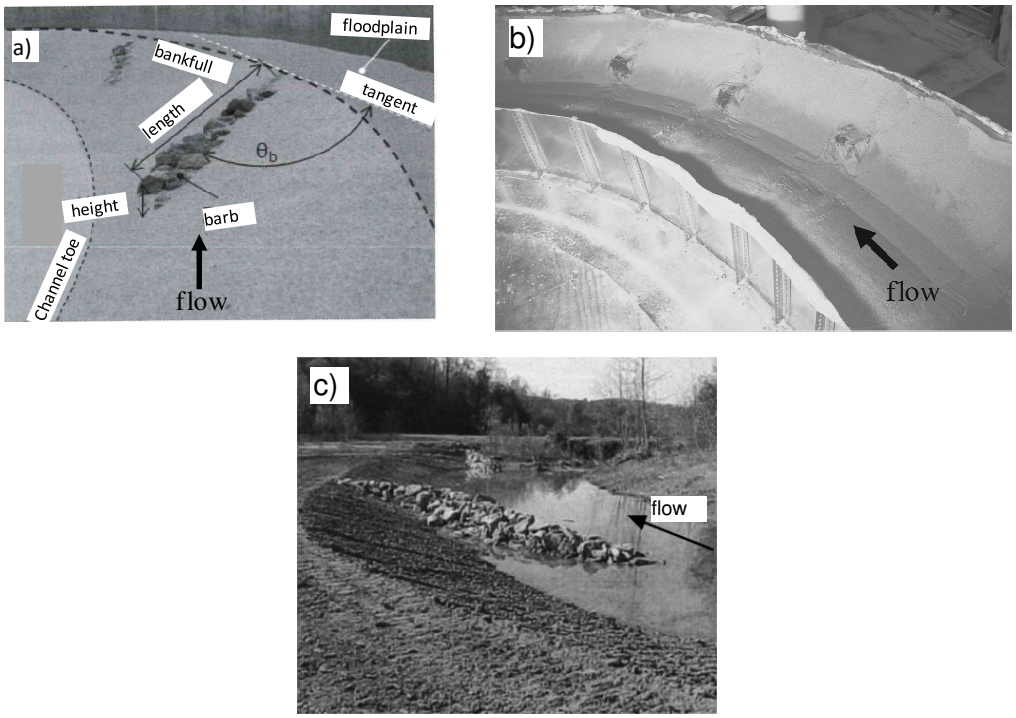

Figure 2.23 Photos of experimental setups: (a) flume with stream barbs of Jamieson et al. 2013a,b, (b) flume with bendway weirs of Cunningham & Lyn 2016, and (c) photo of a natural river with stream barbs by Bressan & Papanicolaou (2012).

All the above mentioned studies on in-stream structures in which mobile bed material was used were carried out under clear water conditions, i.e. without grain feeding except the studies of Johnson et al (2001), Bhuiyan et al. (2010) and Hemmati et al. (2012) carried out tests in a sediment re-circulating flume.

Scurlock et al. (2015) carried out extensive laboratory experiments on spur dikes and bendway weirs on a scaled physical model of Rio Grande River with the aim of developing a mathematical framework of induced transverse in-stream structure hydraulics as a function of geometric parameters of the bend and the structures. One result of their experiments consists in the prediction of the maximum and the average velocity ratios in the inner, centre and outer region of the curve. Although the framework of Scurlock et al. (2015) do not give the optimum setup of the structure, the ve-

locities that the framework predict can be used as a criteria to find the optimum setup of the structures.

In general the investigations of the in-stream structures incorporate a large number of parameters. To describe the channel geometry parameters like width, depth and radius are needed. The in-stream structure parameters include length, width, height, spacing and inclination angle of the structures. Considering the number of parameters involved in the studies of in-stream structures, many tests are required to elaborate on the effect of each parameter. However, in the studies with mobile bed condition, only a limited number of tests were performed. This allowed to draw out some broad recommendations on the structures configuration. Yet, a systematic investigation addressing the hydraulic effect of the single structure parameters is required. Doing so, the experiments with fixed boundaries provide the possibility to run much more tests than mobile bed experiments considering the duration of the experiments. To overcome the need of performing a large number of physical model tests, Khosronejad et al. (2016) proposed a simulation-based optimization of bendway weirs using St. Anthony Falls Laboratory Virtual StreamLab (VSL3D). Two virtual stream bends were setup and numerous simulations were done changing systematically the parameters of the bend way weirs. The projected length of the structures was $W/4$ and the maximum height of the structures was $H/2$. According to the simulations it resulted that the optimum setting of the bendway weirs involves an inclination angle of 50° and a number of three bendway weirs starting from the bend apex to the bend exit (Figure 2.24). The criteria for the optimum setting of bendway weirs were the maximum protection of the outer bank (the least bank erosion) and the least risk of erosion at the inner bank.

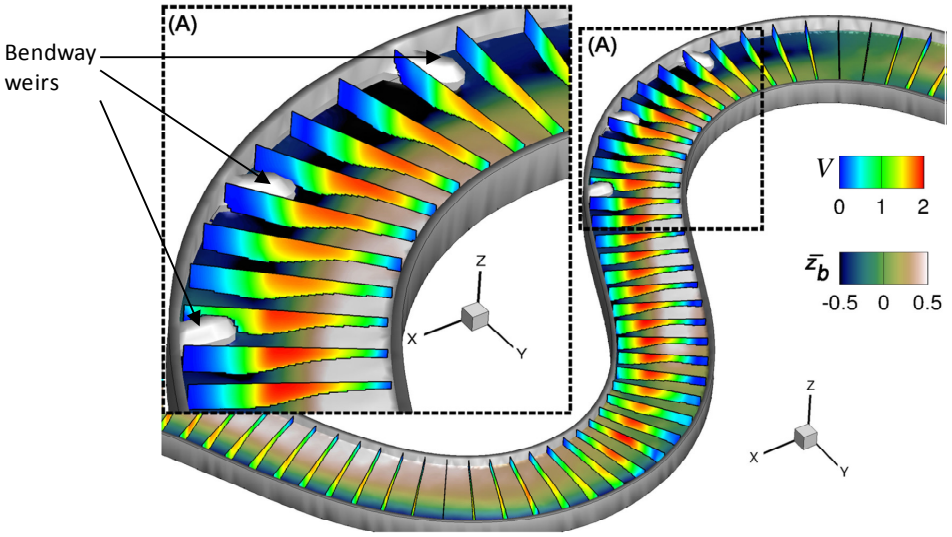

Figure 2.24 *Optimum arrangement of bendway weirs, $\bar{z}_b$ is the bed level, V is velocity magnitude, (Khosronejad et al. 2016)*

2.3.3.2 Design guidelines of stream barbs, bendway weirs and bank-attached vanes

In the following, design guidelines of stream barbs, bendway weirs and bank-attached vanes, which are the close types of in-stream structures to the shallow groynes which are the content of this study, are summarized below. The bases for these design guidelines were physical scale models (Derrick et al. 1994; Scurlock et al. 2015), experiences with the implementation the structures on the field, engineering judgments (Copeland 1983; Radspinner et al. 2010) and several laboratory and numerical studies on different structures types (see Chap.3.3.3.1). Additionally, some studies attempted to group a number of physical model results together with numerical model results to draw design guidelines for some in-stream structures (e.g Julien & Duncan 2003), or to find a mathematical framework to predict the mean velocity ratio at the outer bank for different types of in-stream structures (Scurlock et al. (2015).

Stream Barbs

According to the USDA Kansas Engineering Technical Note No KS-1(Revision1 in January 2013) the first barb should be placed in the downstream quarter of the meander bend or near the downstream end of erosion and stream bank instability. In contrast Matsuura &Townsend (2004) recommended to locate the first barb just upstream of the first scour on the outside bank. Jamieson et al. (2013) suggested that the first barb should be placed in the vicinity of the expected maximum scour and the barb should not extend too far upstream the bend exit because this will compromise the overall channel stability.

The following recommendations are given by the USDA Kansas Engineering Technical Note No KS-1(Revision1 2013) for the design of stream barbs (see Figure 2.24):

- The length of the barb should not exceed $1/3$ of the width of the river at the bank-full discharge.
- The key length which is the part of the barb that needs to penetrate inside the bank should be between $1/3$ - $1/4$ of the barb length.
- The optimum angle θ_{sb} of stream barbs is between 20°-30° but should not exceed 25° if the tortuosity (R/W) is less than 3.

Matsuura &Townsend (2004) found that the optimum angle θ_{sb} of stream barbs is 30°

The height of the barbs (h_b) should be $0.33H \leq h_b \leq 0.5H$, where H is the channel forming flow depth (Matsuura &Townsend 2004), and the spacing can be defined on the bases of geometrical considerations as shown in Figure 2.25. In Figure 2.25 the location of the second barb in a barb field is defined by extending a line at the centre

of the barb and parallel to the tangent at the barb toe in the downstream direction until it intersect with the curve.

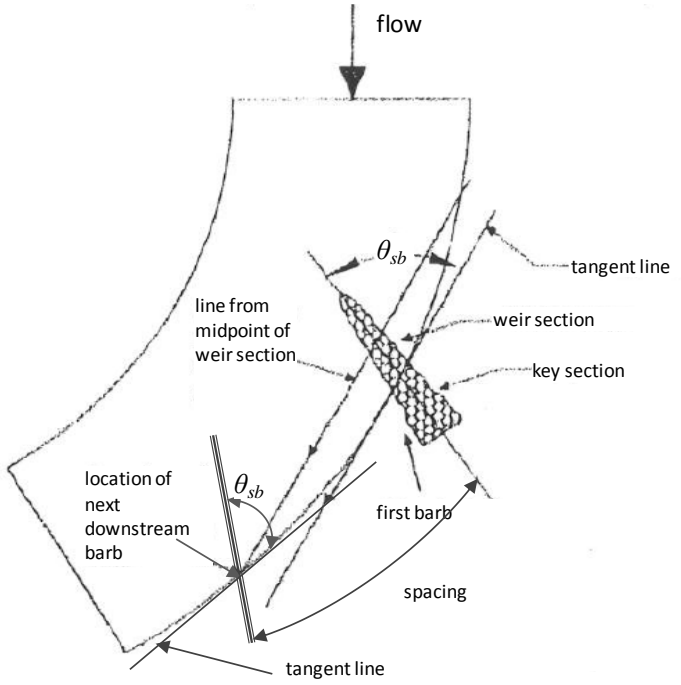

Figure 2.25 Spacing methodology (modified from Matsuura and Townsend 2004)

According to USDA 2013 the first barb should be located near the downstream end of the bend where the bank erosion occurs toward the bend exit. Then the spacing of barbs is defined in the upstream direction by locating the second barb at the intersection of a line at the barb tip extending parallel to the tangent at the barb toe with the curve (see Figrue2.26).

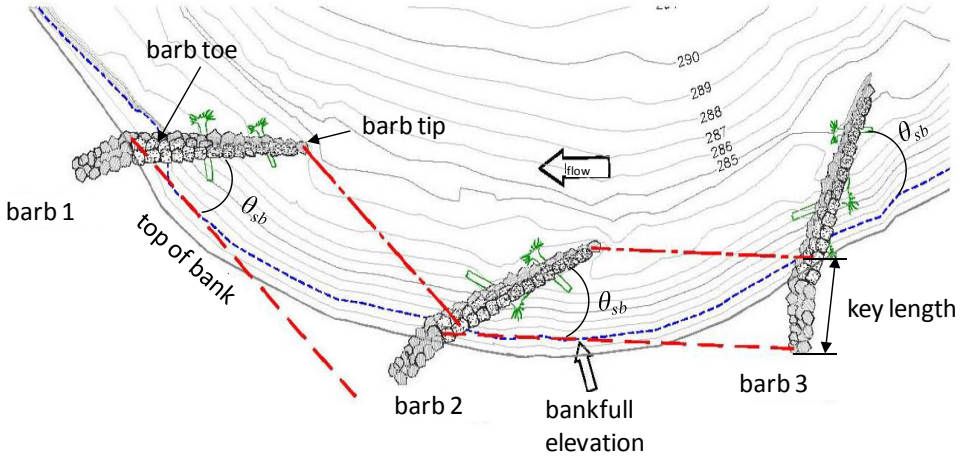

Figure 2.26 Spacing methodology (modified from USDA Kansas Engineering Technical Note No KS-1(Revision1) January 2013)

Bendway weirs

The height of the bendway weirs should be 30%-50 % of the mean annual high water level, below the normal seasonal mean water level and higher than or equal the mean low water level (Federal Highway Administration (FHWA), HEC-23). According to Julien & Duncan (2003) the height of the weir should be dependent on the ratio of the depth clearance above the weir (distance between the weir crest level and the water level) and the total depth of the channel. As the ratio decreases, the influence of the weir on the flow increases.

The inclination angle of the weirs should be 50°-85° in the upstream direction according to HEC-23. Julien & Duncan (2003) and Derrick (1994) recommended that the angle should be 60° and found that an angle less than or greater than 60° reduces the efficiency of the bendway weirs. However, the US Army Corps of Engineers recommended a different range of inclination angle between 20° and 30°.

The maximum length of the bend way weirs is recommended to be 1/3 of the channel width and should be shorter than 1/4 of the channel width for bank protection (HEC-23).

Julien & Duncan (2003) suggested that the length is dependent on the channel geometry and should be defined case by case.

According to HEC-23 and following LaGrone (1995), the spacings S_p between the bendway weirs depends on the length of the weir L , the width of the channel W and the radius of curvature R and are defined as follows:

$$s_p = 1,5L\left[\frac{R}{W}\right]^{0.8}\left[\frac{L}{W}\right]^{0.3}, \tag{2.14}$$

with the maximum spacing $S_{p\text{-max}}$ as:

$$S_{p\_\max} = R\left[1-\left[1-\frac{L}{R}\right]^2\right]^{0.5}. \tag{2.15}$$

Julien & Duncan (2003) recommended that the spacing between the bendway weirs should be 2 to 3 times the length of the bendway weir.

To prevent flanking by the flow the bendway weirs need to be keyed to the bank and the length of the key should be half of the length of the short weir and one fifth of the length of the long weir (HEC-23).

The top width of the weir should be 1 - 4 m but not less than (2 to 3) times the maximum size of the construction material (HEC-23). The side slope is given by the e angle of repose of the riprap rock (Julien & Duncan 2003).

It is to be noted that Cunningham & Lyn (2016) investigated a field of bend way weirs constructed in accordance with (HEC-23) and found that the effect of the bendway weirs in deflecting the flow away from the outer bank was obvious. However, the bank was susceptible to a significant scour even with the presence of the bendway weirs.

The width of the barb should be 1-3 times the maximum D_{100} of the construction material and the slope of the barb should be between 5%– 8%.

Recently Scurlock et al. (2015) developed an empirical equation for the prediction of the maximum velocity ratio MVR_i and the average velocity ratio AVR_i at the inner, centre and outer region of the bend. The maximum velocity ratio is the ratio of maximum velocity with installed in-stream structures to the maximum velocity at the baseline condition without structures. The velocity ratio predicted by Eq. 2.16 can be taken as a criterion for the evaluation of the optimum setup of the structures, i.e. the structures parameters in Eq. 2.16 should be changed to obtain the maximum velocity ratio which is required to protect the bank.

$$MVR_i, AVR_i = a_1 (A^*)^{a_2} \left(\frac{L_{ARC}}{T_W}\right)^{a_3} \left(\frac{R}{T_W}\right)^{a_4} \left(\frac{L_W - PROJ}{T_W}\right)^{a_5} \left(\frac{D_B}{D_B - \triangle_Z}\right)^{a_6} \left(\frac{2\theta_s}{\pi}\right)^{a_7} \quad (2.16)$$

where:

a_1 to a_7 = regression coefficients

A^* = area contraction ratio

L_{ARC} = arc length between weirs along design waterline (L)

$L_W - PROJ$ = projected length of weir measured from the baseline water surface along the horizontal plane to a cross-section perpendicular to the flow (L)

T_W = channel top width (L)

R = radius of curvature for channel bend (L)

= baseline flow depth (L)

= difference between structure crest elevation and water surface level.

= planmetric angle of structure crest with bank-line tangent.

Bank-attached vanes

The spacing S_p between bank-attached vanes can be calculated according to Eq. 2.17 of Bhuiyan et al. (2010):

$$S_p = r_0 \theta_{sv} \quad , \tag{2.17}$$

$$\text{with: } \theta_{sv} = \tan^{-1}\left(\frac{L_v \cos\theta_v}{r_0 - L_v \sin\theta_v}\right), \tag{2.18}$$

Where:

r_o = outer bank radius of the bend (see figure 2.23)

θ_v = angle of vane with upstream tangent

L_v = length of vane

θ_{sv} = angle between vane tip, toe and the curve centre

The projected length of the vane y_t is:

$$y_t = r_0 - L_v \cos\theta_v / \sin\theta_s \, . \tag{2.19}$$

The minimum depth of penetration D_e of the vane (see Figure 2.27) at the tip according to the cross-sectional profile is given as (Bridges 1977):

$$D_e = H_v - D_m \left(\cos\theta_v\right)^{K_{br}\tan\phi}, \tag{2.20}$$

where D_m is the maximum scour depth at the bend and H_v is the design height of the vane.

The number of vanes is given by the ratio θ_c / θ_{sv} ,where θ_c is the bend angle.

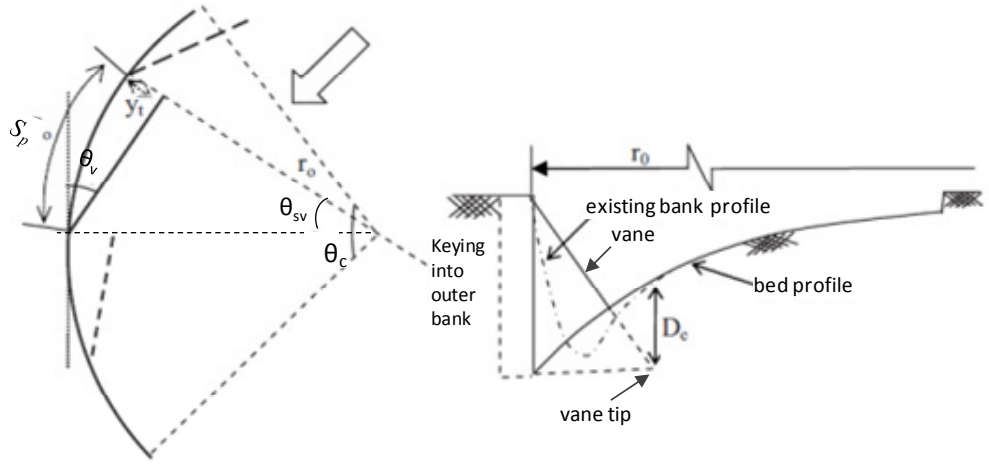

Figure 2.27 Design parameters of bank attached vanes (modified from Bhuiyan et al. 2010)

2.3.4 Shallow groynes as alternative indirect method

Shallow groynes are a new variant of river training structures, under the development of the Leichtweiß-Institut für Wasserbau (LWI). Shallow groynes are submerged type of groynes. They are so shallow, that they are submerged even during low-flow conditions. By being always submerged, shallow groynes have the least obstruction to the activity on the river, aesthetic view and the least effect on the flood level, if any. Shallow groynes produce secondary currents which interact with the primary flow affecting both, the velocity distribution and sediment transport; consequently provide bank protection (Sindelar & Mende 2009).

The investigations with shallow groynes started in a straight, tiltable flume in the laboratory of the LWI (e.g. Mende & Koll 2008, Mende 2014 and Möws & Koll 2014). In the first step, experiments on groups of shallow groynes were carried out in a straight reach of the flume with fixed bed material and glass walls by Mende (2014). The existing flume was 20 m long and had a width of 0.90 m and a depth of 0.60 m. The walls were made of glass and the bottom consisted of fixed gravel with diameters d = 4 to 12 mm. The groynes were built of water resistant wood with flat crest and rounded head (see Figure 2.28). The groyne width w_g was 6 cm and the groyne height h_g = 2 cm. The objective of the investigations of Mende (2014) was the development of design guidelines for shallow groynes for bank protection in straight as well as curved river reaches. Therefore the groyne spacing S_p (measured from the groyne axis), the groyne angle θ_g and the projected length l_p were varied. For these parameters the following values were considered: S_p = 30cm, 60cm and 90cm, for θ_g =30°, 60° and 90°, and for l_p =10cm, 20cm and 30cm. The groynes were installed on one side of the flume in a reach of three meters. Furthermore, the relative height of the groynes h_r (groyne height h_g to water depth H) was varied in the range of h_r =1/10 - 1/4. The investigation with different h_r values had mainly the aim to get an estimation of the effect of the groynes on the water level.

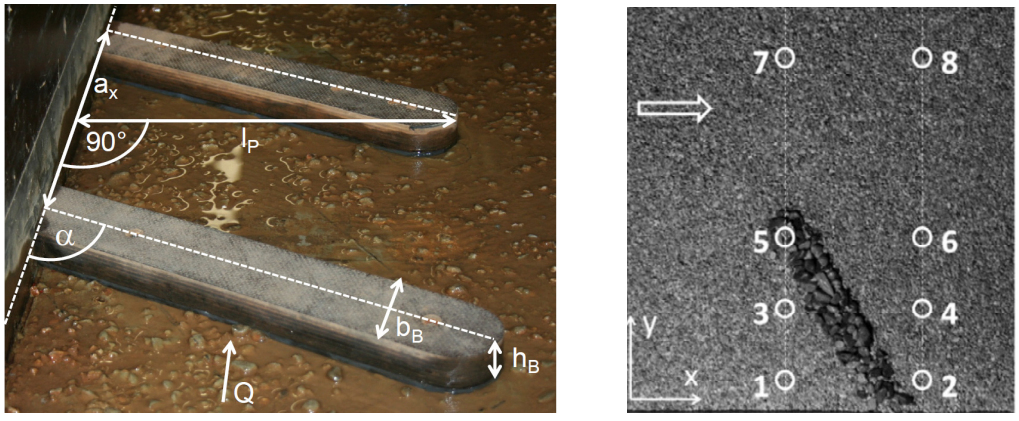

Figure 2.28 Groynes setup, (a) (modified from Mende 2014), (b) (Möws & Koll 2014)

According to Sindelar and Mende (2009) the bank protection effect of shallow groynes consist in the generation of large scale secondary currents which interact

with the main flow and thus influence the velocity distribution and bed load transport. Thereby, the flow attack against the bank will be reduced (redirection method) and the transport of sediment away from the bank will be prevented. As assessment criteria for the effectiveness of the groyne induced secondary currents Mende (2014) used the transverse velocity v or the relative transverse velocity $c = v/U$ (with: U = cross-section averaged velocity). A requirement for bank protection in bend is that c is greater than the relative curvature-induced transverse velocity c_c , i.e. that applies: $c > c_c$. To estimate the relative transverse velocity c_c Mende (2014) recommended the easy handling procedure form Rozoviskii (1957) as: $c_c = \alpha_v W/R$ (with: α_v = secondary flow coefficient $\cong 6.5$, W = channel width and R = bend radius). In river sections were the curve-induced transverse velocity occurs, c_c should be smaller than 0.2.As main result from his investigations in developing design guidelines for shallow groynes in bends Mende (2014) proposed Figure 2.29. The Figure says: if the curvature-induced transverse velocity c_c is known, the relative spacing S_p/l_p for a groyne inclination angle of 60° and relative groyne heights of h_r =1/10 - 1/4 can be estimated. In addition, the evaluation of his data showed that both inclination angles of the groynes directed against the flow (θ_g=30° and 60°) induced secondary currents. In contrary, groynes which were arranged perpendicular to the bank (θ_g=90°) did not generate secondary currents. As the effect of shallow groynes inclination angles (θ_g=30° and 60°) on the secondary flow is only slightly different and due to the higher construction cost of groynes with (θ_g=30°), Mende (2014) recommended for shallow groynes an inclination angle of 60°. For the groyne length l_p values of $l_p = 1/2 b_{s_0} - 2/3 b_{s_0}$ (with: b_{s_0} = width of the channel bottom) are assumed by Mende (2014). Furthermore, it can be withdrawn from Figure 2.29 that the induced secondary current or the transverse velocity is only in a small range dependent on the relative groyne height h_r . From his experiments it resulted as well that no significant increase in the water level is caused by the shallow groynes.

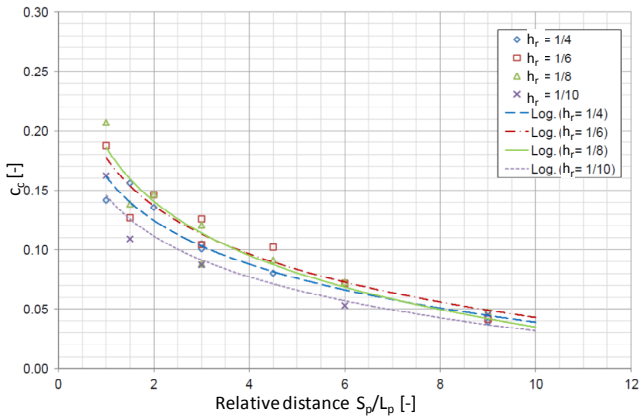

Figure 2.29 Relative transverse velocity c_c as a function of relative spacing S_p/l_p ,relative groyne height h_r and a groyne inclinaion angle of 60 °(modified from Mende 2014)

The investigations on shallow groynes were continued in the same straight flume but with mobile bed material by Möws & Koll (2014). The groynes dimensions were comparable to those of Mende (2014), however, instead of wood; the groynes were made by glued gravel. The aim of the mobile bed condition tests of Möws & Koll (2014) was to investigate effect of a single shallow groyne on the flow field and the morphological effects on the river bed in the near field of the groyne (Figure 2.30). The importance of the investigation of Möws & Koll (2014) was that it helps to understand in which way shallow groynes can be used to increase the morphologic and thus as well the hydraulic heterogeneity in the river which is an important goal in river restoration projects. Möws & Koll (2014) found that the maximum scour was located at a distinct distance downstream of the groyne (Figure 2.30), instead of the groyne head, as noted previously in different studies (e.g. Fang et al. 2006; Kuhnle et al. 2002). They attributed this difference in the location of the maximum scour to the rounded shape of the groyne head, the irregular surface and the shallow height of the groyne they investigated.

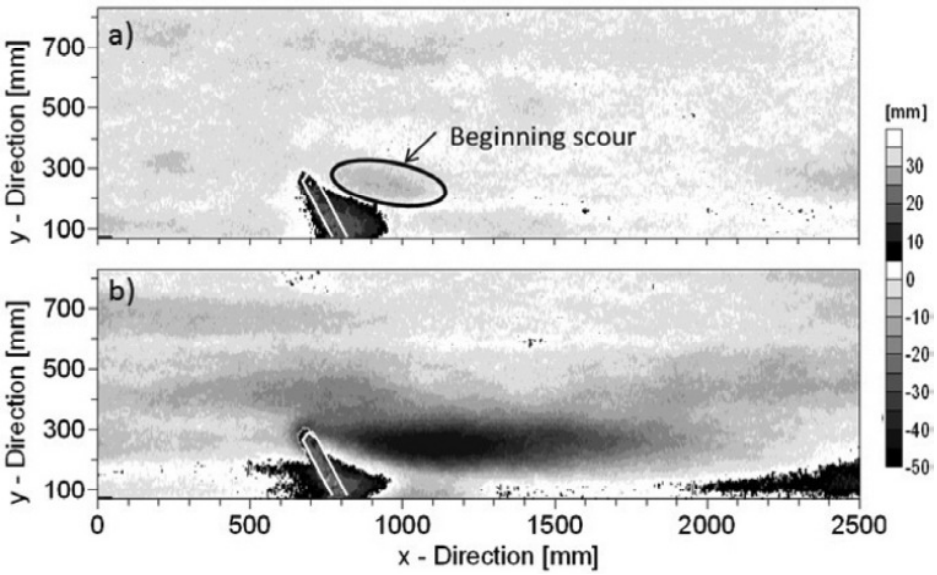

Figure 2.30 *Bed topography for (a) water depth 20 cm slope 1.5 %, (b) water depth 10 cm slope 3%, (Möws & Koll 2014).*

The studies of Mende (2014) and Möws & Koll (2014) on shallow groynes were carried out in a straight flume. However, the flow in river bends is different than in straight reaches, considering the presence of the helical flow, super-elevation and flow separation (see Chap. 2.2.1). In addition, the occurrence of bank erosion in river bends is higher compared to straight reaches. Therefore, it is important to investigate shallow groynes in curved flumes to evaluate the applicability of such structures to protect the bank in bends. To find an optimum setting of shallow groynes the effect of the groyne parameters on the flow field needs to be understood. Examples for the groyne parameters are the groyne inclination angle (Zaid & Koll 2016a) and the location of the groyne within a bend (Zaid & Koll 2016b).

2.4 Synthesis

It results from the literature review that the management of bank erosion is one of the most controversial issues in alluvial corridors. From the available bank protection methods, one can learn that the direct protection methods lead to the loss of valuable habitat. Therefore, to protect the bank in nature-oriented manner indirect methods to decrease the flow acting forces should be applied. In-stream structures belong to indirect methods or redirection methods. With in-stream structures the effective role of the fluvial erosion at the toe of the bank can be avoided and thus, the bank at the mid-basin reaches of rivers will be well protected.

Indirect methods include stream barbs, bendway weirs, vanes groynes, and recently shallow groynes. For the first mentioned indirect methods there are many experiences and results from experimental as well as numerical investigations. By comparing the resulting design guidelines a wide rag of recommendations for the same parameter of the same in-stream structure can be noted. Furthermore to the knowledge of the author none of these studies addressed the effect of the structures on the water level expect the investigation of Mende (2014) on the shallow groynes.

As in Europe, beside the ecological improvement of the river (EU-Water Framework Directive), the flood protection (EU Floods Directive) plays an important role as well, shallow groynes are the preferred indirect method. Therefore, in this study design guidelines for shallow groynes to protect the outer bank of sharp bends ($R/W < 2$) will be developed. Doing so, it can be referred to the experiences gained in straight flumes. However, as the investigations on curved channel showed a different flow pattern than in straight flumes, the design guidelines which are developed in straight flumes are not transferable to sharp bends with a distinct spiral flow and superelevation of the water level. That means investigations in a curved flumes have to be carried out.

It is known from the literature (e.g. Figures 2.8 and 2.9) that in sharp bends ($R/W < 2$) the maximum velocity in bends moves in the stream direction from the inner bank towards the outer bank at some point after the centre of the bend. Stating from this point and moving in the downstream direction the bank is strongly susceptible to erosion and protection must be provided. As this flow pattern is similar whether in laboratory experiments with rectangular cross-sections, natural topographic cross-section or also in natural streams, it was decided to build a curved flume with rectangular cross-section. The walls as well as the flume bottom were made of concrete. Most of the experimental runs were carried out under clear water flow conditions and fixed boundaries to investigate the action of the shallow groynes on the overall flow field. As the secondary current is decisive for shifting the maximum velocity from the inner bank towards the outer bank and the location of the maximum bed shear stress corresponds to the zone of the maximum velocity, implies that velocity measurements are sufficient for the assessment of the stability of the bank material and the optimiza-

tion of groyne configurations. In addition, supplementary test runs were carried out with mobile outer bank material. The objectives of these test runs were to verify the optimum setup of shallow groynes and to investigate the possibility of reducing the local scour at the groynes. The choice of the size of mobile material was done by using the methods from Chow (1959) and Shields (1936) and the assessment of the erosion and sedimentation zones was carried out on the basis of the bank elevation topography.

Unlike other in-stream structures types where the maximum scour is attached to the structure head, the maximum scour of shallow groyne was found to be at a distance downstream the groyne head Möws and Koll (2014). The shape of the structure head play an important role in the scour at the head, therefore it was decided in this study to build the groynes with rounded head.

3 Experiments

From the previous literature review it can be concluded that design guidelines for shallow groynes for bank protection in strong curved (R/W<2) bends is missing. To develop such guidelines, investigations in a curved flume were carried out (see Figure 3.1). The investigations were carried out with two conditions. The first condition with flume fixed bed and bank. The second condition with fixed bed and an outer bank shaped with mobile material. In the first experiments (with fixed bed and bank condition) the groyne parameters, namely, inclination, projected length, width, location and spacing were systematically investigated. Based on the results of the first experiments the optimum groynes group setup was defined. In the second experiments (with mobile outer bank condition) different groyne groups with different groyne lengths and spacing and were tested. Furthermore the local bank erosion at the groyne was investigated.

3.1 Experimental setups

3.1.1 Flume

The experiments were carried out at the laboratory of the Leichtweiß-Institut of the Technische Universität Braunschweig. A large double-curved flume was used for the experiments. The flume was constructed of bricks and concrete. The total length of the flume is 26 m. Starting from the inlet, the flume has a straight reach of 5.24 m to allow for a uniform approaching flow to the first curve. The first curve has a length of 4.08 m at the centre line and a radius of 3.6 m. Between the first curve and the second curve a straight reach of 7.74 m is allocated. The second curve has the same dimensions as the first one. Towards the end of the flume a third straight reach of 4.85 m is located to allow adjusting the flow conditions inside the flume. At the outlet of the flume there is a large reservoir which ends up with a weir to control the water level inside the flume (see Figure 3.1). The cross-section of the flume is rectangular with a width of 2.4 m and a depth of 40-50 cm. The longitudinal slope of the flume is 0.001 m. The bed slope was applied at the centreline of the curves. The projected length of the groyne l_p is defined as a ratio of the channel width w e.g. $l_p = 0.3W$ (see Chap. 2.3.3.2). This is an important aspect to be taken into account in the selection of the flume width, particularly with mobile bank material. Too narrow flumes may result in short groynes that are installed completely on the slope of the bank and do not extend over the bottom of the flume (e.g. Jamieson et al. 2013a,b and Cunningham & Lyn 2016). The implication of narrow flume set up on the groyne installation is shown in Figure 2.23. The flume width in this study was wide enough (2.4 m) to avoid this problem in the mobile outer bank experiments which will be described later. The inlet was adapted in such a way to insure uniform approaching flow to the flume. Three

point gauges were installed in the flume (Figure 3.2), one gauge at each of the three straight reaches of the flume to control the water depth.

The radius of the curves at the centreline is 3.6 m. The curvature ratio (radius to width ratio (R/W) of the bends in the flume is 1.5. Considering that sharp curves have $R/W < 2$ (Blankaert et al. 2013) the flume falls in the range of sharp curves.

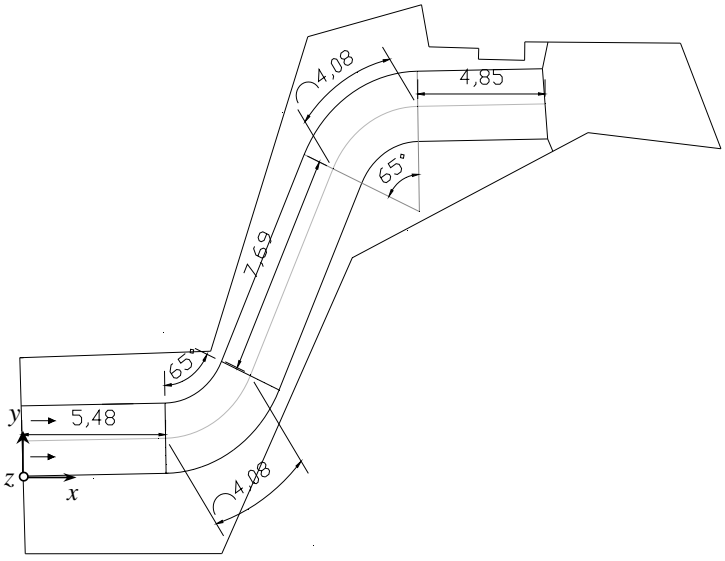

Figure 3.1 Flume layout

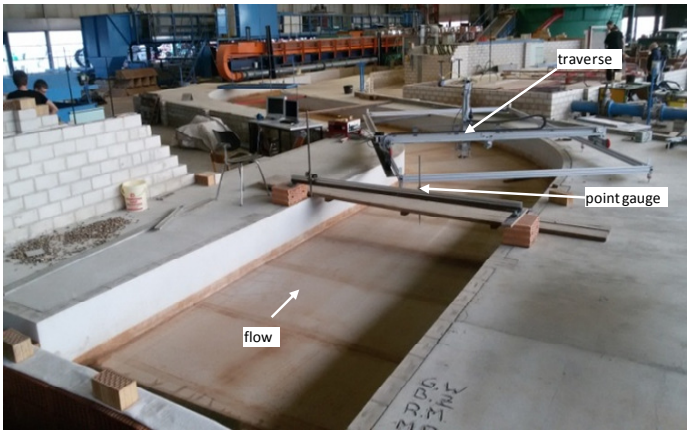

Figure 3.2 Flume photo

3.1.2 Groynes

The basic idea was to construct the groynes in such a way that it will be very close to real groynes in the field. Therefore, the groynes for all the tests were made of glued gravel. The size of the gravels was 6-12 mm. Special glue was poured on the gravel and mixed very well. The mixture was poured into wooden forms to shape the groy-

nes. The groynes were left to dry out, then fixed on a plate of galvanized steel using silicon. The groyne tip was made with a rounded shape to smooth the flow around the tip. Later the groynes were fixed on the flume bottom using a very thin layer of gypsum. The standard groyne for most of the tests has a rectangular section with a width of 6 cm, a height of 2.5 cm and projected length of 80 cm. However, to investigate the effect of the width and the projected length on the flow field the width and the projected length were varied. Three different widths (3cm, 6cm and 9 cm) and three projected lengths (40 cm, 69.3 cm and 80cm) were tested. The inclination angle of the standard groyne for most of the tests was 60°. This angle was used as well by Möws & Koll (2014) in mobile bed experiments and it was recommended by Mende (2014) in fixed bed experiments, therefore it was used as starting point for the experiments. However, both of the studies mentioned before were carried out in a straight flume, therefore different inclination angles (50°, 55°, 60°, and 70°) where tested to define the optimum inclination angle in bends.

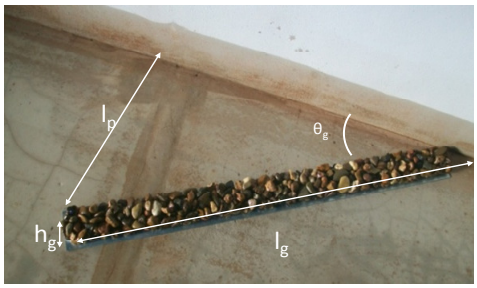

Figure 3.3 Photo of the groyne

3.1.3 Mobile outer bank setup

For mobile outer bank tests, the outer bank of the first curve was shaped with mobile sediment. In addition to the curve, the mobile outer bank material extends 4.25 m in both straight reaches upstream and downstream the curve (Figure 3.4). The placement of the sediment started one meter downstream the inlet to avoid the erosion due to the turbulent flow at the upstream boundary.

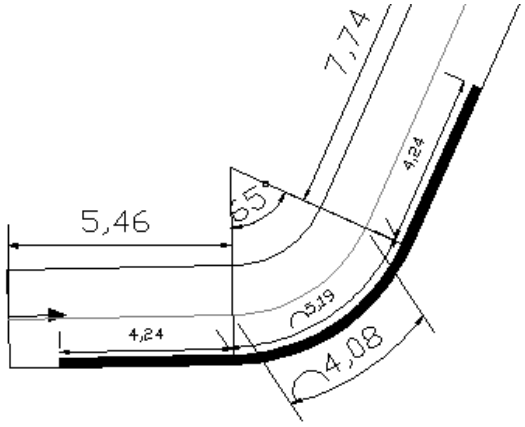

Figure 3.4 Mobile outer bank test layout

The criterion for the selection of the outer bank material was to find sediment with a critical shear stress slightly higher than the maximum boundary shear stress on the bank in the straight reach of the flume. This implies that no erosion will take place in the straight reach of the flume and the erosion within the curve is due to the curvature. To estimate the maximum boundary shear stress on the bank Figure 2.6 was used. The critical shear stress of the sediment on the bank was estimated using the approach of Shields (1936) with a modification of the critical shear stress on the slope of the bank according to Eq. 2.7 of Chow (1959). Accordingly, sediment size in the range of 1 to 5 mm was tested. The sediment material of 1-3 mm (Figure 3.10) was found to be reasonable to visualize the outer bank erosion; accordingly, it was decided to be used for the mobile outer bank tests. For the selected material with d_{50} = 2.5 mm, sediment fiction angle ϕ = 36° and angle of the outer bank material θ_b = 31.9° the critical shear stress on the bank resulted in τ_{c_s} = 0.76 N/m^2. The maximum boundary shear stress at the bank was determined to τ = 0.74 N/m^2 which is slightly lower than the critical shears stress.

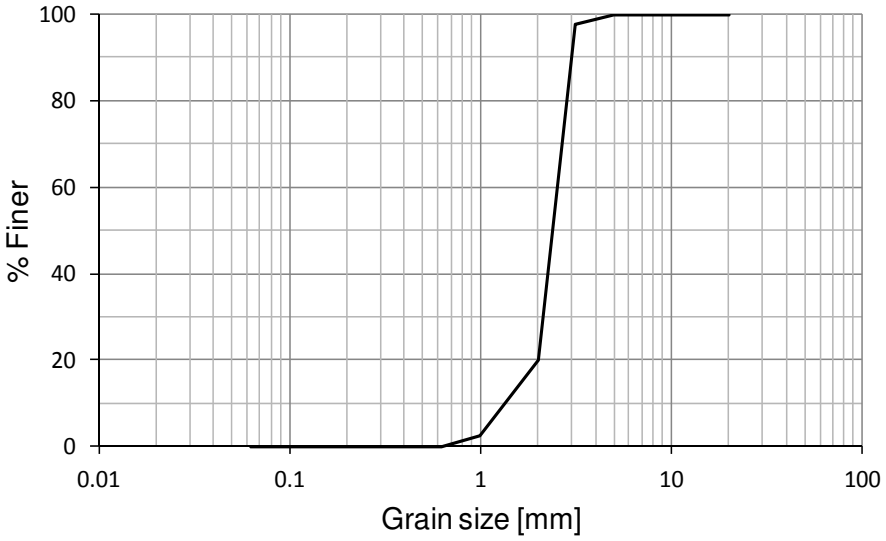

Figure 3.5 Grain size distribution of the bank material

A simple method to shape the outer bank was by using a steel plate. The outer bank mobile material was prepared in the shape of a triangle. The base of the triangle was 22.5 cm and the vertical side has an extension of 14 cm (Figure 3.6a). Since the water depth was 10 cm, 4 cm free board was available. The bank angle was 31.9° evaluated as the angle of repose of the sediment material. A steel plate was used as a form which was carefully scratched along the bank to shape the outer bank material (Figure 3.6b).

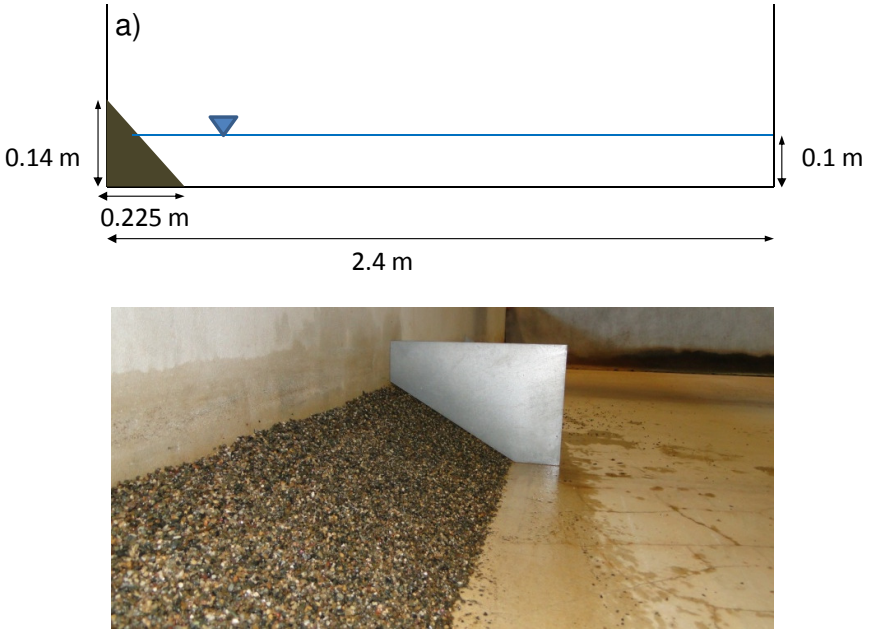

Figure 3.6 Flume cross-section with outer mobile bank (a), outer bank shaping photo (b)

The accuracy of the shaping method was tested using the point gauge measurements shown in Chap. 3.2.2. The bank was shaped three times and the topography of the bank was measured each time. By comparing the topography, it was found that the bank can be shaped with an accuracy of ±0.58 cm. To reduce the inaccuracy associated with the bank shaping, the bank topography was measured before and after running the flume in all the test runs.

3.2 Instrumentations

3.2.1 Velocity measurements

In order to measure the 3D velocities an Acoustic Doppler Velocimeter (Vectrino plus from Nortek) was used. The accuracy of the Vectrino plus is ±0.5% of measured value ±1 mm/s. The device was used to collect point velocity measurements at different locations within the first curve of the flume. The Vectrino was mounted on an automatic traverse which can be moved in x, y and z direction (Figure 3.7). A computer was used to drive the traverse to predefined measuring points using ProNC software. Most of the velocity measurements were done with down-looking Vectrino probe (Figure 3.7a). The orientation of the Vectrino down-looking probe was done with respect to the traverse x axis and the data were rotated later during the processing to the s-n coordinates system (stream line and transverse coordinates). The rotation angles are listed in Table 3.1. The coordinate system of the Vectrino probe is shown in Figure 3.7a (positive transverse velocity *v* means that the flow goes towards the inner bank vice versa). Additional measurements were carried out using a side-

looking probe (Figure 3.7b) to allow for collecting velocity data in the upper half of the water depth.

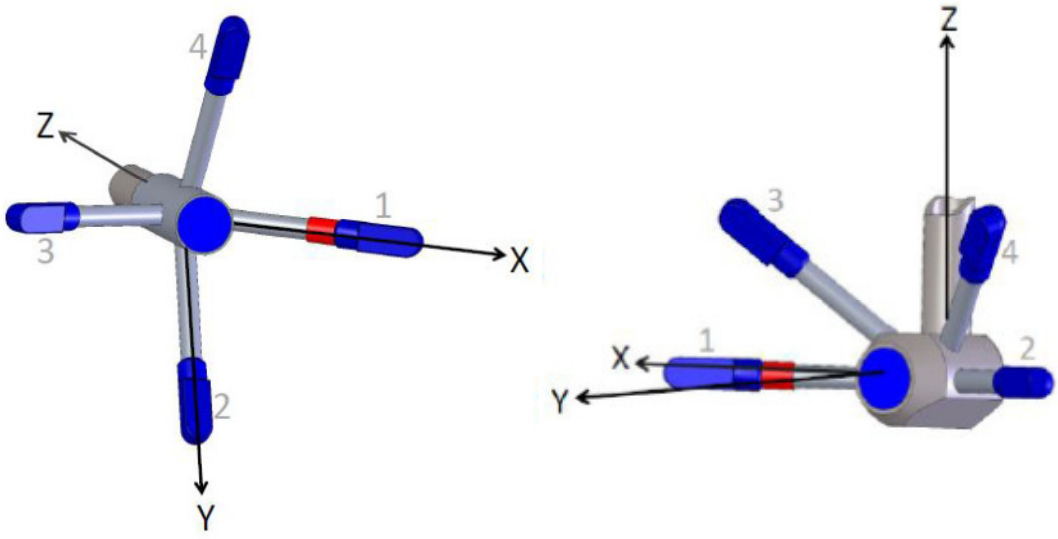

Figure 3.7 Vectrino Plus, (a) down-looking probe, (b) side-looking probe (Norteck 2013)

Table 3.1 Rotation angles at each cross-section.

Cross-section No. [-]	Rotation angle to s-n coordinates [°]	Rotation angle to x-y coordinates [°]
C1	-32.23971	1
C2	-24.11471	9.125
C3	-15.98971	17.25
C4	-7.86471	25.375
C5	0.26029	33.5
C6	8.38529	41.625
C7	16.51029	49.75
C8	24.63529	57.875
C9	32.76029	66
C1_a	-30.96645	2.39353
C9_b	31.48702	64.84702

Due to the sensitivity of the side-looking probe to the transverse velocity which persists in the curve, a rotatable mount was constructed to orient the probe at each cross-section to the s-n coordinates system. This setup of the side-looking probe allows collecting velocity data in most of the measurement points in the curve. However, at the second half of the bend and close to the inner bank it was not possible to

measure with the side-looking probe oriented in s-n coordinates system. It is to be noted that the transverse velocity in this region was very high.

Different parameter settings of the Vectrino were tested in order to acquire data with high quality. The quality of the data can be evaluated by the correlation and the signal to noise ratio (SNR). The optimum setting of the Vectrino was found at a transmit length of 1.8 mm, sampling volume of 7.0 mm and power level (-High, High). The velocity was measured at a frequency of 100 Hz. The sampling duration was investigated and duration of 60 seconds was found to be adequate for estimating the value of time averaged velocities with an accuracy of ± 1.4%. However, when the correlation drops below 70% during the measurements the sampling duration increased to 90 seconds to maintain the same level of accuracy. This is mainly to compensate for the number of samples which will be screened out during the filtering, later in the data data processing. Buffin-Belange & Roy (2005) found that sampling duration in a range of 60 s to 90 s was the optimum for all turbulent statistics in gravel bed rivers. The output data of the Vectrino was processed using WinADV software, originally developed by the US Bureau of Reclamation. During the process the Vectrino data was filtered based on the correlation. All samples with a correlation less than 70% were screened out as recommended by Wahl (2002). Additionally, the spikes were removed by applying the Phase-Space threshold dispiking method of Goring & Nikora (2002) as modified by Wahl (2002).

In order to get the velocities in s-n coordinate system (stream-wise and transverse velocities), the velocity data were rotated using the deviation angle between the probe x axis and the s axis at each cross-section. To obtain the velocities in the global coordinates $(x$-$y)$ with respect to the flume, the rotation angles between the s-n and x-y at each cross-section were used (Table 3.1).

3.2.2 Bank topography measurements

Two methods were used to measure the bank topography in the mobile outer bank experiments described in Chap. 3.1.3. In the first method a photogrammetric technique called Structure from Motion SfM was used and 3D models of the bank were generated. The second method was employing a point gauge which was installed on the traverse to measure the bank topography (Figure 3.9b).

Photogrammetric technique SFM

Structure from motion SfM is a technique for obtaining a high resolution topographic data from multiple overlapping images taken at distinct triangulation angles (Nadal-Romero et al. 2015). The technique has been used recently in a wide range of geosciences applications for example Prosdocimi et al. (2015) applied SfM to investigate bank erosion in agricultural drainage networks. The accuracy of the 3D reconstruction using SfM was investigated at the Leichtweiß-Institut (LWI) in association with

the Bachelor study of Westphal (2016). The results of the investigation showed an accuracy in the order of ±1 mm in x,y,z directions under the tested conditions. Noack et al. (2016) confirmed the accuracy of the SFM technique for many applications in hydraulic laboratories.

The topographic measurements were done by taking photos with enough overlaps and at different angles. The photos were taken for the mobile outer bank starting from the beginning of the bend down to the end of the end of the mobile bank. The locations of the camera and 3D reconstruction of the bank are shown in Figure 3.8 (in point cloud). To take the photos a digital camera Canon DS126191 was used with Sigma DC 18-200mm f/3.5-6.3 Auto Focus OS (Optical Stabilizer) Zoom Lens.

Figure 3.8 Camera locations and 3D model of the bank

To get the 3D topographic model the photos were processed using the free open source software VisualSfM (Changchang Wu 2013). The software has a geographic user interface UGI and computes the 3D reconstruction using the structure from Motion technique (SfM).

For further processing the output data form VisualSfM were imported into MeshLab software (Visual Computing Lab-ISTI-CNR). MeshLab is an open-source software which allows for cleaning, filtering, editing and rendering of the 3D triangular meshes. It also gives the option to export the data (x,y,z) in ASCII format.

Point gauge measurements

For the point gauge measurements a grid of measurements points was defined and the traverse was used to hold the point gauge and drive to the measurement points.

As the focus of the measurement was to study the local erosion at the groyne due to the accelerated flow over the groyne, the measurement grid was set finer in the vicinity of the groyne at C5, in both directions, upstream and downstream of the groyne (Figure 3.9a). The measurements grid contains 6 longitudinal profiles. The spacing between the profiles in the cross-sectional directions is 4 cm. However, the first and the last longitudinal profiles were set at 2 cm distance from the edges of the bank. The grid spacing in the longitudinal direction is 8 cm in the vicinity of the groyne and 17 cm further away from the groyne.

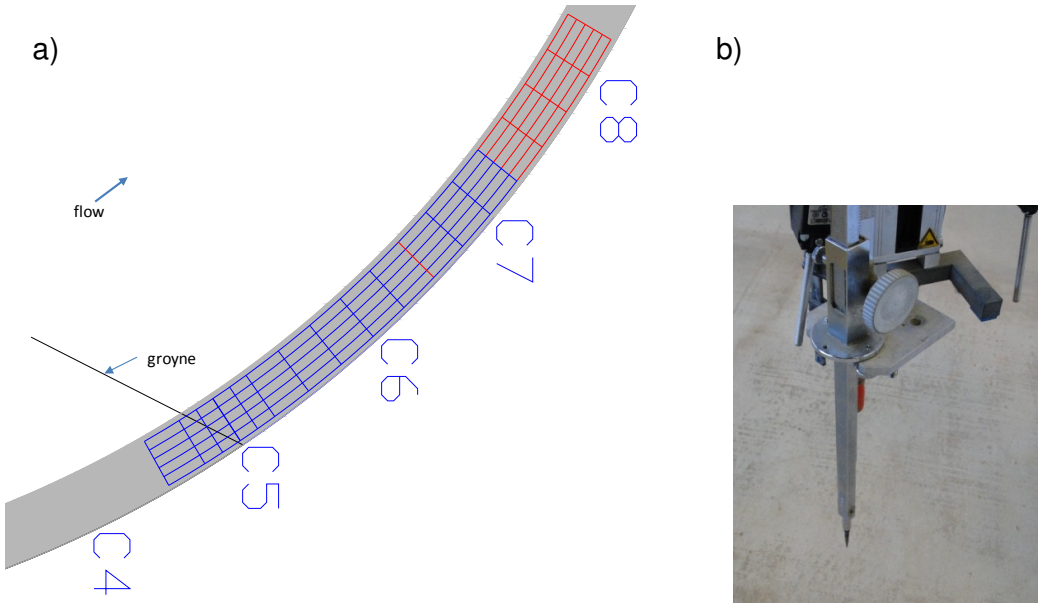

Figure 3.9 *(a) Point gauge measurement grid with red color for grid extension in test runs E8.5 & E8.6, (b) point gauge photo*

3.3 Experimental program

The experimental program was prepared in a systematic way in order to account for the complexity and the large number of parameters affecting the design of shallow groynes. To reduce such complicity, the program started with a fixed rectangular section in which the effect of the groyne inclination, location, spacing, length and width were tested. The fixed bed and bank condition allowed to carry out enough number of tests that can elaborate and give an insight into the hydraulic effect of each of the aforementioned parameters and to optimize the groynes setup. In the way to fine out the optimum setup of shallow groynes, the results of each test run were fed and incorporated in the subsequence test runs. After the fixed bed and bank condition tests were completed, fixed bed and mobile outer bank tests were performed. The aims of the mobile outer bank tests were, to test the optimum groyne settings which came out from the fixed bank condition and to further optimize the groynes spacing to reduce the local bank scour at the groyne due to the accelerated flow over the groyne.

3.3.1 General consideration

The velocity measurements were carried out at the first curve of the flume where the traverse was installed (see Figure 2.2). A grid of a total number of 325 measurement points was set in order to capture the 3D flow field in the curve (Figure 3.10). The curve was divided into 9 cross-sections. Each cross-section was divided laterally into 7 verticals. The spacing between the verticals is 30 cm. Each vertical includes 5 measurement points located at different levels above the bottom (1, 2, 3, 4 and 5 cm above the bottom). Due to some limitation with the traverse, the points of vertical 7 at cross-section C1 and C9 were not possible to measure. Instead, two points were in-

troduced with 10 cm shift in the cross-sectional direction, denoted here with (a) and 10 cm shift in the longitudinal direction denoted with (b).

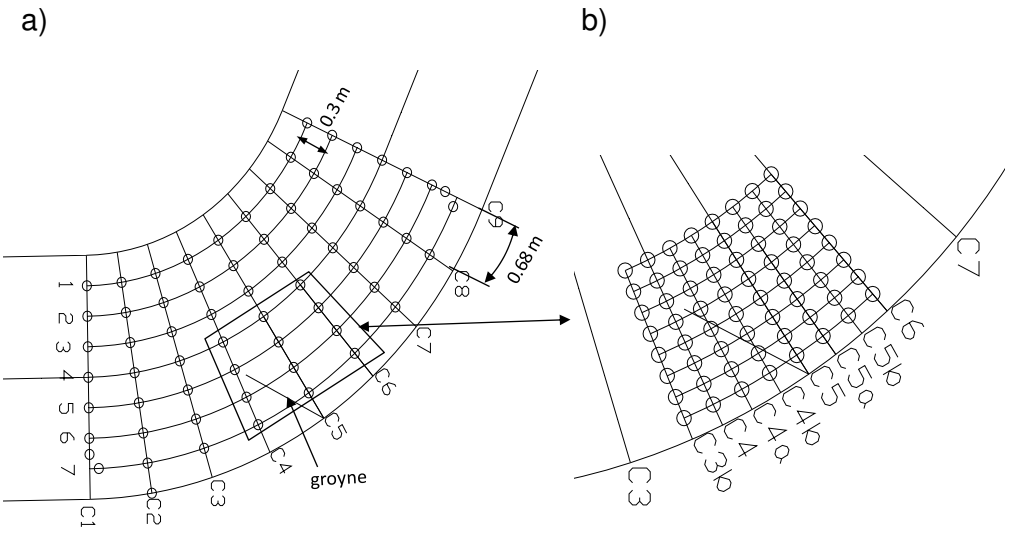

Figure 3.10 (a) Main measurement grid and (a) fine measurement grid

For the additional tests with the side-looking probe the aforementioned measurement grid was extended towards the water surface by adding four points in each vertical to include 6, 7, 8 and 9 cm above the bottom. The side-looking probe measurements were compared with the down-looking probe ones at the level 5 cm above the bottom, and the difference in the stream-wise velocity was less than 5%.

To examine whether the resolution of the measurement grid is fine enough to capture the flow field with a groyne installed, a finer grid was set around cross-section C5 where one groyne was installed. In the fine grid two additional cross-sections in the longitudinal direction were added between the cross-sections of the main grid. In the cross-sectional direction one longitudinal profile was added. In the vertical direction one measurement point was added between the measurement points of the main grid. The vertical spacing in the fine grid is 5 mm instead of 1 cm for the main grid, (see Figure 3.10). The comparison between the velocities of the fine grid and the main grid at longitudinal profile L7 close to the outer bank showed that the main grid was adequate to capture the flow field. However, the fine grid allowed capturing more local details of the flow field around the groyne. Detailed results of the fine grid test are presented in Chap. 4.4.

Repeatability of the measured data

To evaluate the repeatability of the measurements the experiment without groyne (E0) was repeated. The evaluation showed that 96% of the measured stream-wise velocity can be reproduced with an accuracy ± 2 cm/s which is 3.6% of the average velocities at the straight reach of the channel (54 cm/s). Figure 3.7 shows the velocities *u* for the reference test (E0) against the velocities of the repeated test (E0).

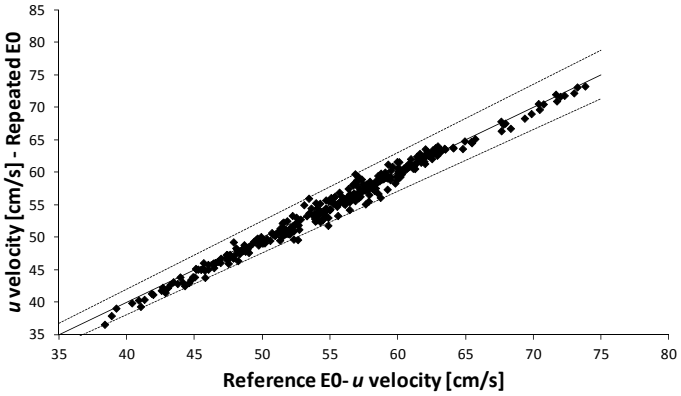

Figure 3.11 Stream-wise velocities u for E0 reference test and E0 repeated test, dotted line ±5 % difference

Approach flow condition

To evaluate the approach flow conditions, a measurement section at 3 m downstream of the inlet was set. The measurements in this section were done using a micro-propeller. In the section, nine verticals were identified. In each vertical there were 4 points in the vertical direction with 2 cm spacing (Figure 3.12). The results showed adequate approach flow to the bend.

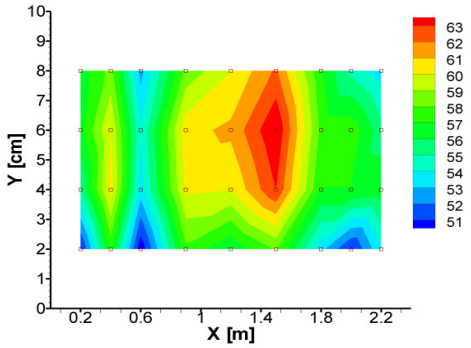

Figure 3.12 Cross-sectional velocity field 3 m downstream of the inlet

3.3.2 Fixed bed experiments

The investigations started with a fixed rectangular section. The baseline flow condition in the flume was measured in the test run E0 in which no groyne was installed. This test is a reference test for the flow field against which the tests with different

groyne configurations were compared. The second experiment E1 was devoted to investigate the effect of the inclination of the groyne on the flow field. This test elaborates on the optimum inclination of the groyne, which was applied to all of the following tests. The third Experiment E2 was carried out to investigate the effect of the location of the groyne on the flow field. To insure that the measurement grid was adequate to capture the flow field with the groyne installed an experiment E3 with a finer grid shown in Figure 3.6 was performed. Further experiments were done to test the effect of the groyne projected length (E4) and the width of the groyne (E5) on the flow field. The experiment E6 was devoted to elaborate and optimize the groynes spacing (group of groynes).

In order to allow comparing the results of the experiments, the boundary conditions in all aforementioned test runs were kept constant (discharge was 130.6 l/s and water depth is 10 cm).

Flow field without groyne (E0)

The objective of this experiment is to measure the baseline flow field without groyne which will be compared with tests with deferent groyne configurations.

Investigation of the groyne inclination angle θ_g (E1)

The optimum inclination angle of shallow groynes in straight flume is 60° (Mende 2017). In curved flume this inclination angle (60°) needs to be checked. To investigate the effect of the groyne inclination on the flow field in bend in order to find out the optimum inclination angle of shallow groynes five test runs were performed. The groyne was installed at the beginning of the curve at cross-section C1. The inclination angle was varied from 50° to 70° in 5° steps. The projected length which is the perpendicular distance from the groyne tip to the bank was kept constant. The projected length was set to one third of the flume width (80 cm) as recommended in the literature for different in-stream structures (see Chap.2.3.3.2). In each test the flow field was measured over the entire measurement grid. The details of the test runs are shown in Table 3.2.

Table 3.2 Experiment E1 groyne setup

Run No.	Inclination [°]	Projected length [cm]	Groyne length [cm]
E1.1	50°	80	104.4
E1.2	55°	80	97.7
E1.3	60°	80	92.4
E1.4	65°	80	88.3
E1.5	70°	80	85.1

Investigation of the groyne location (E2)

The experiment E2 was carried out to investigate the effect of the location of the groyne on the flow field. Eight test runs were performed. One groyne was used in each test run. The inclination angle of the groyne was 60° which was a result of the first experiment E1. The projected length of the groyne was 80 cm. In the first test the groyne was located at cross-section C1. The groyne was moved to C2, then C3 and so on until C9 (Table 3.3). In each test the flow field was measured on the entire measurement grid except for the test run E2.6 and E2.8, where only the longitudinal profile L7 was measured. The width of the groyne was 6 cm and the height was 2.5 cm.

Table 3.3 Experiment E2 groyne setup

Run No.	Location of the groyne [-]	Longitudinal Distance [m]
E2.1*	C1	0
E2.2	C2	0.64
E2.3	C3	1.28
E2.4	C4	1.92
E5.5	C5	2.56
E2.6	C6	3.20
E2.7	C7	3.84
E2.8	C8	4.48
E2.9	C9	5.12
* E2.1 is the same as in E1.1		

Fine grid measurements (E3)

In experiment E3 one groyne at cross-section C5 was installed. The groyne has a projected length of 80 cm and a width of 6 cm. The velocity measurements were taken at the measurement point of the fine grid shown in Figure 3.6. The results of the experiment E3 are compared with test run E2.5 to evaluate the adequacy of the main measurement grid.

Investigation of the groyne projected length l_p (E4)

This experiment is devoted to investigate the effect of the groyne projected length on the flow field. The recommendation on the length of in-stream structures e.g. bend-way weirs and stream barb is in the range between one third and one fourth the channel width (see Chap. 2.3.3.2). In this experiment the projected length was tested in the range of . From Four runs with two different projected lengths were performed, (Table 3.4). However, two runs from experiment E2 with 80 cm (

$l_p/W = 0.3$), one at C1 and the second at C2, are relevant here and the six runs are discussed in Chap. 4.5. Two runs with projected length of 68.3 cm which corresponds to ($l_g/W = 0.3$). Shorter groynes with projected length of 40 cm ($l_p/W = 0.6$) were also tested. The location of the groyne at C1 and C2 was decided based on the results of the experiment E2 in which the effect of the groyne located at the beginning of the curve was found to be higher than in case of at the middle or the end of the curve.

Table 3.4 Groyne setup for experiment E4

Run No.	Projected length [cm]	Groyne location [-]
E4.1	68.3	C1
E4.2	68.3	C2
E4.3	40	C1
E4.4	40	C2
E2.1	80	C1
E2.2	80	C2

The velocity measurements were done at the longitudinal profile L7 except for E2.1 and E2.2 where the entire grid was measured.

Investigation of the groyne width w_g (E5)

The recommendations on the width of different in-stream structure e.g. bendway weirs and stream barbs were related to the stability of the structures (see Chap. 2.3.3.2). The recommended width is defined interims of the maximum size of the construction material of the structures e.g. two or three times the maximum construction material. However, the hydraulic effect of the structure width is missing. Therefore, the effect of the groyne width on the flow field was investigated in this experiment (E5). The width of the groyne is directly connected to the amount of the construction material of groyne which needs to be minimized.

Four test runs were performed using two different groyne widths (9 cm and 3 cm). Two runs from experiment E2 with a groyne width of 6 cm are relevant here and the six runs are discussed in Chap. 4.6. The bases for selecting the cross-sections C1 and C2 to test the groyne width is the same as in experiment E4. The velocity measurements were carried out at L7 except for E2.1 and E2.2 where the entire grid was measured.

Table 3.5 Groyne setup for experiment E5

Run No.	Groyne width [cm]	Groyne location [-]
E5.1	9	C1
E5.2	9	C2
E5.3	3	C1
E5.4	3	C2
E2.1	6	C1
E2.2	6	C2

Investigation of the groyne spacing S_p (E6)

The experiment E6 was carried out to elaborate on the effect of groyne number and spacing on the flow field. Eleven different combinations of groynes were tested. Combinations of two, three and four groynes at different locations were investigated. To find the optimum configuration of the groynes the projected length of the groynes was varied taking into account the results of E4. The velocity measurements were taken at the longitudinal profile L7 close the outer bank for the test run E6.1 to E6.7. For the test runs from E6.8 to E6.11 the measurements were taken at the longitudinal profile L1 and the longitudinal profile L7. As a result of the test run E6.1 to E6.5 a geometric method to define the location of the second groyne was proposed.

Table 3.6 Experiment E6 groynes setup

Run No.	Groyne number [-]	Projected length [cm]	Groyne location [-]
E6.1	3	80	C1, C5, C9
E6.2	2	80	C1, C9
E6.3	2	80	C1,C5
E6.4	2	80	C5,C9
E6.5	3	80	C1,C3,C5
E6.6	2	69.3	C1, Constr.*
E6.7	2	69.3	C1,C5
E6.8	2	40	C1, Constr.*
E6.9	3	40	C1, Constr.*, Constr.*
E6.10	4	40	C1, Constr.*, Constr.*, Constr.*
E6.11	3	40	C1, Constr.**, Constr.**
E6.12	4	40	C1, Constr.*, Constr.*, C9

Constr.* :constructed location

Constr.**: constructed location starting from downstream to upstream direction (USDA 2013)

The location defined with this method is called ''constructed'' location and referred to as the location at the intersection of the curve with a line at the tip of the groyne, extending parallel to the tangent at the toe of the groyne in the downstream direction (Figure 4.21).

The details of all the test runs with the groyne group settings is shown in Table 3.6

3.3.3 Mobile outer bank experiments

Two experiments were performed with mobile outer bank condition, namely, E7 and E8.

The flow boundary condition of the entire mobile outer bank tests was kept constant. The discharge was 125 l/s instead of 130.6 l/s in the fixed bed condition tests to obtain the same water depth of 10 cm. Two point gauges in the straight reaches of the mobile outer bank area were used in order to control the water depth.

To perform the mobile outer bank condition tests the flume was filled slowly up to around 15 cm water depth with low discharge of 35 l/s. To start the test the back water was reduced carefully by lowering the weir at the outlet until the water depth of 10cm at discharge of 125l/s is reached. The duration of the mobile outer bank test was constant (two hours) of all the tests. This was because in the test run without groyne the outer bank was completely eroded downstream of the bend for a length of one meter in two hours.

Investigation of groups of groynes (E7)

The experiment was done to further investigate the optimum configuration of the groyne including the spacing and the projected length. The outer bank topography was documented with photos and a 3D model of each test was constructed using VisualSfM software. Velocity measurements were done at longitudinal profile L1 and L7. The mobile outer bank tests give information on the scour which was found to have the maximum value downstream the bend exit, where velocity measurements are not available. The groynes setup of the test runs of E7 is shown in Table 3.7.

Table 3.7 Groyne setup for experiment E7

Run No.	Groyne number [-]	Projected length [cm]	Groyne location [-]
E7.1	-	-	-
E7.2	3	80	C1,C5,C9
E7.3	3	40	C1, Constr.*, Constr.*
E7.4	4	40	C1, Constr.*, Constr.*, Constr.*
E7.5	4	40	C1, Constr.*, Constr.*, C9
E7.6	3	80	C1, C2, C5, C9
Constr.* :constructed location			

Investigation of the local erosion at the groyne location (E8)

The experiment E8 was performed to investigate the local scour at the groyne toe. The objective was to find the best configuration of the groynes that helps to avoid or to produce the smallest local scour at the groyne toe. Mainly the spacing between the gryones was changed and the bank topography was measured before and after each test using a point gauge (Figure 14a). The projected length of the groyne was 80 cm for all test runs. Mainly the spacing between the groynes was changed

Table 3.8 Groyne setup for experiment E8

Run No.	Groyne number [-]	Groyne location [-]
E8.1	-	-
E8.2	1	C5
E8.3	2	C5,C6
E8.4	3	C5,C6,C7
E8.5	3	C5,C6.5*,C8
E8.6	3	C5.C6,C7.5*
E8.7	1	C7
C6.5: at mid-distance between C5 and C6 C7.5: at mid-distance between C7 and C8		

4 Results

4.1 Bend flow field without groynes, experiment E0

Observations of the 3D flow field without groynes are very important because it gives the reference flow condition, against which the flow field with different groyne configurations can be compared. Thus, the characteristics of the bend flow including the velocity distributions and secondary flow are reported here. The results are shown in cross-sectional plots and global top plots. The global top plots show top views of the flow field over the entire curve at different level above the flume bottom. The measured 3D velocities at all the measurements points are shown in a tabular form in Annex I.

The 3D velocity measurements show that the core of the maximum stream-wise velocity is shifted towards the inner bank and lower stream-wise velocities were observed close to the outer bank. The stream-wise velocities close to the outer bank at longitudinal profile L7 show a decreasing trend throughout the curve until the middle of the curve, and then increase towards the end of the curve (Figure 4.1 & Figure 4.2). Contrarily, the stream-wise velocities close to the inner bank at longitudinal profile L1 increase from the beginning to the middle of the curve C5 and decreases towards the end of the curve.

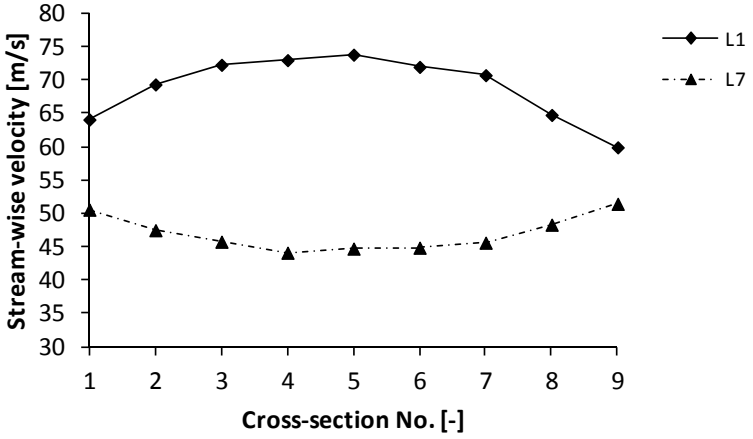

Figure 4.1 Stream-wise velocities at 3 cm above the bottom at longitudinal profiles L1 and L7

The flow depth was 10 cm in the straight reaches of the flume. In the curve a super-elevation took place due to centrifugal force, and thus the flow depth varies. The maximum super-elevation was measured at the middle of the curve. However, super-elevations of 0.94 cm and 1.21 cm were measured at C1 and C9 respectively (see Table 4.1). This implies that the effect of the curve on the water elevation extends beyond the two ends of the curve.

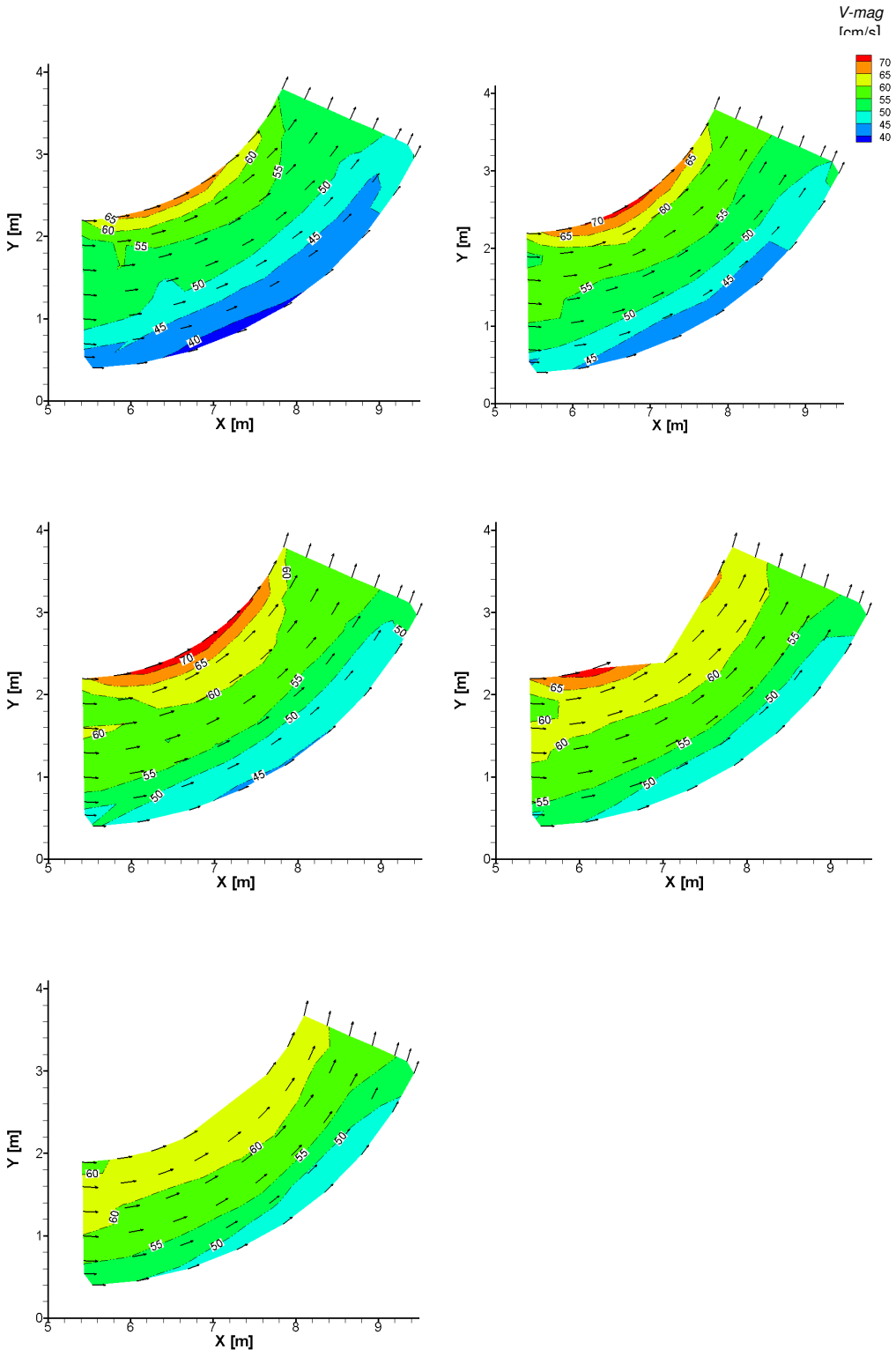

Figure 4.2 *Global 3D flow field at different levels above the bottom, V-mag is the velocity magnitude*

Table 4.1 Water depth (h) and super-elevation

Cross-section No		Distance from Left bank [m]			Δh [cm]
		0.1	1.2	2.3	
C1	h [cm]	9.12	9.73	10.06	0.94
C5	h [cm]	7.88	9.72	10.16	2.28
C9	h [cm]	8.94	9.91	10.15	1.21

Due to the super-elevation and the submergence requirement of 5 cm of the Vectrino probe the entire longitudinal profile L1 at 5 cm above the bottom in addition to four points at 4 cm above the bottom were not possible to measure, see Figure 4.2.

The super-elevation in the curve generates a radial pressure gradient. The local imbalance between the centrifugal force and radial pressure gradient generates a secondary flow circulation. Figure 4.3 shows the cross-sectional 3D flow field in which, the vectors show the transverse and vertical velocities (v,w) and the stream-wise velocity (u) is shown in contour colour. It is to be recalled that the upper 5 cm of the cross-section was not possible to measure with the down-looking Vectrino probe; accordingly complementary tests were carried out with side-looking probe to extend the measurements up to 9 cm above the bottom. Due to the sensitivity of the side-looking probe to the transverse velocity which was very high toward the end of the curve, it was not possible with the current setting to get good measurements close to the inner bank after C6. That explains why the cross-sections from C7 to C9 were not extended up to a depth of 9 cm in (Figure 4.3) where only the down-looking probe measurements were included.

At the first cross-section C1, the velocity vectors show that the flow is moving toward the inner bank and no circulation was observed. The circulation of secondary flow becomes appreciable starting from cross-section C2 (8.125°) and increases toward the end of the curve. The circulation of the secondary current starts between cross-section C1 and C2. The direction of the secondary current is towards the outer bank in the upper part of the flow and towards the inner bank in the lower part close to the bottom. This shows that the circulation of the primary secondary current cell is clockwise. It can be noted that the retaining flow towards the inner bank was observed up to 2 cm from the bottom at C2 to C8 and at the end of the curve C9 the retaining flow is observed up to 1 cm above the bottom, see the velocity vectors in Figure 4.3.

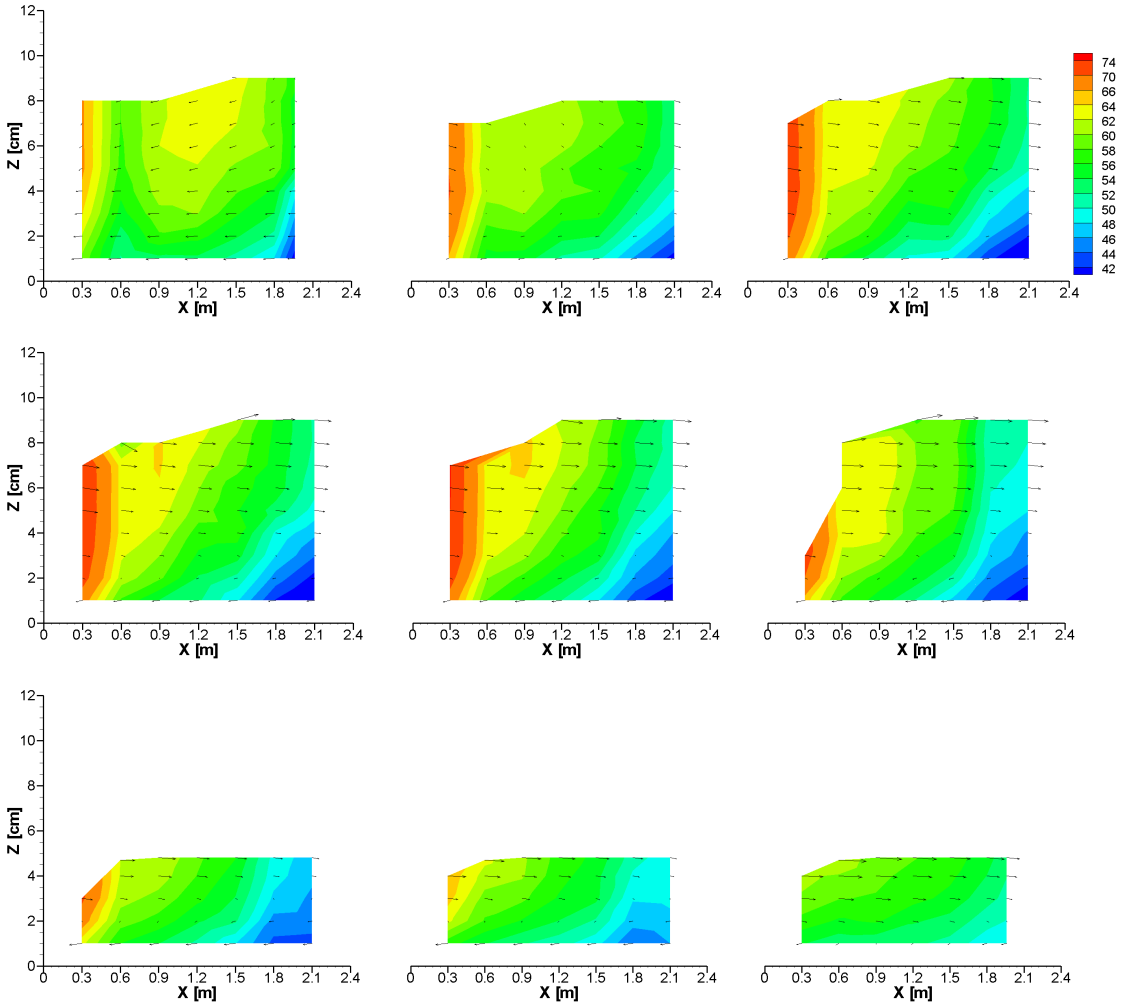

Figure 4.3 Cross-sectional view of the 3D flow field (E0)

4.2 The effect of the groyne inclination angle on the flow field, experiment E1

The objective of experiment E1 is to investigate the effect of the groyne inclination angle on the flow field and to elaborate on the optimum angle for shallow groynes. One groyne was installed at cross-section C1 and the groyne inclination angle was varied from 50° to 70° (see Table 3.2). The projected length l_p was kept constant at 80 cm (one third of the flume width). The results of the flow velocity measurements show clearly the flow redirection effect of the shallow groyne. The flow velocity close to the outer bank was reduced due to the installation of the shallow groyne. The flow was redirected towards the inner bank and the flow velocity close to the inner bank was increased. Figure 4.4 shows, exemplary, the stream-wise velocity u for the test run E1.1 at the longitudinal profiles L1 and L7 and 3 cm above the bottom. Close to the outer bank at L7, the groyne caused a reduction of 44% in the velocity u at C1, immediately behind the groyne. The reduction in the velocity u continued to the end of the curve at C9 and the velocities did not recover the initial velocities without groyne.

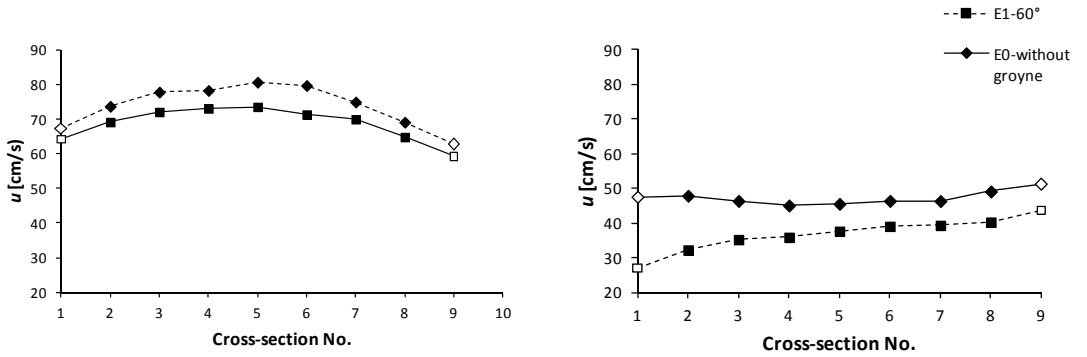

Figure 4.4 *Stream-wise velocities u; at 3 cm above the bottom for (a) for longitudinal profile L1 and (b) for longitudinal profile L7 for test run E1 and E0. White filled symbols indicate longitudinal shifted position (modified from Zaid & Koll 2016a)*

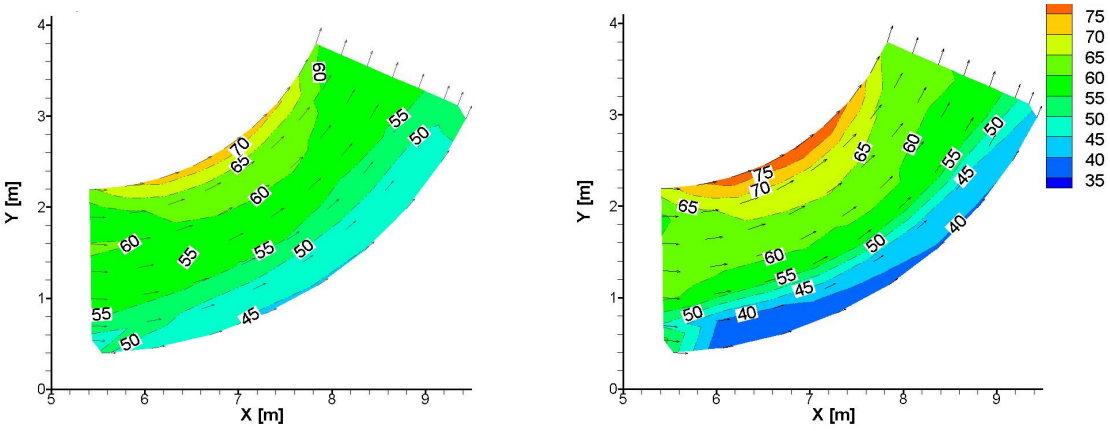

Figure 4.5 *Flow field at 3 cm above the bottom (a) without groyne and (b) with groyne at C1 (E1.1)*

Towards the inner bank at L1, the velocity u increases from 5% at the beginning and the end of the curve to a maximum of 11% at the middle of the curve. Figure 4.5 shows, exemplarily, the top view of the flow field with and without groyne. The cross-sectional view of the flow field of test run E1.1 shows that the entire flow is directed towards the inner bank as in the case of E0 (Figure 4.3a) and no circulation was noted. However in the vicinity of the groyne larger transverse velocities (v) were observed, indicating stronger redirection of the flow towards the inner bank. Starting from cross-section C2, a clock-wise secondary circulation can be noted (Figure 4.6b). In addition, the velocity vectors at the rightmost vertical (Y=2.1 m) show that the flow is going towards the outer bank, indicating another circulation. Two secondary flow cells were observed at the cross-section where the groyne was located from C2 to C9 and will be discussed later in experiment E2.

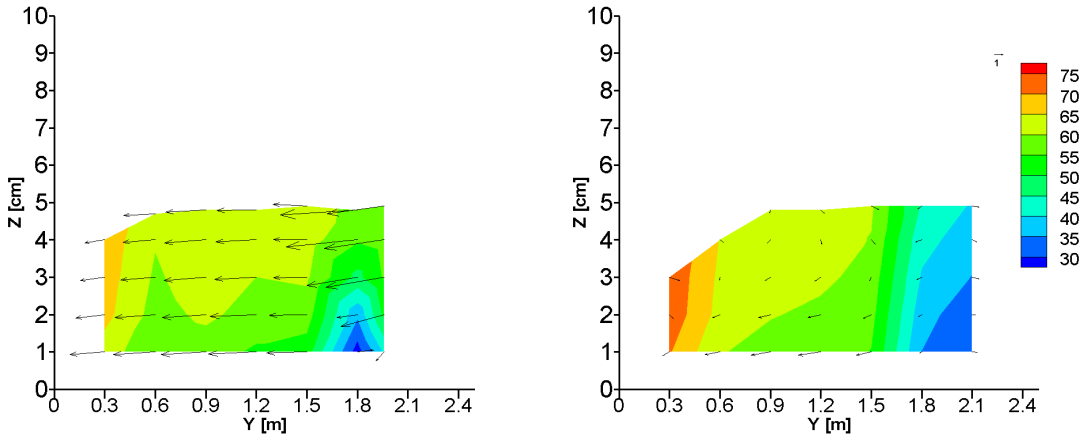

Figure 4.6 Flow field for test run (E1.1), (a) cross-section C1, (b) cross-section C2

To elaborate on the optimum groyne inclination angle the flow field with different groyne inclination angles needs to be understood. As the reduction of the velocity close to the outer bank is a main objective for any bank protection measure (see Chap. 2), it has been taken as criteria for evaluating different groyne configurations. Furthermore the maximum velocity and boundary shear stress zones were found to be coincident in river bend see Figure 2.10 and Figure 2.14. Therefore minimizing the velocity throughout the curve at all vertical levels close to the outer bank was considered as criteria for the optimization of the groyne parameters. In this study, the longitudinal profile L7 which provides the closest velocities to the outer bank at different levels above the bottom, become of high importance in the evaluation of the groyne setups. Therefore, the velocities at L7 for the test runs E1.1 to E1.5 were plotted exemplarily at 3 cm above the bottom (Figure 4.7). The level 3 cm above the bottom was selected because it is the first measurement level above the groyne crest which has a height of 2.5 cm. (Figure 4.7a) shows the effect of the groyne inclination angle on the stream-wise velocities *u*. The maximum effect on the inclination angle was noted at C1, immediately next to the groyne, and decreases throughout the curve. In

fact, when the groyne inclination angle is varied the distance from the groyne to the measurement point at C1 also varied, this contributes to the high differences in the velocities *u* at C1 associated with different inclination angles. A similar pattern was observed at 4 cm, 2 cm and 1cm above the bottom (Figure 4.8). It can be noted that, the differences in the stream-wise velocities at 5, 4 and 3 cm above the bottom due to the inclination angle compared to the case without groyne is insignificant from C2 to C9, except for test run (E1.5) with an inclination angle of 70°. For the flow close to the bottom and below the crest of the groyne the differences in the stream-wise velocities are obvious until around C4 (Figure 4.8). In the vertical direction at 5 cm above the bottom the differences in the velocities due to inclination angle of the groyne becomes small (see Figure 4.8a). This indicates that the effect of the inclination angle decays in the vertical direction.

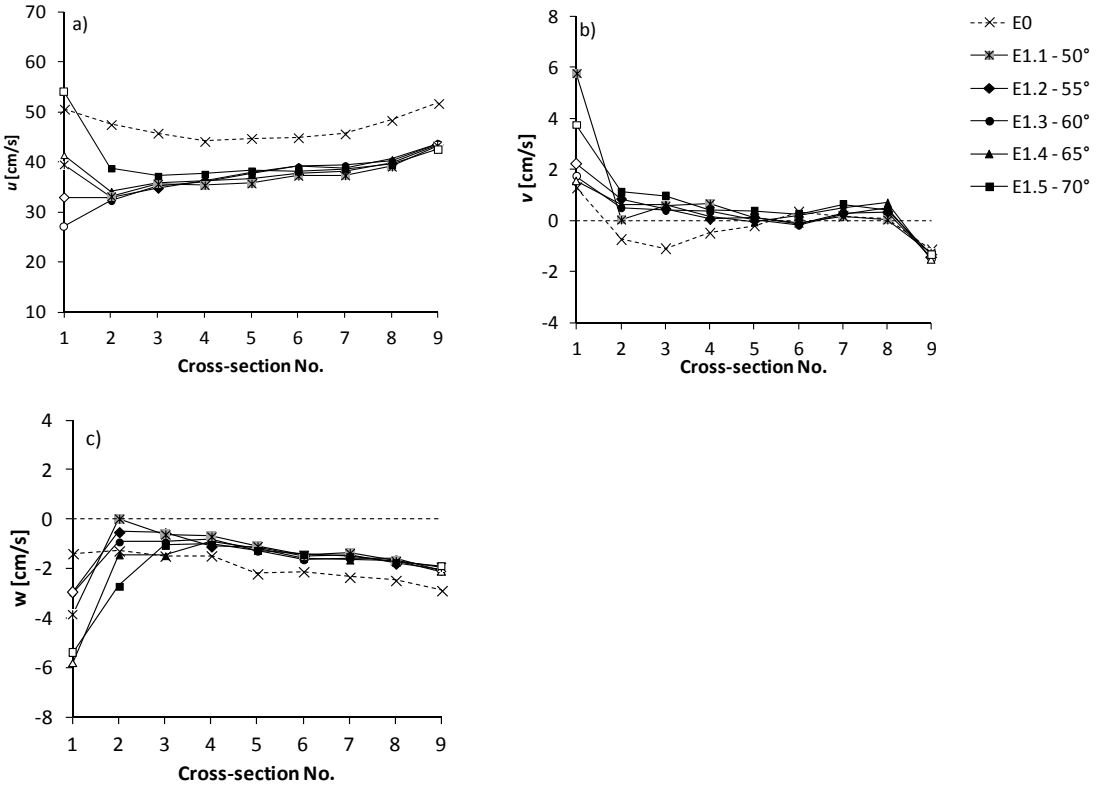

Figure 4.7 *Longitudinal profile L7 3 cm above the bed of (a) stream-wise velocities u, (b) transversal velocities v, and (c) vertical velocities w for inclination angles of 50° to 70°(white filled symbols indicate longitudinally shifted positions)*

The transverse velocities *v* show strong differences at C1; however a relation with the inclination could not been drawn. The strong negative *v* velocities at C9 show the effect of the end of the curve (Figure 4.7b). The changes in the vertical component *w* cannot be sorted according to the inclination angle at C1 whereas at C2 the magnitude of the vertical components *w* increases with increasing inclination angle (Figure 4.7c). The high values of the vertical components *w* at C1 indicate strong redirection of the flow toward the bottom. In the cross-sectional direction, the effect of the inclina-

tion angle was very clear in the longitudinal profile L7 and L6 which are affected by the blockage of the groyne to the flow (see Figure 3.10). From the longitudinal profile L5, the effect of the groyne inclination angle vanishes. At L1 close to the inner bank there was no effect of the inclination angle on the flow field (Figure 4.9). This result is important because the selection of the optimum inclination angle based on the maximum reduction on the velocity close to the outer bank has no effect on increasing the velocity toward the inner bank.

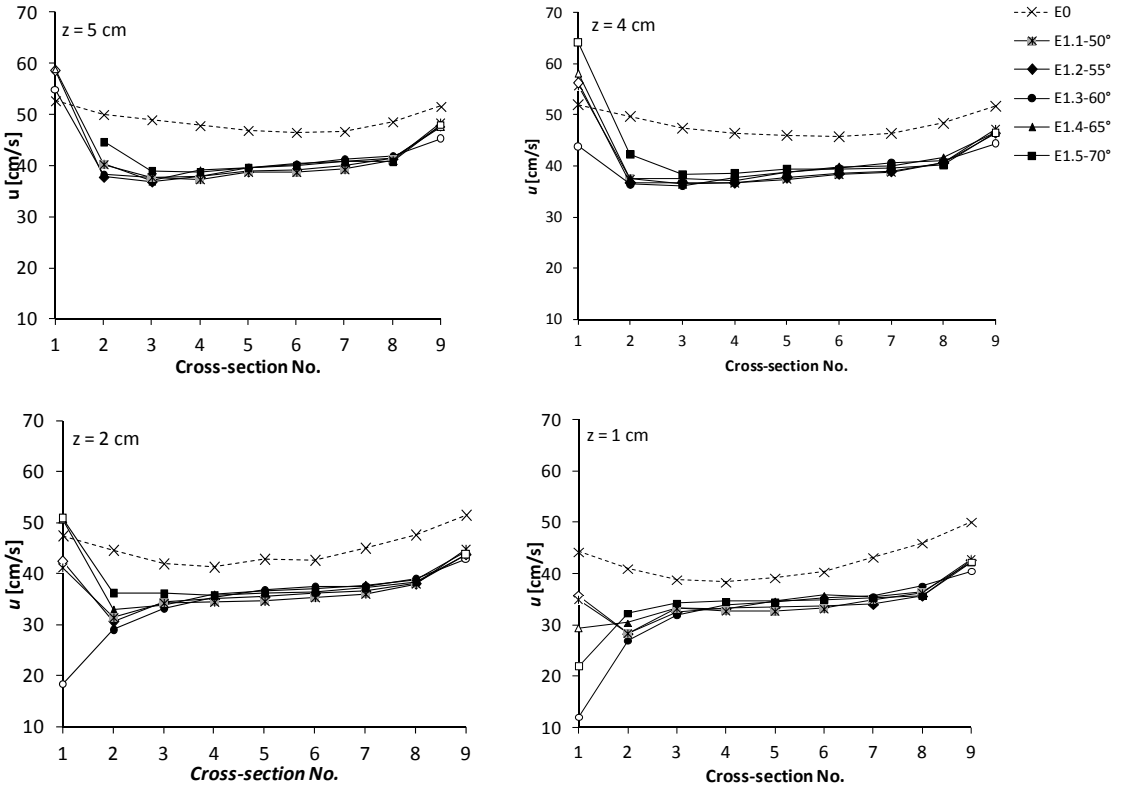

Figure 4.8 Steam-wise velocities at longitudinal profile L7 for inclination angles of 50° to 70° (z is the height above the bottom)

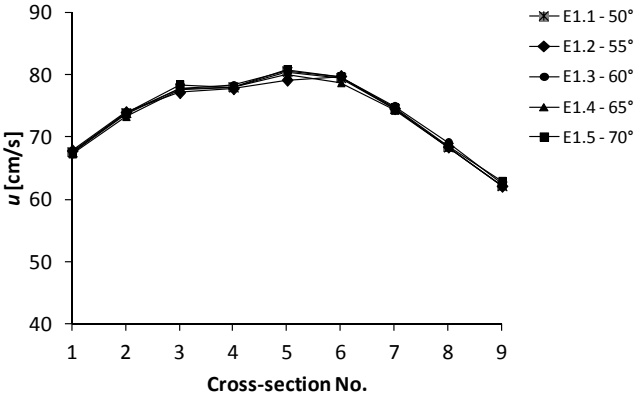

Figure 4.9 Stream-wise velocities at longitudinal profile L1 at 3 cm above the bottom for inclination angles of 50° to 70°

The results show that the effect of the inclination is highly local in the cross-sectional direction, vertical direction and the longitudinal direction. In the longitudinal direction the effect on the inclination extends to approximately cross-section C3 and C4. This local range of the effect of the inclination angle becomes important, considering that the shallow groynes are installed in a series and the second one was found to be at C5 for the groynes with projected length of 80 cm (see Chap.4.4). Accordingly, the evaluation of the reduction in stream-wise velocity over the range from C1 to C4 and over the vertical range from 1 cm to 5 cm above the bottom is necessary in selecting the optimum inclination angle of the shallow groynes. Therefore, the velocities *u* at the levels from 1cm to 5cm above the bottom for the each test run were normalized with the velocities *u* of the same point for the test without groyne (E0). The average normalized velocities for each test run for the range from C1 to C4 and from 1cm to 5cm above the bottom were compared (see Figure4.10). It can be seen from Figure 4.10 that the inclination of 60° provides the lowest average normalized velocity indicating the highest reduction of the stream-wise velocities.

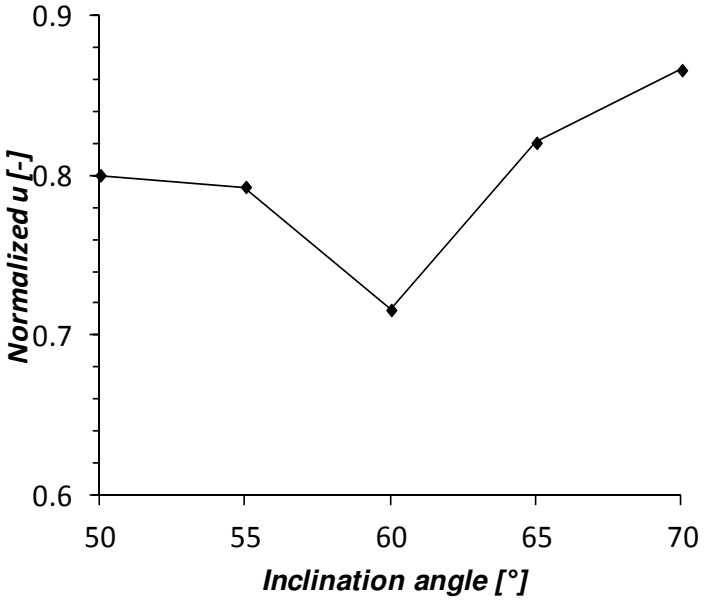

Figure 4.10 Normalized velocity (u/u_0) with respect to the inclination angles (50° to 70°) of the groyne

Furthermore, from the stream-wise velocity at C1, it can be noted that the inclination of 60° provides the heights reduction of *u* velocity from 1 to 4 cm above the bottom (Figure 4.11). At 5 cm above the bottom an acceleration of the flow due to the presence of the groyne was noted. Nevertheless, the inclination of 60° causes the least acceleration of the flow. Accordingly, it can be concluded that the optimum inclination of the shallow groyne is 60°. From this analysis the inclination of 60° can be concluded to be the optimum for the shallow groyne and it was applied for the subsequent experiments for the investigations on other groyne parameters.

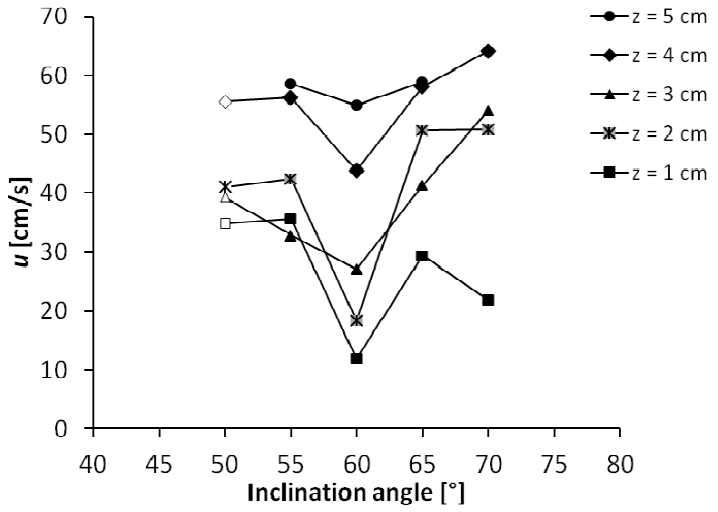

Figure 4.11 Stream-wise velocity u at different z level above the bottom

4.3 The effect of the location of the shallow groyne on the flow field - E2

Groynes are typically installed in a series. The location of the first groyne of the groyne field is an important parameter to be investigated. In order to give a recommendation for the location of the first groyne in the curve, the effect of the groyne location on the flow field need to be understood. Therefore, nine test runs were performed with one groyne located at nine different locations throughout the curve from C1 to C9 (Table 3.3). In each test run the 3D flow field was measured. The results of the test runs were compared against each other and against the test run without groyne (E0). Regarding the groyne inclination angle, the outcome of the experiment E1 was considered and the inclination of 60° was taken for the all the test runs.

The results of the test run E2.1 with the groyne installed at C1 were discussed previously in the test run E1.1. The redirection effect of the groyne was obvious and the velocities towards the outer bank were reduced, on the other hand the velocities close to the inner bank were increased (Figure 4.5b).

In the cross-sectional direction and similar to what was mentioned before in Chap. 4.1 and Chap. 4.2, the primary cell of the secondary flow circulation (clock-wise) was developed always between C1 and C2, independent of the location of the groyne. However, locally where the groyne was installed, except at C1 (Figure 4.6a), a smaller outer secondary flow cell was found. Both secondary flow cells are presented exemplarily at C5 (Figure 4.12a). At C9 the outer circulation was somehow different (Figure 4.12b). This could be attributed to the shifted position of the measurement point at L7 which is upstream the groyne (Figure 3.6). The outer cell circulates in a counter-clock-wise direction, opposite to the primary secondary flow cell.

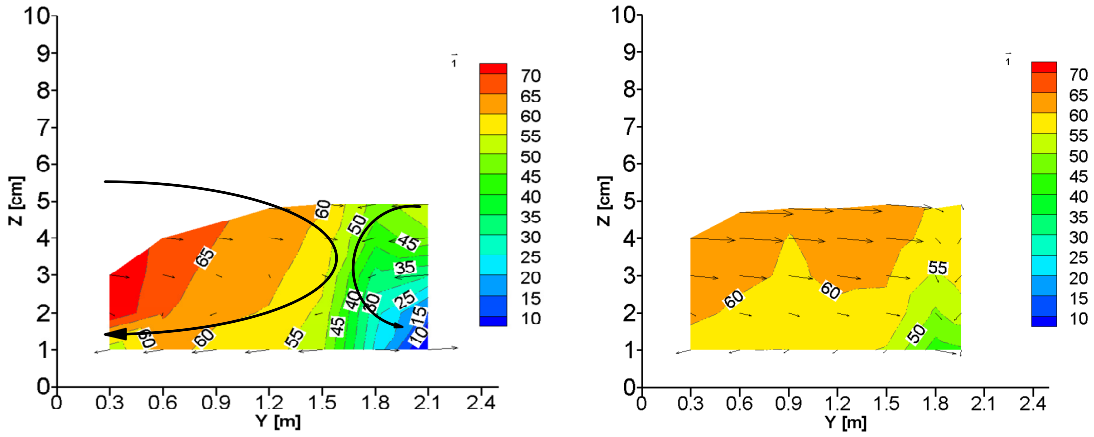

Figure 4.12 3D Flow field, (a) at cross-section C5 (b) at cross-section C9

To evaluate the effect of the groyne location on the flow field, the longitudinal profile L7 was selected. The stream-wise velocities of all test runs of E2 are shown in Figure

4.13. Regardless of the location of the groyne, a significant effect of the groyne on the flow field was evident locally at the cross-section where the groyne is located and the following cross-section in the downstream direction. The effect of the groyne decays in the downstream direction. In the region upstream of the groyne the effect of the groyne is minor compared to the downstream effect; however, at the end of the curve from C7 to C9 the upstream effect and the downstream effect are comparable (Figure 4.13).

In the vertical direction the experimental data show that the effect of the groyne on the flow field is very much dependent on the height above the bottom. This can be related to the obstruction of the flow by the groyne, and whether the flow is above or below the groyne crest level. Due to the obstruction caused by the groyne an accelerated flow was observed at the cross-section where the groyne is installed at (z = 5 and 4 cm) (see Figure 4.13a,b). The accelerated flow is plunging behind the groyne forming water surface with standing waves (Figure 4.14). This flow condition around and behind the groyne is favourable for local bank erosion; therefore, investigations were carried out to reduce this effect (Chap.4.9). It can be noted that the acceleration due to installing the groyne towards the end of the bend (second half of the bend) is higher than towards the first half of the bend (Figure 4.13a,b). After the acceleration zone, the highest reduction of the stream-wise velocity takes place at the cross-section immediately after the groyne. At (z = 5 and 4 cm) the maximum reduction on the stream-wise velocity was found when locating the groyne at C1. In depended of the groyne location the velocity line of the test run E2.2 to E2.8 collides with the velocity line of run E2.1. The level z = 3 cm is only 5 mm above the groyne crest which is 2.5 cm from the flume bottom. At this level and at (z = 2 cm and 1 cm) the velocity u was always decreased for all the test runs. In this region there is a significant reduction of the velocities u at the location of the groyne. This indicates the high influence of the groyne on the near bed flow. Although the reduction of the velocity u downstream the groyne decreases throughout the curve, the velocities dose not recover to the case without the groyne (E0).

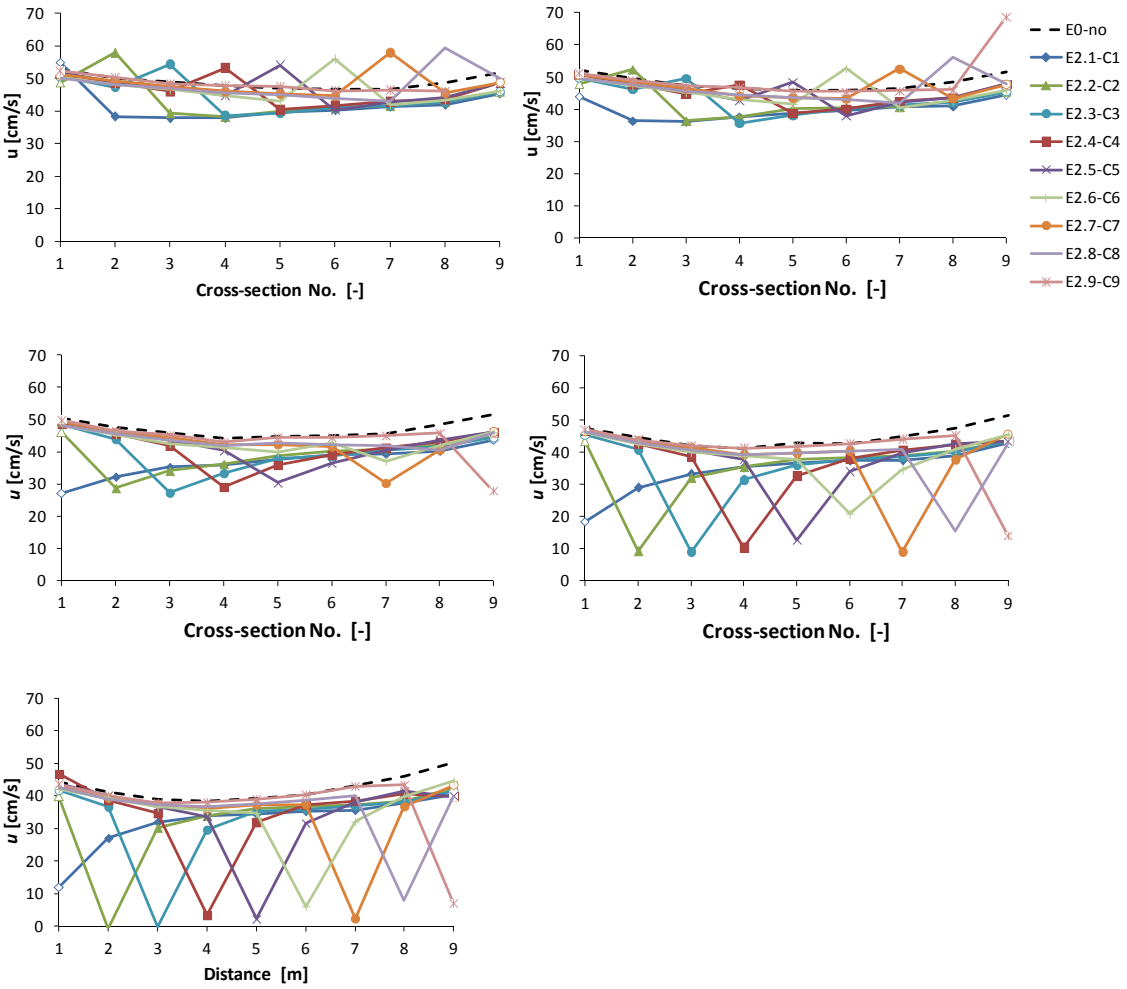

Figure 4.13 Stream-wise velocities u at longitudinal profile L7

Figure 4.14 Photo of the waves downstream of the groyne at C5

It can be noted that at z = 2 cm and 1 cm the reduction in the stream-wise velocities at the location of the groyne for the test run E2.1 is less than the test runs E2.2 to E2.9, except of E2.9 at z = 2 cm. This can be attributed to the effect of the shifted position at C1 (see the measurement grid, Figure 3.6). This effect of the measurement location at C1 can be noted also on the acceleration at z = 5 cm and 4 cm for

the test run E2.1, in which less acceleration was noted whereas higher acceleration was expected (Figure 4.13a, b).

The transverse velocities v at the longitudinal profile L7 are plotted in Figure 4.15. The overall direction of the transverse velocities at 5 cm above the bottom is towards the outer bank (indicated with negative v values), however, locally at the cross-section where the groyne is located, strong redirection of the flow toward the outer bank was noted (Figure 4.15a). On the other hand at 1 cm above the bottom the general direction of the velocities v is towards the inner bank (indicated with positive v values) whereas at the location of the groyne strong redirection toward the outer bank is evident (indicated with negative v values). The high v values at the groyne location indicate the outer bank cell which circulates in the opposite direction of the primary secondary cell. It can be noted from Figure 4.15 that the strength of the outer bank secondary cell is higher towards the end of the curve.

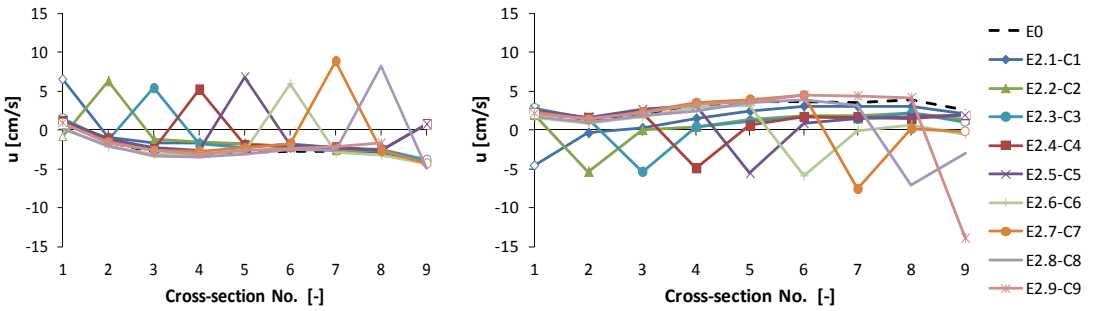

Figure 4.15 Transverse velocities v at the longitudinal profile L7, (a) 5 cm above the bottom (b) 1 cm above the bottom

The analysis of the stream-wise velocities at L7 shows the advantage of placing the groyne toward the beginning of the curve. In this region the reduction in the stream-wise velocities is higher than towards the end of the curve. At the same time the acceleration of the velocity due to the installation of the groyne is less at the first half of the curve than the second half.

The aforementioned analysis was done using the measured data up to 5 cm above the bottom (half the water depth) due to some limitation of the down-looking Vectino probe. In order to get information on the flow field in the upper half of the water depth, complementary measurements with the Vectrino side-looking probe were carried out for the experiment E0, E2.1 and E2.5. The stream-wise velocities at L7 at the levels from 5 cm to 9 cm above the bottom for E2.1 and E2.5 were normalized with the stream-wise velocities of the corresponding levels at E0 (see Figure 4.16). If the normalized < 1 means that the groyne causes a reduction in the velocity of E0, whereas normalized velocities > 1 that means the groyne causes higher velocity than in case without groyne E0 (acceleration).

The results of the side-looking probe showed that the local effect of the submerged groyne on the stream-wise velocity was evident thoughtout the water depth. Figure 4.16a shows that the reduction in the velocity downstream of the groyne at C2 and C3 depends on the level above the bottom. Figure 4.16b for the test run E2.5 shows that the acceleration in the flow is very obvious and the reduction in velocity is very minor. It is to be noted that the side-looking probe velocities were higher than the down-looking probe velocities by 4.5 cm/s and 5.8 cm/s at C5 and C6 where the difference for the other cross-section was in the order of ± 2 cm/s. The measurements with the side-looking probe are supporting the conclusion made before that locating the groyne towards the beginning of the bend gives higher reduction in the stream-wise velocities and lower local acceleration at the groyne location.

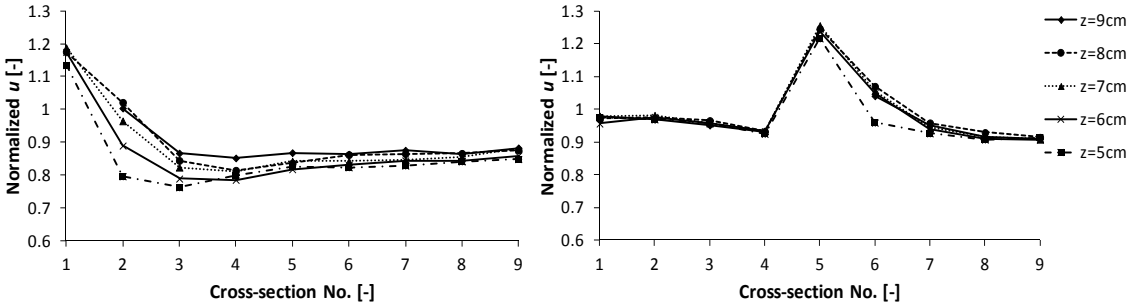

Figure 4.16 Normalized stream-wise velocities (u/u_{E0}) at L 7 for different levels above the bottom (side-looking probe)

4.4 Detailed flow field around the groyne - fine grid - E3

Detailed velocity measurements with a fine grid were carried out with one groyne installed at C5. The objective was to investigate the flow field around the groyne with finer resolution and to check whether the regular coarse grid (Figure 3.6) has enough resolution to capture the flow field with a groyne installed. The detailed setup of the test run with fine grid is shown in Chap. 3.2.

The results of the velocity measurement are shown exemplarily at 4 cm and 1 cm above the bottom. Figure 4.17a shows the accelerated flow over the groyne at 4 cm above the bottom. It can be seen that there are three zones of high velocity, one at the groyne tip, the second in middle of the groyne and the third adjacent to the bank. The high velocity zone in the middle of the groyne is extending further downstream with two adjacent low velocity zones. The velocity vectors immediately behind the groyne show redirection of the flow towards the outer bank. Close to the bottom, the groyne provided significant reduction on the flow velocity and no high velocity zone was noted around the groyne except close to the groyne tip (Figure 4.17b).

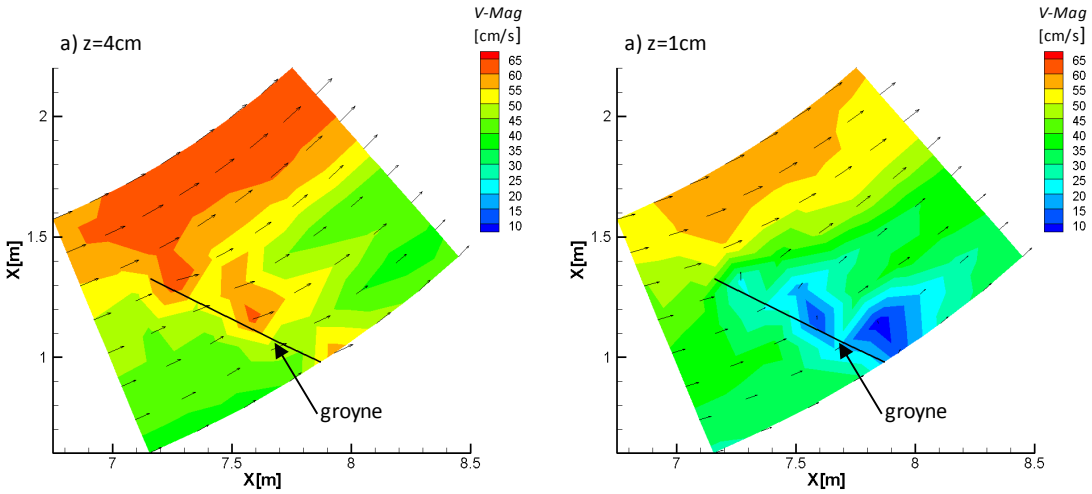

Figure 4.17 *3D Velocity field for the fine grid measurements at z=4 (a) and z=1cm above the bottom (b), V-mag is the velocity magnitude*

To compare the fine grid with the coarse grid measurements, three vertical velocity profiles in three measurement points at the longitudinal profile L7 were used (Figure 4.18). The comparison showed that the vertical and longitudinal resolution of the coarse grid is adequate to capture the flow field with the groyne installed at C5. However, the fine grid showed the local accelerated flow at the groyne location (see Figure 4.18e). In the cross-sectional direction the 3D velocity field at C5 for both grids is shown in Figure 4.19. The stream-wise velocities show an almost similar pattern, however, the fine grid shows the high velocity zone in the middle of the groyne on the M-shaped pattern at the lower right part of the cross-section (Figure 4.19b).

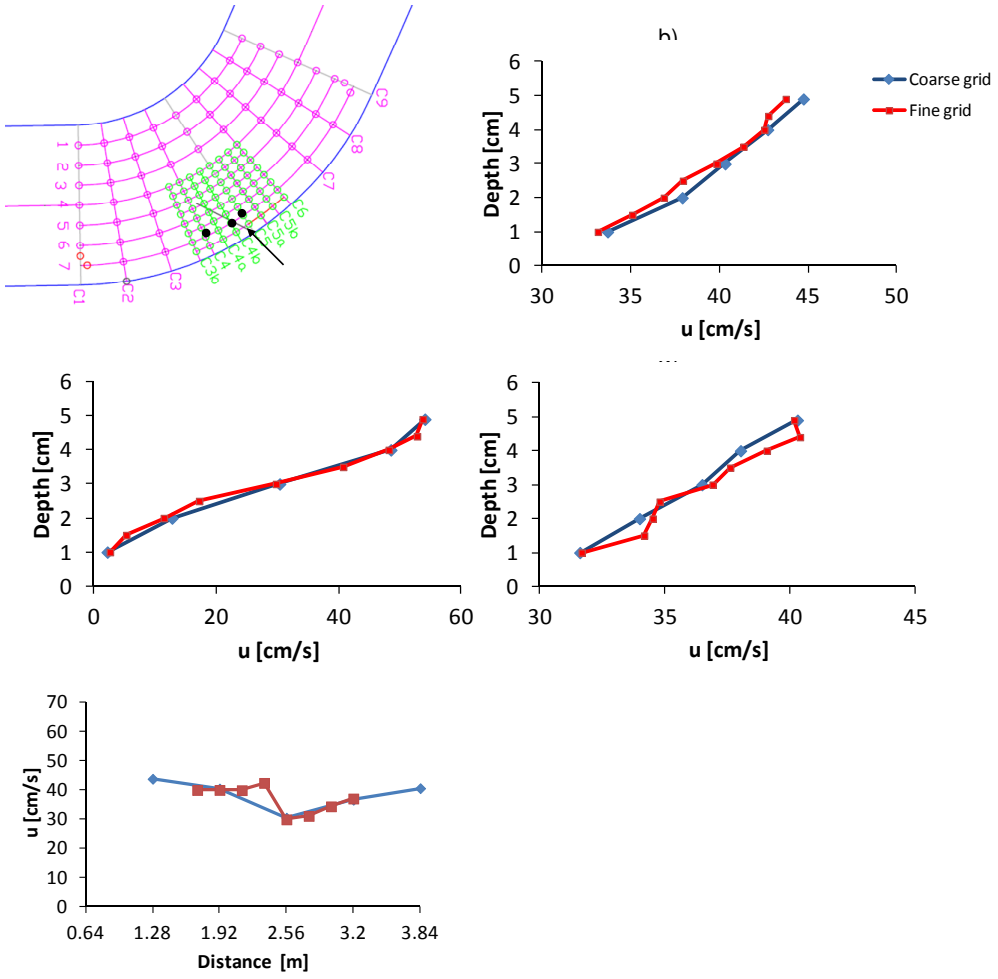

Figure 4.18 *a) Definition sketch of the coarse and fine grid. Stream-wise velocities at L7, in front of the groyne (b), at the groyne (c), downstream the groyne (d) and (e) at longitudinal profile L7, 3 cm above the bed*

The velocity vectors of both grids show comparable patterns. The main clock-wise secondary cell and outer counter-clock-wise secondary cell were obvious in both grids. The measurements confirm the adequacy of the coarse grid capturing the flow field in the presence of a groyne.

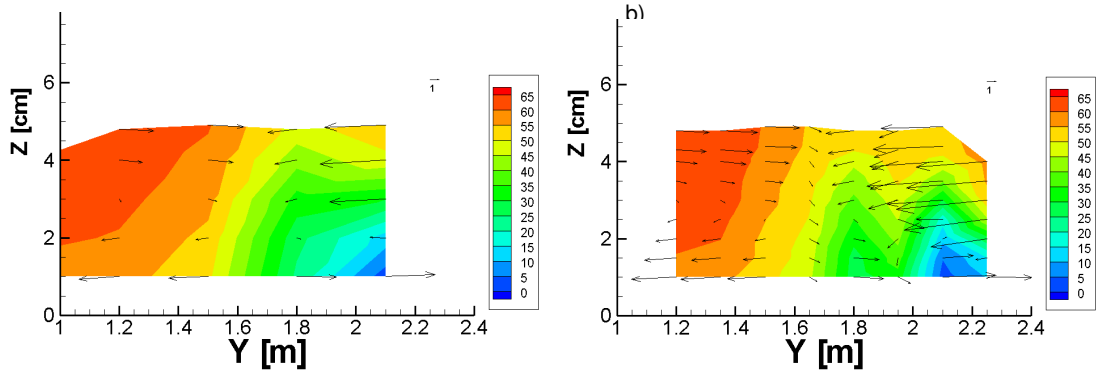

Figure 4.19 *Cross-sectional 3D view at cross-section C5, (a) with coarse grid (b) with fine grid*

4.5 The effect of the projected length of the groyne on the flow field E4

The projected length is the perpendicular distance from the groyne tip to the tangent at the bank. The projected length of the groyne is an important parameter to be studied as it determines the length at which the groyne obstructs the flow. To investigate the effect of the projected length, three groynes with three different lengths were built (80 cm, 69.3 cm and 40 cm). The projected length of 69.3 cm corresponds to groyne length of 80 cm. In each test one groyne was used (see Table 3.4). The test runs E1.1 and E2.2 represent the test with 80 cm projected length at C1 and C2 respectively. The selection of C1 and C2 for the test was based on the results of experiment E2 in which the effect of the groyne was found to be stronger at the beginning of the curve than at the end of the curve. To evaluate the effect of the projected length of the groyne, again the velocities at the longitudinal profile L7 were considered. Figure 4.20 shows the stream-wise velocities of L7, at 5 cm, 3 cm and 1 cm above the bottom.

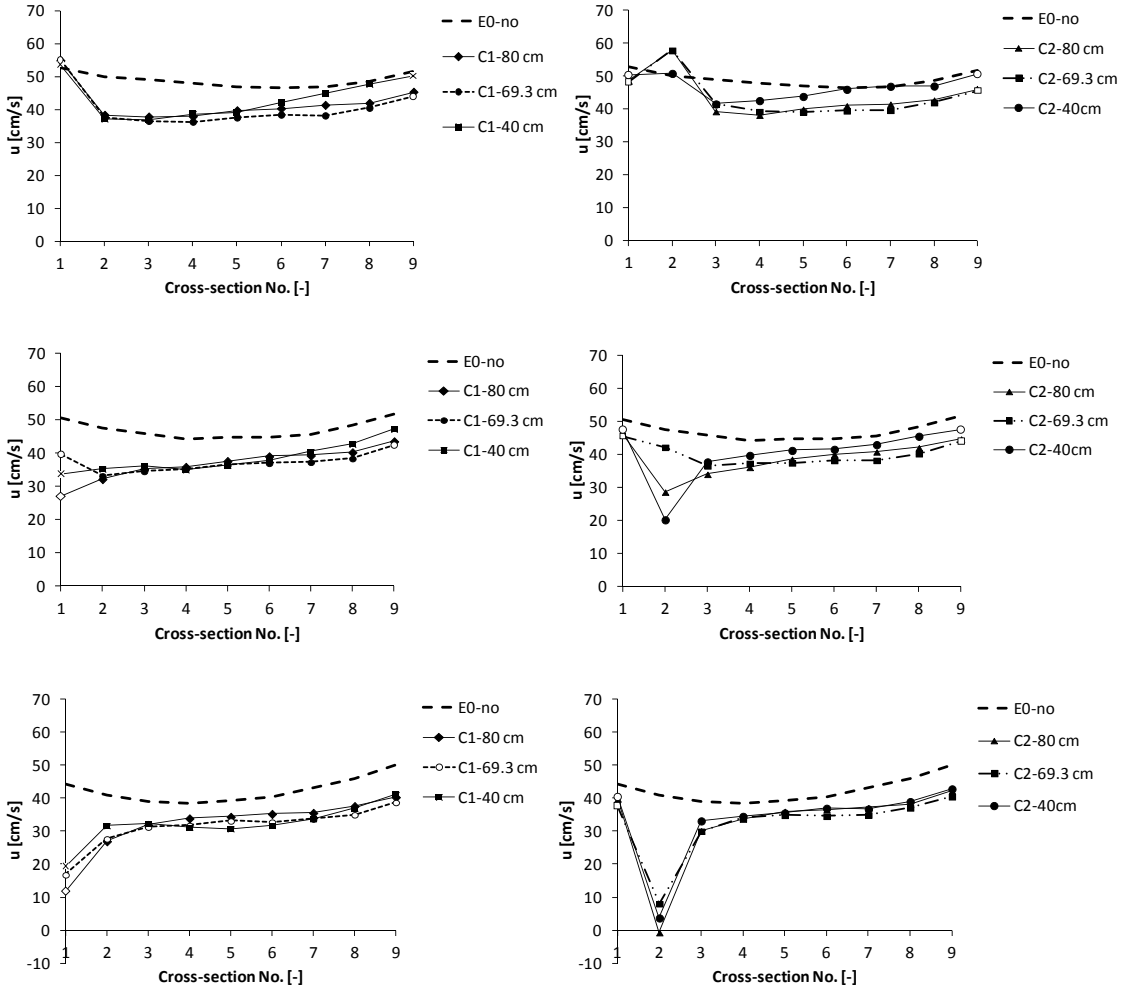

Figure 4.20 Stream-wise velocities at longitudinal profile L7 for the groyne at C1, (a) 5cm, (c) 3cm and (e) 1cm above the bottom and at C2 (b) 5cm, (d) 3cm and (f) 1cm above the bottom

It can be noted from Figure 4.20 that at 5 cm and 1 cm above the bottom the stream-wise velocities of the projected lengths of 80 cm and 69.3cm are comparable with a difference less than 5%, except at C1, where the projected lengths of 80 cm shows higher reduction in the stream-wise velocities at all levels above the bottom.

A similar pattern was noted at 3 cm above the bottom for the groyne of 80 cm and 69.3 projected length, however, the stream-wise velocities at C2 for the groyne of 69.3 cm were significantly higher than for the groyne of 80 cm projected length (Figure 4.20d). In case of the groyne with 40 cm projected length, the stream-wise velocities at 5 cm above the bottom at C1 show comparable patterns to groynes with of 80 cm and 69.3 cm projected lengths until C6 after which the velocities start to increase till they recover to the case without groyne around C8 (Figure 4.20a). At C2 the stream-wise velocities were recovering earlier at around C6 (Figure 4.20b). At 3 cm above the bottom at C1 the recovery of the velocities close to the end of the curve was obvious in case of 40 cm projected length. At the same level at C2 the stream wise velocities of 40 cm was always higher than at 80 cm and 69.3 cm except at C2 where the velocities were the least. The results of experiment (E4) show the advantage of using groyne with longer projected length than shorter ones. Longer groynes provide higher reduction on the stream-wise velocities close to the outer bank. The extent of the reduction in the velocities is longer in the case of longer groynes than in the case of shorter groynes, where the velocities recover at the second half of the curve. Considering the fact that groynes are installed typically in a series, the option of 40 cm projected length still need to be studied in connection with the study of the groyne spacing. This is because installing the second groyne before the velocities recover can maintain the reduction of the stream-wise velocity for longer distance throughout the curve; therefore groups of groynes with 40 cm projected length were tested as well and discussed in Chap. 4.7. In addition to that, the projected length of 40 cm shows very minor acceleration of the velocities at C2 at 5 cm above the bottom and no acceleration at 4 cm whereas 80cm and 69.3 cm projected lengths show highly accelerated flow at both aforementioned levels above the bottom.

4.6 The effect of the groyne width on the flow field - E5

To investigate the effect of the groyne width on the flow field three groynes with different widths were used (3 cm, 6 cm and 9 cm). The projected length of the groynes was kept constant (80 cm). The three groynes were tested at C1 and C2 for the same reason described before in Chap. 4.5. The details of the test runs are shown in Table 3.5.

The results of the test runs show that the effect of the groyne width is highly local in both the longitudinal and vertical directions. In the longitudinal direction the effect of the width vanishes from C3. In the vertical direction the effect vanishes at 5 cm and 2 cm above the bottom (Figure 4.21a). The differences in the velocities due to the width can be noted at 4 cm and 3 cm above the bottom (Figure 4.21b,c). At these levels the widths of 3 cm and 6 cm show comparable results, however at C1 6 cm groyne give higher reduction in *u* and 3 cm groyne gives higher reduction at C2. The wider groyne (6 cm) gives significantly higher stream-wise velocities at 4 cm and 3 cm above the bottom. This accelerated flow due to wider groynes is favouring local scour around the groyne. Since the wider groynes (i) increase the accelerated flow (ii) requires more construction material and (iii) did not yield in higher reduction on the stream-wise velocities; it is not recommended to use groyne wider than 6 cm. The results also show (Figure 4.21) that the thin groyne (3 cm) can also be used to get the same order of reduction in the velocities as in case of 6 cm groyne.

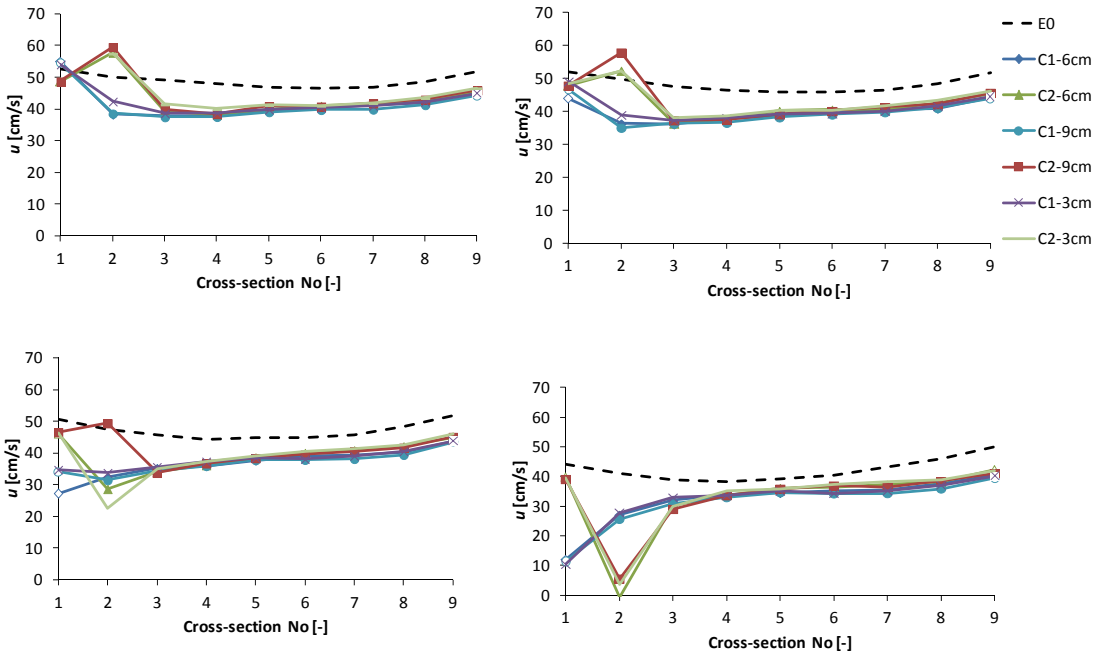

Figure 4.21 Stream-wise velocities at L7 and groyne at C1and C2, (a) 5cm, (b) 4cm, (c) 3cm and (d) 2 cm above the bottom

4.7 The effect of group of groynes on the flow field - E6

In this experiment different groups of groynes were investigated. The number, spacing, location and the length of groynes were varied and the flow field was measured. The objective of the test was to optimize the group of groynes in order to find out the optimum location and the spacing between the groynes. The criterion for the optimum spacing is the least number of groynes that provide the maximum reduction of the stream-wise velocity at L7 close to the outer bank. Twelve test runs were performed; five of which with a projected length of 80 cm, two runs with a projected length of 69.3 cm and five runs with a projected length of 40 cm (see Table 3.6). To evaluate the results, the test runs with two groynes and a projected length l_p= 80 cm were evaluated together. The location of the two groynes was varied and the spacing was kept the same. In the experiment E6.2 the groynes were located at C1 and C9 whereas in run E6.3 at C5 and C9 and in run E6.4 at C1 and C5. Figure 4.22 shows exemplarily the stream-wise velocities at L7 at 5 cm, 3 cm and 1 cm above the bottom. The test run E6.4 showed the lowest stream-wise velocities at all the measured level except at C9 at 3 cm and 1 cm above the bottom. This is due to the high local effect of the groyne located at C9 in the other two test runs. Installing one groyne at C1 and at C9 (E6.2) showed the same order of stream-wise velocities at 5 cm above the bottom in the beginning of the curve with increasing trend in the velocity towards the end of the curve. The water depth at C9 was smaller than 10cm due to high accelerated flow over the groyne. That why the point at C9 at 5 cm above the bottom could not be measured.

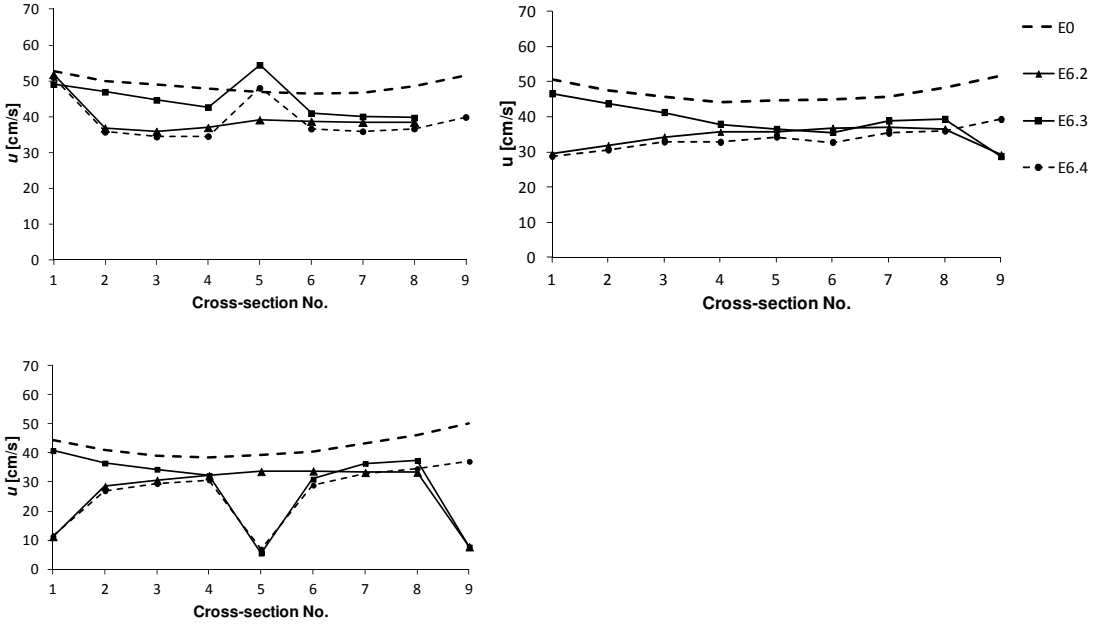

Figure 4.22 Stream-wise velocities u at longitudinal profile L7 measured at (a) z=5cm, (b) z=3cm and (c) z=1cm above the bottom for three different groyne location in E6.2, E6.3 and E6.4 using two groynes (l_p =80cm) and test run E0 without groyne

At 3 cm above the bottom the velocities of E6.2 were slightly higher than E6.4 whereas at 1 cm above the bottom the velocities where comparable with E6.4 except at C5 where the effect of the groyne in E6.4 is noticeable. In the case of E6.3 where one groyne was installed at C5 and another one at C9, the stream-wise velocities at 5 cm above the bottom were the highest, showing the least reduction of the stream-wise velocities among the three test runs. At 3 cm and above the bottom the velocities at the beginning of the curve were the highest and from C4 the velocities were comparable to E6.3 with a slight increase in the velocities at C7 and C8. The same trend was noted at 1 cm above the bottom, except at C5 for E6.2 where no groyne was installed. From this analysis it can be concluded that installing two groynes at the beginning of the curve (C1 and C5) resulted in the highest reduction in the stream-wise velocities at L7 except at C9. However, considering that the maximum scour at the bank was observed downstream of the bend exit (Figure 4.32a) the need for a groyne at C9 becomes obvious. For further analysis the test run E6.4 with two groynes was compared with run E6.1 with three groynes at the same spacing as will come later in this chapter. The test runs with three groynes having a projected length of 80 cm are shown in Figure 4.23. In this test the spacing between the groynes of each group was different; 2.72 m in test run E6.1 and 1.36 m in test run E6.5. It can be seen from Figure 4.23a that the three groynes at smaller spacing (E6.5) resulted in slightly lower stream-wise velocities except at C3 where a significant increase in the velocity was induced by the presence of the groyne at C3.

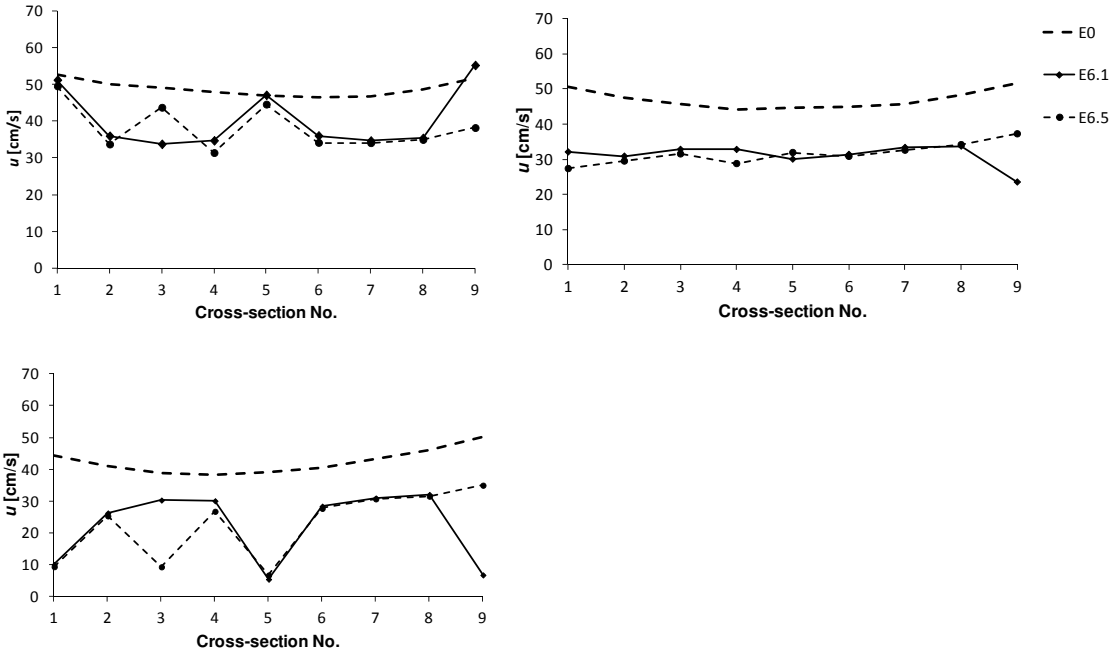

Figure 4.23 Stream-wise velocities u at Longitudinal profile L7 measured at (a) z=5cm, (b) z=3cm and (c) z=1cm above the bottom for three groynes with two different spacings (E6.1 and E6.5 ; l_p =80cm) and test run E0 without groyne

The maximum reduction in *u* at 5 cm above the bottom was 7% higher than in case of larger spacing (E6.1). Countrarily, the velocity *u* at C3 was 30% higher than in large spacing tests (E6.1).

At 3 cm above the bottom (Figure 4.23b) slightly lower velocity at the first half of the curve with smaller spacing was noted whereas at C9 the velocity was higher because there was no groyne installed at C9. At 1 cm above the bottom (Figure 4.23c) the effect of the two spacings on the stream-wise velocities was the same except at C3 and C9 where a groyne was installed in E6.5 and E6.1, respectively. Considering the miner effect on the velocity of the small spacing compared to the large spacing, it was decided to select the large spacing test (E6.1) as the optimum spacing for the group of groynes.

The aforementioned analysis on the tests with three groynes and on two groynes yielded two optimum groups of groyne, E6.4 in case of two groynes and E6.1 in case of three groynes. It is therefore important to compare the two groups of groyne that came out from the first and the second analysis. To do so, the stream-wise velocities at L7 for E6.1 and E6.4 were plotted in Figure 4.24 which shows that the velocities of E6.4 and E6.1 are comparable except at C9. Because there is no groyne at C9 for run E6.4 slightly increasing trend in the velocities can be observed from C6 to the end of the curve. Considering this comparison and the results of the scour down-stream the bend exit, the configuration of (E6.1) with three groynes (C1, C5 and C9) was considered to be the optimum.

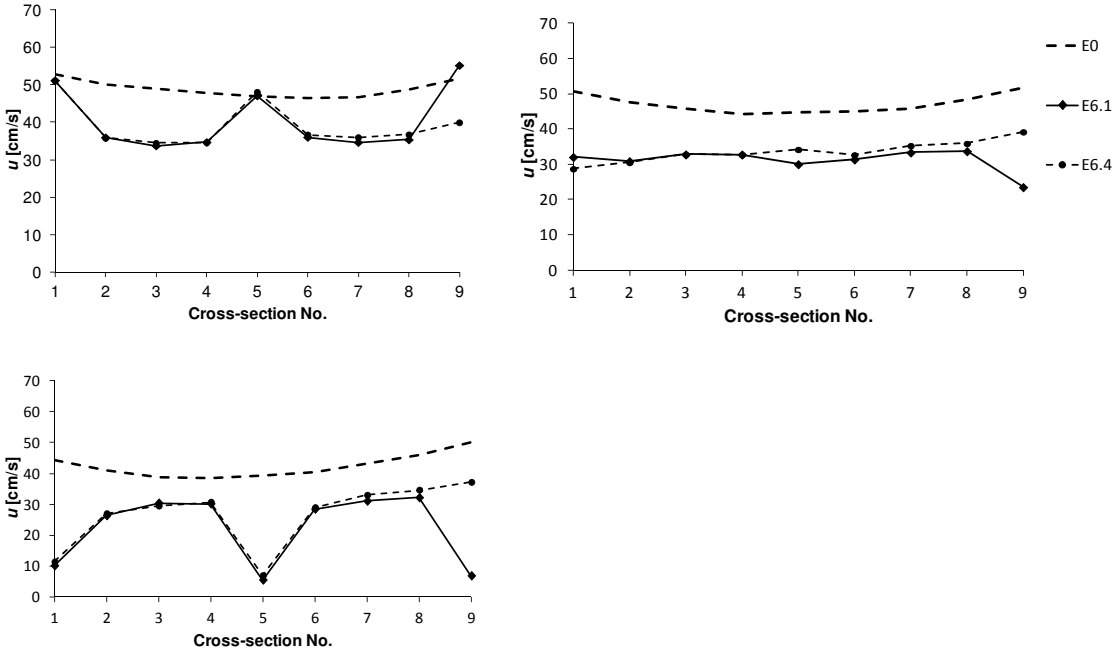

Figure 4.24 Stream-wise velocity u at Longitudinal profile L7 at (a) z=5cm, (b) z=3cm and (c) z=1cm above the bottom for test runs with three groynes (E6.1), two groynes (E6.4) and E0 without groyne

The location of the groynes in the optimum configuration (E6.1) was studied in order to draw a method to describe it. Figure 4.25 shows the location of the groynes in E6.1 with respect to a line at the groyne tip which is parallel to the tangent at the groyne toe and extends in the downstream direction until crossing the curve. It was found that the second groyne is located only 8 cm upstream of the intersection point between the extended line from the groyne tip to the curve. In the case of the third groyne the difference was 14 cm. Considering that the spacing between the groynes is 2.7 m, the difference of 8 cm and 14 cm account to 3% and 5% of the spacing length respectively and can be considered negligible. Therefore, the geometric method shown in Figure 4.25 was proposed to determine the location of the groynes in the groyne field. In the following tests the location of the groyne which was determined using this geometric method is referred to as 'constructed location'.

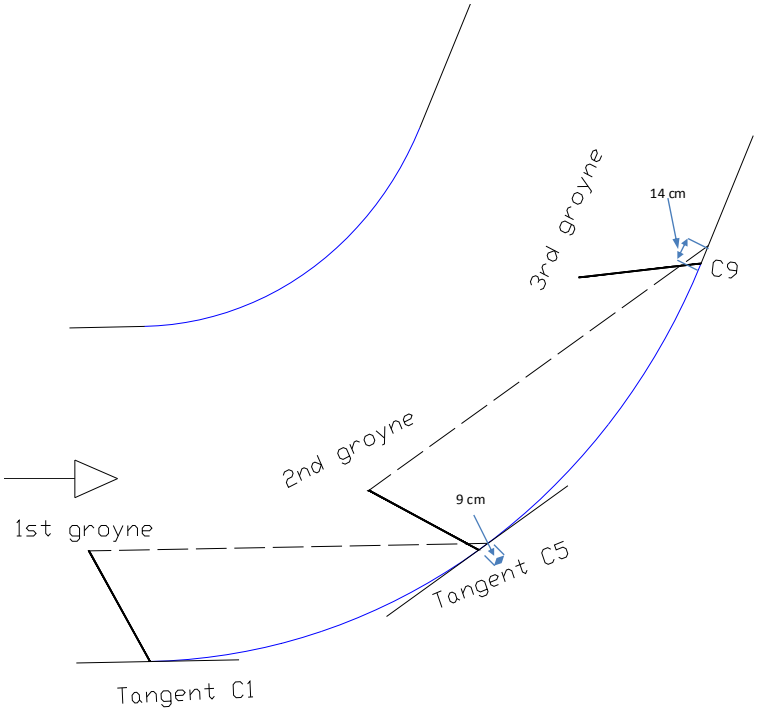

Figure 4.25 Geometric method to determine the groyne location

The analysis of the test run E1.1 with one groyne at C1 gives an explanation for the geometric method described before. As can be seen in Figure 4.4a for the streamwise velocities at L7 at 3 cm above the bottom the reduction of the velocities is very high at C1 where the groyne is located and decreases in the downstream direction until C5, after which the reduction becomes almost constant. Therefore, the next groyne should be located where the local effect of the groyne becomes constant.

This geometric method to determine the position of the groynes was checked in the subsequent test with groynes having a projected length of l_p = 69.3 cm. The comparison between the test run E6.6 with two groynes, one located at C1 and the second

one at the constructed location and the test run E6.7 with two groynes one located at C1 and the second at C5 is shown in Figure 4.26. It can be noted that at 5 cm above the bottom, E6.6 shows slightly lower velocities at the beginning of the curve and significantly lower velocities at C5 compared to E6.7 (see Figure 4.26a). At 3 cm above the bottom the velocities of E6.6 and E6.7 are almost the same. Close to the bottom E6.7 shows significantly lower velocities at 1 cm above the bottom.

The geometric method for determining the groyne location was applied as well for two shorter groynes having a projected length of 40 cm (E6.8) where the first groyne was located at C1 and the second one at the constructed location. Figure 4.26 shows that for the shorter groynes (E6.8) the velocities *u* are lower in the first half of the curve at 5 cm and 3 cm above the bed. However, the velocities *u* are increasing in the second half of the curve. Close to the bottom, the velocities were in the same order of E6.7 and E6.6 except at the location of the second groynes. At C9 a slight increase of the velocities in (E6.8) can be noted. The trend of the velocity recovery in the second half of the curve in case of the short groynes (l_p =40 cm) indicates the need for a third groyne to keep the reduction in the velocity achieved in the first half of the curve. Accordingly, three groynes with a projected length of 40 cm were investigated in test run E6.9.

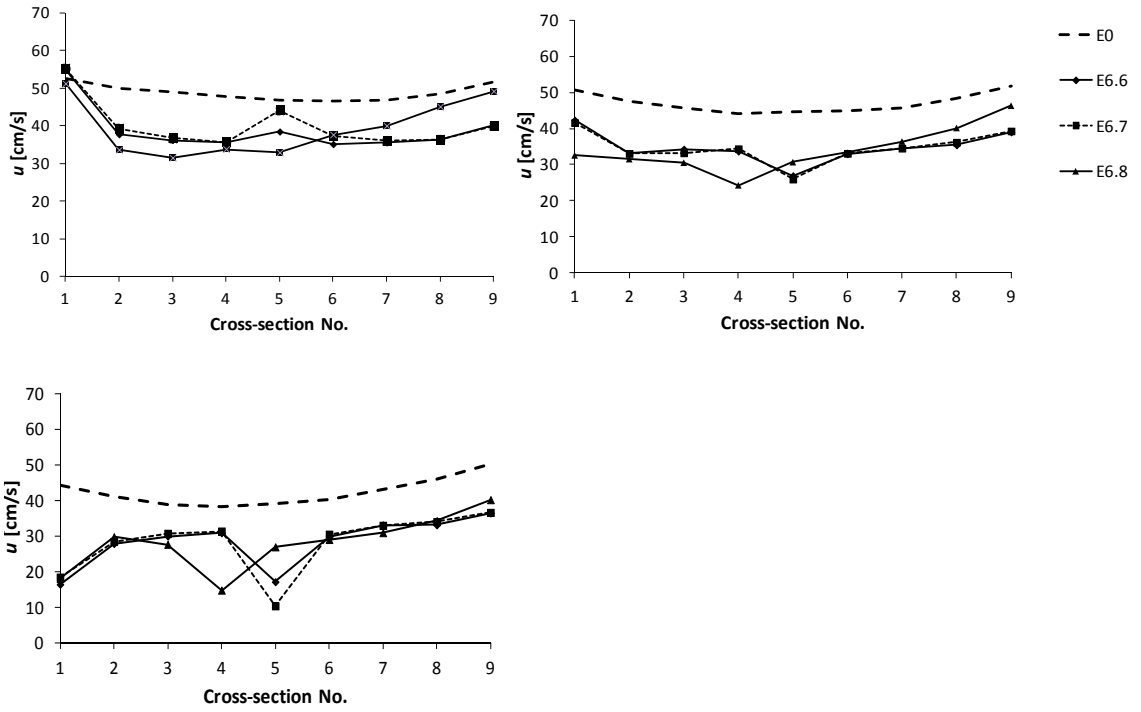

Figure 4.26 Stream-wise velocities at L7 at (a) z=5cm, (b) z=3cm and (c) z=1cm above the bottom for test runs with two groynes E6.6, E6.7 and E6.8 and test run E0 without groyne

To finalize the investigations of the groyne spacing the test run E6.1 with three groynes (l_p =80 cm) which was found to be the optimum was compared with the test run

E6.9 with three groynes having a projected length of 40 cm and a location defined by the geometric method discussed before. An additional test E6.11 was carried out with three short groynes; the first one located at C9 and the second and the third were defined with the geometric method but in the upstream direction. The spacing setting in E6.11 complies with the spacing method recommended for stream barbs by the USDA Kansas Engineering Technical Note No KS-1 2013 (see Figure 2.21). The results of the aforementioned three tests are shown in Figure 4.27. At 5 cm above the bottom E6.11 show slightly smaller velocities till C7 compared with E6.1, except at C5 where the velocity is significantly slower than at E6.1. This is due to the acceleration over the groyne at C5 in E6.1. It was observed that the shorter groynes (l_p =40 cm) introduce less acceleration at the location of the groyne and the flow surface shows less waves than in the case of long groynes (l_p =80cm) (see Figure 4.27a). At C8 and C9 the velocity *u* was significantly increasing implying that three short groynes (l_p =40cm) are not enough and an additional fourth groyne is required. At the same level above the bottom, the test run E6.11 showed the smallest reduction of the velocity *u.* At 3 cm above the bottom E6.9 shows lower velocities at C4 and C7 and increasing velocities at C8 and C9 compared to E6.1. E6.11 shows the smallest reduction in *u* except locally close to the groynes location (C9, C6 and C3) where the reduction in the velocities *u* was significantly higher than the other two tests (Figure 4.27b).

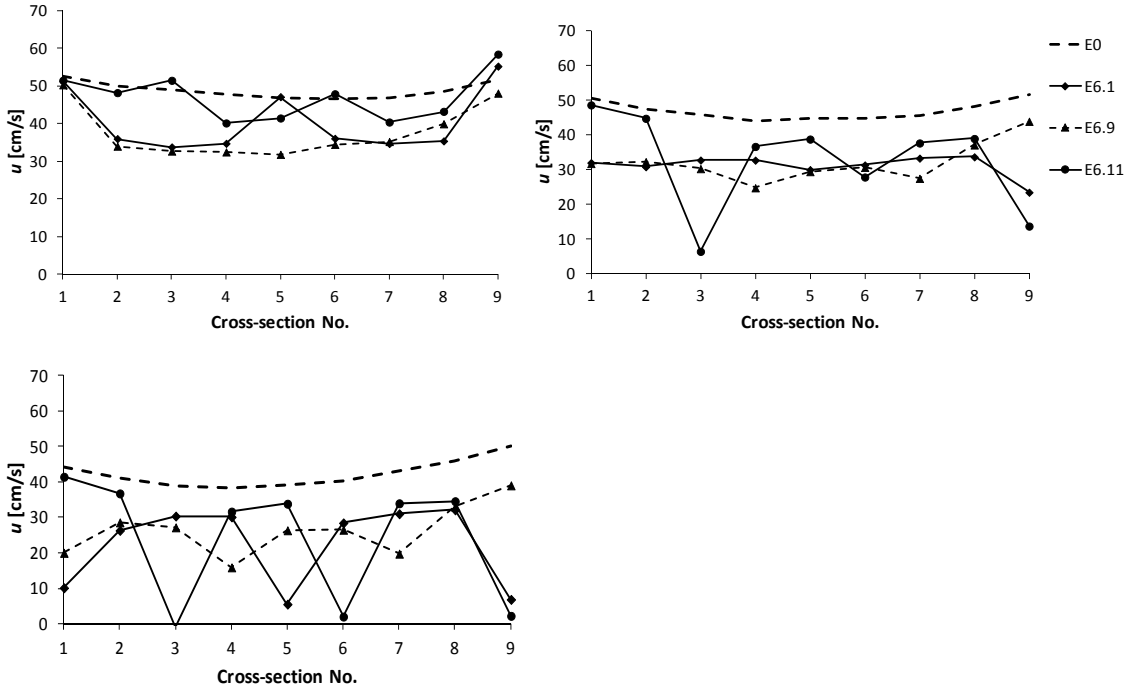

Figure 4.27 Stream-wise velocity at L7 at (a) z=5cm, (b) z=3cm and (c) z=1cm above the bottom for test runs with three groynes E6.1 (lp=80cm), E6.9 (lp=40cm) and E6.11 (lp=40cm) and test run E0 without groyne

At 3 cm above the bottom the test runs E6.9 shows the minimum reduction of the velocities *u* close to the location of the groynes (C1, C4 and C7) whereas the local reduction in *u* close to the groynes location in E6.1 and E6.11 where significantly higher than at E6.9.

A further test run with four shorter groynes (l_p =40 cm) was carried out (E6.10). The first groyne was installed at C1 and the locations of the following three groynes were defined according to the geometric method proposed before. The last groyne was located 57 cm downstream of the end of the curve. The results are shown exemplarily at 5 cm above the bottom (Figure 4.28). The installation of the fourth groyne in E6.10 shows a slight reduction of the velocities *u* in the second half of the curve compared to three groynes in E6.9. However, the trend of increasing velocities towards the end of the curve is still evident.

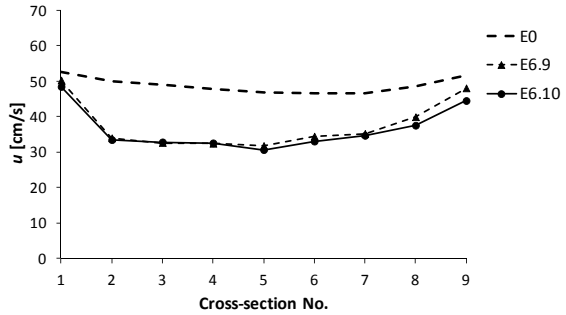

Figure 4.28 Stream-wise velocities at L7 at 5cm above the bottom for test runs E6.9 with three groynes (lp=40cm), E6.10 with four groynes (lp=40cm) and E0 without groyne

Considering the aforementioned analysis it can be concluded that the three groynes with l_p =80 cm in the test run E6.1 and run E6.10 with four short groynes show comparable reduction of the stream-wise velocities at L7 (Figure 4.29). The long groynes show a high locally accelerated flow at the location of the groyne followed with high standing waves whereas shorter groynes showed more smooth surface flow. The acceleration of the flow at the location of the short groynes cannot be evaluated here; hence the groynes from the second to the fourth are not located exactly at the cross-sections where the measurements were done. It is nevertheless noted that one short groyne (l_p = 40) showed less acceleration at C2 compared to longer groynes in the test run E4 (see Figure 4.20b).

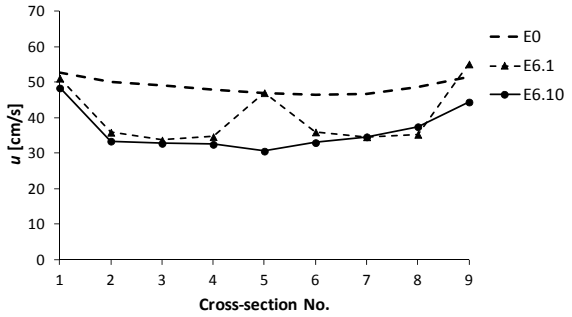

Figure 4.29 *Stream-wise velocities at longitudinal profile L7 at 5cm above the bottom for the test runs E6.1 with three groynes (lp=80cm), E6.10 with four groynes (lp=40cm) and E0 without groyne*

A Further comparison between E6.1 and E6.10 was done at the longitudinal profile L1 close to the inner bank at 3 cm above the bottom (Figure 4.30). It can be seen that both groyne groups cause an increase in the stream-wise velocities close to the inner bank. The short groynes of E6.10 show higher velocities in the first half of the curve compared to the long groynes in E6.1. In the second half of the curve the velocities of E6.10 are lower than in E6.1.

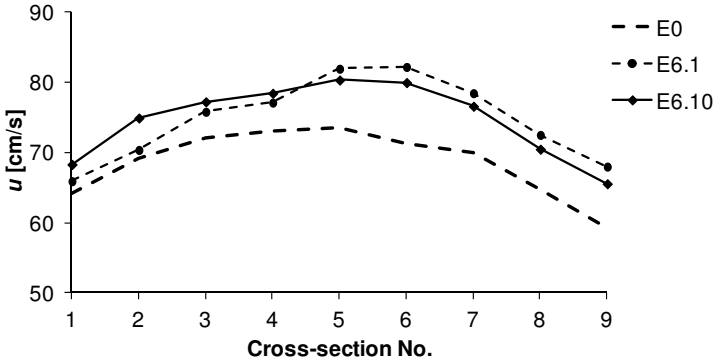

Figure 4.30 *Stream-wise velocities at the longitudinal profile L1 at 5cm above the bottom for the test runs E6.1 with three groynes (lp=80cm), E6.10 with four groynes (lp=40cm) and E0 without groyne*

Complementary measurements with the side-looking Vectrino probe were carried out for the test runs E6.1 and E6.12 in order to get velocity measurements in the upper half of the water depth, which was not possible with the down-looking Vectrino probe. The test run E6.12 with four short groynes was introduced as a result of the mobile outer bank test E7.5 (see Chap. 4.8) where installing the last groyne at C9 provided better results on the bank erosion than at the constructed location as in the case of E6.10. It can be noted from the normalized velocities (u/u_{E0}) in Figure 4.31 that towards the beginning of the curve the short groynes in E6.12 cause lower velocities than long groynes in E6.1. Towards the end of the curve the short groynes in E6.12

give lower reductions in the velocities compared to E6.1 and the reduction in the velocities decreases in the vertical direction towards the water surface (see Figure 4.31a and 4.31b). Both of the long and short groynes causes acceleration at C1 and C9, however the short groynes in the middle did not yield in velocities higher than the velocities without groyne as in the case of the middle long groyne.

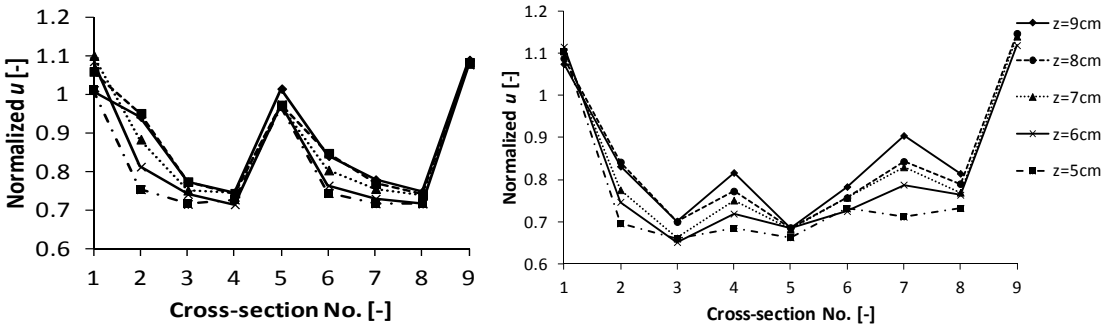

Figure 4.31 Normalized velocities (u/u_{E0}) at longitudinal profile No.7

The investigations with the short groyne (l_p = 40 cm) were further continued with mobile outer bank conditions and the results are documented in the following chapter.

4.8 Mobile outer bank test - group of groynes - E7

The outer bank was built with mobile material in order to define the optimum configuration of the groyne by visualizing the erosion at the bank for different groups of groynes. The importance of this test is that it gives information on the bank scour which was found to be the maximum downstream the bend exit where no velocity measurements are available (see the measurement grid in Figure 3.6). Six test runs were carried out. The outer bank topography was documented with photos and 3D models of the outer bank were generated using photogrammetric technique (SFM). The first test run was done without groyne to observe the erosion pattern on the outer bank and to compare it with different groynes groups. The second test run (E7.2) was done with long groynes (l_p = 80cm). Three test runs with short groynes (l_p = 40cm) were carried out as well. The details of the test runs can be found in Table 3.7. The outer bank erosion was documented with photos, and 3D reconstruction of the bank was done using photogrammetric technique. The resulting erosion on the outer bank for the test run E7.1 without groynes is shown in Figure 4.32. The maximum scour was found downstream the bend exit where the bank material was completely eroded for about one meter

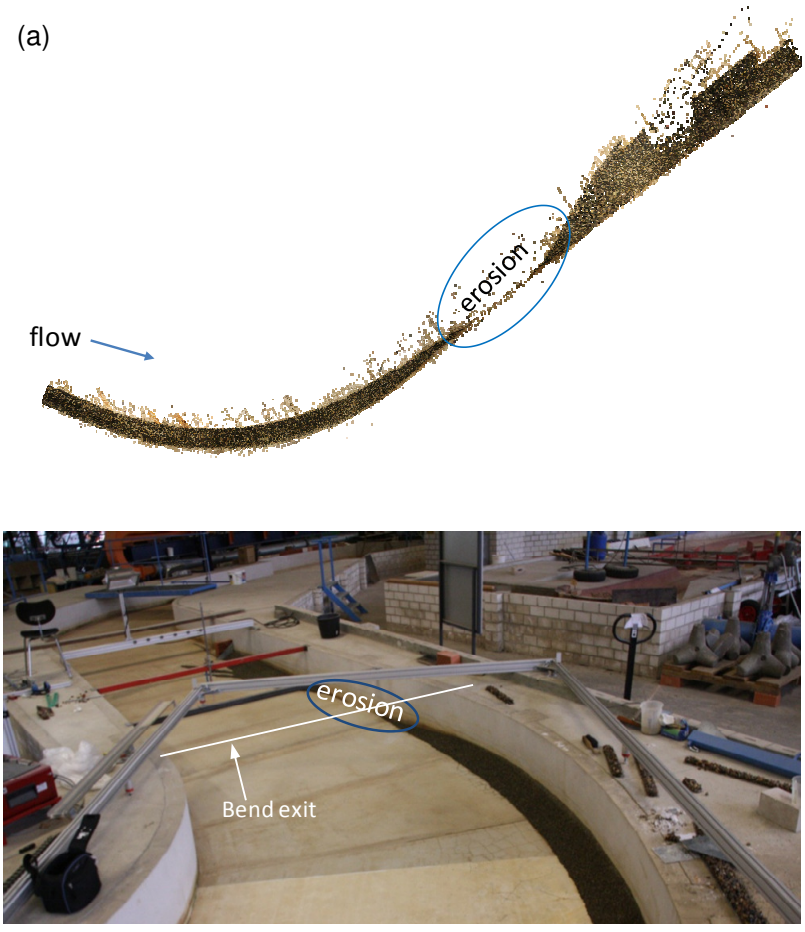

Figure 4.32 3D model of the outer bank (a) and photo around the bend exit (b) for the test run E7.1 without groynes

In the following test runs different groups of groynes were tested in order to confirm the optimum setting of the groynes which provide protection to the outer bank from the erosion shown in Figure 4.32.

In the test run E7.2 three long groynes (l_p = 80 cm) were installed at C1, C5 and C9. The results of the test show that the groynes provided significant protection for the bank. Figure 4.33 shows that the area of the maximum scour downstream the bend exit (Figure 4.32a) is well protected with the groyne. The test results confirm the efficiency of the setup of the long groynes in protecting the bank, however applying longer groynes means more construction material and work. Therefore, shorter groynes with (l_p = 40 cm) were tested in order to explore the possibility of protecting the bank with the least possible amount of material and work.

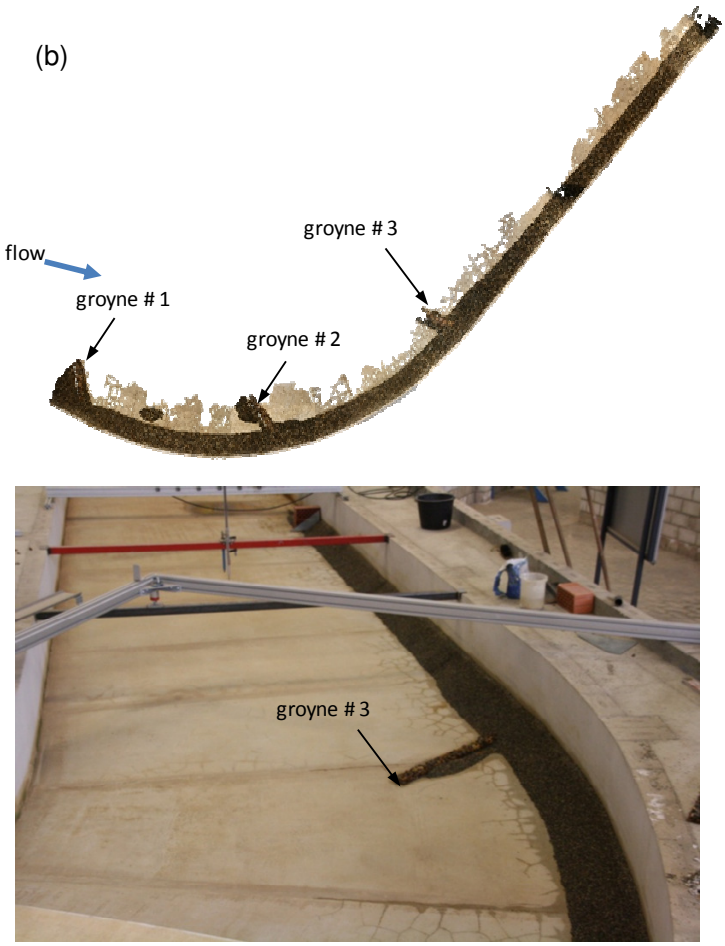

Figure 4.33 3D model of the outer bank (a) and photo around the bend exit (b) for the test run E7.2 with three groynes (l_p=80cm)

In the test run E7.3 three short groynes (l_p = 40) were tested. The location of the second and the third groyne was defined according to the geometric method described before. The resulting outer bank scour is shown in Figure 4.34. The results show significant erosion downstream the bend exit and a deposition of the eroded material can be seen at the end of the mobile outer bank zone. Although the bank was not

eroded completed, the extent of the erosion area in Figure 4.34 was very large compared to test run E7.1 This large erosion can be explained by the quick recovery trend of the stream-wise velocities after the third groyne which was observed in the test run E4.9 (see Figure 28). The excessive erosion observed in this test run implies that three short groynes (l_p =40 cm) are not enough to protect the outer bank. Accordingly, a fourth short groyne was added to test the possibility of protecting the outer bank with four short groynes instead of three groynes. It is to be noted that although the number of groynes in the case of four short groynes is higher compared to test run E7.2 with three long groynes, the volume of the groyne material is one third less in case of four short groynes.

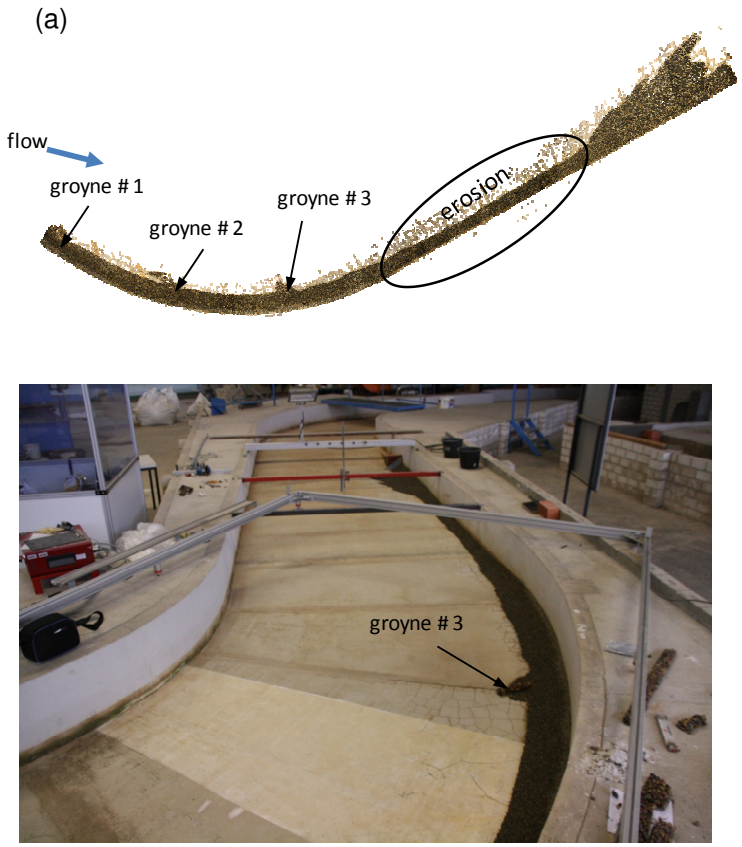

Figure 4.34 3D model of the outer bank (a) and photo around the bend exit (b) for the test run E7.3 with three groynes (l_p=40cm)

In test run E7.4 four short groynes (l_p =40 cm) were used. The first groyne was installed at C1 and the three following groynes were located according to the geometric method descried in Figure 4.25. The geometric method resulted in the last groyne to located 57 cm downstream the bend exit. The results show that significant protection for the outer bank was achieved, however, noticeable erosion was observed around the last groyne (Figure 4.35). To reduce this local erosion, a similar test run with four short groynes with the last groyne shifted to the end of the curve (C9) was carried out (E7.5). The results show a significant reduction of the scour compared to E7.4 (see

Figure 4.36). It was concluded that with short groynes (l_p = 40 cm) four groynes are required to protect the bank and the last groyne should be placed at the end of the curve (C9). This highlights the importance of installing a groyne at the bend exit (C9).

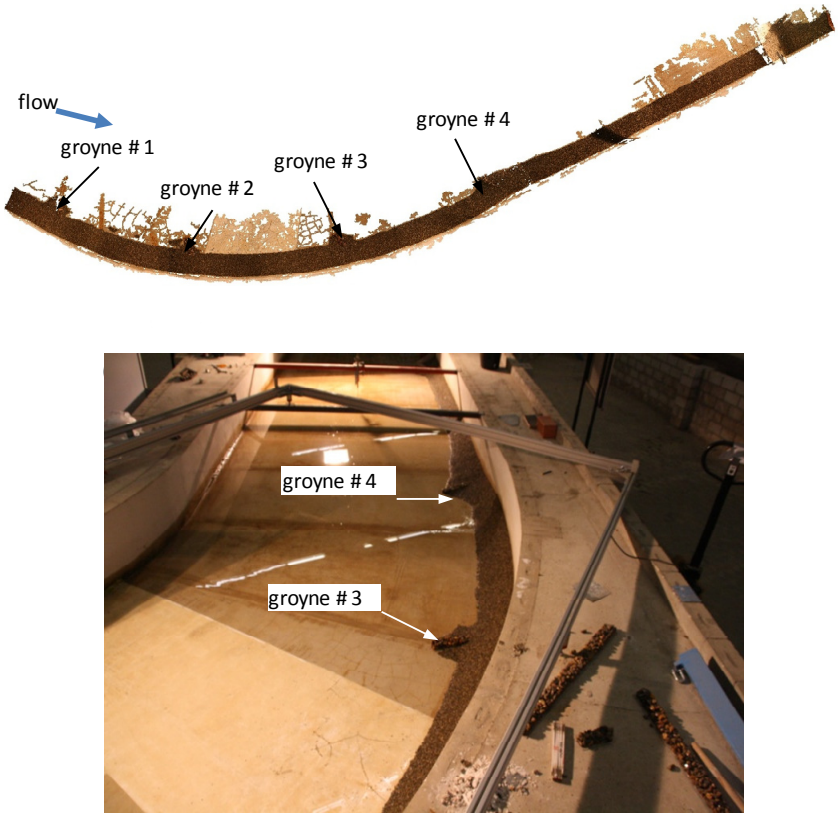

Figure 4.35 3D model of the outer bank (a) and photo around the bend exit (b) for the test run E7.4 with four groynes (l_p=40cm)

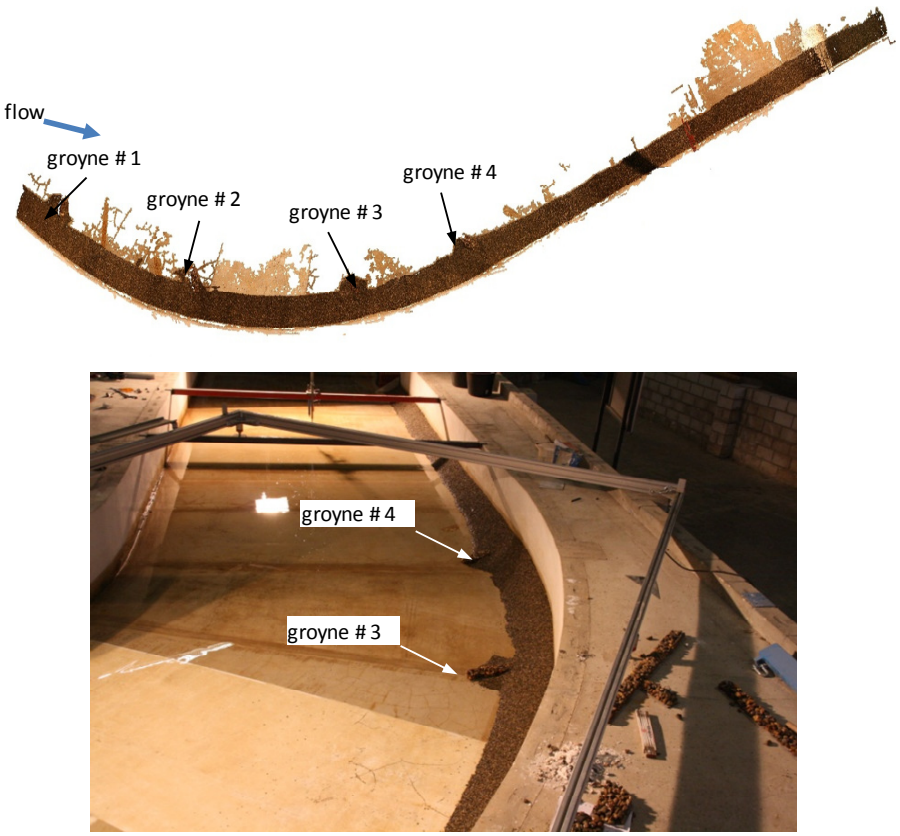

Figure 4.36 3D model of the outer bank (a) and photo around the bend exit (b) for the test run E7.5 with four groynes (l_p=40cm)

In the test run E7.6 four groynes with l_p = 80 cm were used. The second groyne was installed at C2 (one cross-section spacing). The test run E7.6 combines the results of the experiments E7 and E8. In the test run E7.2 the three long groynes provide good protection for the outer bank, nevertheless, at C1 high local scour around downstream the groynes is observed (Figure 4.37b). The investigation of the local scour at the groyne location was tested in E8 and the results show that installing the second groyne at a close distance to the first one (one cross-section spacing) provides better results in reducing the local scour (Figure 4.39). The local erosion at the groyne at C1 and be seen in Figure 4.37a. Installing the second groyne at C2 as in (E7.6) reduces the local scour at C1 (Figure 4.37b). Accordingly it is recommended when using long groynes to install the additional groyne at C2 to reduce the local scour wherever it is necessary.

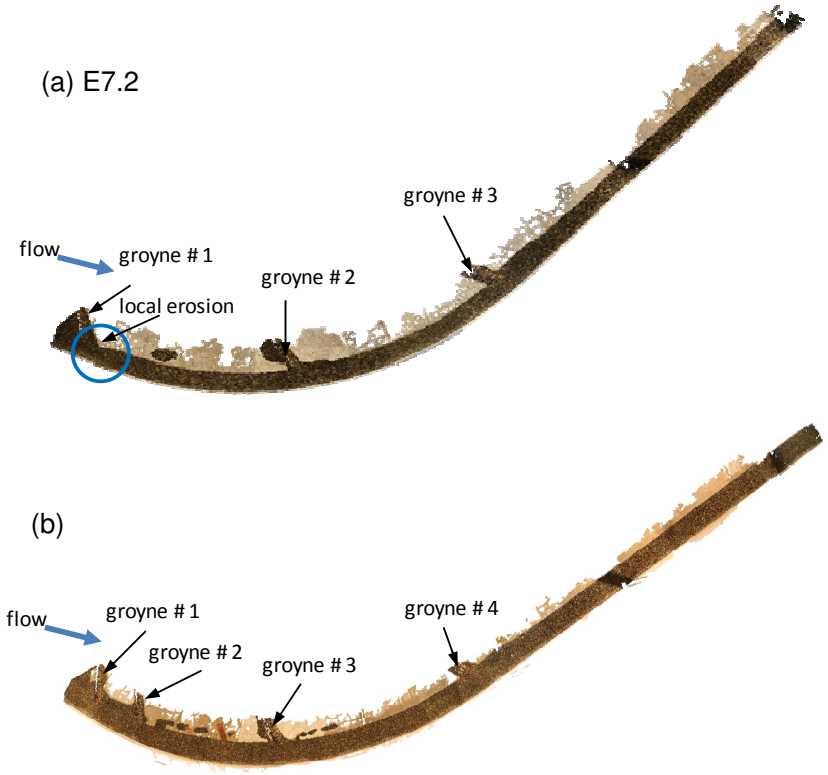

Figure 4.37 *3D model for the outer bank in test run E7.2 with three grones lp=80cm (a) and with four groynes in test run E7.6 (b)*

4.9 Mobile outer bank - local scour at the groyne - E8

The obstruction of the flow by the groyne causes the flow to accelerate over the groyne. This acceleration at the groyne location was discussed in Chap. 4.3 where the velocities at 5 cm above the bottom were found to be 11 - 24 % higher than the velocity in the case without groyne. The aforementioned variation of the acceleration depends on the location of the groyne throughout the curve.

This experiment E8 was carried out to investigate the local erosion at the groyne and to how it can be reduced by using different spacings between the groynes. Seven test runs were carried out (see Table 3.8).

The first test run E8.1 was carried out without groyne and no erosion was observed at cross-section C5. In the second test run E8.2 with one groyne was installed at C5 and the local scour at the groyne was observed (see Figure 4.38 and Figure 4.39a). The maximum scour depth and the scour extent were measured using point gauge (see Table 4.2).

Figure 4.38 Local bank scour at the groyne (E8.2)

The scour at the test run E8.2 with one groyne at C5 was taken as a reference scour to be minimized by adding further groynes with different spacings. In the test run E8.3 two groynes were installed one at C5 and the second at C6 some 68 cm downstream of C5. The scour depth at C5 in the test run E8.3 was noticeably increased larger than in E8.2 (see Figure 4.39b) in addition to a second scour at the groyne at C6 (see Table 4.2).

In the test run E8.4 three groyne were installed at C5, C6, and C7 (same spacing 68 cm) and the results show a reduction of the scour at C5 of 0.4 cm and at C6 of 0.41 cm and additional scour of 1.32 cm was noted at C7 (see Figure 4.39c).

Table 4.2 Outer bank local scour depth and extent

Test	Groyne location	Scour at 1st groyne		Scour 2nd groyne		Scour 3rd groyne	
		Depth [cm]	Extent [m]	Depth [cm]	Extent [m]	Depth [cm]	Extent [m]
E8.1	-	-	-	-	-	-	-
E8.2	C5	2.41	0.50	-	-	-	-
E8.3	C5-C6	3.02	0.41	2.29	0.66	-	-
E8.4	C5-C6-C7	2.01	0.41	1.88	0.33	1.32	0.33
E8.5	C5-C6.5-C8	2.42	0.74	1.88	0.33	0.95	0.33
E8.6	**C5-C6-C7.5**	**1.92**	**0.50**	**1.68**	**0.33**	**0.89**	**0.33**
E8.7	C7	2.01	1.32	-	-	-	-

It was concluded from test run E8.4 that three groynes induce less local scour at the outer bank. Accordingly, it was decided to test three groynes in the test run E8.5 with larger spacing (50% larger than the distance between the cross-sections). According to this spacing the location of the second gronye was in the middle between C6 and C7 and here referred to as C6.5. The results of E8.5 show that the scour at C5 increases to the same order of the scour in E8.2 while the extent of the sour increases significantly more than in case of E8.2 (see Figure 4.39e). At C6.5 the scour depth and magnitude remained the same as in E8.4. At C8 the scour depth was slightly less than E8.4 whereas the extent remained the same.

To optimize the spacing of the groyne with an objective to reduce the local scour at the bank the outcome of E8.4 and E8.5 where combined. In the test run E8.6 three groynes were used with one cross-section spacing for the second groyne and 1.5 cross-section spacing for the third groyne. The scour depth at C5 in E8.6 was the minimum scour of all the previous tests and the extent remained the same. This result shows that the local scour at the groyne can be reduced with group of groynes taking into account that the second groyne is installed at smaller spacing (68 cm) and the spacing can be increased for the following groyne to 102 cm. It is nevertheless evident that the reduction of the local scour was achieved on the cost of additional scour at the second and the third groyne. This can be justified by the fact that groynes are typically installed in a series and only one groyne cannot protect the bank.

(a) E8.2 (b) E8.3 Δ h [cm]

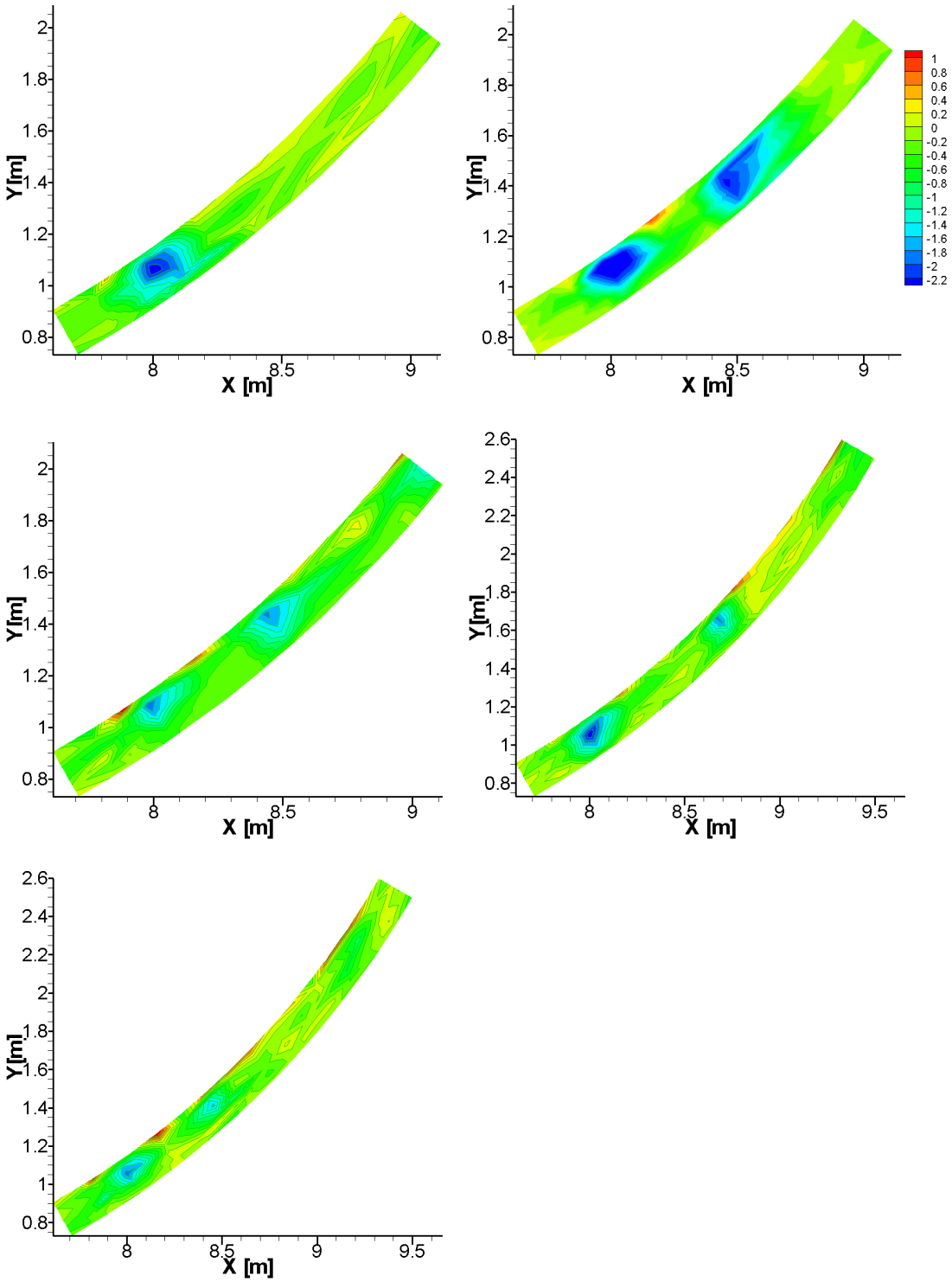

Figure 4.39 Difference in outer bank topography (Δ h) before and after the test runs

5 Discussion

5.1 Flow field without groyne (E0)

The flow filed without groynes measured in the experiment E0 is similar to what was found in the literature, i.e. the core of the maximum velocity shifts towards the inner bank upon entering the curve and shifted gradually throughout the curve towards the outer bank (e.g. Chow 1959; Shukry 1950; Novak 2004; Blankaert et al. 2013). However, the curve has only 65° which is not long enough to show clearly the deviation of the core of the maximum velocity zone towards the outer bank which starts at 60-65° according to Shukry (1950) (see Figure 2.9).

The super elevation estimated using Eq.2.8 was 1.98 cm and 1.80 cm which is 13% less than the measured one at C5 (2.28 cm). It is to be noted that the difference in the super-elevation calculation is expected to be higher considering that the measured super-elevation was done at 10 cm away from the flume side walls.

The secondary flow circulation was observed at C2 which means that the secondary flow developed somewhere between cross-section C1 and C2. At C1 the transverse velocities were directed towards the inner bank. This could be related to the aforementioned fact that the core of the maximum velocity is moved toward the inner bank upon entering the curve (see Figure 2.9).

The outer bank secondary flow cell which was noted by e.g. Graf and Blankaert 2002 was not observed heir. It is to be noted that Graf & Blankaert 2002 used mobile bed material with lateral slope compared to the fixed flat bed used in this study.

5.2 The inclination angle θ_g of shallow groynes (E1)

The installation of the groyne at C1 shows a clear redirection of the flow towards the inner bank. The groyne causes significant reduction on the stream-wise velocities immediately behind the groyne. The reduction of the velocities decrease thought the curve.

The cross-sectional view of the flow at C1 where the groyne was installed showed that no outer bank cell was noted and the inter flow is redirected to the inner bank. This can be attributed to the straight reach upstream the groyne at C1 and to the result of E0 that the flow circulation started somewhere between C1 and C2.

The groyne inclination angle of 60° showed the highest reduction on the stream-wise velocities and the least flow acceleration over the groyne. Therefore the inclination angle of 60° was defined as the optimum inclination angle of shallow groynes. In fact the inclination angle of 60° was also recommended by Mende (2014) for shallow groynes in a straight flume. Mende (2014) found that the inclination angle of 30° and 60° similar secondary flow pattern (clock-wise). However, the inclination angle of 60°

provides shorter groynes than in case of 30° considering that the projected length is constant. Therefore, Mende (2014) recommended 60° to reduce the construction material of the groynes. Similarly Julien & Duncan (2003) and Derrick (1994) recommended an inclination angle of 60° for bendway weirs. However, the USDA 2013 recommended an inclination angle of stream barbs of 20°-30°, similarly Matsuura & Townsend (2004) recommended an inclination angle of 30° for stream barbs. Considering the inclination angle shallow groynes are closer to bendway weirs than stream barbs.

5.3 The effect of the groyne location on the flow field (E2)

The results of the cross-sectional view of the flow field in E2 showed that two secondary flow cells were observed at the cross-section where the groyne is installed expect at C1 (the reason was discussed before). The presence of these two secondary flow cells was noted in connection with in-stream structures by Bhuiyan et al. (2010), Jamieson et al. (2013) and Zaid & Koll (2016b). In the case of shallow groynes, the outer bank cell is larger than that one noted in bends without groyne and it circulates over larger lateral span covering around one third of the cross-section width (see Figure 4.12a). This induced outer bank secondary cell is very important as it widens the outer bank boundary layer reducing the dynamic forces on the outer bank and reduces bank erosion (Blankaert et al. 2013). The induced secondary flow by shallow groynes was noted also in straight flume by Mende (2014).

The results of the experiment runs E2 support the installation of the first groyne at the beginning of the curve. This is due to the high reduction of the stream-wise velocities and the low acceleration of the flow caused by the groyne at the beginning of the curve. The recommendation of installing the groyne at the beginning of the curve is in line with the recommendation of HEC-23 for bendway weirs. However, compared to stream barbs the first groyne is recommended to be installed close to the bend exit according to USDA 2013. Matsuura & Townsend (2004) recommended to locate the first groyne just upstream the first scour at the outer bank. Similarly, Jamieson et al. (2013) recommend to install the first groyne in the vicinity of the expected maximum scour at the bank and not too far upstream the bend exit. The recommendation of installing the groyne towards the end of the curve as per USDA 2013, Matsuura & Townsend (2004) and Jamieson et al. (2013) was tested in the experiment with groyne group E6 and it resulted in boor results with respect to the velocity reduction close to the outer bank. Therefore, it is recommend to install the first groyne at the beginning of the curve.

5.4 Detailed flow field around the groyne (E3)

The measurements of the flow field at 1 cm above the bottom did not show significant high velocity zone around the groyne tip. Thus, no significant scour is expected to

develop at the groyne tip. In the same context Möws & Katinka (2014) found that the maximum scour of the bed due to shallow groynes is located at a distinct distance downstream of the groyne head (Figure 2.18) and not attached to the groyne head. The 3D velocity view at 5cm above the bottom showed accelerated flow over the groyne and high velocity zone close to the outer bank. This high velocity zone is expected to cause local bank erosion at the groyne toe therefore it has been investigated in more detail the experiments E8.

5.5 Investigation of the groyne length l_g (E4)

The results of this experiment show the advantage of using groynes with longer projected length (l_p = 80cm; 1/3 the flume width) compared to the shorter ones. Longer groynes provide higher reduction on the stream-wise velocities close to the outer bank. However, groynes with shorter projected length of lp = 40 cm showed lower velocity accelerations at the location of the groyne compared to longer ones. This gives shorter groynes the advantage of causing lower local bank erosion around the groyne which is well connected to the accelerated flow around the groyne.

The extent of the reduction of the velocities in the downstream direction is longer in the case of longer groynes than in the case of shorter groynes. The velocities in the case of shorter groynes (lp = 40 cm 1/6 the flume width) recover to those in the case without groynes at the second half of the curve (around C6). This means that the effect of the short groynes in the stream-wise velocities finish at the second half of the curve.

Compared to other in-stream structures, like stream barb, the USDA 2013 recommends length of is 1/3-1/4 of the channel width. Similarly, the length of the bend way weirs should be 1/3-1/4 of the channel width according to the HEC 23.

For shallow groynes the recommend projected length is 1/3-1/6 the width of the channel.

5.6 Investigation of the groyne width w_g (E5)

The results shows that wider groyne w_g > 6 cm show higher acceleration over the groyne. This leads to higher local erosion at the groyne location in addition to higher construction costs. On the same time narrow a groyne of 3 cm width shows the same order of reduction in the velocities as groyne with 6 cm width. This gives the opportunity for the uses of large wood as shallow construction material for groynes as they may have the same order of width as the thin groyne investigated here.

5.7 Spacing of shallow groynes S_g (E6)

The results of the experiment E6 support locating the groynes starting from the beginning of the curve because of the high reduction on the stream-wise velocities.

The analysis of the experiment E6 helped to develop a geometric method for locating the groynes (Figure 4.25). In the geometric method a line at the tip of the previous groyne is extended in the downstream direction parallel to the tangent at the toe. The intersection of this line with the curve defines the location of the next groyne. The geometric method was verified with deferent groyne projected lengths. Thus, the geometric method developed here is similar to the one proposed by the USDA 2013 for stream barbs but applied in the opposite direction. According to the SUSDA 2013 the installation of the groynes starts from the end of the curve (where the highest erosion is expected to take place) and continuo in the upstream direction Figure 2.26. The installation of the groynes according to the USDA 2013 show less protection of outer bank as high velocities were observed close to the outer bank (see E6.11 in Figure 4.23). Similarly Matuura & Townsend 2004 proposed a geometric method for determining the location of stream barbs within a barb field (Figure 2.25). Instead of expending a line from the groyne tip as proposed here, Matuura & Townsend 2004 proposed extending a line from the centre of the barb which results in shorter spacing between the barbs. A shorter spacing implies higher number of groynes. The results of E6.3 showed only insignificant higher reduction on the velocities compared to E6.1 although the spacing in E6.3 was half of the spacing in E6.1. This means reducing the spacing between the groynes more than the spacing defined by the geometric method proposed here will not result in significant reduction on the velocities. Accordingly the geometric method of Matuura & Townsend (2004) will increase the number of groynes without significant reduction of the velocities.

Using Eq. 2.4 of LaGrone (1995) for defining the spacing of bedway weirs (HEC 23) the spacing between the groynes result in S_p = 1.49 m. This value of the spacing equals half the spacing recommended here. As discussed before reducing the spacing to half did not yield significant reduction on the velocities, therefore Eq. 2.4 is not suitable for shallow groynes. According to Eq. 2.17 for the spacing of bank attached vanes by Bhuiyan et al. (2010) the spacing of the groyne result in S_p = 0.58 m which is too small compared to the optimum spacing investigated here (2.8 m). Therefore, Eq. 2.17 is as well not applicable for shallow groynes. It is to be noted that there are significant geometrical differences between shallow groynes and bank attached vanes which might be the reason for the large difference in spacing mentioned before.

5.8 Mobile outer bank experiment to optimize the configuration of the groynes (E7)

The results of the mobile outer bank experiment (E7) supported the applicability of shallow groynes to protect the outer bank in river bends. In the test run E7.1 without groyne the maximum erosion on the bank was found downstream the bend exit. Matsuura & Townsend (2004) found similar patterns for the maximum scour in the curve

of Θ_b = 90°, whereas the curve of Θ_b = 135° showed that the maximum scour was just upstream the bend exit.

Blankaert et al (2013) carried out experiments in a curved flume under mobile and immobile bed conditions (Figure 5.1). In the mobile bed tests the maximum scour depth was found at the bend exit (90°). The location of the maximum scour in this case is slightly upstream of what was found in the test run E7.1. Blankaert et al (2013) found also that the flow pattern over the immobile bed show similar patterns to the one over the mobile bed which indicates that the dominant hydrodynamic processes in sharp curved bends are similar in a relatively wide range of curvature ratio, bend length, roughness and under Froude number conditions. However, in the straight reach downstream of the first bend the topographic steering of the flow causes considerable differences in the flow field between mobile and immobile bed conditions. The flow in case of mobile bed conditions was recovering towards homogenous velocity distributions whereas in the case of immobile bed conditions the high velocity zone remained attached to the outer bank (Blankaert et al. 2013). In fact, the aforementioned results from the literature and test run E7.1 on the similarity between the flow pattern in sharp bends in mobile bed and immobile bed experiments and the similarity of in the scour location help to generalize the results obtained here with immobile bed conditions. Considering the differences between immobile bed and mobile bed tests downstream the first bend of Blankaert et al. (2013) it can be concluded that the results of the group of groynes in the experiment E7 are expected to be more conservative as the zone of high velocities remains attached to the outer bank whereas in immobile bed condition the velocities tend to recover to homogenous destitutions. The geometric method for determining the spacing of shallow groynes was verified with different groyne projected lengths. With long groynes l_p = 80cm the outer bank was protected with three groynes. In the case of short groynes l_p = 40cm four groynes were needed to protect the outer bank. It was noted that the last groyne should be moved to the bend exit if the geometric method defines the location of the last groyne far away from the bend exit. This can be related to the location of the maximum scour at the bank which was found to be downstream or close to the bend exit as discussed before.

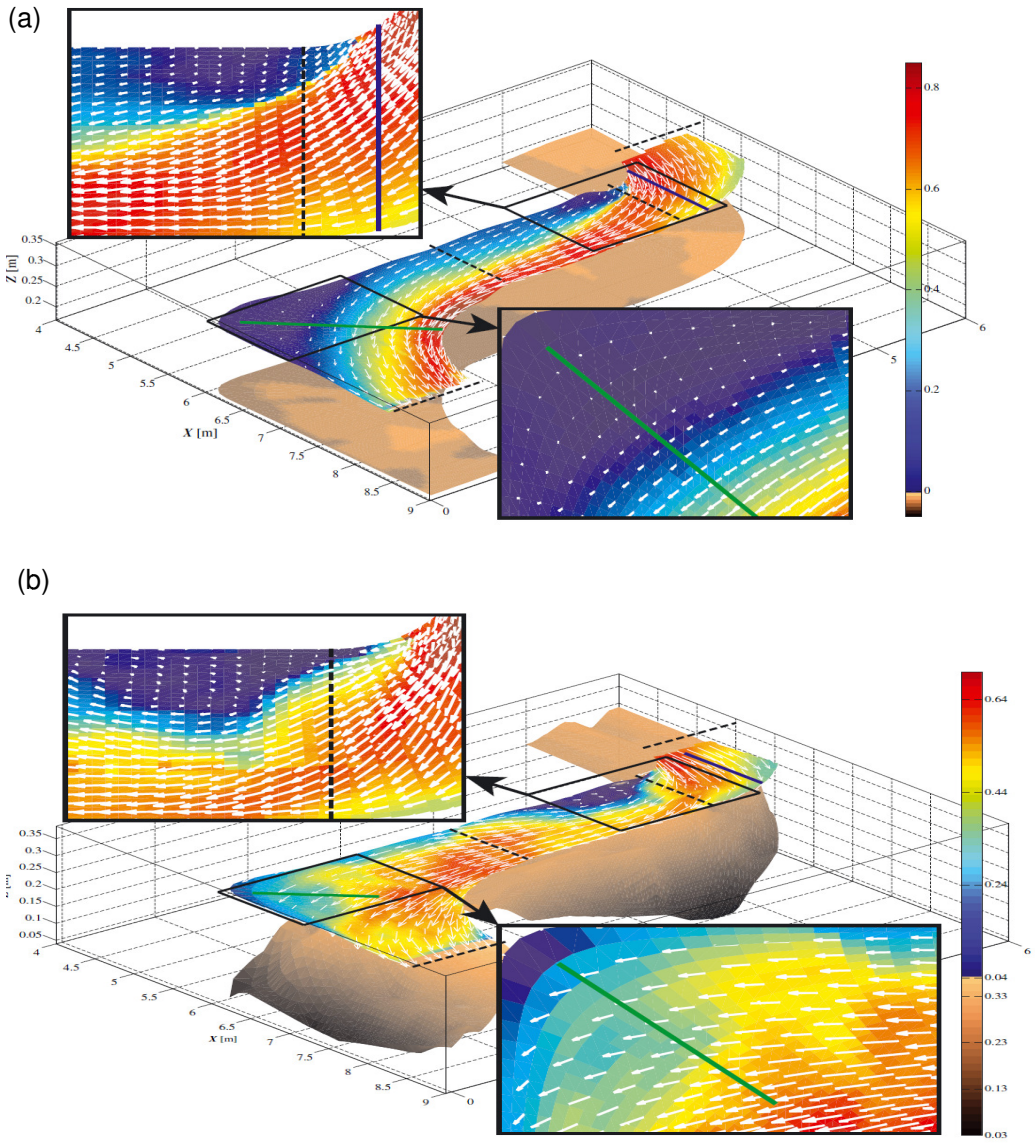

Figure 5.1 *Velocity vectors at the water surface (a) immobile bed experiment, (b) mobile bed experiment (Blankaert et al 2013).*

5.9 Mobile outer bank experiment for local scour at the groyne (E8)

Due to obstruction of the flow by the groyne the flow accelerate over the groyne. This acceleration of the flow caused local scour at the groyne. The results of the experiment E8 helped to reduce this local scour by adjusting the spacing of the second groyne in the groyne field. The second groyne should be located close to the first one at distance of one cross-section (68 cm) to reduce the local sour. Recently El Kadi et al. 2014 and Aelbrecht et al. 2014 highlighted the concept of contorted bank erosion to generate alluvial dynamics where the bank was weakened to allow for limited bank erosion. Considering this concept the local scour at the groyne might be in some cases desirable to enhance the fluvial dynamics which is important to sustain the ecosystem.

6 Conclusions and outlook

6.1 Conclusions

Shallow groynes are introduces as in-stream structures for river bank protection in a nature-oriented manner which takes into account the environmental benefits of the structures on creating heterogeneous river habitat. The investigation on shallow groynes started at *LWI* in straight flume experiments (Mende 2014; Möws & Koll 2014). As far as the river bank protection is concerned, the need to investigate shallow groynes in river bends where bank erosion is more frequent is obvious.

In this study the investigations of shallow groynes in a curved flume were carried out in fixed bed and bank conditions and fixed bed with mobile outer bank conditions. The effect of the groynes parameters on the flow field was addressed in the fixed bed and bank experiments where a comprehensive testing program was performed. Furthermore the combination of groyne parameters in different groups of groynes were tested and optimized. The optimum setup of the groyne was further tested in a fixed bed and mobile outer bank condition.

The applicability of shallow groynes as a bank erosion counter measure in river bends was experimentally tested and verified with the mobile outer bank tests. Although shallow groynes have a low height compared to the water depth (1/4 H) the protection effect for the outer bank was very clear.

The flow redirection effect of shallow groynes was obvious, i.e. the velocity close to the outer bank was decreased whereas the velocity towards the inner bank was increased. This supports the application of shallow groynes as nature-oriented structures (indirect bank protection method) where the aim is to reduce the flow acting force rather than increasing the bank resisting force (e.g. riprap).

In the test without groyne the secondary flow developed at the very beginning of the curve, i.e. between cross-section C1 and C2 and the main secondary flow cell circulate in clock-wise direction. The installation of the groyne generated, locally, an outer bank secondary flow cell which circulated in a counter-clock-wise direction. Unlike the outer bank cell observed in curved flume (Blankaert & de Vriend 2004) or in natural river bends (Bathurst et al. 1979) the outer bank cell here circulated deeper toward the bottom and covered about one third of the cross-section (Zaid & Koll 2016b). In straight flume the secondary flow circulation over the groyne fields was noted by Mende (2014) for groynes with an inclination angle of 30° and 60° whereas an inclination angle of 90° showed no secondary flow circulation.

The systematic investigation of shallow groyne parameters and the effect of changing these parameters on the flow field allowed for better understanding of the hydraulic

effect of the groyne parameters. Accordingly, the following conclusions and recommendations for the design of shallow groynes are made:

- Shallow groyne height was kept constant to one fourth of the water depth ($h_g = 1/4\,H$). For the design purpose, a design water depth needs to be identified to determine the height of the groynes. The design water depth can be calculated based on the discharge which controls the channel morphology e.g. bank-full discharge or effective discharge; however, the design water depth was not part of the scope of this study.
- The investigation of the inclination of the groynes was carried out with inclination angles varied from 50° to 70° with steps of 5°. The optimum inclination of shallow groynes was found to be 60° at which the highest reduction of the steam-wise velocity close to the outer bank was noted (Zaid & Koll 2016a). Therefore the recommended inclination angle of shallow groynes is $\theta_g = 60°$.
- Three different groyne projected lengths (l_p) were tested (80 cm, 69.3 cm and 40 cm). The effect of the long and medium groynes (80 cm, 69.3 cm) on the velocities close to the outer bank was in the same order of magnitude. The shorter groynes (l_p =40 cm) showed a faster recovery trend of the stream-wise velocities close to the outer bank to the initial velocities without groynes compared to the long groynes (l_p =80 cm). However, when testing the short groynes in connection with the experiment with groyne groups (E6) it was possible to maintain the reduction on the velocity by adding more short groynes in the downstream direction. So it was possible to get the same order of velocity reduction as in the case of three long groynes (l_p =80 cm) by using four short groynes (l_p =40 cm). Although the number of groynes in case of short groynes is higher, the volume of the groynes' material is one third less compared to long groynes. Short groynes showed also less accelerated flow over the groyne and less wavy water surface which in turn results in less local erosion at the groyne. At this stage of investigation the projected length l_p is recommended to be $1/3 - 1/6$ the channel width.
- The investigation of the groyne width $w_g = 3cm = 0.3H$ and $w_g = 6cm = 0.6H$ showed comparable results of the stream-wise velocities close to the outer bank. The use of a wider groyne ( ) did not result in more reduction of the velocity close to the outer bank; at the same time it increased the accelerated flow over the groyne which leads to more local erosion at the groyne toe. In addition, the volume of the groyne material is considerably high. Accordingly, shallow groyne width should be

.

- The location of the first groyne in a groyne field is an important parameter. The results showed a significant effect of the groyne location on the flow field. At the groyne location two secondary flow cells were noted independent of the location of the groyne except at the beginning of the curve (C1). Regarding the stream-wise velocity close to the outer bank the results showed the advantage of installing the groyne towards the beginning of the curve on reducing the stream-wise velocities and inducing less flow acceleration at the groyne location. The maximum reduction on the stream-wise velocities was obtained when the groyne was installed at the beginning of the curve (C1). It is therefore recommended to start the shallow groynes field at the beginning of the curve.
- Shallow groynes are installed in a series and the spacing between the groynes was investigated with different groyne group setups. A geometric method to define the location of the groyne was proposed in which the spacing is dependent on the projected length of the groyne. Longer groynes have larger spacing compared to shorter ones. In the geometric method the subsequent groyne locations are defined by the intersection of a line extending in the downstream direction from the groyne tip, parallel to the tangent at the groyne toe, with the curve (see Figure 4.25). It is very important to consider the necessity of installing a groyne right at the end of the curve if the geometric method results in a location for the last groyne away from the end of the bend.
- The installation of shallow groynes causes the flow to accelerate locally at the groyne location causing local bank erosion. The highest local erosion in a groyne group was observed at the first groyne at the beginning of the curve and at the last one at the end of the curve. In order to reduce the local erosion at the groyne at the beginning of the curve, it was found that an additional groyne needs to be installed at a distance of $0.85l_p$ in the downstream direction.

The experiments in this study were performed in a curved channel with a radius-width ratio of $R/W = 1.5$. This curvature radio put the curve in the flume in the range of sharp open channel bends ($R/W \leq 2$) (Blankaert et al. 2013). The curvature ratio can be considered as an index for the effect of the bend geometry on the hydraulic forces in the bend (USDA 2013) i.e. low curvature ratio (sharp bends) means high hydraulic forces in the bend. Therefore the recommendation on shallow groynes described here, can be expected to be applicable in river bends with higher curvature ratio. The average curvature ratio in natural rivers is about ( ). However, it is necessary to verify the applicability of the recommendations on the design of shallow groynes in bends with different geometry ( ).

Design guidelines for shallow groynes

From the summary of the information of this and previous chapters, the following recommendations for the design of shallow groynes can be given to the practitioner:

- The investigations were done in a curved channel with a radius-width ratio of $R/W = 1.5$. The results are therefore applicable for sharp open channel bend with $R/W = 2$.
- The investigations have shown that the groynes should have the following dimensions: $\theta_g = 60°$, $1/3 \leq l_p \leq 1/6$, $0.3H \leq w_g \leq 0.6H$ and $h_g = 1/4\,H$
- Regarding the arrangement of the groynes, it is important that the first groyne to be located at the beginning of the river bend and the last one should be right at the end of the curve.
- For the determination of the distance of the further groynes the application of the geometrical method is recommended with which the location of the groynes can be determined (Figure 4.25).
- To reduce the local scour at the first groyne toe, the installation of additional groyne at a distance of $0.85lp$ downstream of the first groyne is recommended.

6.2 Outlook

The investigation on shallow groyne was carried out with constant hydraulic boundary condition (water depth of 10 cm). It is therefore necessary to examine the design recommendation of shallow groynes under different hydraulic boundary conditions. This can be achieved in compilation with the flume bed roughness change; by using higher bed roughness instead of smooth bed in the current setup.

All the experiments were done with a flat fixed bed. Therefore no information on the bed topographical changes associated with the structures could be gained. Thus the extension of the measurements on shallow groynes to mobile bed conditions is needed. This will allow to elaborate on the effect of shallow groynes on the river thalweg. It shows also how far shallow groynes are able to relocate the thalweg away from the outer bank which is an important criterion for the performance of the structure for protecting the outer bank. The mobile bed conditions will allow investigating the local erosion at the groyne tip. Although this local erosion at the groyne tip was found to be at a distinct distance downstream the shallow groyne in straight flume experiments (Möws & Koll 2014) it is necessary to check it in a curved flume. The erosion at the groyne tip is important considering the stability of the groynes.

Ultimately, the final tests on shallow groynes should be carried out with mobile bed and bank conditions and in a pilot project on a natural river. This can be combined with biological measurements to evaluate the effect of shallow groynes on the river ecology.

7 References

Abad, J.D., Rhoads, B.L., Günerlap, I., Garcia, M.H. (2008): Flow structure at different stages in a meander-bend with bendway weirs. J. Hydraul. Eng., Vol.134, No. 8, 1052-1063.

Aelbrecht, D., Clutier, A., Barillier, A., Pinte, K., El-Kadi-Abderrezzak, K., Die-Moran, A., Lebert, F. (2014): Morphodynamics restoration of the Old Rhine through controlled bank erosion: Concept, laboratory modeling, and field testing and first results on a pilot site. River Flow 2014, Lausanne, Switzerland – Schleiss et al. (Eds) © 2014 Taylor & Francis Group, London, ISBN 978-1-138-02674-2.

Arulanandan, K., Gillogley, E., Tully, R. (1980): Development of a Quantitative Method to Predict Critical Shear Stress and Rate of Erosion of Natural Undisturbed Cohesive Soils. Report GL-80-5, U.S. Army Engineers, Waterways Experiment Station: Vicksburg, Mississippi.

Baird, D.C, Fotherby, L., Klumpp, C.C., Sculock, S.M. (2015): Bank Stabilization Design Guidelines. Report No.: SRH-2015-25, Bureau of Reclamation, Technical Service Center, Denver, Colorado.

Bathurst J.C., Thorne C. R., Hey R.D. (1979): Secondary flow and shear stress at river bends. J. Hydraul. Div. Vol. 105, No. 10, 1277-1295.

Bathurst, J.C., Thorne, C.R., Hey, R.D. (1977): Direct measurements of secondary currents in river bends. Nat., 269, 504–506.

Bejestan, M. S., Jarrah, F., Ramesh, S. (2010): Experimental study on Bendway weirs. River Flow 2010 - Dittrich, Koll, Aberle & Geisenhainer (eds) - © 2010 Bundesanstalt für Wasserbau ISBN 978-3-939230-00-7

Bhuiyan, A.F., Hey, R. (2007): Computation of three-dimensional flow field created by weir-type structures. Journal of Engineering Application of Computational Fluid Mechanics Vol.1, No.4, 350-360.

Bhuiyan, F., Hey, R.D., Wormleaton, P.R. (2009): Effects of vanes and w-weir on sediment transport in meandering channels. J. Hydraul. Eng., Vol. 135, No.5, 339-349.

Bhuiyan, F., Hey, R.D., Wormleaton, P.R. (2010): Bank-attached vanes for bank erosion control and restoration of river meanders. J. Hydraul. Eng., Vol. 136No. 9, 583-596.

Blanckaert, K, de Vriend, H.J. (2003): Non-linear modeling of mean flow redistribution in curved open channels. Water Resour. Res., Vol. 39 No.12, 1375.

Blanckaert, K, Graf, W.H. (2004): Momentum transport in sharp open channel bends. J. Hydraul. Eng., Vol. 130, No.3,186-198.

Blanckaert, K. (2010): Topographic steering, flow recirculation, velocity redistribution and bed topography in sharp meander bends. Water Resour. Res. 46: W09506. DOI: 10.1029/2009WR008303.

Blanckaert, K. (2011): Hydrodynamic processes in sharply-curved river bends and their morphological implications. J. Geophys. Res., Vol. 116: F01003. DOI: 10.1029/2010JF001806.

Blanckaert, K., de Vriend, H.J. (2004): Secondary flow in sharp open-channel bends. J. Fluid Mech., Vol. 498, 353-380.

Blanckaert, K., de Vriend, H.J. (2004): Secondary flow in sharp open-channel bends. J. Fluid Mech., Vol. 498, 353-380

Blanckaert, K., Graf, W.H. (2001): Mean flow and turbulence in open-channel bends. J. Hydraul. Eng., 127(10), 835-847.

Blanckaert, K., Kleinhans, M.G., McLelland, S J., Uijttewaal, W.S.J., Murphy, B.J., Anja van de Kruijs, Parsons, D.R., Chen, Q. (2013): Flow separation at the inner (convex) and outer (concave) banks of constant-width and widening open-channel bends. Earth Surf. Process. Landforms, Vol.38, 696-716.

Bravard, J.P., Kondolf, G.M., Pie´gay, H. (1999): Environmental and societal effects of river incision and remedial strategies. In Incised River Channels, Simon A, Darby SE (eds). John Wiley and Sons: Chichester; 303-341.

Chang, H. (1988): Fluvial Processes in River Engineering. Wiley-Interscience, Wiley, NY.

Chow, V.T. (1959): Open Channel Hydraulics, McGraw-Hill.

Clark, L.A., Wynn, T.M. (2007): Methods for determining streambank critical shear stress and soil erodibility: Implications for erosion rate predictions. Transactions of the American Society of Agricultural and Biological EngineersVol. 50, No.1, 95-106.

Couper, P., Maddock, I., (2001): Subaerial River Bank Processes and Interaction with other Bank Erosion Mechanisms on the River Arrow, Warwickshire, UK. Earth Surf. Process. Landforms, 26 (6). pp. 631-646.

Darby, S.E., Thorne C.R. (1996): Numerical simulation of widening and bed deformation of straight sand-bed rivers. II: Model evaluation. J. Hydraul. Eng., Vol. 122, No. 4, 194-202.

Das, T.K, Haldar, S.K., Gupta, I.D, Sen, S. (2014): River Bank Erosion Induced Human Displacement and Its Consequences. Living Reviews Landscape Research URL (accessed): http://www.livingreviews.org/lrlr-2014-3

de Vriend, H.J. (1979): Flow measurements in a Curved Rectangular Channel." Report No. 79-9, Lab. Fl. Mech., Dept. Civ. Eng., Delft Univ. Techn., Delft, Netherlands.

de Vriend, H.J., Geldof, H.J. (1983): Main flow velocity in short and sharply curved river bends. Report No. 83-6, Lab. Fl. Mech., Dept. Civ. Eng., Delft Univ. Techn., Delft, Netherlands

Derrick, D.L., Boyd, M.B., Crutchfield, J.P., Henderson, R.R., Pokrefke, T.J. (1994): Design and development of bendway weirs for the Dogtooth Bend reach, Mississippi River, hydraulic model investigation. Technical Rep. HL-94-10, Waterways Experiment Station, Vicksburg, MS.

Dey, S. (2014): Fluvial hydrodynamics, GeoPlanet: Earth and Planetary Sciences, Springer Berlin Heidelberg.

Dietrich, W.E., Smith, J. D. (1983): Influence of the point bar on flow through curved channels. Water Resourc. Res., AGU, Vol. 19, No. 5, 1173-1192.

Dietrich, W.E., Smith, J.D., Dunne, T. (1979): Flow and sediment transport in sand beded meander. Journal of Geology, Vol. 87, pp. 305-315.

Dittrich, A. (1998): Wechselwirkung Morphologie/Strömung naturnaher Fließgewässer. Mitteilung des Instituts für Wasserwirtschaft und Kulturtechnik, Universität Karlsruhe (TH), Heft 198.

Dittrich, A.; Koll, Ka.; Aberle, J.; Geisenhainer, P. (Ed.) (2010): Proceedings of the International Conference on Fluvial Hydraulics, Braunschweig, Germany, September 08-10, 2010: River flow 2010.

Diplas, P., Vigilar, G. (1992): Hydraulic geometry of threshold channels. J. Hydrail. Eng., Vol. 118, No. 4, 597-614.

Downs, PW, Simon, A. (2001): Fluvial geomorphological analysis of the recruitment of large woody debris in the Yalobusha river network, Central Mississippi, USA. Geomorphology, Vol. 37, Issu. 1-2, 65–91.

El kadi Abderrezzak, K., Die Moran, A., Mosselman, E., Bouchard, J-P., Aelbrecht, D. (2014): A physical movable bed model for non-uniform sediment transport, fluvial erosion and bank failure in rivers. Journal of Hydro-Environment Research Volume 8, Issue 2, pp. 95–114.

Fang, D., Sui, J., Thring, R.W. (2006): Impacts of dimension and slope of sumberged spur dikes on local scour processes - an experimental study. Int. J. Sediment Res., Vol. 21, No.2, 89-100.

FISRWG (1998). Stream Corridor Restoration: Principles, Processes, and Practices. Federal. Interagency Stream Restoration Working Group (FISRWG). GPO Item No. 0120-A.

Florsheim, J.L., Mount J.F., Chin A. (2008): Bank erosion as a desirable attribute of rivers. BiosScience, Vol. 58, No.6, 519-529.

Fox, J.F., Papanicolaou, A.N., Hobbs, B., Kramer, C., and Kjos, L. (2005): Fluid-sediment dynamics around a barb: An experimental case study of a hydraulic structure for the Pacific Northwest. Can. J. Civ. Eng., Vol. 32, No.5, 853-867.

Goring, D.G., Nikora, V.I. (2002): Despiking acoustic Doppler velocimeter data. J. Hydraul. Eng., Vol. 128, No. 1, 117-126.

Han, S.S., Ramamurthy, A.S., Biron, P.M. (2011): Characteristics of Flow around Open Channel 90° Bends with Vanes. J. Irrig. Drain. Eng. Vol. 13, No.10,668-676.

Hanson, G.J., Simon, A. (2001):Erodibility of cohesive streambeds in the loess area of the Midwestern USA. Hydrol. Processes Vol.15, No.1, 23-38.

Hemmati, M., Ghomeshi, M., Mahmood Kashefipour, S., Mahmood Shafai-Bejestan, M., Lanzoni, S. (2012): Experimental Investigation of the Effects of Angle and Length of Bendway Weirs on Scouring and Sedimentation in a Meander River. J. Am. Sci., Vol. 8, No.9, 912-917.

Hooke, R.L. (1975): Distribution of sediment transport and shear stress in a meander bend: J. Geol., Vol. 83, No.5, 543-565.

Jamieson, E.C., Rennie, C.D., Townsend, R.D. (2013): 3D flow and sediment dynamics in a laboratory channel bend with and without stream barbs. J. Hydraul. Eng., Vol.139, No.2, 154-166.

Jamieson, E.C., Rennie, C.D., Townsend, R.D. (2013): Turbulence and Vortices in a Laboratory Channel Bend at Equilibrium Clear-Water Scour with and without Stream Barbs. J. Hydraul. Eng., Vol.139, No.3, 259-268.

Johnson, P.A., Hey, R.D., Tessier, M., Rosgen, D.L. (2001): Use of vanes for control of scour at vertical wall abutments.J. Hydraul. Eng., Vol. 127, No. 9, 772-778.

Julien, P.Y., and Duncan, J.R. (2003): Optimal design criteria of bendway weirs from numerical simulations and physical model studies. Technical Paper, Dept. of Civil Engineering, Colorado State Univ., Fort Collins, CO.

Khosronejad, A., Diplas, P., Sotiropoulos, F. (2016): Simulation-based optimization of in–stream structures design: bendway weirs. Environ. Fluid Mech. Vol. 17, No.1, 79-109.

Kikkawa, H., Ikeda, S., Kitagawa, A. (1976): Flow and bed topography in curved open channels. J. Hydraul. Div., Vol. 102, No.9, 1327-1342.

King, H. (2015): The use of groynes for river bank erosion protection and river stabilization: State of art report 2015. DOI: 10.13140/RG.2.1.2773.3203.

Kondolf, GM, H Piégay (2016): Tools in fluvial geomorphology. John Wiley & Sons, Chichester UK., 2nd edition.

Kuhnle, R.A., Alonso, C.V. (2002): Local scour associated with angled spur dikes. J. Hydraul. Eng., Vol. 128, No. 12, 1087-1093

Laderoute, L., Bauer B. (2013): River bank erosion and boat wakes along the lower Shauswap River, British Columbia. Final project report submitted to the Regional District of North Okanagan Fisheries and Oceans Canada.

Lagasse, P.F., Byars, M.S., Zevenbergen, L.W., Clopper, P.E.(1997): Bridge scour and stream instability countermeasures: Experience, selection, and design guidance. HEC-23 - FHWA-HI-97-030, Washington, D.C.

Lagasse, P.F., Clopper, P.E., Pagán-Ortiz, J.E., Zevenbergen, L.W., Arneson, L.A., Schall, J.D., Girard, L.G. (2009): Bridge scour and stream instability countermeasures: Experience, selection, and design guidance: Third edition (Hydraulic Engineering Circular No. 23,) Report No. FHWA-NHI-09-111). Washington, DC: Federal Highway Administration.

Lagasse, P.F., et al. (2009): Bridge scour and stream stability countermeasures." HEC-23, FHWA-NHI-09-111, Federal Highway Administration, U. S. Dept. of Transportation, Washington, DC.

LaGrone, D.L., (1996): Bendway Weir General Guidance Memorandum. U.S. Army Corps of Engineers, Omaha District, Omaha, Nebraska, revised from 1995.

Lawler, D. M. (1995): The impact of scale on the processes of channel-side sediment supply: A conceptual model. In Effects of Scale on Interpretation and Management of Sediment and ater Quality. IAHS Pub. 226. Wallingford, U.K.: International Association of Hydrological Sciences.

Lawler, D.M. (1992): Process dominance in bank erosion systems. In: Lowland Floodplain Rivers: Geomorphological Perspectives, P. A. Carling and G. E. Petts (eds.), John Wiley, Chichester, UK, 117-143.

Leopold, L., Wolman, M., Miller, P. (1964): Fluvial Processes in Geomorphology, Dover Publications, Inc., New York, New York.

Leopold, L.B. and Wolman, M.G. (1960): River meanders. Bulletin of the Geological Society of America, Vol. 71, No.6, 769-794.

Leopold, L.B., Wolman, M.G. (1957): River channel patterns: Braided, meandering, and straight. Geological Survey Professional Paper 282 B, Physiographic and Hydraulic Studies of Rivers, U.S. Dept. of the Interior, U.S. Government Printing Office, Washington, DC.

Marion, A., Nikora, V., Puijalon, S., Bouma, T., Koll, Ka., Ballio, F., Tait, S., Zaramella, M. Sukhodolov, A. O'Hare, M., Wharton, G., Aberle, J., Tregnaghi,

M., Davies. P., Nepf, H., Parker, G., Statzner, B. (2014): Aquatic interfaces: a hydrodynamic and ecological perspective. J. Hydraul. Res., Vol. 52, No. 6, 744-758.

Matsuura, T., and Townsend, R. (2004): Stream-barb installations for narrow channel bends—A laboratory study. Can. J. Civ. Eng., Vol. 31, No.3, 478-486.

Mende, M. (2014): Naturnaher Uferschutz mit Lenkbuhnen – Grundlagen, Analytik und Bemessung. Dissertation, Fakultät für Architektur, Bauingenieurwesen und Umweltwissenschaften der Technischen Universität Braunschweig.

Mende, M., Sindelar, C. (2010): Instream River Training - Lenkbuhnen und Pendelrampen. Beitrag zum 15. Gemeinschafts-Symposium der Wasserbau-Institute TU München, TU Graz und ETH Zürich vom 1.-3. Juli 2010 in Wallgau, Oberbayern, S. 35-44.

Mende, M.; Koll, K. (2008): Wissenschaftliche Beratung und Begleitung innovativer Sicherungs-und Strukturmaßnahmen an Gewässern 1. Ordnung (hauptsächlich Wiese in Lörrach)– Teilmaßnahme 2: Monitoring der morphodynamischen Enwicklung. LWI-Bericht Nr. 970,

Nadal-Romero, E., Revuelto, J., Errea, P., López-Moreno, J. I. (2015):The application of terrestrial laser scanner and SfM photogrammetry in measuring erosion and deposition processes in two opposite slopes in a humid badlands area (central Spanish Pyrenees). SOIL, Vol. 1, No. 2, 561–573.

Nardi, L. (2011): Numerical and physical modelling of bank retreat in gravel-bed rivers. PhD dissertation, Department of Architecture, Civil engineering and Environmental Sciences University of Braunschweig – Institute of Technology and the Faculty of Engineering University of Florence.

Natural Resources Conservation Service (2013): ENG-Design of Stream Barbs, Kansas Engineering Technical Note No. KS-1 (Revision 1). US Department of Agriculture, 760 South Broadway, Salina, Kansas 67401-4604.

Nezu, I., Nakagawa, H. (1993): Turbulence in open-channel flows, IAHR-monograph, Balkema.

Nikora, V.I., Goring, D.G. (1998): ADV measurements of turbulence: Can we improve their interpretation?. J. Hydraul. Eng., Vol. 124, No. 6, 630–634.

Noack, M., Schmid, G., Thom, M., Wieprecht, S. (2016): Testing ‘Structure-from-Motion’ photogrammetry for high-resolution topographic surveys in hydraulic laboratories. Int. Conf. on Fluvial Hydraulics, River Flow 2016, Saint Louis, USA, Edited by Constantinescu, Garcia & Hanes, Taylor & Francis Group, London, ISBN 978-1-138-02913-2, 1286-1292.

Nortek AS (2013): Principles of Operation Measuring Current and waves.

Odgaard, A.J. (2009): River Channel Stabilization with Submerged Vanes. In C. T. Yang, L. K. Wang (eds.), Advances in Water Resources Engineering, Handbook of Environmental Engineering, Volume 14, DOI 10.1007/978-3-319-11023-3_3.

Odgaard, A.J., and Wang, Y. (1991): Sediment management with submerged vanes. I: Theory. J. Hydraul. Eng. Vol. 117, No. 3, 267-283.

Odgaard, A.J., Bergs, M.A. (1988): Flow processes in a curved alluvial channel. Water Resour. Res., Vol. 24, No. 1, 45-56.

Osman, A.M., Thorne, C.R. (1988): Riverbank stability analysis: I. Theory. J. Hydraulic Eng. Vol. 114, No. 2, 134-150.

Ottevanger, W., Blanckaert, K., Uijttewaal, W.S.J (2012): Processes governing the flow redistribution in sharp river bends. Geomorphology, Vol. 163–164, 45–55.

Palmer, J.A., Schling, K.E., Isenhart, T.M., Schultz, R.C, Tomer, M.D. (2014): Streambank erosion rates and loads within a single watershed: Bridgin the gap between temporal and spatial scales. Geomorphology Vol. 209, 66–78.

Papanicolaou, A.N., M. Rinaldi, S. Dey, Mazumdar, A. (2006): Research issues for Riverine bank stability analysis in the 21st Century. IIHR-Hydroscience & Engineering College of Engineering the University of Iowa, IIHR Technical Report No. 457,

Parker, G., Andrews, E.D. (1985): Sorting of Bed Load Sediment by Flow in Meander Bends. Water Resour. Res., Vol. 21, No. 9,1361-1373,

Partheniades, E., (1965): Erosion and deposition of cohesive soils. J Hydraul. Div., Vol. 91, No.1, 105-139.

Piegay, H., Darby, S.E., Mosselman, E., Surian, N. (2005): A review of techniques available for delimiting the erodible river corridor: a sustainable approach to managing bank erosion. River Res. Applic., Vol. 21, No.7, 773-789.

Pollen, N., (2006): Temporal and spatial variability in root reinforcement of streambanks: Accounting for soil shear strength and moisture. Catena, Vol. 69, No. 3,197-205.

Pollen-Bankhead, N., Simon, A., (2009): Enhanced Application of Root-Reinforcement Algorithms for Bank-Stability Modeling. Earth Surf. Process. Landf., Vol. 34, No. 4, 471–480.

Prosdocimi, M., Calligaro, S., Sofia, G., Fontana, G.D., Tarolli, P. (2015): Bank erosion in agricultural drainage networks: new challenges from structure-from-motion photogrammetry for post-event analysis. Earth Surf. Process. Landf., Vol. 40, No. 14, 1891–1906.

Prosser, I.P., Hughes, A.O., Rutherford, I.D. (2000): Bank erosion of an incised upland channel by subaerial processes. Tasmania, Australia. Earth Surf. Process. Landf., Vol. 25, No. 10, 1085-1101.

Przedwojeski, (1957): Flow of water in bends of open channels, Academy of Science of Ukrainian .SSR, Kiev.

Radspinner, R.R., Diplas, P., Lightbody, A.F., and Sotoropoulis, F. (2010): River training and ecologic enhancement potential using in-stream structures. J. Hydraul. Eng., Vol. 136, No. 12, 967–980.

Rinaldi, M., Casagli, N., (1999): Stability of streambanks formed in partially saturated soils and effects of negative pore water pressures: The Sieve River (Italy). Geomorphology, Vol.26, No.4, 253-277.

Rinaldi, M., Darby, S.E., (2008): Modelling river-bank-erosion processes and mass failure mechanisms: progress towards fully coupled simulations. In: Habersack, H., Piégay, H., Rinaldi, M. (Eds), Gravel-Bed Rivers 6 - From Process Understanding to River Restoration. Series Developments in Earth Surface Processes, 11, Elsevier, Netherlands, 213-239.

Rosgen, D.L. (1996): Applied river morphology, Wildland Hydrology. Pagosa Springs, Colo.

Scottish Environment Protection Agency (2008): Engineering in the Water Environment Good Practice Guide Bank Protection: Rivers and Lochs. Document reference: WAT-SG-23.

Scurlock, S. M. (2014): Quantification of hydraulic effects from transverse in-stream structures in channel bends. Ph.D. dissertation, Dept. of Civil and Environmental Engineering, Colorado State Univ., Fort Collins, CO.

Scurlock, S.M.; Thornton, C.I, Baird, D.C., Abt, S.R. (2015): Quantification of transverse in-stream structure hydraulics. J. Hydraul. Eng. Vol. 141, No. 2, DOI: 10.1061/(ASCE)HY.1943-7900.0000952.

Shields, F. D., Knight, S. S., and Cooper, C. M. (1998): Addition of spurs to stone toe protection for warmwater fish habitat rehabilitation. J. Am. Water Res. Assoc., Vol. 34, No. 6, 1427-1436.

Shields, F. D., Knight, S. S., and Cooper, C.M. (2000): Warmwater stream bank protection and fish habitat: A comparative study. Environ. Manage., Vol. 26, No3, 317-328.

Shields, F.D. Jr., Cooper, C.M., Knight, S.S. (1995): Experiment in stream restoration. J. Hydraul. Eng., Vol. 121, No. 6, 494-502.

Shiono, K., Muto, Y. (1998): Complex flow mechanisms in compound meandering channels with overbank flow. J. Fluid Mech. 376, 221–261.

Shukry, A. (1950): Flow around bends in an open flume. Transactions of the American Society of Civil Engineers, Vol. 115, No. 1, 751-779.

Simon, A., Curini, A., Darby S.E., Langendoen, E.J. (2000): Bank and near-bank processes in an incised channel. Geomorphology, Vol. 35, No.3-4, 193-217.

Simon, A., Wolfe, W.J., Molinas, A., (1991): Mass-wasting algorithms in an alluvial channel model. Proceedings of the 5th Federal Interagency Sedimentation Conference, Las, edited by Drs. Shou-Shan Fan and Yung-Huang Kuo. Vegas, Nevada, 2, 8, 22-29.

Smerdon, E.T., and R.P. Beasley (1961): Critical tractive forces in cohesive soils. Agric. Eng. Vol. 42, No.1, 26-29.

Temple, D.M., Hanson, G.J. (1994): Headcut development in vegetated earth spillways. Appl. Eng. Agric., Vol.10, No.5, 677-682.

Trimble, S.W. (1997): Contribution of stream channel erosion to sediment yield from an urbanizing watershed. Science (Washington), Vol. 278, No. 5342, 1442-1444.

U.S. Department of Agriculture (USDA). (2005): Design of stream barbs. Engineering Technical Note No. 23, Version 2.0, Natural Resources Conservation Service Oregon, Portland, OR.

Wahl, TL (2002): Discussion of ‘despiking acoustic Doppler velocimeter data’ by Derek G Goring and Vladimir I Nikora” J. Hydraul. Eng., Vol 129, No 6, 484-486.

Wallbrink, P.J., Murray, A.S., Olley, J. M., Olive, L.J. (1998): Determining sources and transit times of suspended sediment in the Murrumbidgee River, New South Wales, Australia, using fallout ^{137}Cs and ^{210}Pb. Water Resour. Res., Vol. 34, No.4, 879-887.

Westphal, C (2016): Eignung von Open-Source Photogrammetriesoftware für Vermessungsaufgaben im wasserbaulichen Versuchswesen. Bachelorarbeit, Leichtweiß-Institut für Wasserbau.

Wu, C. (2013): Towards Linear-time Incremental Structure from Motion. International conference on 3D Vision.

Yu, G., Knight, D.W. (1998): Geometry of self-formed straight threshold channels in uniform material. Proc., of the Institution of Civil Engineers - Water and Maritime Engineering London, 130 (March), 31-41.

Zaid, B., Koll, Ka. (2016): Sensitivity of the flow to the inclination of a single shallow groyne in a curved flume. In: PM Rowiński & A Marion (eds), Hydrodynamic and Mass Transport at Freshwater Aquatic Interfaces: 34th International School of Hydraulics. GeoPlanet: Earth and Planetary Sciences, Springer, Żelechów, Poland, 245-254.

Zaid, B.A., Koll, Ka. (2016): Experimental investigation of the location of a shallow groyne for bank protection. Int. Conf. on Fluvial Hydraulics, River Flow 2016, Saint Louis, USA, Edited by Constantinescu, Garcia & Hanes, Taylor & Francis Group, London, ISBN 978-1-138-02913-2, 1286-1292.

Zeng J, Constantinescu G, Blanckaert K, Weber L. (2008): Flow and bathymetry in sharp open channel bends: experiments and predictions. Water Resources Research 44: W09401.

Annexes

Annex A

Annex B

Annex A1: Experiment E1 for the inclination angle of shallow groynes

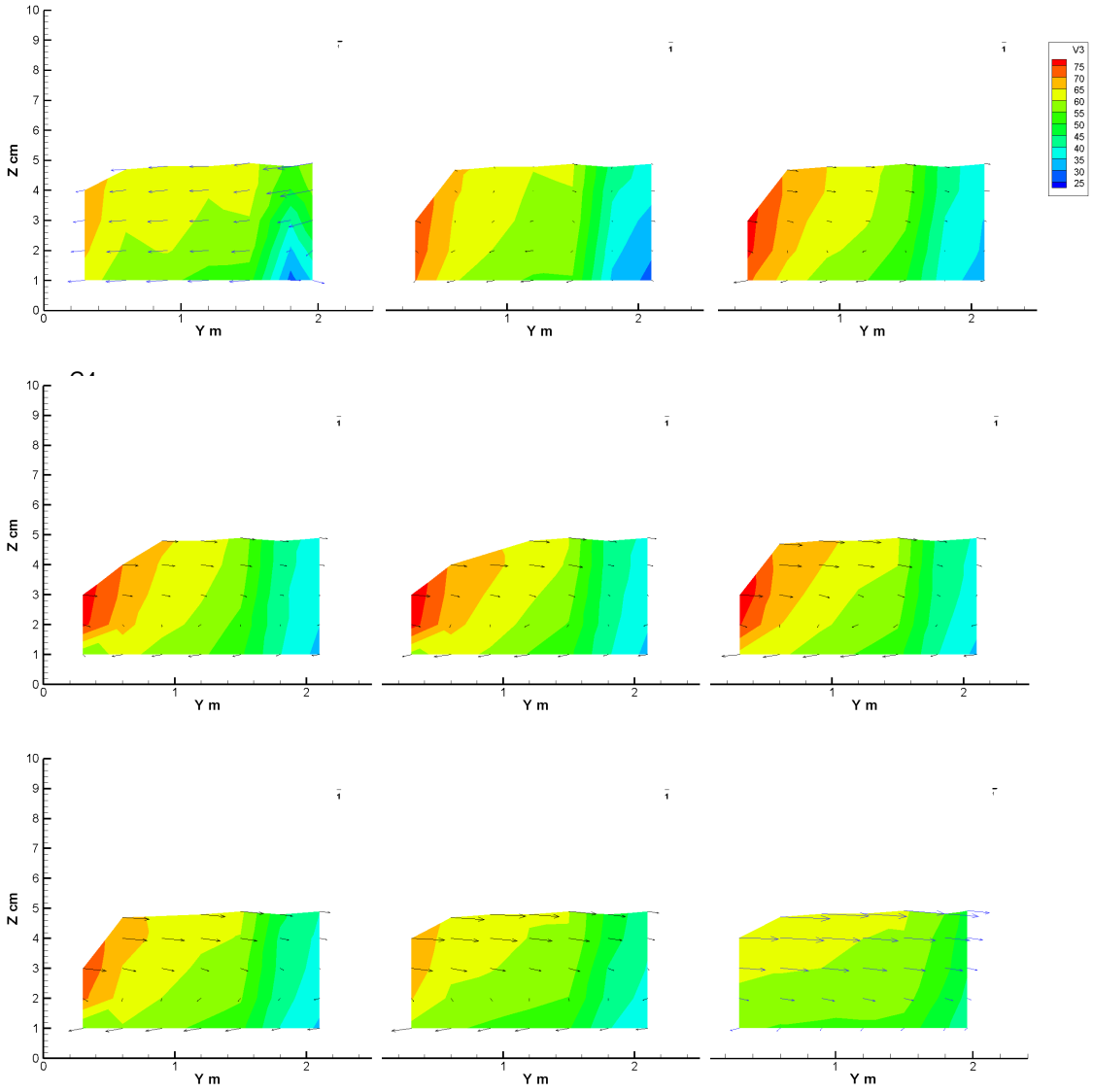

Figure A1 *Cross-sectional view of the 3D velocity field in the test run E1.2*

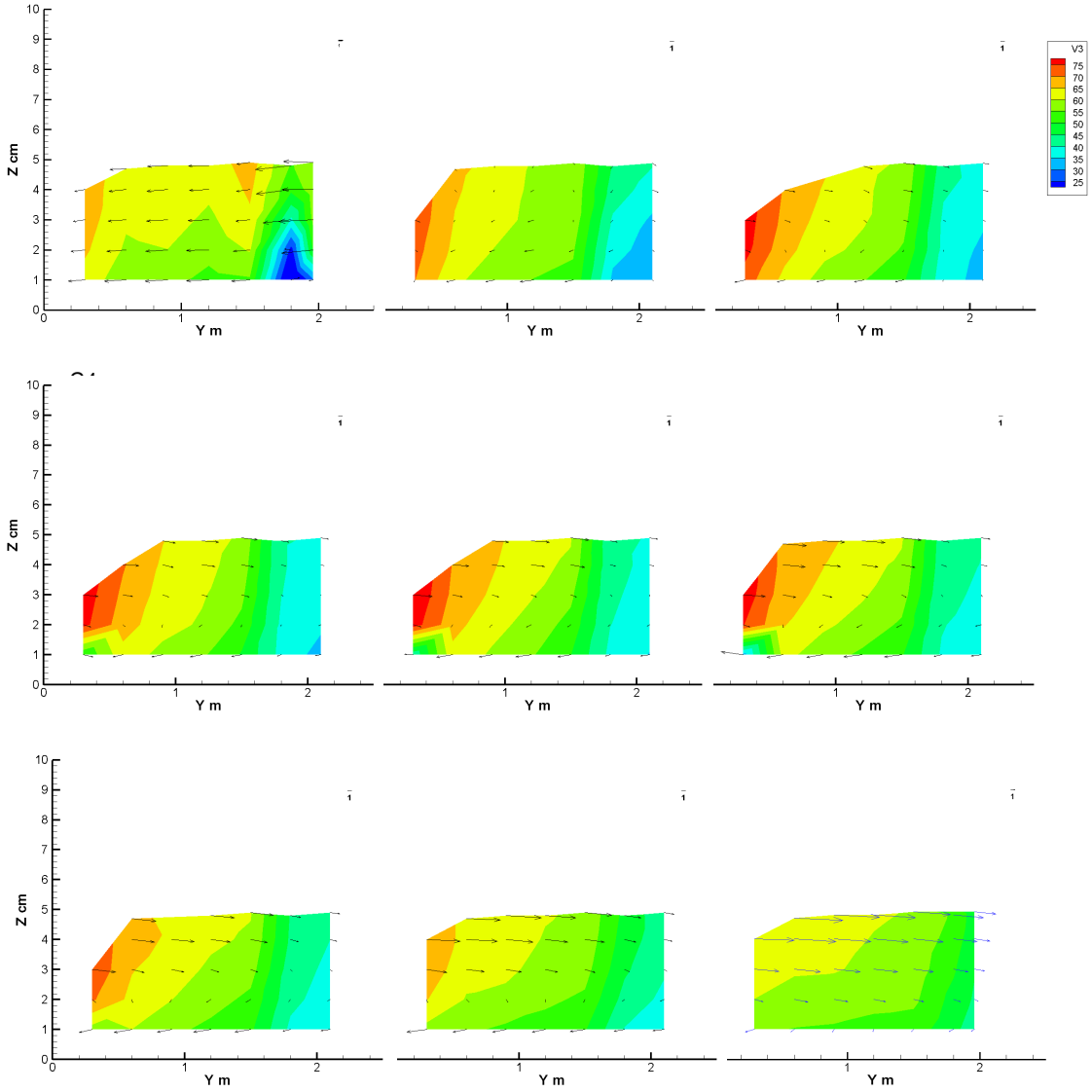

Figure A2 Cross-sectional view of the 3D velocity field in the test run E1.3

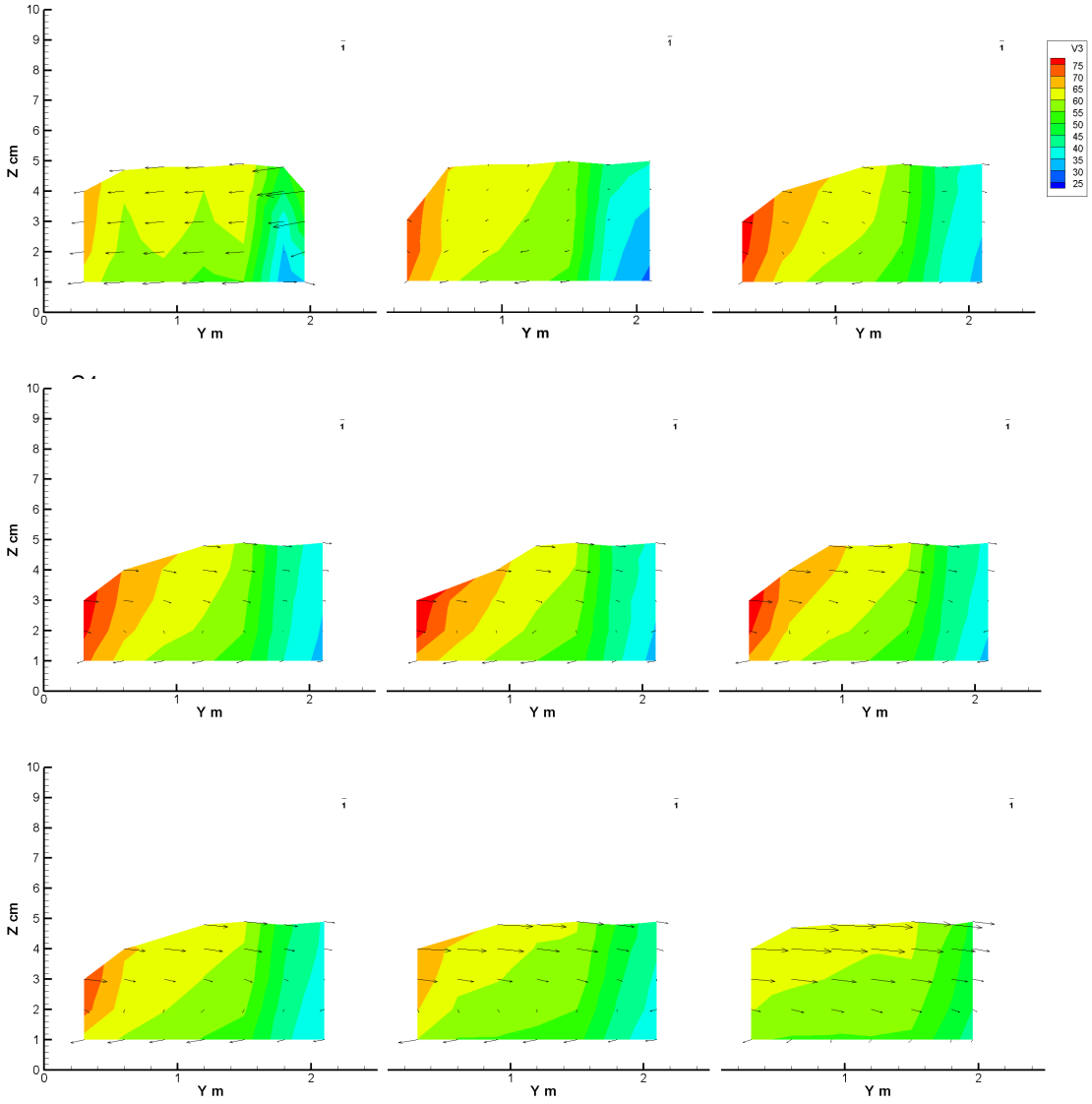

Figure A3 Cross-sectional view of the 3D velocity field in the test run E1.4

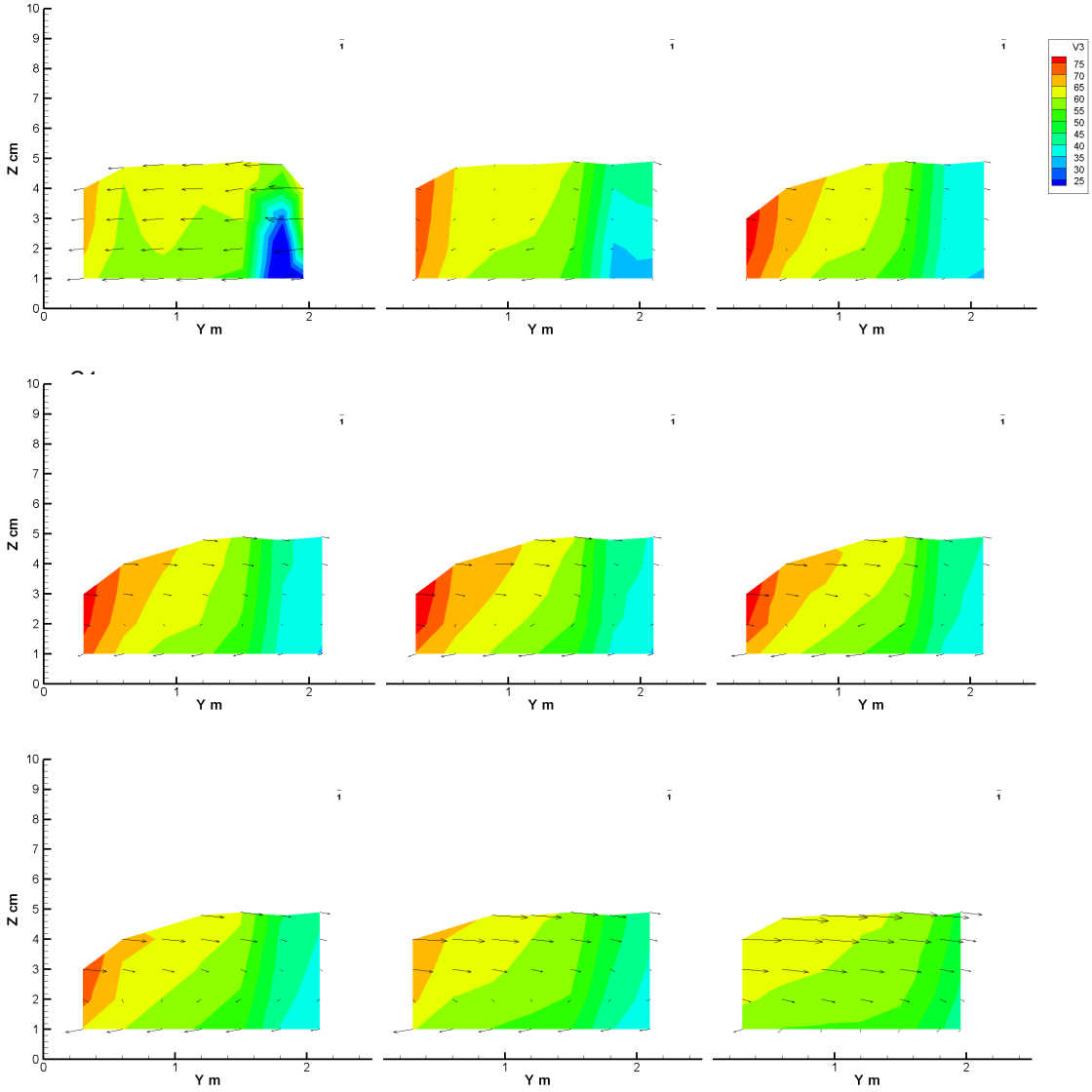

Figure A4 Cross-sectional view of the 3D velocity field in the test run E1.5

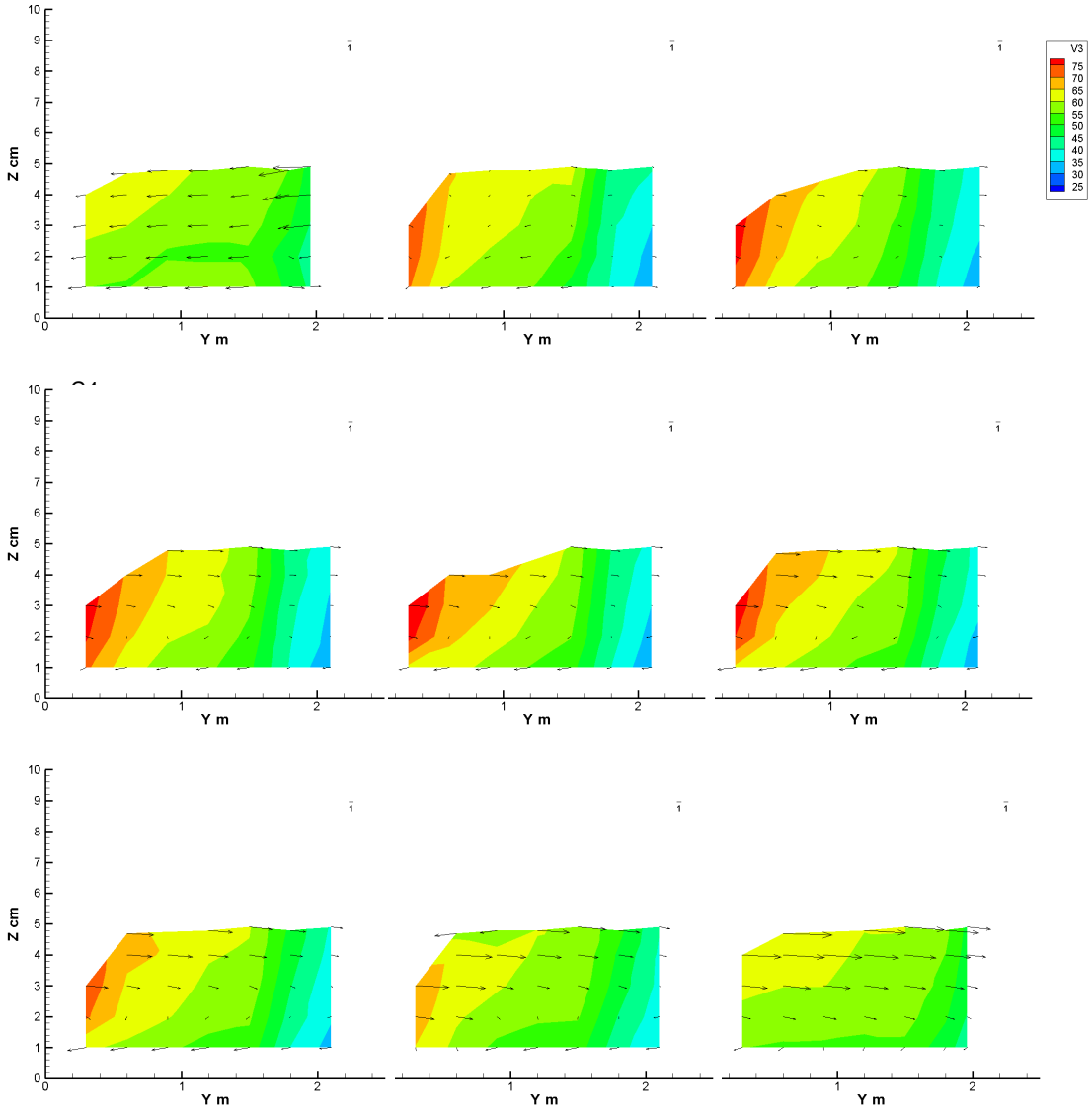

Figure A5 Cross-sectional view of the 3D velocity field in the test run E1.6

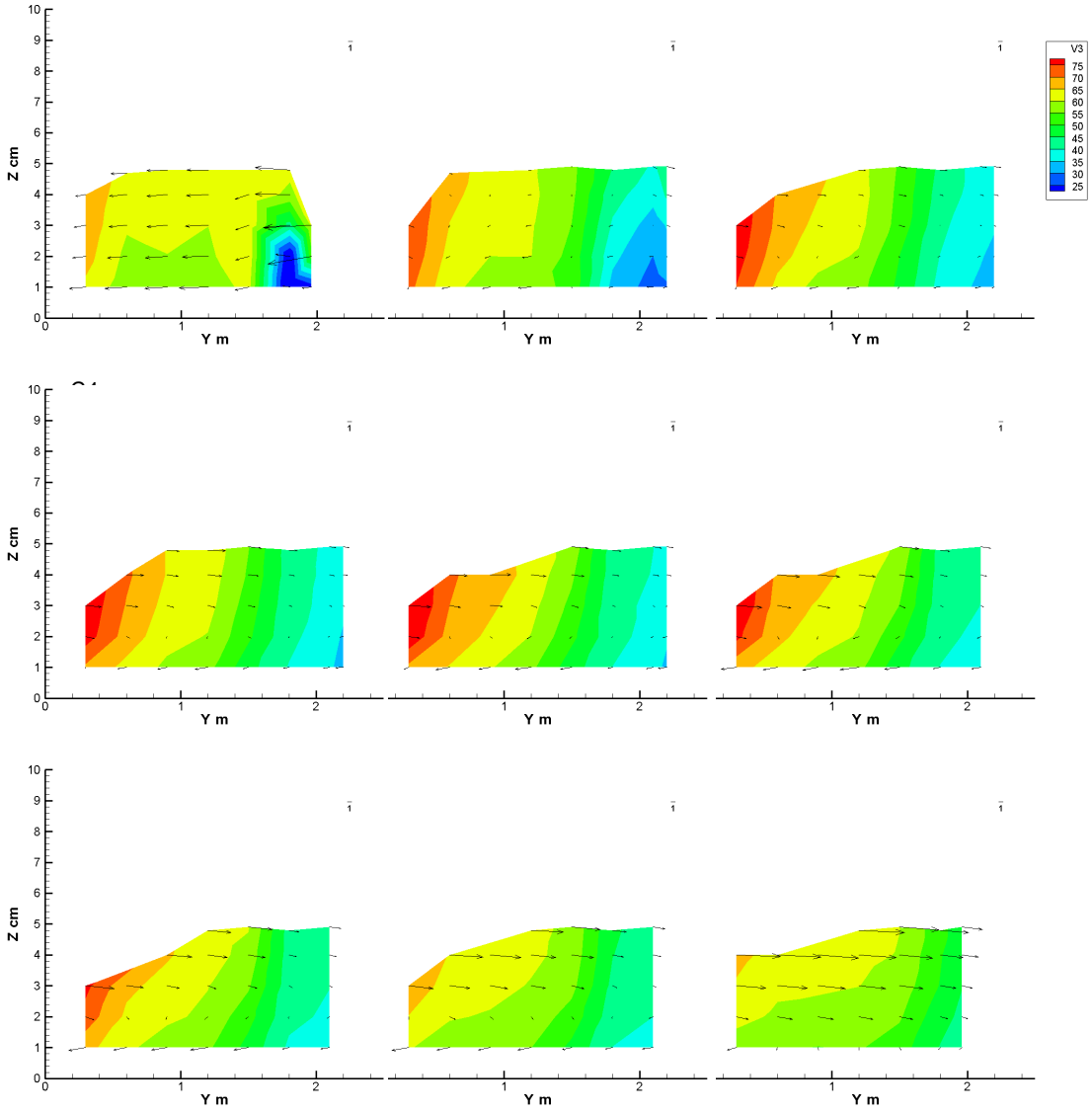

Figure A6 Cross-sectional view of the 3D velocity in the test run E1.7

Annex A2: the effect of the groyne location on the flow field (E2)

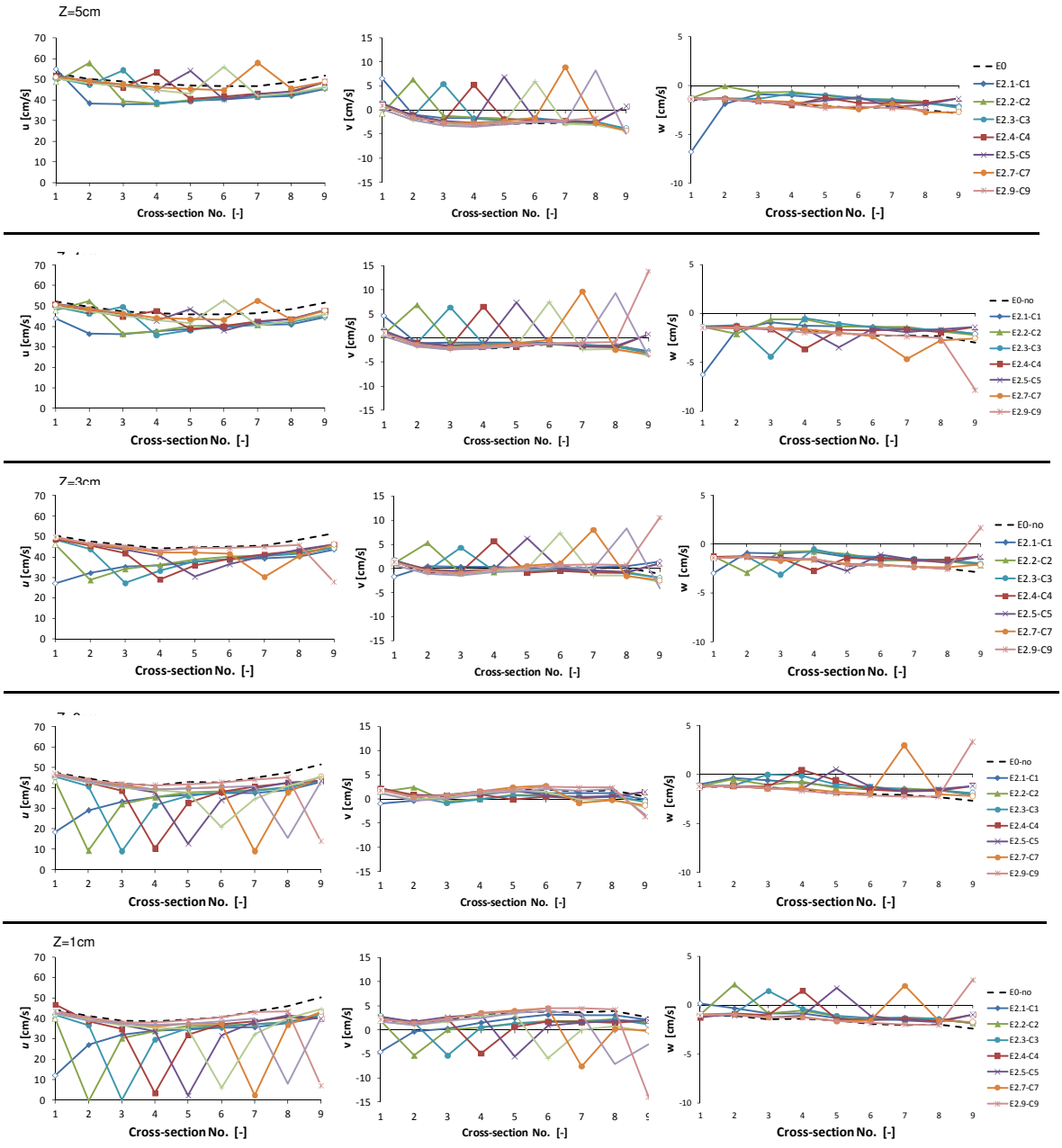

Figure A7 *3D flow field at the longitudinal profile L7 at different levels above the bottom (z=1 to 5cm) and for different groyne locations from C1 to C9*

Annex A3: Experiment E3 for the detailed flow field around one groyne installed at C5

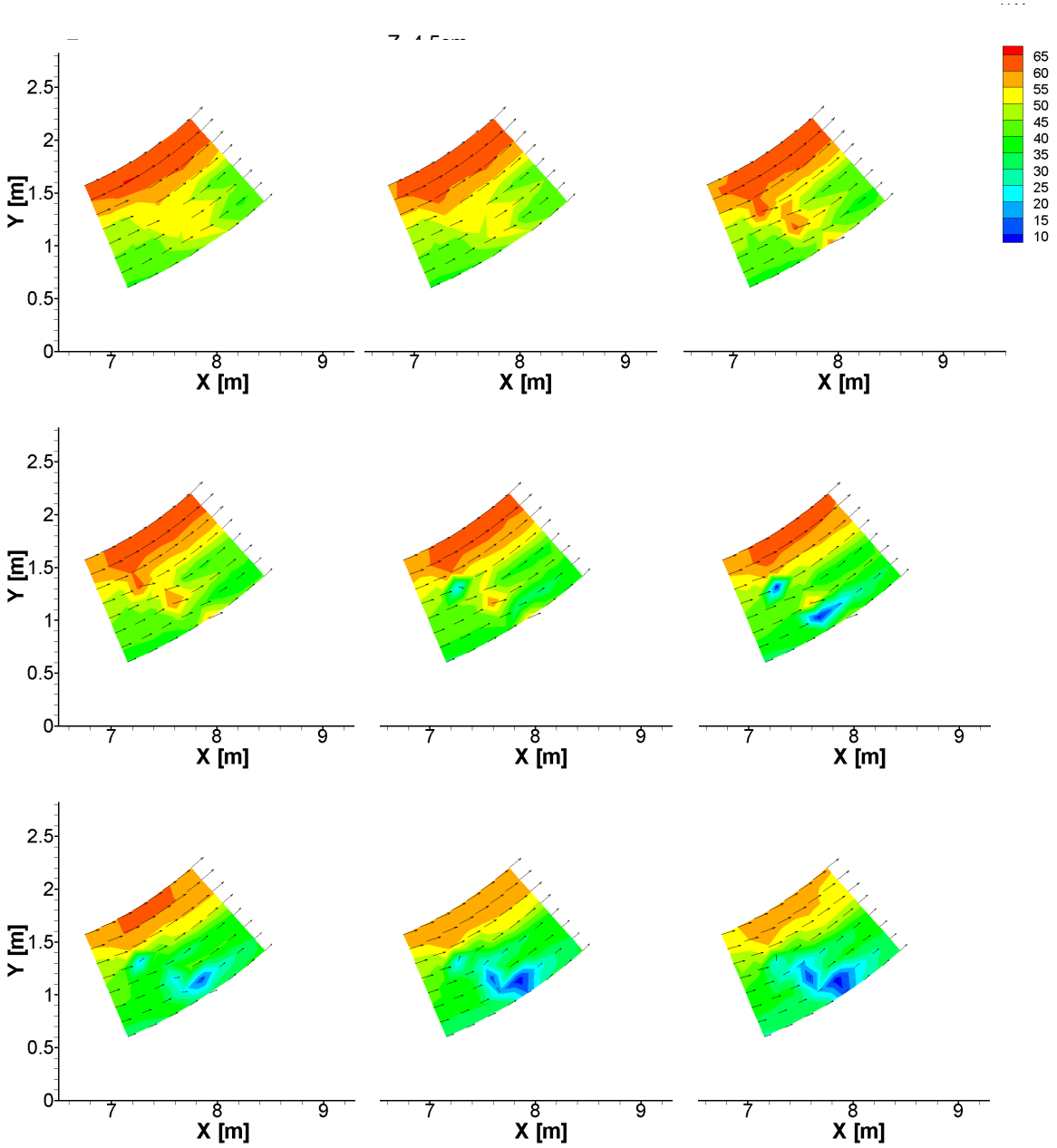

Figure A8 *Top view of the flow field at different levels above the bottom (z=1 to 5cm) with fine grid measurements*

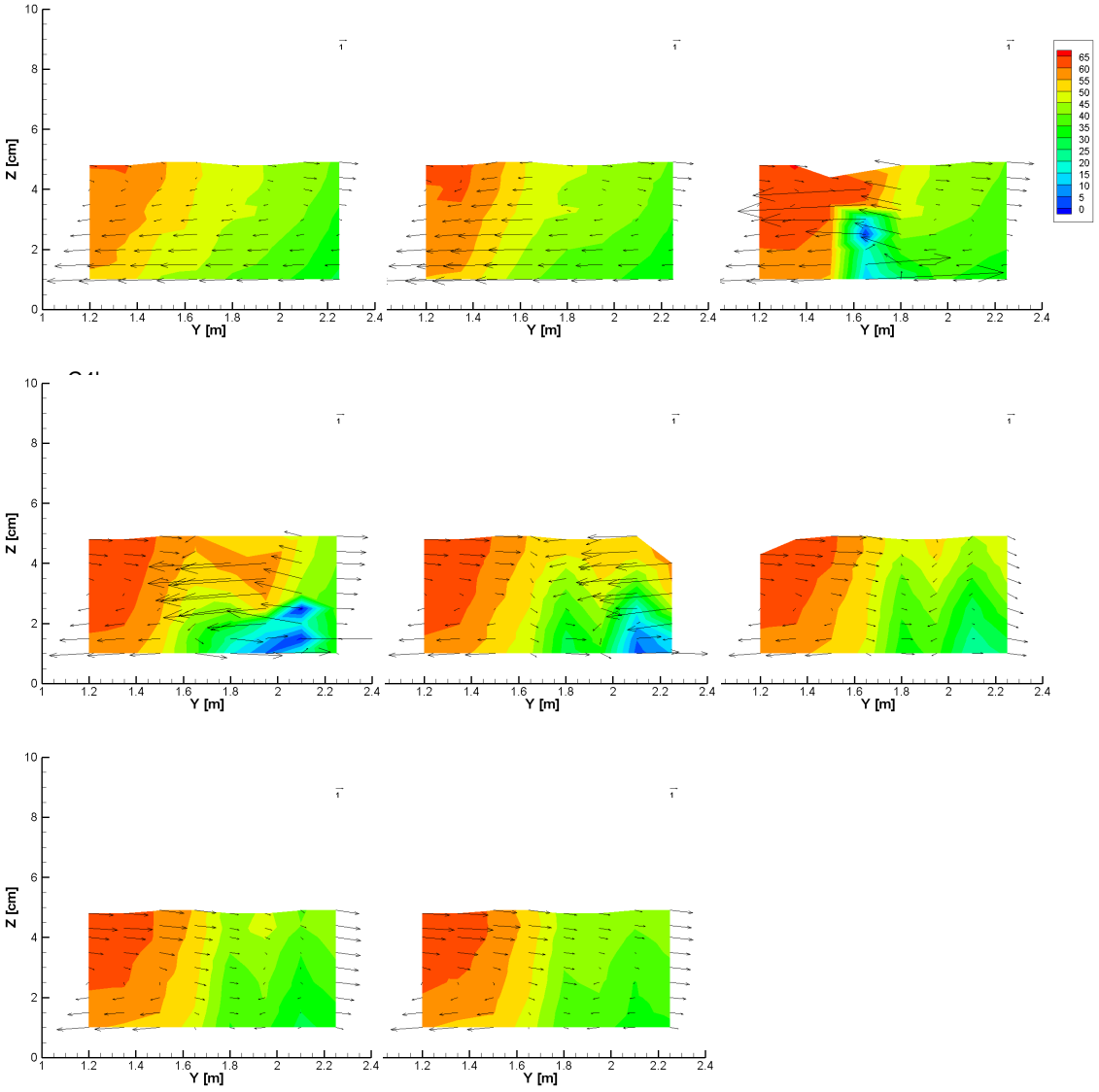

Figure A9 Cross-sectional view of the 3D velocity field with the fine grid measurements (E3)

Annex A4: Experiment E4 on the effect of the groyne projected length (l_p) on the flow field

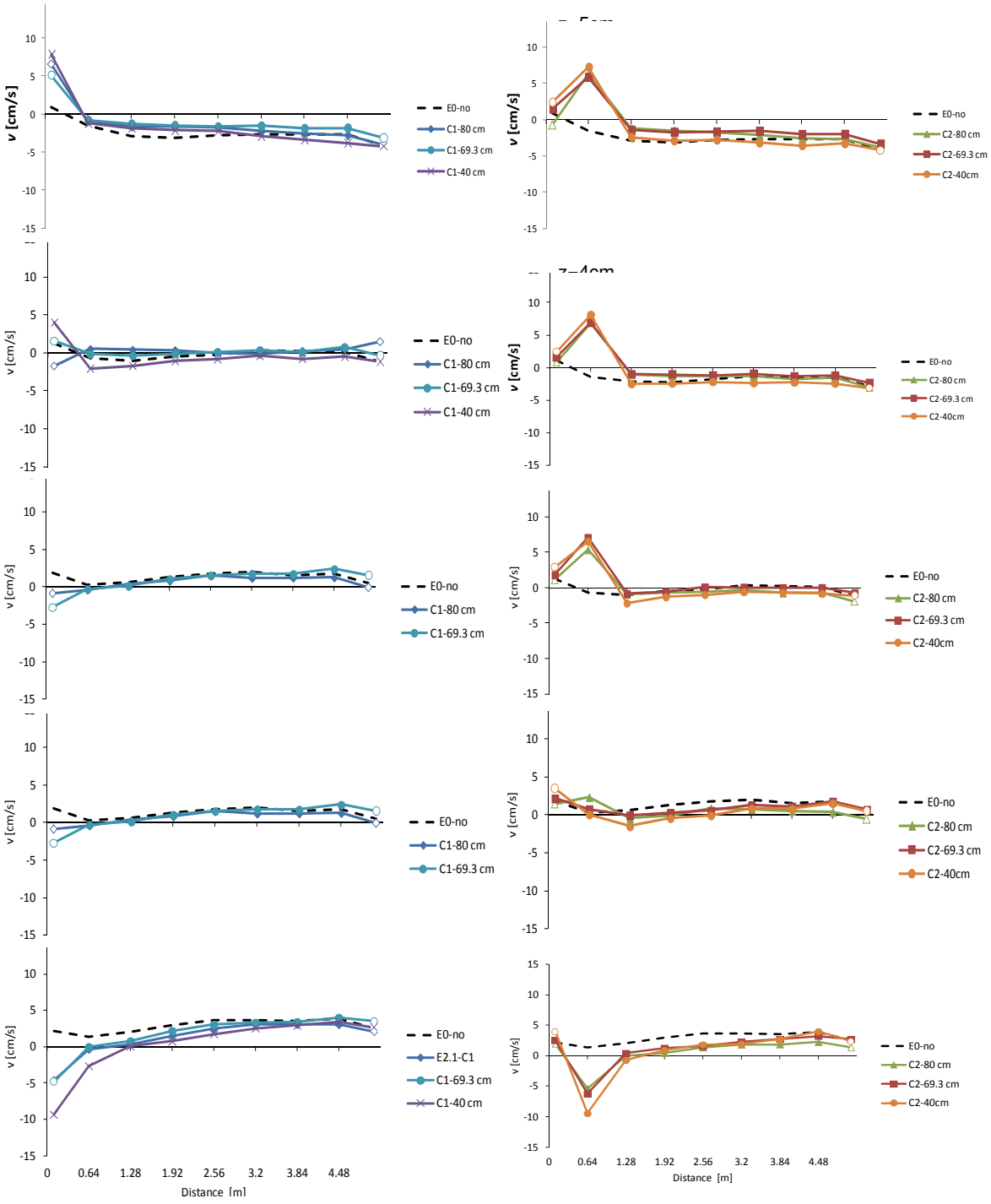

Figure A10 *Transverse velocity v at the longitudinal profile L7 a different levels above the bottom (z=1 to 5cm) for different groyne projected lengths installed at C1 and C2*

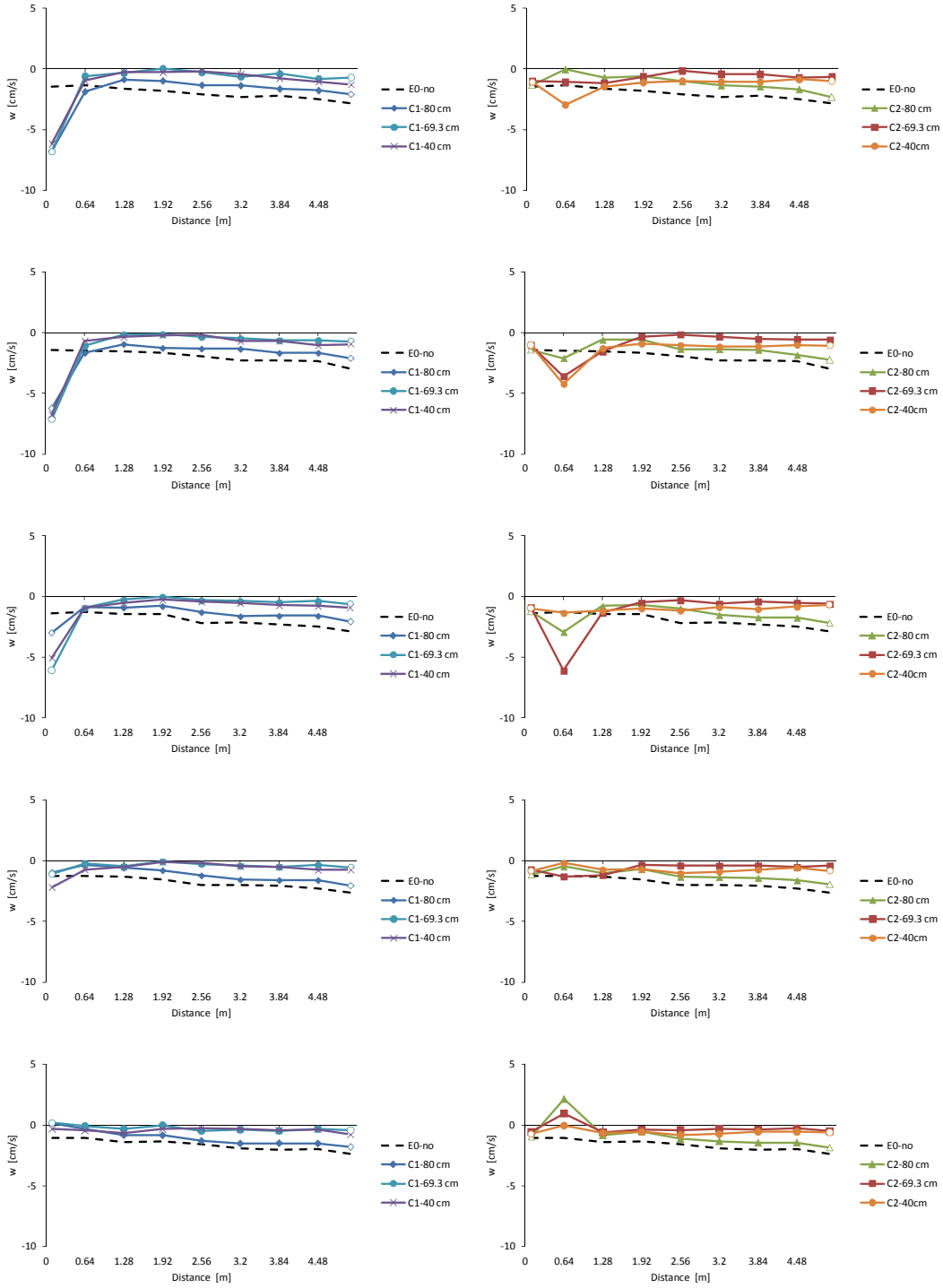

Figure A11 *Vertical velocity w at the longitudinal profile L7 a different levels above the bottom (z=1 to 5cm) for different groyne projected lengths installed at C1 and C2*

Annex A5: The effect of the groyne width (w_g) on the flow field (E5)

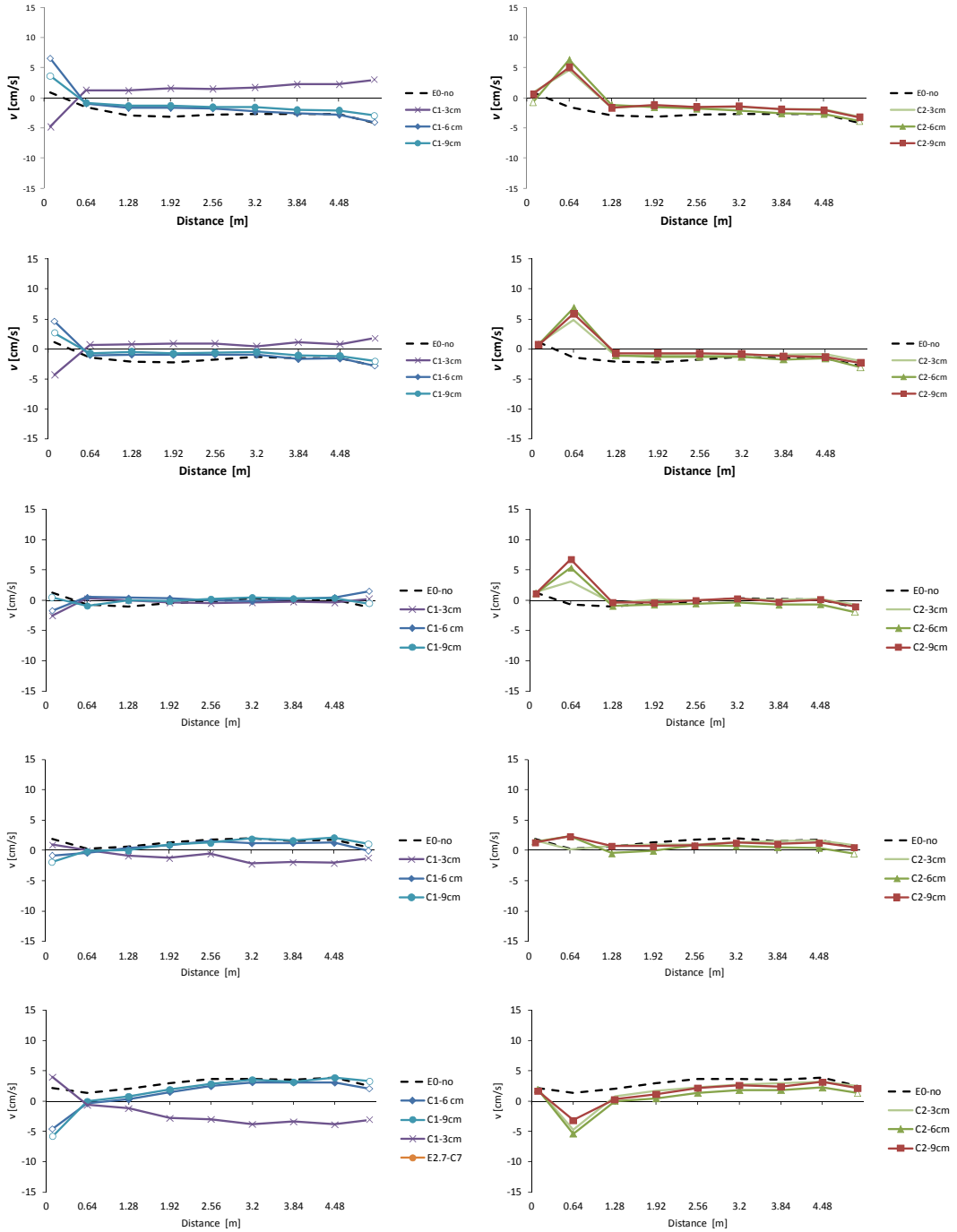

Figure A12 Transverse velocity v at the longitudinal profile L7 a different levels above the bottom (z=1 to 5cm) for groynes with different widths (w_g) installed at C1 and C2

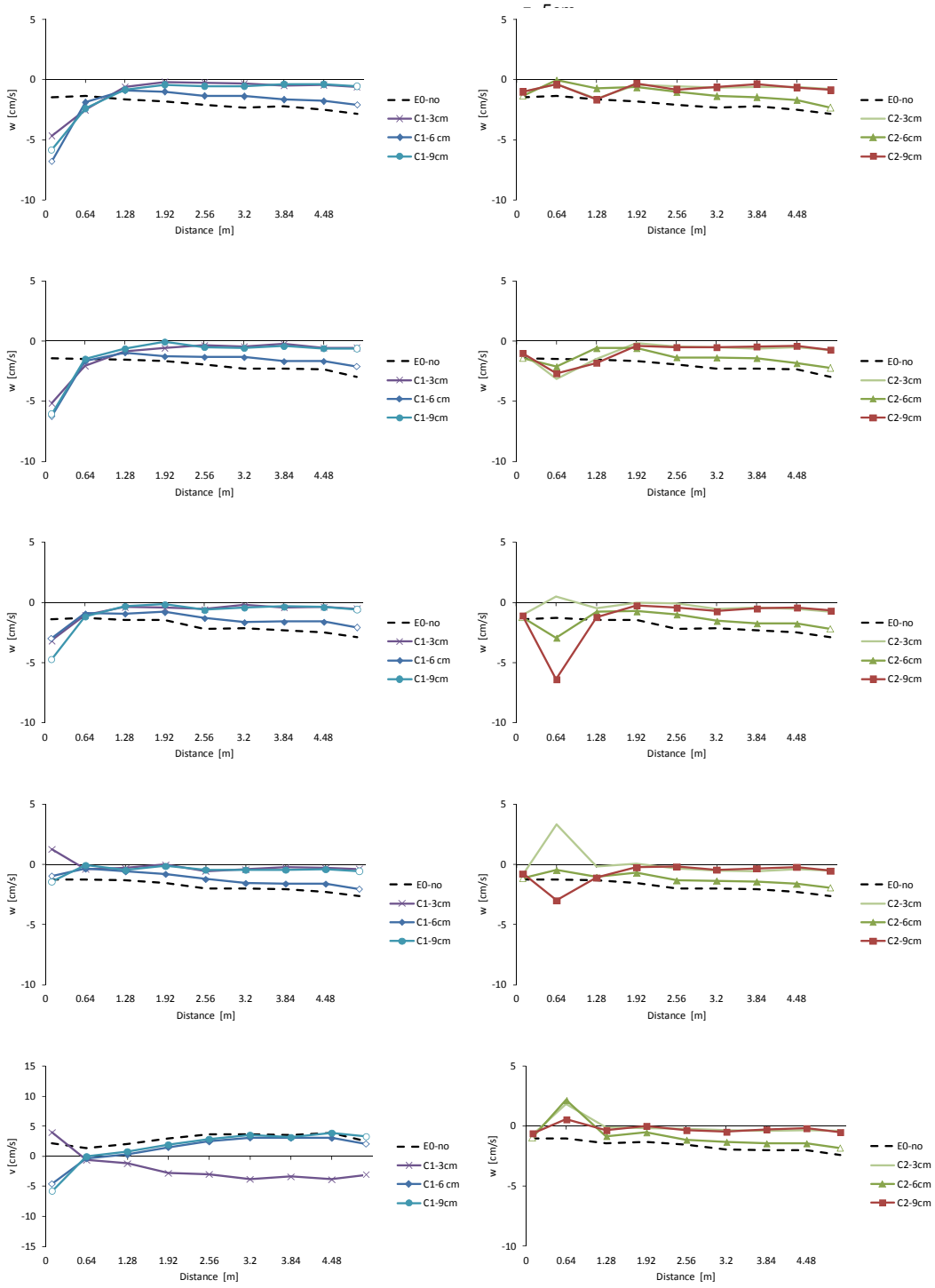

Figure A13 *Vertical velocity w at the longitudinal profile L7 a different levels above the bottom (z=1 to 5cm) for groynes with different widths (w_g) installed at C1 and C2*

Annex A6: Flow field due to the groynes group in the test run E6.1

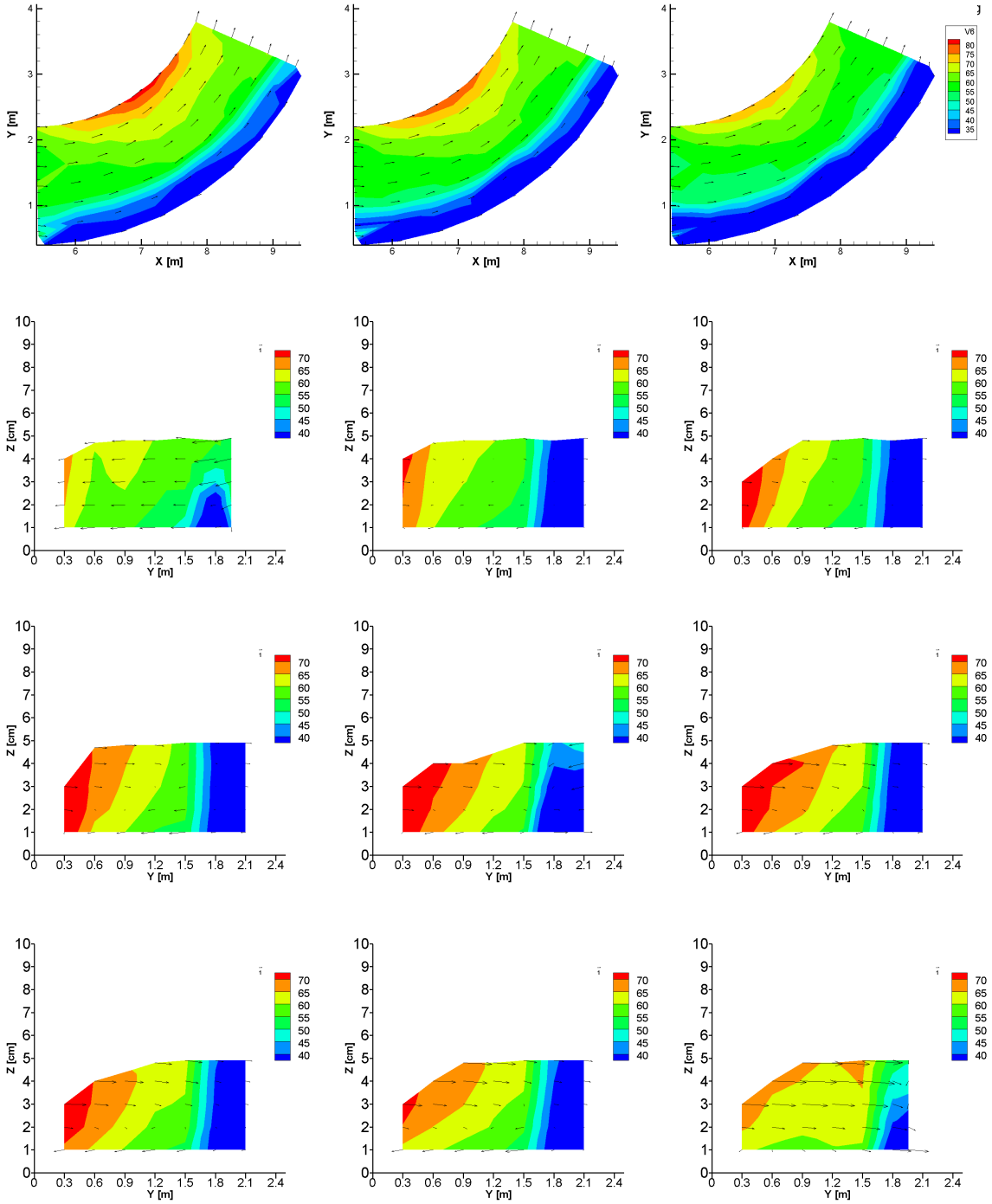

Figure A14 *Flow field in test run E6.1 with three groyne at C1, C5 and C9, top view at z=1, 2 and 3cm above the bottom and cross-sectional view of the 3D velocities at C1 to C9*

Annex B1: Velocity data of the experiment (E0) without groyne

Point	Y [m]	u [cm/s]	v [cm/s]	w [cm/s]	V-Mag [cm/s]
C111	0.3	N/A	N/A	N/A	N/A
C112	0.3	65.41	-2.34	-1.48	65.47
C113	0.3	64.09	-2.79	-1.56	64.17
C114	0.3	61.85	-3.33	-1.61	61.96
C115	0.3	59.44	-4.10	-1.37	59.60
C121	0.6	57.54	-3.25	-0.82	57.64
C122	0.6	56.45	-3.38	-1.24	56.57
C123	0.6	55.26	-3.50	-1.45	55.39
C124	0.6	53.08	-4.08	-1.42	53.25
C125	0.6	51.82	-4.66	-1.29	52.05
C131	0.9	61.24	-4.00	-1.12	61.38
C132	0.9	60.92	-4.13	-1.57	61.08
C133	0.9	59.48	-4.32	-1.54	59.65
C134	0.9	57.67	-4.49	-1.50	57.86
C135	0.9	53.45	-5.12	-1.30	53.71
C141	1.2	62.18	-3.94	-1.45	62.32
C142	1.2	60.95	-4.03	-1.64	61.11
C143	1.2	60.08	-4.32	-1.62	60.26
C144	1.2	56.70	-4.61	-1.54	56.90
C145	1.2	53.60	-4.93	-1.52	53.85
C151	1.5	59.80	-3.49	-1.37	59.92
C152	1.5	58.27	-3.67	-1.66	58.41
C153	1.5	56.24	-3.97	-1.54	56.40
C154	1.5	54.28	-4.29	-1.44	54.47
C155	1.5	51.29	-4.94	-1.45	51.55
C161	1.8	56.35	-2.80	-1.32	56.43
C162	1.8	55.68	-3.10	-1.45	55.79
C163	1.8	53.95	-3.54	-1.43	54.09
C164	1.8	51.48	-4.12	-1.22	51.66
C165	1.8	47.87	-4.36	-1.19	48.09
C171_a	1.96	50.17	-1.82	-0.71	50.21
C172_a	1.96	48.75	-2.05	-1.01	48.80
C173_a	1.96	46.38	-2.48	-0.90	46.46
C174_a	1.96	43.74	-2.66	-0.84	43.83
C175_a	1.96	40.87	-2.87	-0.69	40.98
C171_b	2.1	52.71	-0.84	-1.47	52.74
C172_b	2.1	52.02	-1.12	-1.43	52.05
C173_b	2.1	50.57	-1.29	-1.38	50.61
C174_b	2.1	47.43	-1.88	-1.24	47.49
C175_b	2.1	44.28	-2.17	-1.05	44.34
C211	0.3	N/A	N/A	N/A	N/A
C212	0.3	70.46	1.81	-1.35	70.49
C213	0.3	69.35	1.10	-1.92	69.39
C214	0.3	67.93	0.02	-2.12	67.96
C215	0.3	65.70	-0.96	-1.79	65.73
C221	0.6	60.62	0.33	-1.18	60.64
C222	0.6	60.84	0.36	-1.20	60.85
C223	0.6	59.10	-0.39	-1.69	59.13
C224	0.6	56.98	-1.12	-1.65	57.01
C225	0.6	55.36	-2.31	-1.40	55.42
C231	0.9	62.13	0.09	-1.24	62.15
C232	0.9	61.41	-0.34	-1.57	61.43
C233	0.9	60.06	-0.48	-1.81	60.09
C234	0.9	57.59	-1.30	-1.64	57.63
C235	0.9	55.07	-2.17	-1.65	55.14
C241	1.2	59.60	0.21	-0.78	59.60
C242	1.2	58.75	-0.17	-1.38	58.76
C243	1.2	56.69	-0.41	-1.30	56.70
C244	1.2	54.69	-1.35	-1.28	54.72
C245	1.2	51.56	-2.54	-1.60	51.65
C251	1.5	59.23	0.48	-1.43	59.24
C252	1.5	57.88	0.03	-1.74	57.90
C253	1.5	56.43	-0.33	-1.71	56.46
C254	1.5	54.02	-1.57	-1.54	54.06
C255	1.5	50.32	-2.51	-1.28	50.40
C261	1.8	54.78	0.85	-1.44	54.81
C262	1.8	53.87	0.34	-1.62	53.90
C263	1.8	51.88	-0.40	-1.51	51.91
C264	1.8	48.89	-1.46	-1.25	48.92
C265	1.8	45.47	-2.42	-1.16	45.55
C271	2.1	50.02	1.59	-1.33	50.07
C272	2.1	49.72	1.43	-1.46	49.76
C273	2.1	47.50	0.74	-1.27	47.52
C274	2.1	44.59	-0.31	-1.25	44.61
C275	2.1	41.02	-1.38	-1.05	41.06
C311	0.3	N/A	N/A	N/A	N/A
C312	0.3	73.24	3.33	-1.78	73.34
C313	0.3	72.30	2.23	-2.13	72.36
C314	0.3	70.38	0.72	-2.25	70.42
C315	0.3	67.79	-1.70	-2.20	67.84
C321	0.6	62.91	2.25	-0.85	62.96
C322	0.6	62.03	1.58	-1.39	62.06
C323	0.6	61.61	1.00	-1.63	61.64
C324	0.6	59.95	-0.33	-1.68	59.97
C325	0.6	57.07	-2.29	-1.62	57.14
C331	0.9	62.77	2.32	-0.95	62.82
C332	0.9	61.41	1.68	-1.68	61.45
C333	0.9	59.27	0.87	-1.65	59.30
C334	0.9	57.33	-0.53	-1.91	57.36
C335	0.9	53.43	-2.09	-1.63	53.49
C341	1.2	58.53	2.33	-0.88	58.59
C342	1.2	56.84	1.59	-1.34	56.88
C343	1.2	54.88	0.70	-1.28	54.90
C344	1.2	52.43	-0.89	-1.25	52.45
C345	1.2	49.55	-2.74	-1.26	49.64
C351	1.5	58.56	2.59	-1.69	58.64

* **The measurement point C*i,j,k* :**

i is the cross-section number, j is the longitudinal profile number and k is the vertical level of the point (1, 2,3,4 and 5 correspond to 5, 4, 3, 2 and 1cm above the bottom)

Pioint	Y	u	v	w	Mag
	[m]	[cm/s]	[cm/s]	[cm/s]	V-Avg
C352	1.5	57.62	1.749	-1.93	57.674
C353	1.5	55.57	0.85	-1.86	55.61
C354	1.5	52.62	-0.96	-1.82	52.66
C355	1.5	48.59	-2.82	-1.55	48.70
C361	1.8	52.82	2.45	-1.60	52.90
C362	1.8	51.16	1.43	-1.66	51.20
C363	1.8	48.69	0.31	-1.62	48.72
C364	1.8	46.39	-1.08	-1.61	46.43
C365	1.8	42.55	-2.39	-1.36	42.64
C371	2.1	49.00	2.90	-1.67	49.11
C372	2.1	47.41	2.10	-1.56	47.48
C373	2.1	45.77	1.10	-1.48	45.81
C374	2.1	41.94	-0.57	-1.31	41.96
C375	2.1	38.87	-2.05	-1.41	38.95
C411	0.3	N/A	N/A	N/A	N/A
C412	0.3	N/A	N/A	N/A	N/A
C413	0.3	73.00	2.83	-2.49	73.10
C414	0.3	71.73	0.95	-2.66	71.78
C415	0.3	67.64	-2.60	-2.56	67.74
C421	0.6	63.50	3.30	-1.43	63.60
C422	0.6	63.19	2.98	-1.88	63.29
C423	0.6	62.26	1.47	-2.13	62.32
C424	0.6	61.12	-0.25	-2.29	61.16
C425	0.6	57.68	-3.02	-1.98	57.79
C431	0.9	63.13	3.92	-1.26	63.26
C432	0.9	61.70	3.13	-1.80	61.81
C433	0.9	60.01	1.51	-1.85	60.06
C434	0.9	58.36	-0.22	-2.06	58.40
C435	0.9	53.85	-3.00	-1.85	53.96
C441	1.2	58.81	3.50	-1.05	58.92
C442	1.2	57.04	2.63	-1.60	57.12
C443	1.2	55.66	0.88	-1.68	55.69
C444	1.2	53.76	-0.80	-1.68	53.79
C445	1.2	52.31	-3.56	-2.00	52.47
C451	1.5	57.84	3.75	-1.93	57.99
C452	1.5	56.86	2.56	-2.18	56.96
C453	1.5	54.85	0.77	-2.24	54.90
C454	1.5	51.42	-1.29	-1.95	51.48
C455	1.5	48.20	-3.37	-1.90	48.36
C461	1.8	51.32	3.05	-1.71	51.43
C462	1.8	49.59	1.79	-1.62	49.65
C463	1.8	48.05	0.18	-1.60	48.08
C464	1.8	45.13	-1.37	-1.63	45.18
C465	1.8	41.83	-2.95	-1.30	41.95
C471	2.1	47.85	3.12	-1.82	47.99
C472	2.1	46.43	2.30	-1.67	46.52
C473	2.1	44.12	0.49	-1.47	44.15
C474	2.1	41.29	-1.30	-1.55	41.34

Pioint	Y	u	v	w	Mag
	[m]	[cm/s]	[cm/s]	[cm/s]	V-Avg
C475	2.1	38.37	-2.96	-1.35	38.5034
C511	0.3	N/A	N/A	N/A	N/A
C512	0.3	N/A	N/A	N/A	N/A
C513	0.3	73.82	3.65	-2.70	73.96
C514	0.3	71.66	0.99	-2.89	71.72
C515	0.3	68.32	-2.76	-3.10	68.45
C521	0.6	N/A	N/A	N/A	N/A
C522	0.6	62.94	4.18	-1.54	63.10
C523	0.6	62.57	2.43	-2.25	62.66
C524	0.6	60.09	0.17	-2.56	60.14
C525	0.6	57.93	-3.06	-2.32	58.05
C531	0.9	64.06	5.02	-1.21	64.27
C532	0.9	62.08	3.57	-1.69	62.21
C533	0.9	60.46	1.51	-2.12	60.51
C534	0.9	57.41	-0.73	-2.24	57.46
C535	0.9	54.68	-3.78	-2.13	54.85
C541	1.2	59.05	4.28	-1.11	59.22
C542	1.2	58.33	3.04	-1.90	58.44
C543	1.2	56.77	0.74	-2.00	56.81
C544	1.2	54.59	-1.53	-2.14	54.65
C545	1.2	52.00	-3.88	-2.08	52.18
C551	1.5	58.72	4.21	-2.35	58.91
C552	1.5	56.45	2.70	-2.27	56.56
C553	1.5	54.86	0.59	-2.44	54.92
C554	1.5	51.51	-1.59	-2.34	51.59
C555	1.5	48.01	-4.08	-1.92	48.22
C561	1.8	50.70	3.25	-1.74	50.83
C562	1.8	49.85	1.85	-1.80	49.91
C563	1.8	47.36	0.06	-1.56	47.38
C564	1.8	45.66	-1.43	-1.61	45.71
C565	1.8	42.77	-3.61	-1.45	42.94
C571	2.1	46.91	2.86	-2.10	47.04
C572	2.1	46.01	1.80	-1.96	46.09
C573	2.1	44.73	0.20	-2.20	44.79
C574	2.1	42.85	-1.77	-2.01	42.93
C575	2.1	39.21	-3.61	-1.56	39.41
C611	0.3	N/A	N/A	N/A	N/A
C612	0.3	N/A	N/A	N/A	N/A
C613	0.3	71.98	4.28	-3.22	72.18
C614	0.3	69.86	1.05	-3.19	69.94
C615	0.3	64.93	-3.64	-3.11	65.11
C621	0.6	N/A	N/A	N/A	N/A
C622	0.6	62.94	4.44	-2.21	63.13
C623	0.6	61.48	2.37	-2.48	61.58
C624	0.6	59.98	-0.31	-2.75	60.04
C625	0.6	57.62	-4.08	-2.68	57.82
C631	0.9	63.44	5.79	-1.80	63.72
C632	0.9	62.90	4.41	-2.53	63.10

Pioint	Y	u	v	w	Mag
	[m]	[cm/s]	[cm/s]	[cm/s]	V-Avg
C633	0.9	60.68	2.069	-2.65	60.777
C634	0.9	57.00	-0.73	-2.68	57.07
C635	0.9	55.21	-3.99	-2.73	55.42
C641	1.2	59.47	4.99	-1.81	59.70
C642	1.2	58.32	3.27	-2.21	58.45
C643	1.2	56.26	0.98	-2.25	56.31
C644	1.2	55.01	-1.48	-2.42	55.08
C645	1.2	51.74	-4.45	-2.38	51.99
C651	1.5	57.10	4.33	-2.23	57.30
C652	1.5	55.99	2.89	-2.46	56.12
C653	1.5	54.46	0.42	-2.45	54.51
C654	1.5	51.46	-1.87	-2.47	51.56
C655	1.5	47.42	-4.91	-1.99	47.71
C661	1.8	49.26	3.00	-2.00	49.39
C662	1.8	48.66	1.85	-1.91	48.73
C663	1.8	47.37	0.20	-2.02	47.42
C664	1.8	45.08	-1.61	-1.90	45.15
C665	1.8	43.02	-3.44	-1.85	43.19
C671	2.1	46.53	2.74	-2.31	46.67
C672	2.1	45.75	1.29	-2.30	45.82
C673	2.1	44.87	-0.34	-2.11	44.92
C674	2.1	42.65	-1.96	-2.01	42.74
C675	2.1	40.37	-3.70	-1.93	40.59
C711	0.3	N/A	N/A	N/A	N/A
C712	0.3	N/A	N/A	N/A	N/A
C713	0.3	70.75	4.12	-2.93	70.93
C714	0.3	67.62	0.16	-3.29	67.70
C715	0.3	62.62	-4.95	-3.20	62.90
C721	0.6	62.00	5.77	-1.15	62.28
C722	0.6	61.84	5.15	-1.61	62.08
C723	0.6	60.81	2.82	-2.25	60.92
C724	0.6	58.94	-0.45	-2.62	59.00
C725	0.6	56.03	-4.16	-2.64	56.25
C731	0.9	61.94	6.69	-2.17	62.34
C732	0.9	61.09	5.02	-2.76	61.36
C733	0.9	59.33	2.39	-2.81	59.45
C734	0.9	57.25	-0.53	-2.79	57.32
C735	0.9	54.04	-3.48	-2.75	54.22
C741	1.2	58.41	4.92	-2.34	58.67
C742	1.2	57.95	4.10	-2.59	58.16
C743	1.2	56.56	1.45	-2.59	56.64
C744	1.2	54.35	-0.86	-2.45	54.41
C745	1.2	51.54	-4.22	-2.52	51.78
C751	1.5	56.09	4.46	-2.28	56.32
C752	1.5	54.98	2.83	-2.41	55.10
C753	1.5	53.91	0.87	-2.55	53.97
C754	1.5	52.31	-1.61	-2.63	52.40
C755	1.5	48.13	-4.35	-2.21	48.38

Pioint	Y	u	v	w	Mag
	[m]	[cm/s]	[cm/s]	[cm/s]	V-Avg
C761	1.8	49.38	3.44	-2.15	49.544
C762	1.8	48.90	2.09	-2.18	49.00
C763	1.8	47.56	0.14	-2.16	47.61
C764	1.8	45.26	-1.76	-2.14	45.35
C765	1.8	43.43	-3.86	-2.00	43.65
C771	2.1	46.72	2.69	-2.21	46.85
C772	2.1	46.40	1.52	-2.30	46.48
C773	2.1	45.62	-0.18	-2.33	45.68
C774	2.1	45.01	-1.57	-2.05	45.09
C775	2.1	43.20	-3.57	-2.03	43.40
C811	0.3	N/A	N/A	N/A	N/A
C812	0.3	65.45	7.37	-1.61	65.89
C813	0.3	64.78	4.13	-2.76	64.97
C814	0.3	62.51	0.29	-3.17	62.59
C815	0.3	56.85	-4.88	-2.69	57.13
C821	0.6	62.46	7.87	-2.50	63.00
C822	0.6	61.17	6.13	-2.67	61.53
C823	0.6	59.25	3.12	-2.95	59.40
C824	0.6	57.78	0.01	-2.92	57.85
C825	0.6	54.12	-4.20	-2.81	54.36
C831	0.9	60.49	7.78	-2.30	61.03
C832	0.9	60.26	5.97	-2.61	60.61
C833	0.9	58.48	3.27	-2.79	58.64
C834	0.9	55.84	-0.03	-2.60	55.90
C835	0.9	52.22	-3.38	-2.54	52.39
C841	1.2	57.22	6.56	-2.50	57.65
C842	1.2	56.76	4.81	-2.65	57.02
C843	1.2	55.77	2.38	-2.79	55.89
C844	1.2	53.95	-0.41	-2.56	54.01
C845	1.2	50.76	-3.40	-2.30	50.92
C851	1.5	55.51	5.43	-2.52	55.83
C852	1.5	54.66	3.92	-2.57	54.86
C853	1.5	54.46	1.49	-2.87	54.56
C854	1.5	51.69	-0.73	-2.44	51.75
C855	1.5	48.77	-3.42	-2.27	48.94
C861	1.8	50.92	4.02	-2.40	51.13
C862	1.8	49.63	2.49	-2.42	49.76
C863	1.8	48.18	0.40	-2.31	48.24
C864	1.8	46.93	-1.53	-2.23	47.01
C865	1.8	43.94	-3.94	-2.02	44.16
C871	2.1	48.60	2.71	-2.49	48.74
C872	2.1	48.36	1.53	-2.35	48.44
C873	2.1	48.32	-0.09	-2.46	48.39
C874	2.1	47.60	-1.76	-2.29	47.69
C875	2.1	45.99	-3.90	-1.98	46.20
C911	0.3	N/A	N/A	N/A	N/A
C912	0.3	60.17	8.76	-2.31	60.85
C913	0.3	59.93	5.67	-2.64	60.25

Pioint	Y	u	v	w	Mag
	[m]	[cm/s]	[cm/s]	[cm/s]	V-Avg
C914	0.3	57.23	1.971	-2.59	57.323
C915	0.3	54.17	-2.09	-2.63	54.28
C921	0.6	61.26	11.21	-2.83	62.34
C922	0.6	59.88	9.50	-3.29	60.72
C923	0.6	58.13	6.11	-3.28	58.54
C924	0.6	55.71	2.26	-3.12	55.85
C925	0.6	52.65	-1.12	-2.87	52.74
C931	0.9	59.11	10.54	-2.87	60.11
C932	0.9	58.64	8.59	-3.23	59.36
C933	0.9	57.78	5.94	-3.20	58.17
C934	0.9	56.29	2.98	-3.10	56.46
C935	0.9	52.51	0.03	-2.65	52.57
C941	1.2	58.18	9.53	-2.88	59.03
C942	1.2	57.22	7.75	-3.06	57.83
C943	1.2	56.71	5.21	-2.98	57.03
C944	1.2	54.26	2.21	-2.75	54.37
C945	1.2	52.39	-0.66	-2.74	52.46
C951	1.5	56.97	8.31	-2.65	57.64
C952	1.5	56.46	6.47	-2.85	56.90
C953	1.5	55.40	4.14	-2.75	55.63
C954	1.5	53.28	1.79	-2.61	53.37
C955	1.5	51.38	-0.89	-2.46	51.45
C961	1.8	54.95	6.99	-2.85	55.47
C962	1.8	53.97	5.07	-2.72	54.27
C963	1.8	52.66	3.02	-2.70	52.82
C964	1.8	50.94	0.74	-2.51	51.01
C965	1.8	48.56	-1.84	-2.36	48.65
C971_a	1.96	52.32	5.26	-2.67	52.65
C972_a	1.96	52.06	3.99	-2.68	52.28
C973_a	1.96	51.45	2.07	-2.68	51.56
C974_a	1.96	49.90	0.08	-2.36	49.96
C975_a	1.96	49.03	-2.17	-2.29	49.13
C971_b	2.1	51.60	4.22	-2.87	51.85
C972_b	2.1	51.71	2.88	-2.99	51.87
C973_b	2.1	51.71	1.14	-2.87	51.80
C974_b	2.1	51.47	-0.46	-2.66	51.54
C975_b	2.1	50.10	-2.53	-2.39	50.23

Annex B2: Velocity data for the test run E1.1 with one groyne at C1 and inclination angle of 60°

Point	Y [m]	u [cm/s]	v [cm/s]	w [cm/s]
C111	0.3	N/A	N/A	N/A
C112	0.3	68.18	-2.32	-1.53
C113	0.3	67.45	-2.92	-1.77
C114	0.3	66.57	-3.45	-1.82
C115	0.3	62.72	-4.12	-1.42
C121	0.6	61.50	-3.78	-0.82
C122	0.6	60.36	-3.85	-1.29
C123	0.6	59.30	-4.10	-1.36
C124	0.6	58.12	-4.78	-1.55
C125	0.6	55.76	-4.97	-1.31
C131	0.9	64.98	-4.79	-1.06
C132	0.9	64.01	-4.88	-1.54
C133	0.9	62.87	-4.97	-1.76
C134	0.9	61.12	-5.14	-1.62
C135	0.9	57.29	-5.29	-1.37
C141	1.2	61.98	-4.69	-0.12
C142	1.2	61.22	-4.79	-0.95
C143	1.2	60.01	-4.97	-1.06
C144	1.2	57.72	-5.47	-0.94
C145	1.2	54.24	-5.71	-1.08
C151	1.5	62.67	-4.02	1.01
C152	1.5	62.21	-3.98	0.25
C153	1.5	60.76	-3.98	-0.28
C154	1.5	57.58	-4.44	-0.42
C155	1.5	52.36	-4.76	-0.63
C161	1.8	58.36	-9.14	-2.70
C162	1.8	55.57	-8.47	-3.86
C163	1.8	48.50	-6.01	-4.60
C164	1.8	36.11	-2.42	-1.51
C165	1.8	27.53	1.92	0.96
C171_a	1.96	57.57	-6.81	-4.07
C172_a	1.96	57.10	-7.14	-4.68
C173_a	1.96	55.59	-6.93	-5.44
C174_a	1.96	51.26	-5.13	-6.28
C175_a	1.96	40.91	-0.99	-4.79
C175_b	2.1	55.59	6.94	-6.32
C171_b	2.1	50.81	6.12	-7.36
C172_b	2.1	34.81	2.61	-5.34
C173_b	2.1	21.81	-0.38	-1.29
C174_b	2.1	14.52	-3.63	0.25
C211	0.3	0.00	0.00	0.00
C212	0.3	0.00	0.00	0.00
C213	0.3	74.00	1.24	-1.92
C214	0.3	73.45	0.47	-2.19
C215	0.3	70.46	-0.82	-1.92
C221	0.6	0.00	0.00	0.00
C222	0.6	64.83	0.44	-1.29
C223	0.6	63.93	-0.06	-1.62
C224	0.6	63.19	-0.87	-1.7
C225	0.6	60.45	-1.80	-1.51
C231	0.9	64.30	-0.08	-1.36
C232	0.9	62.90	-0.38	-1.70
C233	0.9	62.05	-0.62	-1.80
C234	0.9	60.39	-1.38	-1.74
C235	0.9	57.59	-2.31	-1.71
C241	1.2	62.53	0.42	-1.85
C242	1.2	62.58	0.12	-2.21
C243	1.2	61.30	-0.72	-1.96
C244	1.2	58.67	-1.56	-1.54
C245	1.2	57.18	-2.68	-1.87
C251	1.5	60.69	0.86	-1.80
C252	1.5	59.79	0.46	-2.15
C253	1.5	57.97	-0.19	-1.91
C254	1.5	56.49	-0.98	-1.87
C255	1.5	54.84	-1.76	-1.79
C261	1.8	44.38	-0.44	-1.23
C262	1.8	41.66	-0.73	-1.22
C263	1.8	39.48	-0.61	-1.26
C264	1.8	37.09	-0.37	-0.95
C265	1.8	34.92	-0.23	-0.66
C271	2.1	39.49	0.80	-0.54
C272	2.1	37.49	0.52	-0.99
C273	2.1	34.81	0.81	-0.85
C274	2.1	31.36	0.37	-0.11
C275	2.1	30.19	0.57	-0.37
C311	0.3	N/A	N/A	N/A
C312	0.3	N/A	N/A	N/A
C313	0.3	78.48	2.53	-1.55
C314	0.3	76.67	1.31	-2.08
C315	0.3	73.30	-0.69	-2.00
C321	0.6	N/A	N/A	N/A
C322	0.6	68.72	2.41	-1.21
C323	0.6	67.26	1.47	-1.92
C324	0.6	65.88	0.09	-2.00
C325	0.6	62.65	-1.86	-1.86
C331	0.9	N/A	N/A	N/A
C332	0.9	65.15	2.43	-0.92
C333	0.9	63.77	1.45	-1.30
C334	0.9	61.60	0.25	-1.65
C335	0.9	58.31	-1.53	-1.65
C341	1.2	N/A	N/A	N/A
C342	1.2	61.98	2.78	-0.62
C343	1.2	61.00	1.43	-1.25
C344	1.2	60.27	-0.04	-1.55
C345	1.2	57.12	-2.15	-1.57
C351	1.5	58.94	2.51	-1.53

Point	Y [m]	u [cm/s]	v [cm/s]	w [cm/s]
C352	1.5	57.81	1.9	-1.82
C353	1.5	56.19	1.12	-1.80
C354	1.5	54.21	-0.02	-1.63
C355	1.5	51.58	-1.85	-1.49
C361	1.8	42.28	1.39	-0.89
C362	1.8	40.85	0.97	-0.96
C363	1.8	39.61	0.48	-0.88
C364	1.8	38.97	0.12	-0.77
C365	1.8	37.27	-0.69	-0.90
C371	2.1	37.52	1.53	-0.79
C372	2.1	37.07	1.28	-0.74
C373	2.1	36.18	0.87	-0.93
C374	2.1	34.97	0.18	-0.52
C375	2.1	33.40	-0.84	-0.61
C411	0.3	N/A	N/A	N/A
C412	0.3	N/A	N/A	N/A
C413	0.3	78.10	3.78	-1.71
C414	0.3	76.19	1.81	-2.15
C415	0.3	72.51	-1.51	-2.21
C421	0.6	0.00	0.00	0.00
C422	0.6	69.09	3.84	-0.69
C423	0.6	68.13	2.46	-1.49
C424	0.6	66.62	0.45	-1.93
C425	0.6	62.74	-2.35	-1.91
C431	0.9	N/A	N/A	N/A
C432	0.9	66.35	3.91	-2.53
C433	0.9	64.44	2.48	-2.56
C434	0.9	62.59	0.58	-2.38
C435	0.9	58.90	-2.12	-2.04
C441	1.2	62.36	3.92	-0.74
C442	1.2	61.72	3.24	-1.38
C443	1.2	61.49	1.81	-1.82
C444	1.2	59.45	-0.32	-1.98
C445	1.2	56.05	-2.48	-1.86
C451	1.5	60.45	3.83	-1.69
C452	1.5	59.11	3.07	-2.02
C453	1.5	57.51	1.74	-2.14
C454	1.5	55.39	-0.05	-2.21
C455	1.5	52.09	-2.16	-1.86
C461	1.8	42.71	1.97	-1.16
C462	1.8	41.76	1.35	-1.15
C463	1.8	41.48	0.64	-1.24
C464	1.8	39.79	-0.10	-1.17
C465	1.8	38.67	-0.76	-1.10
C471	2.1	38.33	1.69	-0.72
C472	2.1	37.75	1.10	-0.90
C473	2.1	36.21	0.33	-0.77
C474	2.1	35.42	-0.38	-0.65

Point	Y [m]	u [cm/s]	v [cm/s]	w [cm/s]
C475	2.1	34.06	-1.72	-0.85
C511	0.3	N/A	N/A	N/A
C512	0.3	N/A	N/A	N/A
C513	0.3	80.27	5.01	-1.28
C514	0.3	77.99	2.21	-1.88
C515	0.3	71.75	-1.79	-2.02
C521	0.6	N/A	N/A	N/A
C522	0.6	69.55	3.98	-0.92
C523	0.6	68.57	2.46	-2.07
C524	0.6	66.37	-0.12	-2.42
C525	0.6	63.12	-3.59	-2.44
C531	0.9	N/A	N/A	N/A
C532	0.9	66.94	4.12	-2.29
C533	0.9	65.17	2.51	-2.58
C534	0.9	63.19	-0.01	-2.81
C535	0.9	59.78	-3.08	-2.63
C541	1.2	62.71	4.66	-1.48
C542	1.2	61.87	3.54	-2.01
C543	1.2	60.71	1.11	-2.32
C544	1.2	58.51	-1.22	-2.23
C545	1.2	56.16	-3.78	-2.29
C551	1.5	61.46	4.57	-1.94
C552	1.5	60.28	3.23	-2.37
C553	1.5	58.72	1.75	-2.56
C554	1.5	56.25	-0.57	-2.36
C555	1.5	53.10	-2.95	-2.20
C561	1.8	43.41	2.09	-1.37
C562	1.8	43.14	1.43	-1.48
C563	1.8	42.14	0.60	-1.43
C564	1.8	41.43	-0.28	-1.30
C565	1.8	40.29	-1.69	-1.29
C571	2.1	39.89	2.01	-1.16
C572	2.1	39.58	1.30	-1.41
C573	2.1	37.98	0.31	-1.27
C574	2.1	35.80	-0.97	-1.00
C575	2.1	34.86	-1.91	-1.09
C611	0.3	N/A	N/A	N/A
C612	0.3	N/A	N/A	N/A
C613	0.3	79.40	5.86	-1.66
C614	0.3	75.96	1.88	-2.32
C615	0.3	68.42	-3.45	-2.26
C621	0.6	N/A	N/A	N/A
C622	0.6	68.47	6.04	-1.89
C623	0.6	67.15	3.69	-2.50
C624	0.6	65.20	0.14	-2.60
C625	0.6	61.88	-3.60	-2.77
C631	0.9	66.32	5.77	-2.38
C632	0.9	65.09	4.51	-2.64

Point	Y [m]	u [cm/s]	v [cm/s]	w [cm/s]
C633	0.9	64.3	2.108	-2.91
C634	0.9	62.18	-0.46	-3.17
C635	0.9	57.69	-3.79	-2.77
C641	1.2	63.29	5.60	-1.68
C642	1.2	62.55	3.77	-2.20
C643	1.2	60.94	1.61	-2.67
C644	1.2	58.82	-1.45	-2.48
C645	1.2	55.47	-4.64	-2.47
C651	1.5	61.58	5.21	-2.30
C652	1.5	60.32	3.58	-2.69
C653	1.5	58.18	1.49	-2.79
C654	1.5	55.24	-0.88	-2.53
C655	1.5	51.37	-3.77	-2.49
C661	1.8	44.39	2.37	-1.70
C662	1.8	43.74	1.47	-1.75
C663	1.8	42.86	0.55	-1.49
C664	1.8	41.65	-0.58	-1.80
C665	1.8	40.54	-1.74	-1.70
C671	2.1	41.03	2.43	-1.35
C672	2.1	39.83	1.24	-1.53
C673	2.1	39.53	0.23	-1.58
C674	2.1	37.08	-1.30	-1.36
C675	2.1	35.97	-2.50	-1.32
C711	0.3	N/A	N/A	N/A
C712	0.3	N/A	N/A	N/A
C713	0.3	74.50	5.70	-2.18
C714	0.3	72.00	1.44	-3.18
C715	0.3	63.69	-4.93	-2.85
C721	0.6	N/A	N/A	N/A
C722	0.6	66.27	5.93	-2.66
C723	0.6	65.39	3.39	-3.25
C724	0.6	63.39	0.28	-3.27
C725	0.6	59.99	-4.12	-3.12
C731	0.9	0.00	0.00	0.00
C732	0.9	64.08	5.58	-2.05
C733	0.9	62.50	2.93	-2.50
C734	0.9	59.83	-0.46	-2.69
C735	0.9	56.61	-3.85	-2.65
C741	1.2	61.32	5.74	-2.17
C742	1.2	60.63	4.46	-2.31
C743	1.2	59.16	1.87	-2.67
C744	1.2	56.98	-1.12	-2.65
C745	1.2	54.19	-4.29	-2.62
C751	1.5	60.91	5.74	-2.54
C752	1.5	59.78	4.39	-2.91
C753	1.5	58.09	1.60	-2.93
C754	1.5	54.69	-0.76	-2.71
C755	1.5	51.63	-3.97	-2.71

Point	Y [m]	u [cm/s]	v [cm/s]	w [cm/s]
C761	1.8	45.87	2.799	-1.87
C762	1.8	45.00	1.91	-1.92
C763	1.8	43.86	0.83	-2.02
C764	1.8	42.29	-0.64	-2.02
C765	1.8	40.26	-2.29	-1.89
C771	2.1	41.45	2.95	-1.73
C772	2.1	39.99	1.79	-1.54
C773	2.1	39.55	0.78	-1.67
C774	2.1	38.50	-0.82	-1.75
C775	2.1	36.22	-2.28	-1.51
C811	0.3	N/A	N/A	N/A
C812	0.3	69.50	8.36	-1.67
C813	0.3	68.47	4.76	-2.80
C814	0.3	65.50	0.54	-2.97
C815	0.3	59.58	-4.68	-2.75
C821	0.6	63.64	8.65	-2.27
C822	0.6	63.19	7.20	-2.68
C823	0.6	61.16	4.00	-2.79
C824	0.6	59.27	0.54	-3.08
C825	0.6	55.80	-3.73	-2.91
C831	0.9	63.48	9.15	-2.13
C832	0.9	62.96	7.06	-2.66
C833	0.9	61.29	3.95	-2.89
C834	0.9	58.24	0.73	-2.76
C835	0.9	54.84	-3.09	-2.58
C841	1.2	60.75	7.64	-2.34
C842	1.2	59.78	5.84	-2.70
C843	1.2	58.02	2.97	-2.62
C844	1.2	56.49	0.20	-2.57
C845	1.2	53.17	-3.27	-2.42
C851	1.5	59.71	7.08	-2.69
C852	1.5	59.11	5.25	-2.92
C853	1.5	57.31	2.47	-2.93
C854	1.5	54.56	-0.20	-2.83
C855	1.5	51.52	-3.47	-2.74
C861	1.8	48.91	4.44	-2.32
C862	1.8	47.54	3.06	-2.24
C863	1.8	45.95	1.36	-2.26
C864	1.8	43.37	-0.55	-1.98
C865	1.8	40.80	-2.39	-1.78
C871	2.1	41.50	2.73	-1.81
C872	2.1	41.45	2.00	-1.77
C873	2.1	40.27	0.47	-1.78
C874	2.1	38.94	-0.81	-1.56
C875	2.1	37.71	-2.70	-1.58
C911	0.3	N/A	N/A	N/A
C912	0.3	63.20	9.98	-1.41
C913	0.3	62.58	6.44	-2.18

Point	Y [m]	u [cm/s]	v [cm/s]	w [cm/s]
C914	0.3	60.72	2.532	-2.86
C915	0.3	55.78	-2.24	-2.46
C921	0.6	64.10	12.73	-2.20
C922	0.6	63.62	11.07	-2.66
C923	0.6	60.69	7.41	-2.96
C924	0.6	58.32	3.23	-2.90
C925	0.6	54.87	-0.78	-2.95
C931	0.9	61.92	11.27	-2.70
C932	0.9	61.48	9.24	-2.93
C933	0.9	59.96	6.40	-3.12
C934	0.9	57.89	3.34	-2.80
C935	0.9	54.25	-0.30	-2.65
C941	1.2	60.64	10.60	-2.70
C942	1.2	59.99	8.74	-3.12
C943	1.2	59.27	6.03	-3.12
C944	1.2	56.86	2.97	-2.85
C945	1.2	54.13	-0.19	-2.66
C951	1.5	60.08	9.67	-2.87
C952	1.5	59.44	7.78	-3.05
C953	1.5	58.28	5.19	-3.12
C954	1.5	56.29	2.45	-3.01
C955	1.5	53.49	-0.40	-2.70
C961	1.8	54.43	7.63	-2.85
C962	1.8	53.70	6.16	-2.91
C963	1.8	51.43	4.03	-2.68
C964	1.8	48.81	1.86	-2.45
C965	1.8	45.75	-0.34	-2.32
C971_a	1.96	48.25	5.17	-2.50
C972_a	1.96	47.53	4.07	-2.43
C973_a	1.96	46.19	2.18	-2.35
C974_a	1.96	44.53	0.91	-2.19
C975_a	1.96	42.81	-0.79	-2.13
C971_b	2.1	45.45	4.16	-2.27
C972_b	2.1	44.43	3.10	-2.10
C973_b	2.1	43.51	1.45	-2.14
C974_b	2.1	42.39	-0.09	-2.02
C975_b	2.1	41.13	-1.79	-1.91

Annex B3: Velocity data at the longitudinal profile L7 for the experiment E2 on the effect of the groyne location on the flow field

E2.1					**E2.2**				**E2.3**			
Point	z [cm]	u [cm/s]	v [cm/s]	w [cm/s]	Point	u [cm/s]	v [cm/s]	w [cm/s]	Point	u [cm/s]	v [cm/s]	w [cm/s]
C171_b	5	54.86	6.52	-6.78	C171_b	48.56	-0.75	-1.33	C171_b	50.43	1.51	-1.36
C271	5	38.31	-0.93	-1.88	C271	57.81	6.31	-0.06	C271	47.33	-1.27	-1.29
C371	5	37.79	-1.68	-0.87	C371	39.29	-1.20	-0.71	C371	54.30	5.41	-1.36
C471	5	37.87	-1.68	-0.99	C471	38.19	-1.55	-0.63	C471	38.59	-1.76	-0.81
C571	5	39.68	-1.76	-1.34	C571	39.98	-1.79	-1.02	C571	39.33	-2.23	-0.98
C671	5	40.29	-2.25	-1.37	C671	41.02	-2.15	-1.36	C671	41.00	-1.72	-1.29
C771	5	41.32	-2.56	-1.65	C771	41.53	-2.56	-1.44	C771	41.60	-2.31	-1.51
C871	5	41.93	-2.82	-1.78	C871	42.76	-2.66	-1.69	C871	42.70	-2.45	-1.77
C971_b	5	45.31	-4.05	-2.10	C971_b	45.78	-3.89	-2.34	C971_b	45.91	-3.83	-2.26
C172_b	4	43.85	4.62	-6.26	C172_b	47.75	0.78	-1.40	C172_b	49.65	1.60	-1.35
C272	4	36.40	-1.04	-1.67	C272	52.38	6.85	-2.11	C272	46.30	-1.10	-1.21
C372	4	36.15	-0.96	-0.94	C372	36.40	-1.10	-0.59	C372	49.64	6.34	-4.41
C472	4	37.72	-1.02	-1.27	C472	37.48	-1.28	-0.59	C472	35.74	-1.21	-0.52
C572	4	38.74	-0.95	-1.32	C572	40.19	-1.30	-1.34	C572	38.11	-1.09	-1.04
C672	4	39.55	-0.99	-1.34	C672	40.58	-1.32	-1.37	C672	40.15	-1.32	-1.45
C772	4	40.64	-1.70	-1.68	C772	40.67	-1.74	-1.41	C772	41.23	-1.36	-1.57
C872	4	40.93	-1.61	-1.66	C872	42.47	-1.59	-1.84	C872	42.12	-1.84	-1.70
C972_b	4	44.35	-2.81	-2.12	C972_b	45.31	-3.10	-2.25	C972_b	45.37	-3.09	-2.13
C173_b	3	27.08	-1.73	-2.98	C173_b	46.04	1.08	-1.25	C173_b	48.45	1.76	-1.32
C273	3	32.26	0.50	-0.90	C273	28.68	5.33	-2.91	C273	43.89	-0.45	-1.23
C373	3	35.26	0.40	-0.91	C373	34.07	-0.94	-0.78	C373	27.27	4.34	-3.11
C473	3	35.90	0.36	-0.79	C473	36.17	-0.75	-0.72	C473	33.33	-0.53	-0.52
C573	3	37.66	0.02	-1.28	C573	38.62	-0.54	-0.98	C573	37.85	-0.40	-1.17
C673	3	39.09	-0.18	-1.63	C673	40.04	-0.41	-1.51	C673	38.64	-0.16	-1.32
C773	3	39.35	0.26	-1.59	C773	40.87	-0.76	-1.72	C773	40.50	-0.68	-1.51
C873	3	40.30	0.48	-1.59	C873	42.12	-0.67	-1.74	C873	41.53	-0.95	-1.68
C973_b	3	43.60	1.50	-2.09	C973_b	44.77	-1.96	-2.18	C973_b	44.30	-1.96	-1.96
C174_b	2	18.35	-0.91	-0.97	C174_b	43.33	1.45	-1.15	C174_b	45.36	2.24	-1.14
C274	2	29.03	-0.38	-0.36	C274	9.25	2.36	-0.48	C274	40.77	0.46	-1.12
C374	2	33.23	0.33	-0.58	C374	32.06	-0.46	-1.04	C374	9.01	-0.84	-0.01
C474	2	35.36	0.82	-0.79	C474	35.42	-0.05	-0.71	C474	31.34	-0.08	-0.09
C574	2	36.75	1.51	-1.22	C574	37.80	0.88	-1.33	C574	36.01	0.69	-1.01
C674	2	37.43	1.20	-1.55	C674	38.33	0.77	-1.35	C674	37.89	0.65	-1.25
C774	2	37.55	1.23	-1.60	C774	38.97	0.54	-1.43	C774	38.57	0.26	-1.52
C874	2	38.98	1.26	-1.61	C874	40.43	0.43	-1.62	C874	40.05	0.75	-1.57
C974_b	2	42.84	-0.10	-2.04	C974_b	43.55	-0.57	-1.92	C974_b	43.35	-0.55	-1.86
C175_b	1	11.95	-4.59	0.15	C175_b	39.86	1.93	-0.96	C175_b	41.75	2.81	-0.93
C275	1	27.03	-0.36	-0.29	C275	-0.66	-5.36	2.15	C275	36.59	1.50	-0.86
C375	1	31.97	0.27	-0.82	C375	30.19	0.03	-0.83	C375	-0.09	-5.36	1.48
C475	1	33.96	1.50	-0.84	C475	33.77	0.45	-0.53	C475	29.59	0.45	-0.36
C575	1	34.43	2.44	-1.30	C575	36.07	1.34	-1.14	C575	35.15	1.17	-1.06
C675	1	35.32	3.09	-1.51	C675	36.56	1.81	-1.32	C675	35.87	1.69	-1.29
C775	1	35.63	3.05	-1.49	C775	37.20	1.84	-1.44	C775	36.95	1.44	-1.28
C875	1	37.68	3.04	-1.51	C875	38.21	2.22	-1.44	C875	38.00	2.20	-1.38
C975_b	1	40.40	2.07	-1.82	C975_b	42.26	1.32	-1.84	C975_b	41.45	1.04	-1.83

E2.4					**E2.5**				**E2.6**			
Point	z [cm]	u [cm/s]	v [cm/s]	w [cm/s]	Point	u [cm/s]	v [cm/s]	w [cm/s]		u [cm/s]	v [cm/s]	w [cm/s]
C171_b	5	51.40	1.18	-1.33	C171_b	51.82	1.23	-1.42	C171_b	50.23	0.24	-1.00
C271	5	48.57	-1.09	-1.39	C271	48.80	-1.12	-1.39	C271	48.17	-2.11	-1.00
C371	5	45.96	-2.47	-1.56	C371	47.28	-2.29	-1.65	C371	46.49	-3.14	-1.20
C471	5	53.21	5.23	-2.01	C471	44.73	-2.68	-1.84	C471	44.78	-3.11	-1.35
C571	5	40.37	-1.95	-1.22	C571	54.06	6.84	-1.58	C571	43.09	-2.71	-1.81
C671	5	41.65	-2.06	-1.80	C671	40.29	-1.90	-1.18	C671	55.91	5.97	-2.39
C771	5	42.86	-2.20	-1.81	C771	42.82	-2.27	-2.21	C771	41.95	-2.88	-1.72
C871	5	43.56	-2.62	-1.76	C871	44.20	-2.57	-1.97	C871	43.37	-3.17	-1.91
C971_b	5	48.56	0.75	-1.33	C971_b	48.56	0.75	-1.33	C971_b	46.19	-4.25	-1.85
C172_b	4	50.75	1.31	-1.45	C172_b	51.05	1.18	-1.46	C172_b	49.51	0.41	-1.10
C272	4	47.75	-0.91	-1.31	C272	48.65	-1.01	-1.49	C272	47.25	-1.74	-1.08
C372	4	44.83	-1.84	-1.60	C372	45.95	-1.58	-1.62	C372	45.16	-2.47	-1.16
C472	4	47.63	6.49	-3.65	C472	42.72	-1.45	-1.59	C472	43.00	-1.89	-1.30
C572	4	38.80	-1.86	-1.67	C572	48.50	7.41	-3.48	C572	41.65	-1.56	-1.60
C672	4	40.12	-1.13	-1.74	C672	38.02	-1.05	-1.57	C672	52.64	7.48	-5.25
C772	4	42.45	-1.76	-1.63	C772	42.23	-1.66	-1.92	C772	40.49	-2.44	-2.05
C872	4	43.61	-1.96	-1.92	C872	43.47	-1.65	-1.64	C872	42.60	-2.31	-1.71
C972_b	4	47.75	0.78	-1.40	C972_b	47.75	0.78	-1.40	C972_b	45.99	-3.57	-1.95
C173_b	3	48.66	1.53	-1.28	C173_b	49.32	1.60	-1.41	C173_b	48.13	0.75	-1.00
C273	3	45.66	-0.17	-1.24	C273	46.05	-0.32	-1.31	C273	45.41	-1.04	-0.91
C373	3	41.84	-0.75	-1.40	C373	43.65	-0.46	-1.37	C373	42.56	-1.27	-1.12
C473	3	29.06	5.72	-2.72	C473	40.31	-0.18	-1.60	C473	41.21	-0.50	-1.17
C573	3	35.89	-0.87	-1.42	C573	30.35	6.27	-2.70	C573	39.98	-0.02	-1.63
C673	3	39.04	-0.46	-1.43	C673	36.48	-0.11	-1.08	C673	42.65	7.38	-6.66
C773	3	41.29	-0.82	-1.65	C773	40.44	-0.33	-1.60	C773	37.08	-1.41	-1.70
C873	3	42.98	-0.84	-1.58	C873	43.62	-0.68	-1.92	C873	41.75	-1.39	-1.69
C973_b	3	46.04	1.08	-1.25	C973_b	46.04	1.08	-1.25	C973_b	46.09	-2.79	-1.91
C174_b	2	46.65	2.16	-1.26	C174_b	46.77	1.94	-1.15	C174_b	46.09	1.20	-0.86
C274	2	42.61	0.89	-1.16	C274	43.72	0.59	-1.15	C274	42.52	-0.12	-0.88
C374	2	38.65	0.69	-1.22	C374	40.57	0.87	-1.38	C374	40.01	0.26	-0.95
C474	2	10.38	0.96	0.47	C474	37.89	1.53	-1.45	C474	38.95	1.30	-1.19
C574	2	32.62	-0.11	-0.57	C574	12.77	1.78	0.55	C574	37.76	1.85	-1.48
C674	2	37.98	0.42	-1.51	C674	33.98	0.67	-1.24	C674	20.81	1.45	-2.73
C774	2	40.49	0.15	-1.72	C774	39.83	0.37	-1.74	C774	34.53	-0.14	-1.02
C874	2	42.33	0.45	-1.65	C874	42.55	0.51	-1.49	C874	40.87	-0.27	-1.75
C974_b	2	43.33	1.45	-1.15	C974_b	43.33	1.45	-1.15	C974_b	45.35	-1.70	-1.78
C175_b	1	46.65	2.16	-1.26	C175_b	43.61	2.61	-1.06	C175_b	42.05	1.66	-0.77
C275	1	38.62	1.57	-0.86	C275	40.13	1.66	-1.05	C275	39.27	0.91	-0.81
C375	1	34.65	2.20	-1.03	C375	36.71	2.64	-1.23	C375	36.58	1.69	-0.88
C475	1	3.37	-4.89	1.50	C475	33.68	3.12	-1.06	C475	35.48	2.90	-0.94
C575	1	31.87	0.59	-1.46	C575	2.21	-5.56	1.77	C575	34.67	3.23	-1.18
C675	1	37.15	1.69	-1.52	C675	31.60	0.87	-1.10	C675	6.08	-5.88	0.43
C775	1	38.41	1.66	-1.38	C775	38.10	1.44	-1.58	C775	32.10	-0.03	-0.90
C875	1	40.55	1.50	-1.63	C875	41.40	1.77	-1.72	C875	39.78	0.68	-1.42
C975_b	1	39.86	1.93	-0.96	C975_b	39.86	1.93	-0.96	C975_b	44.56	-0.52	-1.66

E2.7					**E2.8**				**E2.9**			
Point	z [cm]	u [cm/s]	v [cm/s]	w [cm/s]	Point	u [cm/s]	v [cm/s]	w [cm/s]	Point	u [cm/s]	v [cm/s]	w [cm/s]
C171_b	5	51.05	0.91	-1.39	C171_b	50.15	0.14	-0.94	C171_b	52.26	0.90	-1.39
C271	5	49.02	-1.52	-1.36	C271	48.06	-2.06	-1.06	C271	50.20	-1.62	-1.38
C371	5	47.59	-2.66	-1.56	C371	46.84	-3.29	-1.28	C371	48.23	-2.63	-1.61
C471	5	45.96	-2.71	-1.69	C471	45.64	-3.49	-1.26	C471	47.62	-3.05	-1.91
C571	5	45.21	-2.30	-2.08	C571	45.04	-3.08	-1.66	C571	47.42	-2.62	-2.31
C671	5	44.52	-1.74	-2.43	C671	43.76	-2.55	-1.90	C671	46.17	-2.33	-2.15
C771	5	57.85	8.88	-1.83	C771	42.99	-2.59	-2.01	C771	46.37	-2.12	-2.34
C871	5	45.42	-2.66	-2.73	C871	59.42	8.26	-2.31	C871	45.93	-1.67	-2.48
C971_b	5	48.73	-4.30	-2.72	C971_b	50.10	-4.90	-4.64	C971_b	N/A	N/A	N/A
C172_b	4	50.61	0.97	-1.46	C172_b	49.71	0.39	-1.11	C172_b	51.06	1.00	-1.48
C272	4	48.55	-1.41	-1.48	C272	47.69	-1.85	-1.07	C272	49.02	-1.34	-1.44
C372	4	46.35	-2.08	-1.49	C372	45.56	-2.44	-1.24	C372	47.16	-2.09	-1.58
C472	4	44.24	-1.74	-1.63	C472	44.33	-2.22	-1.49	C472	46.84	-1.97	-1.96
C572	4	43.60	-1.05	-1.98	C572	43.47	-1.72	-1.71	C572	45.67	-1.47	-2.06
C672	4	43.31	-0.37	-2.33	C672	43.05	-1.17	-1.70	C672	45.46	-1.10	-2.15
C772	4	52.58	9.66	-4.66	C772	41.99	-1.36	-1.92	C772	45.75	-1.01	-2.36
C872	4	43.44	-2.46	-2.78	C872	56.19	9.24	-5.34	C872	46.05	-0.82	-2.51
C972_b	4	47.66	-3.35	-2.57	C972_b	47.90	-3.91	-4.32	C972_b	68.56	13.85	-7.83
C173_b	3	49.39	1.39	-1.38	C173_b	48.05	0.69	-1.05	C173_b	49.79	1.38	-1.40
C273	3	46.09	-0.54	-1.24	C273	45.62	-1.14	-0.98	C273	46.57	-0.57	-1.28
C373	3	44.56	-0.87	-1.68	C373	43.58	-1.44	-1.23	C373	45.24	-1.03	-1.50
C473	3	42.05	-0.12	-1.53	C473	41.86	-0.77	-1.12	C473	43.09	-0.14	-1.48
C573	3	42.28	0.56	-1.99	C573	42.68	-0.33	-1.65	C573	44.55	0.27	-2.13
C673	3	41.61	1.09	-2.07	C673	42.11	0.40	-1.73	C673	44.49	0.76	-2.12
C773	3	30.29	8.04	-2.33	C773	41.82	0.00	-1.85	C773	45.05	0.79	-2.30
C873	3	40.58	-1.55	-2.39	C873	40.48	8.33	-5.72	C873	45.89	0.74	-2.54
C973_b	3	46.19	-2.44	-2.09	C973_b	45.85	-4.15	-4.25	C973_b	27.69	10.60	1.68
C174_b	2	46.58	1.88	-1.16	C174_b	46.39	1.21	-0.91	C174_b	47.10	1.76	-1.20
C274	2	43.43	0.45	-1.15	C274	42.80	-0.31	-0.82	C274	43.74	0.34	-1.15
C374	2	41.33	0.74	-1.44	C374	40.51	0.05	-1.03	C374	41.98	0.71	-1.38
C474	2	39.32	1.63	-1.38	C474	39.20	1.06	-1.05	C474	41.27	1.62	-1.64
C574	2	39.64	2.45	-1.78	C574	39.66	1.39	-1.46	C574	41.89	1.98	-1.94
C674	2	40.38	2.74	-1.93	C674	40.41	2.05	-1.54	C674	42.60	2.53	-2.10
C774	2	9.04	-0.87	3.00	C774	40.83	1.73	-1.73	C774	44.10	2.36	-2.25
C874	2	37.73	-0.21	-1.98	C874	15.64	2.04	0.31	C874	45.15	2.37	-2.23
C974_b	2	45.69	-1.34	-2.18	C974_b	42.76	-3.23	-3.67	C974_b	13.85	-3.65	3.36
C175_b	1	43.25	2.31	-0.98	C175_b	42.45	1.70	-0.78	C175_b	43.46	2.12	-1.03
C275	1	39.33	1.37	-0.90	C275	38.85	0.98	-0.77	C275	40.11	1.43	-0.97
C375	1	37.58	2.32	-1.23	C375	37.24	1.88	-1.02	C375	37.83	2.25	-1.23
C475	1	36.06	3.52	-1.17	C475	36.75	2.40	-1.06	C475	38.06	3.35	-1.25
C575	1	37.24	3.95	-1.63	C575	37.45	3.54	-1.34	C575	39.03	3.71	-1.60
C675	1	37.30	4.49	-1.55	C675	38.52	3.85	-1.49	C675	40.40	4.48	-1.82
C775	1	2.36	-7.57	2.00	C775	40.01	3.19	-1.70	C775	42.97	4.43	-1.95
C875	1	36.76	0.18	-1.57	C875	8.08	-7.10	0.57	C875	43.39	4.19	-2.01
C975_b	1	43.18	-0.15	-1.72	C975_b	39.85	-3.02	-2.46	C975_b	7.04	-13.91	2.60

Annex B4: Velocity data at the longitudinal profile L7 for the experiment E4 on different groyne projected lengths

E4.1					E4.2				E4.3				E4.4			
Point	z [cm]	u [cm/s]	v [cm/s]	w [cm/s]	Point	u [cm/s]	v [cm/s]	w [cm/s]	Point	u [cm/s]	v [cm/s]	w [cm/s]	Point	u [cm/s]	v [cm/s]	w [cm/s]
C171_b	5	54.97	5.07	-6.83	C171_b	48.17	1.49	-1.02	C171_b	53.63	7.85	-6.18	C171_b	50.30	2.38	-1.08
C271	5	37.53	-0.87	-0.58	C271	57.91	5.84	-1.09	C271	37.15	-1.24	-0.98	C271	50.88	7.23	-2.96
C371	5	36.49	-1.33	-0.34	C371	41.49	-1.46	-1.19	C371	36.95	-1.83	-0.27	C371	41.59	-2.44	-1.45
C471	5	36.24	-1.52	0.02	C471	39.27	-1.72	-0.64	C471	38.60	-2.16	-0.29	C471	42.62	-2.91	-1.12
C571	5	37.52	-1.71	-0.29	C571	39.15	-1.69	-0.16	C571	38.94	-2.24	-0.18	C571	43.88	-2.80	-1.00
C671	5	38.39	-1.59	-0.65	C671	39.50	-1.59	-0.43	C671	42.17	-2.94	-0.45	C671	46.04	-3.20	-1.07
C771	5	38.12	-1.92	-0.40	C771	39.66	-2.04	-0.45	C771	44.87	-3.39	-0.77	C771	46.97	-3.58	-1.07
C871	5	40.46	-1.86	-0.81	C871	41.98	-2.02	-0.73	C871	47.68	-3.80	-1.05	C871	47.04	-3.31	-0.86
C971_b	5	43.96	-3.14	-0.72	C971_b	45.58	-3.35	-0.65	C971_b	50.15	-4.29	-1.31	C971_b	50.68	-4.23	-1.01
C172_b	4	51.72	4.00	-7.14	C172_b	47.60	1.55	-1.02	C172_b	48.24	7.14	-6.74	C172_b	49.84	2.41	-1.03
C272	4	35.39	-0.64	-1.10	C272	54.99	6.90	-3.59	C272	35.83	-1.18	-0.66	C272	44.51	8.10	-4.22
C372	4	35.13	-0.84	-0.15	C372	39.56	-1.03	-1.57	C372	36.44	-1.39	-0.35	C372	39.81	-2.53	-1.28
C472	4	36.66	-0.86	-0.13	C472	37.52	-1.03	-0.33	C472	36.72	-1.70	-0.21	C472	41.54	-2.47	-0.91
C572	4	37.40	-1.13	-0.36	C572	38.34	-1.21	-0.15	C572	38.36	-1.72	-0.19	C572	43.80	-2.22	-1.03
C672	4	37.02	-0.85	-0.48	C672	38.50	-0.94	-0.33	C672	41.50	-1.93	-0.70	C672	44.82	-2.40	-1.15
C772	4	38.37	-1.10	-0.64	C772	39.48	-1.34	-0.53	C772	43.86	-2.36	-0.68	C772	45.60	-2.30	-1.12
C872	4	39.41	-0.73	-0.63	C872	41.04	-1.23	-0.54	C872	45.21	-2.21	-1.05	C872	47.95	-2.47	-1.00
C972_b	4	43.19	-1.83	-0.73	C972_b	44.78	-2.35	-0.58	C972_b	48.92	-2.91	-0.95	C972_b	50.37	-3.14	-1.07
C173_b	3	39.65	1.54	-6.10	C173_b	45.58	1.80	-0.88	C173_b	33.72	4.04	-5.04	C173_b	47.58	2.88	-0.98
C273	3	33.21	-0.17	-0.93	C273	42.25	7.03	-6.10	C273	35.23	-2.03	-0.93	C273	20.28	6.52	-1.34
C373	3	34.55	-0.34	-0.25	C373	36.62	-0.88	-1.33	C373	36.14	-1.69	-0.54	C373	37.82	-2.20	-1.18
C473	3	35.24	-0.10	-0.02	C473	37.39	-0.58	-0.50	C473	35.00	-1.07	-0.26	C473	39.80	-1.32	-0.97
C573	3	36.43	0.12	-0.31	C573	37.51	0.05	-0.30	C573	36.33	-0.83	-0.41	C573	41.31	-1.00	-1.15
C673	3	36.99	0.35	-0.39	C673	38.26	0.03	-0.59	C673	37.81	-0.36	-0.53	C673	41.65	-0.59	-0.87
C773	3	37.30	0.14	-0.47	C773	38.29	-0.04	-0.41	C773	40.55	-0.78	-0.72	C773	43.06	-0.70	-1.03
C873	3	38.41	0.75	-0.37	C873	40.30	-0.03	-0.51	C873	42.71	-0.48	-0.76	C873	45.61	-0.84	-0.84
C973_b	3	42.47	-0.33	-0.62	C973_b	43.99	-0.75	-0.60	C973_b	47.22	-1.16	-0.93	C973_b	47.45	-1.13	-0.69
C174_b	2	23.77	-2.75	-1.10	C174_b	42.11	2.20	-0.72	C174_b	22.14	-0.75	-2.18	C174_b	44.19	3.49	-0.85
C274	2	29.83	-0.26	-0.21	C274	19.15	0.78	-1.30	C274	34.21	-2.83	-0.73	C274	6.51	0.08	-0.18
C374	2	33.20	0.17	-0.45	C374	33.30	-0.05	-1.18	C374	33.62	-0.96	-0.50	C374	34.54	-1.48	-0.73
C474	2	34.01	1.08	-0.06	C474	35.36	0.29	-0.35	C474	33.00	-0.39	-0.12	C474	36.90	-0.41	-0.69
C574	2	35.31	1.57	-0.26	C574	36.81	0.57	-0.40	C574	33.63	0.61	-0.18	C574	39.01	-0.05	-1.03
C674	2	35.61	1.80	-0.42	C674	36.92	1.28	-0.41	C674	35.51	0.98	-0.47	C674	39.91	0.86	-0.90
C774	2	36.31	1.76	-0.50	C774	37.51	1.13	-0.40	C774	37.57	0.76	-0.51	C774	40.68	0.84	-0.74
C874	2	36.62	2.41	-0.32	C874	38.83	1.78	-0.53	C874	40.99	1.46	-0.76	C874	41.82	1.56	-0.58
C974_b	2	41.16	1.55	-0.57	C974_b	42.91	0.71	-0.40	C974_b	44.97	0.48	-0.76	C974_b	46.51	0.52	-0.85
C175_b	1	16.85	-4.81	0.19	C175_b	37.76	2.54	-0.56	C175_b	19.39	-9.33	-0.31	C175_b	40.28	3.96	-0.74
C275	1	27.75	-0.02	-0.06	C275	8.09	-6.23	0.96	C275	31.74	-2.62	-0.45	C275	3.79	-9.45	-0.04
C375	1	31.31	0.78	-0.31	C375	30.07	0.40	-0.59	C375	32.34	0.06	-0.64	C375	33.20	-0.72	-0.66
C475	1	31.81	2.19	0.00	C475	34.05	1.26	-0.37	C475	31.20	0.74	-0.33	C475	34.58	0.90	-0.55
C575	1	33.18	3.06	-0.48	C575	34.87	1.58	-0.40	C575	30.78	1.75	-0.26	C575	35.61	1.82	-0.82
C675	1	32.83	3.33	-0.38	C675	34.58	2.30	-0.29	C675	31.77	2.53	-0.32	C675	37.03	1.96	-0.73
C775	1	33.72	3.42	-0.48	C775	34.97	2.72	-0.36	C775	33.81	2.91	-0.42	C775	36.79	2.69	-0.55
C875	1	35.04	4.00	-0.33	C875	37.13	3.23	-0.28	C875	36.98	3.42	-0.34	C875	39.05	4.00	-0.56
C975_b	1	38.78	3.50	-0.40	C975_b	40.51	2.71	-0.50	C975_b	41.27	2.65	-0.78	C975_b	42.90	2.35	-0.59

Annex B5: Velocity data at the longitudinal profile L7 for the experiment E4 on different groyne widths

E5.1					E5.2				E5.3				E5.4			
Point	z	u	v	w	Point	u	v	w	Point	u	v	w	Point	u	v	w
	[cm]	[cm/s]	[cm/s]	[cm/s]		[cm/s]	[cm/s]	[cm/s]		[cm/s]	[cm/s]	[cm/s]		[cm/s]	[cm/s]	[cm/s]
C171_b	5	54.42	3.61	-5.85	C171_b	48.69	0.59	-1.00	C171_b	54.10	-4.82	-4.66	C171_b	48.98	0.92	-1.03
C271	5	38.60	-0.86	-2.39	C271	59.54	5.07	-0.40	C271	42.40	1.26	-2.52	C271	57.50	4.54	-0.38
C371	5	37.47	-1.36	-0.83	C371	39.94	-1.66	-1.65	C371	38.66	1.19	-0.61	C371	41.46	-1.68	-1.60
C471	5	37.56	-1.31	-0.41	C471	38.45	-1.22	-0.32	C471	38.80	1.58	-0.19	C471	40.03	-1.28	-0.46
C571	5	39.06	-1.55	-0.53	C571	40.95	-1.51	-0.81	C571	39.87	1.49	-0.24	C571	41.31	-1.53	-0.53
C671	5	39.75	-1.59	-0.53	C671	40.80	-1.39	-0.63	C671	40.40	1.73	-0.34	C671	41.04	-1.53	-0.66
C771	5	39.87	-2.01	-0.37	C771	41.81	-1.91	-0.36	C771	40.96	2.24	-0.47	C771	41.88	-1.87	-0.61
C871	5	41.28	-2.10	-0.37	C871	42.99	-2.06	-0.64	C871	42.31	2.25	-0.44	C871	43.53	-1.87	-0.63
C971_b	5	44.10	-2.98	-0.55	C971_b	45.96	-3.22	-0.86	C971_b	44.91	2.98	-0.62	C971_b	46.63	-3.19	-0.77
C172_b	4	46.69	2.67	-6.07	C172_b	47.88	0.70	-1.00	C172_b	49.15	-4.33	-5.15	C172_b	48.47	0.92	-1.05
C272	4	35.11	-0.74	-1.47	C272	57.93	5.86	-2.68	C272	39.01	0.69	-2.07	C272	52.38	4.82	-3.12
C372	4	36.34	-0.45	-0.62	C372	37.38	-0.71	-1.81	C372	37.39	0.77	-0.83	C372	38.13	-1.20	-1.49
C472	4	36.62	-0.78	-0.05	C472	37.59	-0.71	-0.41	C472	38.14	0.88	-0.58	C472	38.72	-0.93	-0.19
C572	4	38.27	-0.65	-0.50	C572	39.19	-0.76	-0.51	C572	39.19	0.90	-0.34	C572	40.20	-1.14	-0.44
C672	4	39.13	-0.52	-0.57	C672	40.19	-0.83	-0.51	C672	39.39	0.44	-0.43	C672	40.41	-1.04	-0.51
C772	4	39.83	-1.09	-0.42	C772	41.37	-1.26	-0.45	C772	40.14	1.10	-0.22	C772	41.76	-1.02	-0.61
C872	4	41.09	-1.18	-0.60	C872	42.28	-1.36	-0.40	C872	41.62	0.79	-0.55	C872	43.38	-0.81	-0.50
C972_b	4	43.93	-2.06	-0.63	C972_b	45.70	-2.31	-0.73	C972_b	44.45	1.77	-0.56	C972_b	46.28	-2.02	-0.74
C173_b	3	34.03	0.43	-4.76	C173_b	46.59	1.10	-1.07	C173_b	34.80	-2.55	-3.16	C173_b	46.39	1.33	-1.07
C273	3	31.47	-0.92	-1.15	C273	49.41	6.74	-6.37	C273	33.82	0.29	-1.02	C273	22.58	3.03	0.51
C373	3	34.52	-0.03	-0.28	C373	33.75	-0.35	-1.19	C373	35.66	0.02	-0.37	C373	34.97	-0.50	-0.48
C473	3	35.93	-0.16	-0.14	C473	36.75	-0.42	-0.22	C473	37.36	-0.41	-0.43	C473	37.19	0.07	-0.04
C573	3	37.78	0.21	-0.61	C573	38.42	-0.03	-0.42	C573	38.48	-0.50	-0.55	C573	39.13	-0.06	-0.06
C673	3	37.86	0.48	-0.41	C673	39.52	0.27	-0.72	C673	38.08	-0.39	-0.21	C673	40.48	0.15	-0.56
C773	3	38.15	0.29	-0.33	C773	40.62	-0.29	-0.49	C773	39.10	-0.26	-0.39	C773	41.35	0.05	-0.42
C873	3	39.43	0.38	-0.37	C873	41.72	0.15	-0.40	C873	40.56	-0.42	-0.34	C873	42.55	0.25	-0.53
C973_b	3	43.43	-0.55	-0.58	C973_b	45.11	-1.05	-0.67	C973_b	43.81	0.20	-0.52	C973_b	45.95	-0.71	-0.79
C174_b	2	20.45	-1.95	-1.45	C174_b	42.60	1.35	-0.77	C174_b	18.63	0.96	1.28	C174_b	43.36	1.67	-0.88
C274	2	27.08	-0.11	-0.06	C274	24.80	2.34	-3.00	C274	30.80	0.00	-0.38	C274	7.03	0.12	3.31
C374	2	34.16	-0.01	-0.47	C374	31.07	0.75	-1.10	C374	34.59	-0.85	-0.30	C374	31.31	0.78	-0.17
C474	2	35.44	0.96	-0.13	C474	34.80	0.68	-0.24	C474	35.13	-1.26	-0.01	C474	35.22	0.94	0.08
C574	2	36.76	1.26	-0.44	C574	36.98	0.83	-0.18	C574	38.23	-0.54	-0.55	C574	38.36	1.00	-0.35
C674	2	36.97	1.97	-0.45	C674	37.97	1.27	-0.44	C674	37.02	-2.19	-0.41	C674	39.24	1.27	-0.50
C774	2	37.21	1.70	-0.44	C774	38.91	1.09	-0.33	C774	37.56	-1.91	-0.23	C774	39.83	1.50	-0.54
C874	2	38.16	2.16	-0.40	C874	39.93	1.28	-0.21	C874	39.30	-2.07	-0.28	C874	41.39	1.67	-0.37
C974_b	2	41.96	1.04	-0.57	C974_b	43.33	0.54	-0.53	C974_b	42.60	-1.28	-0.38	C974_b	44.77	0.89	-0.49
C175_b	1	11.40	-5.82	0.27	C175_b	39.11	1.68	-0.60	C175_b	10.42	3.98	1.36	C175_b	39.47	2.03	-0.73
C275	1	25.68	-0.02	-0.11	C275	5.54	-3.17	0.55	C275	27.84	-0.64	-0.25	C275	3.49	-4.77	1.82
C375	1	30.82	0.80	-0.35	C375	29.03	0.28	-0.34	C375	32.91	-1.20	-0.37	C375	30.02	0.83	-0.12
C475	1	33.00	1.94	0.14	C475	33.67	1.17	0.01	C475	33.73	-2.79	-0.01	C475	35.24	1.72	-0.19
C575	1	34.67	2.87	-0.38	C575	35.84	2.18	-0.34	C575	35.13	-2.98	-0.48	C575	35.81	2.25	-0.23
C675	1	34.27	3.55	-0.39	C675	36.90	2.63	-0.48	C675	34.35	-3.78	-0.36	C675	37.23	2.75	-0.33
C775	1	34.36	3.16	-0.31	C775	36.45	2.40	-0.29	C775	35.26	-3.38	-0.26	C775	38.37	2.91	-0.43
C875	1	35.93	3.89	-0.35	C875	38.44	3.16	-0.18	C875	37.18	-3.86	-0.23	C875	38.90	3.19	-0.34
C975_b	1	39.44	3.26	-0.41	C975_b	41.13	2.14	-0.50	C975_b	40.18	-3.09	-0.41	C975_b	41.89	2.54	-0.40

Annex B6: Velocity data at the longitudinal profile L7 for the experiment E6 on different groups of groynes

E6.1					E6.2				E6.3			
Point	z	u	v	w	Point	u	v	w	Point	u	v	w
	[cm]	[cm/s]	[cm/s]	[cm/s]		[cm/s]	[cm/s]	[cm/s]		[cm/s]	[cm/s]	[cm/s]
C171_b	5	51.18	4.95	-6.75	C171_b	51.82	4.92	-7.29	C171_b	49.08	0.34	-0.96
C271	5	35.93	-1.17	-0.08	C271	36.87	-1.00	-0.21	C271	46.97	-1.82	-1.07
C371	5	33.73	-1.39	-0.24	C371	35.95	-2.12	-0.41	C371	44.70	-2.69	-1.18
C471	5	34.69	-2.07	-0.81	C471	36.99	-2.13	-0.54	C471	42.70	-3.05	-1.51
C571	5	47.06	4.89	-3.68	C571	39.16	-2.42	-1.08	C571	54.46	5.30	-2.25
C671	5	36.01	-2.20	-1.61	C671	38.72	-2.64	-1.12	C671	41.02	-2.26	-1.66
C771	5	34.64	-2.19	-0.93	C771	38.45	-2.61	-1.24	C771	40.08	-2.32	-1.88
C871	5	35.34	-2.78	-1.20	C871	38.47	-3.00	-1.48	C871	39.77	-2.28	-1.64
C971_b	5	55.18	7.41	-3.68	C971_b	N/A	N/A	N/A	C971_b	N/A	N/A	N/A
C172_b	4	46.71	5.03	-7.17	C172_b	45.09	4.47	-8.08	C172_b	48.44	0.57	-1.05
C272	4	33.82	-1.08	-0.05	C272	34.63	-0.97	-0.07	C272	46.24	-1.59	-1.12
C372	4	33.78	-1.27	-0.16	C372	35.21	-1.61	-0.70	C372	43.24	-2.06	-1.19
C472	4	33.73	-1.51	-0.60	C472	35.74	-1.33	-0.55	C472	40.44	-1.68	-1.34
C572	4	42.58	5.18	-5.21	C572	37.52	-1.54	-1.13	C572	50.40	6.54	-4.39
C672	4	33.66	-1.46	-1.88	C672	38.01	-1.70	-1.26	C672	38.77	-1.53	-1.82
C772	4	34.06	-1.51	-1.15	C772	37.74	-1.64	-1.33	C772	39.20	-1.37	-1.79
C872	4	34.42	-2.09	-1.08	C872	38.04	-2.00	-1.62	C872	39.74	-1.69	-1.51
C972_b	4	52.03	9.98	-6.47	C972_b	57.10	11.70	-6.96	C972_b	60.06	9.86	-7.69
C173_b	3	32.09	0.76	-5.18	C173_b	29.46	1.95	-5.79	C173_b	46.53	0.86	-0.97
C273	3	30.90	-0.34	0.10	C273	31.81	-0.91	-0.16	C273	43.66	-0.77	-0.97
C373	3	32.83	-0.45	-0.12	C373	34.24	-0.72	-0.40	C373	41.21	-0.75	-1.21
C473	3	32.80	-0.72	-0.67	C473	35.62	-0.72	-0.55	C473	37.86	-0.38	-1.28
C573	3	30.05	4.08	-4.55	C573	35.62	-0.36	-0.93	C573	36.39	5.27	-4.86
C673	3	31.40	-0.60	-1.18	C673	36.79	-0.34	-1.00	C673	35.56	-0.62	-1.71
C773	3	33.38	-0.87	-1.19	C773	37.01	-0.39	-1.13	C773	38.81	-0.57	-1.68
C873	3	33.75	-1.01	-0.85	C873	36.54	-0.81	-1.32	C873	39.26	-1.00	-1.40
C973_b	3	23.55	7.12	1.07	C973_b	29.17	9.83	-0.68	C973_b	28.70	8.06	1.23
C174_b	2	18.74	-1.81	-1.55	C174_b	16.62	-0.60	-1.13	C174_b	44.19	1.27	-0.83
C274	2	28.73	-0.59	0.07	C274	29.50	-0.54	0.34	C274	40.58	0.20	-0.74
C374	2	31.70	0.02	-0.44	C374	32.67	-0.39	-0.14	C374	37.62	0.68	-0.90
C474	2	32.60	0.04	-0.63	C474	33.47	0.14	-0.29	C474	35.18	1.52	-1.02
C574	2	12.89	1.76	-0.97	C574	35.08	0.60	-1.02	C574	17.04	1.11	-1.53
C674	2	30.34	0.42	-1.14	C674	36.12	0.57	-1.36	C674	32.75	0.18	-1.25
C774	2	31.98	0.07	-1.15	C774	35.64	0.74	-1.34	C774	37.56	0.51	-1.42
C874	2	32.57	-0.25	-0.90	C874	35.41	0.84	-1.36	C874	38.50	0.28	-1.27
C974_b	2	13.29	-3.58	3.81	C974_b	13.10	-1.85	4.22	C974_b	14.83	-5.20	5.67
C175_b	1	10.18	-3.32	1.25	C175_b	11.27	-4.16	0.07	C175_b	40.77	1.93	-0.76
C275	1	26.37	-0.22	0.12	C275	28.45	-0.70	-0.14	C275	36.53	1.04	-0.64
C375	1	30.41	0.75	-0.43	C375	30.64	0.57	-0.23	C375	34.40	2.34	-1.05
C475	1	30.18	1.47	-0.31	C475	32.19	1.66	-0.34	C475	32.24	2.84	-0.79
C575	1	5.57	-2.76	-0.11	C575	33.64	1.78	-1.05	C575	5.59	-3.25	1.11
C675	1	28.49	1.62	-1.10	C675	33.83	2.38	-0.99	C675	31.00	1.37	-0.91
C775	1	31.06	1.28	-1.02	C775	33.30	2.43	-1.13	C775	36.39	2.02	-1.29
C875	1	32.17	0.37	-0.92	C875	33.42	1.92	-1.14	C875	37.40	1.03	-1.20
C975_b	1	6.91	-14.04	3.03	C975_b	7.77	-13.11	4.51	C975_b	7.68	-13.95	5.60

E6.4					**E6.5**				**E6.6**			
Point	z	u	v	w	Point	u	v	w	Point	u	v	w
	[cm]	[cm/s]	[cm/s]	[cm/s]		[cm/s]	[cm/s]	[cm/s]		[cm/s]	[cm/s]	[cm/s]
C171_b	5	51.04	5.40	-7.17	C171_b	49.49	5.58	-6.77	C171_b	54.98	4.82	-6.70
C271	5	35.79	-0.19	0.07	C271	33.68	-0.72	-0.23	C271	37.70	4.90	-0.58
C371	5	34.45	-1.66	-0.33	C371	43.68	4.09	-4.17	C371	36.21	-1.17	-0.32
C471	5	34.59	2.93	-0.48	C471	31.36	-1.68	-0.92	C471	35.66	-1.65	-0.24
C571	5	48.07	4.98	-3.14	C571	44.54	4.62	-3.81	C571	38.42	2.12	-2.24
C671	5	36.68	-2.13	-1.84	C671	34.12	-1.82	-1.35	C671	35.10	-1.75	-0.60
C771	5	35.96	-2.61	-1.07	C771	34.04	-2.28	-0.89	C771	35.53	-1.49	-0.56
C871	5	36.70	-2.96	-1.03	C871	34.92	-2.89	-0.99	C871	36.42	-1.60	-0.20
C971_b	5	39.93	-4.17	-1.40	C971_b	38.16	-4.21	-1.48	C971_b	40.15	-2.87	-0.63
C172_b	4	46.14	4.90	-7.82	C172_b	43.58	4.72	-7.52	C172_b	51.28	3.79	-7.32
C272	4	33.88	-0.85	0.00	C272	32.76	-0.55	0.04	C272	36.90	4.43	-1.12
C372	4	33.54	-0.87	-0.22	C372	39.89	4.60	-5.78	C372	34.89	-0.69	-0.31
C472	4	34.27	3.38	-0.67	C472	30.68	-1.39	-0.77	C472	35.07	-1.27	-0.42
C572	4	45.64	5.41	-4.75	C572	42.03	5.30	-5.55	C572	34.76	2.24	-2.80
C672	4	34.46	-1.71	-1.57	C672	32.90	-1.35	-1.57	C672	34.82	-1.03	-0.87
C772	4	35.48	-1.94	-1.04	C772	33.94	-1.75	-1.17	C772	35.33	-1.09	-0.52
C872	4	36.30	-2.32	-1.16	C872	35.16	-2.49	-1.24	C872	36.41	-1.14	-0.45
C972_b	4	39.38	-3.57	-1.57	C972_b	37.50	-3.40	-1.49	C972_b	39.39	-2.05	-0.47
C173_b	3	28.75	1.80	-4.32	C173_b	27.37	2.38	-4.32	C173_b	42.31	1.24	-6.60
C273	3	30.56	-0.44	0.09	C273	29.51	-0.72	0.48	C273	33.05	4.19	-0.57
C373	3	32.83	-0.44	-0.40	C373	31.54	3.23	-6.12	C373	34.30	-0.36	0.03
C473	3	32.74	3.88	-0.36	C473	28.78	-0.69	-0.23	C473	33.68	-0.37	-0.20
C573	3	34.23	4.50	-5.24	C573	31.93	4.89	-5.36	C573	26.96	1.24	-1.68
C673	3	32.70	-0.99	-1.73	C673	30.85	-0.94	-1.13	C673	32.94	0.13	-0.44
C773	3	35.32	-1.21	-1.16	C773	32.59	-1.18	-1.02	C773	34.60	-0.04	-0.42
C873	3	35.93	-1.24	-1.16	C873	34.16	-1.74	-0.89	C873	35.42	-0.22	-0.30
C973_b	3	39.22	-2.61	-1.38	C973_b	37.25	-2.72	-1.49	C973_b	39.00	-1.03	-0.49
C174_b	2	16.14	-0.83	-0.93	C174_b	16.19	-0.40	-1.20	C174_b	26.90	-2.24	-2.81
C274	2	28.98	-0.72	0.05	C274	27.72	-0.56	0.01	C274	30.38	4.55	0.04
C374	2	32.00	0.22	0.12	C374	17.11	-0.29	-3.30	C374	33.17	0.79	-0.32
C474	2	31.76	5.09	-0.49	C474	27.20	-0.06	-0.35	C474	32.30	0.95	-0.14
C574	2	16.69	0.96	-2.51	C574	16.24	0.97	-2.07	C574	21.91	-1.18	-1.06
C674	2	29.80	0.30	-1.06	C674	29.50	-0.35	-0.99	C674	30.81	0.92	-0.36
C774	2	34.07	-0.07	-1.09	C774	31.98	-0.26	-1.01	C774	34.04	0.80	-0.39
C874	2	35.55	-0.46	-1.10	C874	34.64	-1.25	-1.35	C874	34.70	0.58	-0.19
C974_b	2	38.44	-1.77	-1.16	C974_b	36.51	-1.48	-1.23	C974_b	38.65	-0.02	-0.50
C175_b	1	11.41	-4.31	0.54	C175_b	9.50	-4.07	1.01	C175_b	16.44	-4.00	0.21
C275	1	26.98	-0.05	0.21	C275	25.45	-0.36	0.18	C275	27.89	4.29	-0.34
C375	1	29.46	0.81	-0.27	C375	9.45	-4.09	-1.05	C375	29.97	1.35	-0.04
C475	1	30.71	5.85	-0.40	C475	26.89	-0.20	-0.35	C475	30.88	1.90	-0.10
C575	1	6.98	-4.68	-0.36	C575	6.87	-3.42	-0.59	C575	17.16	-3.50	0.16
C675	1	28.94	0.70	-1.13	C675	27.81	0.63	-1.02	C675	29.86	1.83	-0.22
C775	1	32.96	0.74	-0.98	C775	30.79	0.52	-0.98	C775	33.09	1.88	-0.28
C875	1	34.61	0.63	-1.06	C875	31.64	0.50	-0.73	C875	33.12	1.58	-0.22
C975_b	1	37.13	-0.33	-1.38	C975_b	35.08	-0.59	-1.21	C975_b	36.44	0.98	-0.37

E6.7					**E6.8**				**E6.9**			
Point	z	u	v	w	Point	u	v	w	Point	u	v	w
	[cm]	[cm/s]	[cm/s]	[cm/s]		[cm/s]	[cm/s]	[cm/s]		[cm/s]	[cm/s]	[cm/s]
C171_b	5	55.21	4.46	-6.63	C171_b	51.20	7.56	-5.74	C171_b	50.23	-7.47	-5.96
C271	5	39.29	-0.87	-0.95	C271	33.62	0.25	0.20	C271	33.94	-0.09	-0.37
C371	5	36.72	-1.22	-0.49	C371	31.49	-0.56	0.67	C371	32.64	0.45	0.53
C471	5	35.64	-1.57	-0.17	C471	33.80	1.91	-2.83	C471	32.41	-1.66	-2.80
C571	5	44.15	4.58	-3.23	C571	32.91	-1.71	0.07	C571	31.76	1.64	0.26
C671	5	37.39	-1.36	-1.03	C671	37.62	-2.23	-0.23	C671	34.41	1.36	-0.36
C771	5	36.04	-1.81	-0.61	C771	39.99	-3.14	-0.09	C771	35.17	0.10	-2.63
C871	5	36.34	-1.81	-0.39	C871	45.09	-3.90	-0.76	C871	39.88	3.98	-0.51
C971_b	5	40.02	-2.82	-0.43	C971_b	49.19	-5.31	-0.83	C971_b	48.02	5.66	-0.50
C172_b	4	51.71	3.57	-7.03	C172_b	46.01	6.83	-5.91	C172_b	44.42	-6.27	-6.52
C272	4	36.02	-0.38	-0.62	C272	32.50	-0.30	0.19	C272	33.59	0.23	-0.58
C372	4	34.58	-0.71	-0.13	C372	31.68	-0.34	0.45	C372	31.10	0.31	0.43
C472	4	35.15	-0.72	-0.34	C472	30.29	1.50	-3.61	C472	28.62	-1.45	-2.93
C572	4	39.42	5.87	-4.21	C572	32.08	-1.26	-0.20	C572	31.07	1.20	0.03
C672	4	34.57	-0.95	-0.37	C672	34.91	-1.11	-0.05	C672	32.77	0.63	-0.20
C772	4	35.69	-1.19	-0.37	C772	39.04	-1.93	-0.52	C772	33.11	0.06	-2.98
C872	4	36.00	-1.36	-0.14	C872	43.13	-2.94	-0.90	C872	38.78	3.31	-0.30
C972_b	4	39.19	-2.22	-0.37	C972_b	46.96	-3.75	-0.63	C972_b	47.89	5.39	-1.15
C173_b	3	41.61	1.52	-6.48	C173_b	32.55	4.11	-3.64	C173_b	31.84	-3.79	-4.22
C273	3	33.06	-0.23	-0.39	C273	31.52	-0.86	-0.26	C273	32.35	1.41	-0.06
C373	3	33.22	-0.12	0.17	C373	30.54	0.15	0.56	C373	30.36	0.03	0.14
C473	3	34.39	-0.04	-0.23	C473	24.28	1.17	-3.45	C473	24.83	0.13	-3.61
C573	3	25.97	4.62	-2.84	C573	30.67	-0.71	-0.16	C573	29.50	0.50	-0.20
C673	3	33.09	-0.54	-0.51	C673	33.31	-0.28	-0.07	C673	30.71	-0.48	-0.17
C773	3	34.52	-0.41	-0.24	C773	36.39	-0.80	-0.24	C773	27.55	0.17	-2.81
C873	3	36.19	-0.17	-0.33	C873	40.13	-1.10	-0.61	C873	37.19	1.90	-0.70
C973_b	3	39.29	-1.29	-0.37	C973_b	46.28	-2.06	-1.06	C973_b	43.99	2.68	-0.87
C174_b	2	26.96	-2.18	-2.40	C174_b	20.99	-0.04	-1.08	C174_b	21.78	0.96	-1.17
C274	2	30.63	0.21	-0.37	C274	30.91	-1.99	0.28	C274	31.20	1.74	-0.23
C374	2	32.13	0.64	0.04	C374	29.21	0.48	0.24	C374	29.77	-0.32	-0.09
C474	2	32.83	0.87	-0.21	C474	18.03	-0.97	-2.62	C474	19.30	0.93	-3.10
C574	2	14.34	0.75	-1.08	C574	29.69	-0.20	-0.15	C574	27.45	-0.27	0.02
C674	2	32.13	0.98	-0.40	C674	30.35	0.71	-0.08	C674	28.01	-1.12	0.03
C774	2	34.87	0.84	-0.53	C774	34.27	0.96	-0.24	C774	23.37	1.17	-2.00
C874	2	35.33	0.42	-0.25	C874	37.99	0.14	-0.52	C874	34.16	1.26	-0.42
C974_b	2	38.17	0.03	-0.22	C974_b	44.16	-0.07	-0.79	C974_b	42.91	2.11	-0.73
C175_b	1	18.46	-4.27	-0.41	C175_b	18.12	-7.86	0.48	C175_b	20.05	8.23	-0.06
C275	1	28.45	0.22	-0.02	C275	29.78	-2.79	0.10	C275	28.64	1.43	0.14
C375	1	30.74	0.77	-0.14	C375	27.67	1.26	0.07	C375	27.23	-1.05	-0.10
C475	1	31.36	2.14	-0.12	C475	14.81	-3.62	-1.05	C475	15.95	3.87	-1.30
C575	1	10.40	-5.42	-0.17	C575	26.94	1.18	-0.16	C575	26.40	-1.04	-0.18
C675	1	30.50	2.07	-0.31	C675	29.01	2.19	-0.29	C675	26.56	-2.61	-0.27
C775	1	32.98	1.57	-0.28	C775	30.93	2.16	-0.38	C775	19.81	1.86	-0.98
C875	1	34.03	1.53	-0.22	C875	34.29	1.77	-0.36	C875	33.05	0.72	-0.32
C975_b	1	36.60	1.00	-0.27	C975_b	40.18	1.32	-0.42	C975_b	39.07	0.45	-0.60

E6.10					**E6.11**			
Point	z	u	v	w	Point	u	v	w
	[cm]	[cm/s]	[cm/s]	[cm/s]		[cm/s]	[cm/s]	[cm/s]
C171_b	5	48.41	-8.06	-5.64	C171_b	51.44	-1.25	-1.15
C271	5	33.42	-0.01	0.03	C271	48.15	0.67	-0.92
C371	5	32.79	0.80	0.16	C371	51.42	-9.72	-1.03
C471	5	32.52	-1.46	-2.79	C471	40.09	2.53	-1.84
C571	5	30.61	1.09	0.35	C571	41.41	1.88	-0.90
C671	5	33.00	1.48	0.24	C671	47.83	-8.68	-2.57
C771	5	34.63	0.52	-2.49	C771	40.34	2.86	-1.08
C871	5	37.49	2.97	-0.18	C871	43.18	2.71	-0.61
C971_b	5	44.45	4.07	-0.66	C971_b	58.37	-7.04	-1.43
C172_b	4	41.87	-6.88	-5.90	C172_b	50.61	-1.31	-1.21
C272	4	33.36	0.17	-0.26	C272	47.29	0.36	-0.92
C372	4	32.70	0.59	0.15	C372	47.65	-12.14	-3.85
C472	4	29.01	-1.36	-3.31	C472	38.16	2.10	-1.58
C572	4	30.81	1.01	-0.11	C572	39.87	1.11	-0.89
C672	4	32.33	0.69	-0.16	C672	44.26	-9.04	-4.90
C772	4	30.47	-0.83	-2.83	C772	38.21	2.09	-1.01
C872	4	36.29	2.70	-0.16	C872	42.06	1.71	-0.76
C972_b	4	42.30	2.80	-0.56	C972_b	46.60	-8.72	-2.54
C173_b	3	29.31	-4.04	-3.62	C173_b	48.73	-1.57	-1.09
C273	3	32.28	1.26	-0.12	C273	44.86	-0.39	-0.88
C373	3	30.92	0.18	0.20	C373	6.51	-6.31	2.91
C473	3	23.72	-0.68	-3.44	C473	36.75	2.29	-1.42
C573	3	28.96	0.68	0.22	C573	38.87	0.22	-1.08
C673	3	29.77	-0.64	-0.18	C673	27.93	-7.70	-3.86
C773	3	27.90	0.10	-2.75	C773	37.75	1.97	-1.35
C873	3	35.67	1.80	-0.29	C873	39.03	0.34	-0.55
C973_b	3	40.94	1.83	-0.49	C973_b	13.79	-3.48	5.58
C174_b	2	19.50	0.26	-1.68	C174_b	45.60	-2.24	-0.82
C274	2	32.37	2.27	-0.29	C274	41.51	-1.49	-0.78
C374	2	29.91	-0.23	0.30	C374	1.02	-0.57	2.95
C474	2	18.67	0.92	-2.23	C474	34.01	1.28	-1.21
C574	2	27.60	-0.30	0.13	C574	35.29	-0.96	-0.61
C674	2	28.30	-1.46	-0.29	C674	9.28	-2.14	0.31
C774	2	22.79	0.29	-1.65	C774	35.68	0.96	-0.90
C874	2	31.22	-0.10	0.11	C874	37.91	-0.52	-0.32
C974_b	2	38.22	0.08	-0.53	C974_b	7.29	0.89	3.05
C175_b	1	19.26	8.22	-0.40	C175_b	41.50	-2.77	-0.68
C275	1	30.56	2.20	-0.23	C275	36.80	-2.66	-0.52
C375	1	27.99	-0.73	-0.23	C375	-0.93	0.03	2.12
C475	1	14.74	3.09	-1.44	C475	31.67	0.68	-0.53
C575	1	25.56	-1.21	0.04	C575	33.89	-2.31	-0.75
C675	1	26.43	-2.67	-0.19	C675	2.07	7.25	1.00
C775	1	19.61	1.45	-1.15	C775	34.02	0.49	-0.87
C875	1	30.50	-1.04	-0.27	C875	34.60	-2.39	-0.18
C975_b	1	34.58	-1.15	-0.39	C975_b	2.27	13.25	3.56